Design and Synthesis of Organic Functional Materials for Energy Conversion and Storage Applications

Francis Lin

A dissertation

submitted in partial fulfillment of the

requirements for the degree of

Doctor of Philosophy

University of Washington

2019

Reading Committee:

Alex Jen, Chair

Samson Jenekhe

Christine Luscombe

Program Authorized to Offer Degree:

Chemistry

University of Washington

Abstract

Design and Synthesis of Organic Functional Materials for
Energy Conversion and Storage Applications

Francis Lin

Chair of the Supervisory Committee:
Dr. Alex Jen
Materials Science and Engineering

Carbon emission from consumption of fossil fuels has led to global warming accompanying with a large number of environmental issues. In order to lessen the strong dependence on fossil fuels in modern society, it is crucial to develop new energy sources which are clean, renewable and environmentally friendly. Solar energy is one of the leading candidates to fulfill the foreseeable growing demand of clean energy in near future. In the past few decades, tremendous efforts have been devoted to research on organic photovoltaics (OPVs) as the electrochemical and optical properties of OPV materials can be customized through judicious molecular engineering. Though OPV devices gave power conversion efficiencies (PCEs) no more than 0.1% while conceptually demonstrated in late 1950s, nowadays scientists have achieved PCEs over 17% utilizing new material systems and device fabrication techniques. Beside performance,

OPVs can be easily fabricated through solution methods and the device properties are highly tunable, facilitating the application of OPVs in next-generation solar energy system.

While OPVs demonstrate great potential to efficiently convert light into electricity, yet all solar energy systems possess a major drawback that sun does not provide a constant stream of energy. A proper energy storage system is necessary to be coupled with the solar energy system to store up the energy harvested from sunlight and maintain stable power supply no matter day or night. Li-S battery made of a sulfur cathode and a metallic Li anode is cost-effective for large-scale energy storage due to its high capacity and energy density. However, the infamous "shuttle effect" in sulfur cathode caused by formation of soluble lithium polysulfide (Li_2S_x, $3 \leq x \leq 8$) during charge/discharge strongly inhibits the commercialization of Li-S battery. An effective material system capable of mitigating the shuttle effect is in urgent need.

This dissertation elucidates my research efforts on design and synthesis of organic functional materials for OPVs and sulfur cathodes, respectively. The goal of my research aims at establishing novel structure-property relationships and exploiting rationales on molecular designing which may address current challenges in the fields. Chapter 1 gives a brief overview on the evolution of OPV materials and the design principles. Chapter 2 demonstrates the effect of selenium substitution on ladder-type non-fullerene acceptors for polymer solar cells. Chapter 3 explores the possibility of coupling selenium substitution with β-alkylation on central donor cores of non-fullerene acceptors as a strategy to further enhance photovoltaic performance. Chapter 4 provides a basic summary on rationales of designing organic materials for the sulfur cathode of Li-S batteries, and shows a class of polymethacrylates designed and synthesized as a component for a self-healing and polysulfide-trapping polyelectrolyte in Li-S batteries.

TABLE OF CONTENTS

LIST OF FIGURES

LIST OF SCHEMES

LIST OF TABLES

CHEMICAL STRUCTURE INDEX

Intermediates

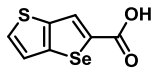

2-1

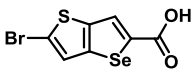

2-2

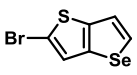

2-3

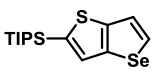

2-4

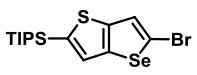

2-5

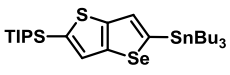

2-6

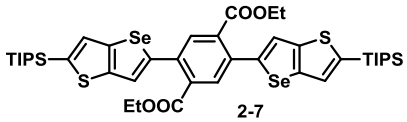

2-7

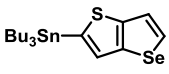

2-8

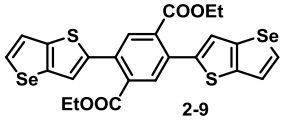

2-9

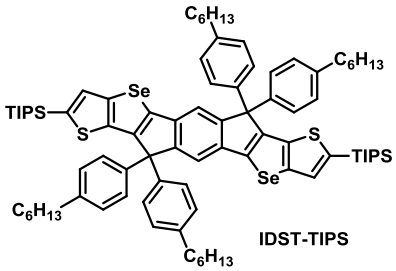

IDST-TIPS

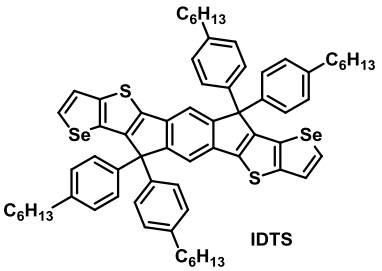

IDTS

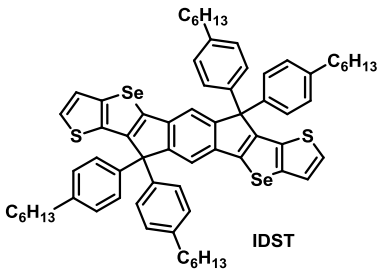

IDST

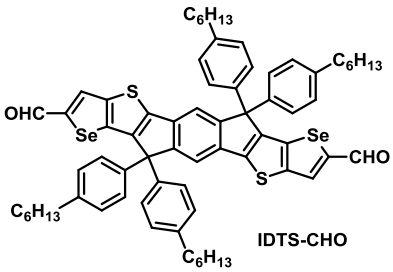

IDTS-CHO

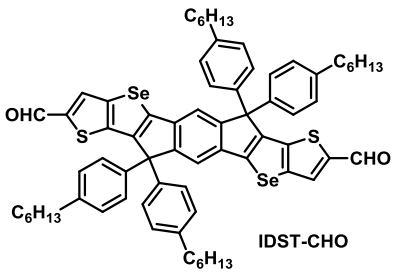

IDST-CHO

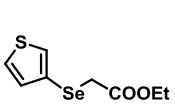

3-1

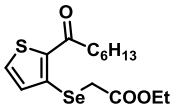

3-2

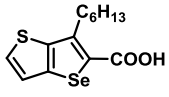

3-3

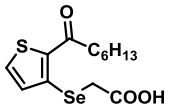

3-3a

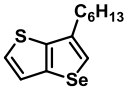

3-4

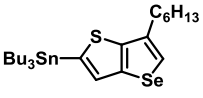

3-5

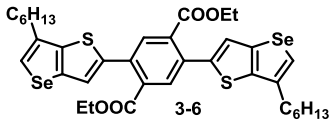

3-6

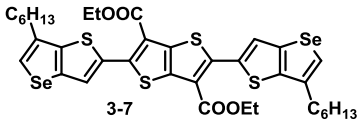

3-7

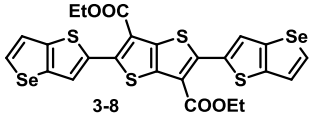

3-8

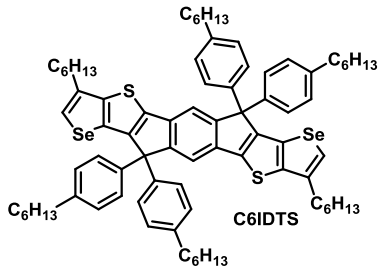
C6IDTS

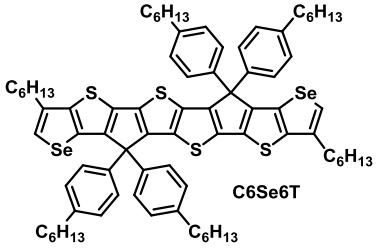
C6Se6T

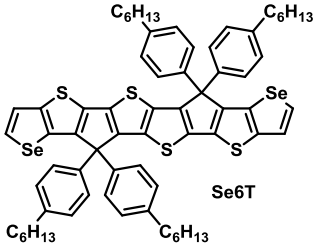
Se6T

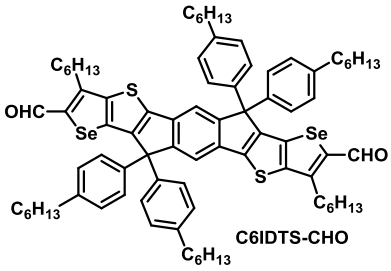
C6IDTS-CHO

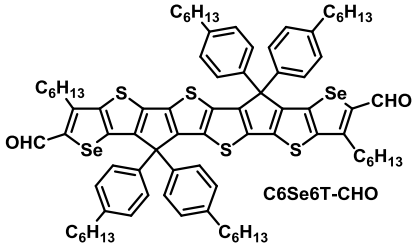
C6Se6T-CHO

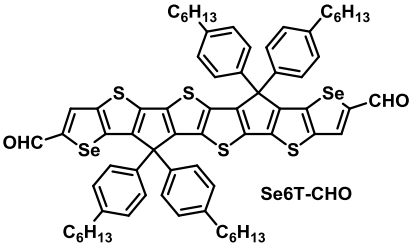
Se6T-CHO

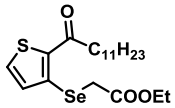
3-9

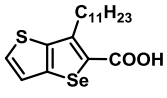
3-10

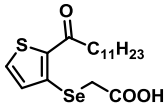
3-10a

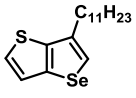
3-11

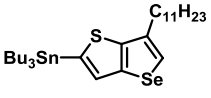
3-12

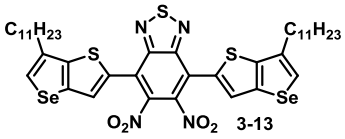
3-13

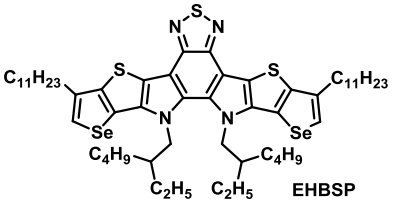
EHBSP

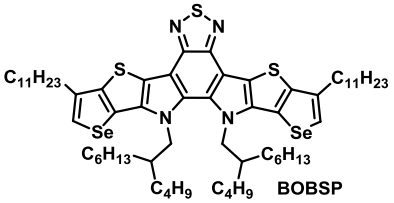
BOBSP

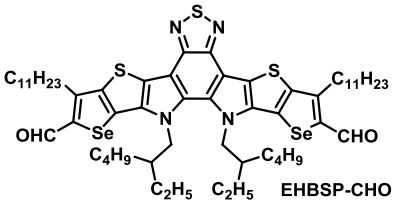
EHBSP-CHO

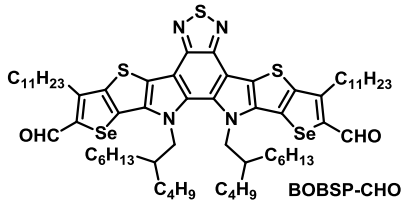
BOBSP-CHO

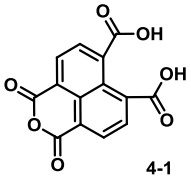
4-1

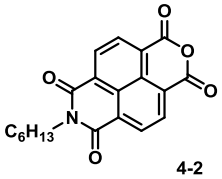
4-2

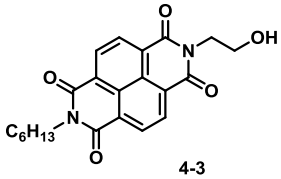
4-3

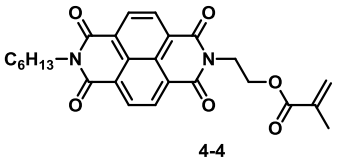
4-4

Target Compounds

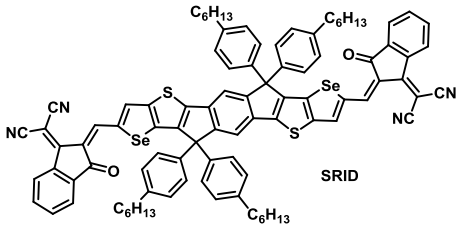
SRID

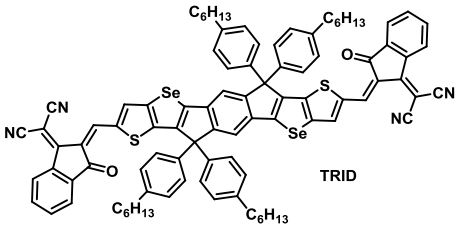
TRID

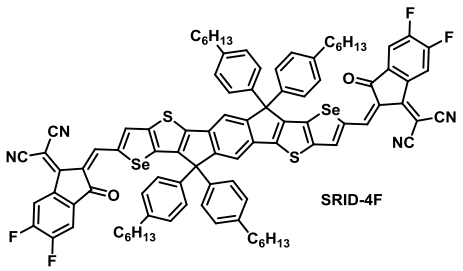
SRID-4F

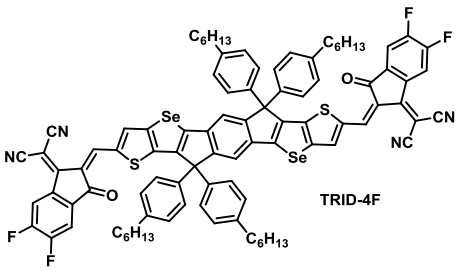
TRID-4F

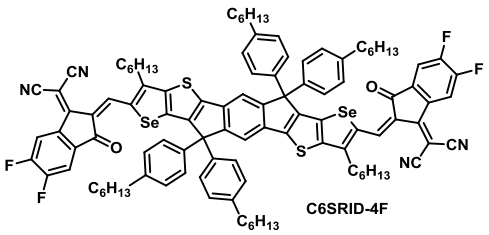
C6SRID-4F

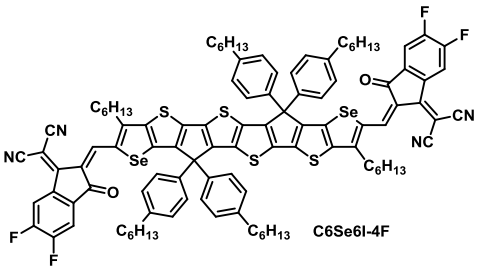
C6Se6I-4F

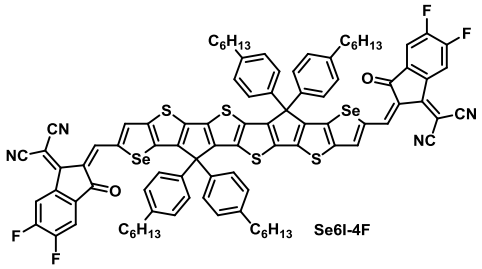
Se6I-4F

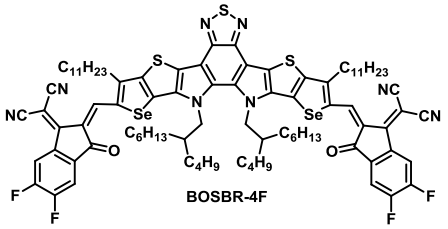
BOSBR-4F

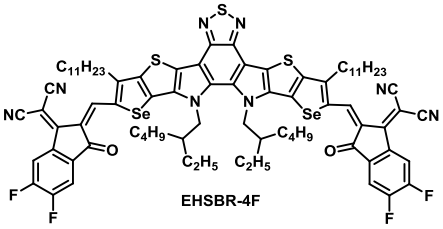
EHSBR-4F

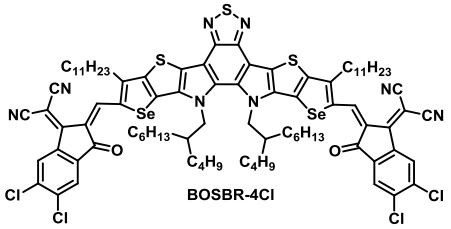
BOSBR-4Cl

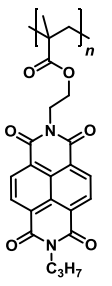
PNDI-C_3

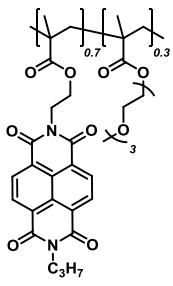
PENDI-C_3

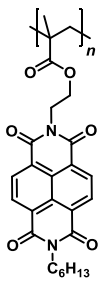
PNDI-C_6

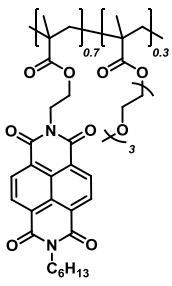
PENDI-C_6

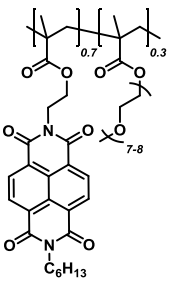
PENDI-350

ACKNOWLEDGEMENTS

Going to the United States to pursue a Ph.D. degree is probably the biggest decision that I have ever made in my life. The past 5 years has been a whole new experience in terms of research and lifestyle for me. I would like to thank my advisor, Prof. Alex Jen for his support and guidance during my Ph.D. study, as well as Dr. Sei-Hum Jang, Prof. Chu-Chen Chueh and Prof. Jingdong Luo. I also want to thank the students and postdocs, including Burny, Dr. Shen-Wen Brian Cheng, Dr. Po-Wei Liang, Dr. Ting Zhao, Dr. Adharsh Rajagopal, Dr. Xueliang Shi, Dr. Jingbo Zhao, Dr. Bin Kan, Dr. Ke Gao, Dr. Sae Byeok Jo and other members in Jen Research Group for the companionship, collaboration and numerous help on my research. It is my great pleasure to work with you guys.

This dissertation couldn't have been finished without the help from Dr. Lijian Zuo for the majority part of OPV device fabrication, Dr. Jiangsheng Yu for part of the OPV device fabrication, Dr. Yuyin Xi for part of the GIWAXS measurement, Dr. Werner Kaminsky for the single-crystal X-ray crystallography analysis, Porf. Feng Liu for RSoXS and part of the GIWAXS measurement, Mr. Dion Hubble and Mr. Jiaxu Qin for battery fabrication and part of the material characterization. Every effort of yours has made this dissertation closer to its completion.

Toward my life outside of the lab, I want to thank my EMB roommates in L-407, Stephen and POA, for the memorable days. I also want to thank the friendship between me and my college friends, Alex, Freddy, Marco and Timothy, as we are all pursuing or have already got our Ph.D. degree in the United States. I am also thankful to my old friends and new friends in Seattle,

including Christina, Joe, Maggie, Henry and Jasmine, who have brought me joy during the nice summer days and warmness during the rainy winter days.

I would like to thank people who have inspired and encouraged me to pursue chemistry, including my senior high school chemistry teacher Mr. Che Chau Yang, my undergraduate research advisor Prof. Ken-Tsung Wong, and my mentor Dr. Li-Yen Lin. I also want to give special thanks to Chun-Kai Wang, who was a mentee of mine and was just awarded his Ph.D. in NTU. We know we are not alone on our journey to Ph.D. in Chemistry.

Finally, I want to show my greatest gratitude to my parents and my sister for their support. I also want to thank D. L. and C.-Y. H., who had taught me lessons of life and provided me great emotional support when I was struggling, as a lover or as friends, so that I was able to persist in the pursuit of my Ph.D.

DEDICATION

Chapter 1. EVOLUTION AND DESIGN OF ORGANIC FUNCTIONAL MATERIALS FOR SOLAR ENERGY CONVERSION

1.1 INTRODUCTION

The concept of organic photovoltaics (OPVs), in which organic dyes are used as the absorber in solar cells, was first demonstrated in the late 1950s. While studying the photoconductivity of semiconducting organic dyes, mainly phthalocyanine or chlorophyll derivatives, scientists observed formation of photocurrent on a simple device fabricated simply by sandwiching a single layer of organic dyes between electrodes with different work functions.[1,2] However, a major issue in this type of solar cells is that the internal electric field built by the metal electrodes in the devices is not strong enough to efficiently split the excitons into free charge carriers, while the low charge carrier mobilities of organic dyes further worsens the charge transport in the devices. As a result, these solar cells only gave very low power conversion efficiencies, mostly less than 0.1%.

In 1986, Tang reported the first example of binary OPVs with a bilayer configuration, which contains two layers of organic dyes between the electrodes.[3] This type of bilayer configuration is also known as planar heterojunction. By depositing a layer of copper phthalocyanine (CuPc) on the indium tin oxide (ITO) substrate, and subsequently another layer of perylene bisbenzimidazole (PV) on top, finally a layer of Ag as the electrode, the device delivered a PCE of 0.95% under AM2 illumination (Figure 1-1). The two organic dyes with different electron affinities and ionization potentials create strong local electric field at the heterojunction, namely the interface. As the exciton forms under illumination, the two dyes can act as an electron donor and an electron acceptor, respectively, to efficiently split excitons into charge carriers, thus to enhance the

photovoltaic performance. The work has been regarded as a main breakthrough which opened the era of current OPV research.

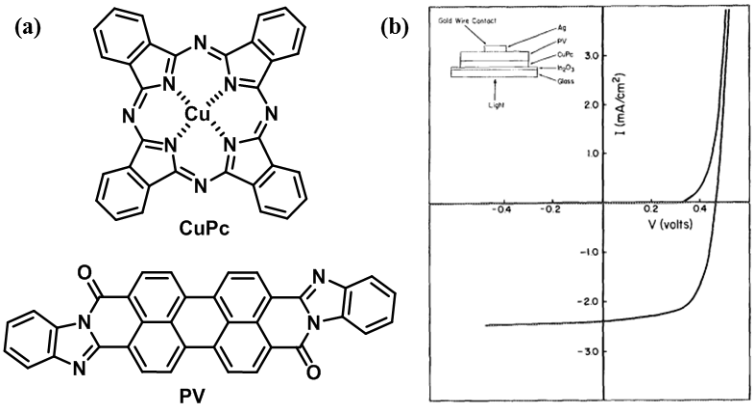

Figure 1-1. (a) Chemical structures of CuPc and PV. (b) Photovoltaic device architecture and *J*-*V* curve of CuPc:PV bilayer OPV.

With the concept of binary OPVs being established, scientists started to explore different materials for donor/acceptor combination. In 1993, Heeger, Wudl *et al.* first reported planar heterojunction devices employing conductive polymers:C_{60} as donor:acceptor.[4] C_{60} possesses high electron affinity, high electron mobility and stable electrochemical properties, and this is the first time of fullerenes being used as the electron acceptor in OPVs. Along with exploration on new material systems, new processing techniques were also developed. One year later in 1994, Heeger *et al.* further expanded the concept of heterojunction from the simple planar heterojunction into a much more complicated "bulk heterojunction (BHJ)".[5] In the BHJ, electron donor and electron acceptor are blended together to form a bicontinuous interpenetrating network, thus the surface area between the donor:acceptor phase can be greatly enlarged and leads to higher charge separation efficiency at donor:acceptor interfaces.

The morphology of BHJ is highly dependent on the interaction between donor/acceptor, which is strongly affected by the crystallinity and miscibility of the materials. Though widely used as an electron acceptor in early studies, the high crystallinity of C_{60} had always been an issue which prohibited the formation of high quality polymer:C_{60} BHJ due to strong self-aggregation of C_{60} in blended films. To solve this problem, Wudl *et al.* reported a series of chemically modified fullerenes with reduced crystallinity, enhanced solubility and processability in 1995, one of which being the very well-known phenyl-C_{61}-butyric acid methyl ester ($PC_{61}BM$).[6] From then on, BHJ employing fullerenes, including C_{60}, C_{70} and their derivatives, has dominated the field of OPV research for almost two decades.[7] Different classes of donor materials have also been designed to accommodate to different processing techniques, including vacuum processing and solution processing (Figure 1-2 & 1-3).[8-12] The issues in terms of light harvesting, exciton generation, exciton diffusion, charge separation and charge transport can also be addressed from the perspective of material design. Researchers were able to finally achieve 10% PCE on devices based on PTB7-Th:$PC_{71}BM$ BHJ,[13,14] and further reached a higher PCE of 11% based on polymers designed by Yan *et al.* (Figure 1-3b).[15]

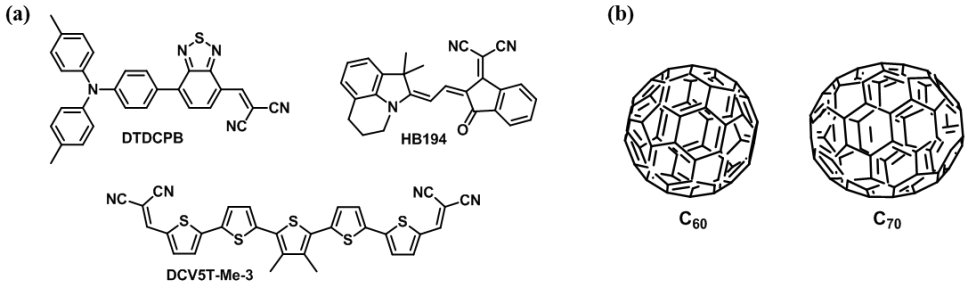

Figure 1-2. Chemical structures of (a) vacuum-deposited small-molecule donors, and (b) C_{60} and C_{70}.

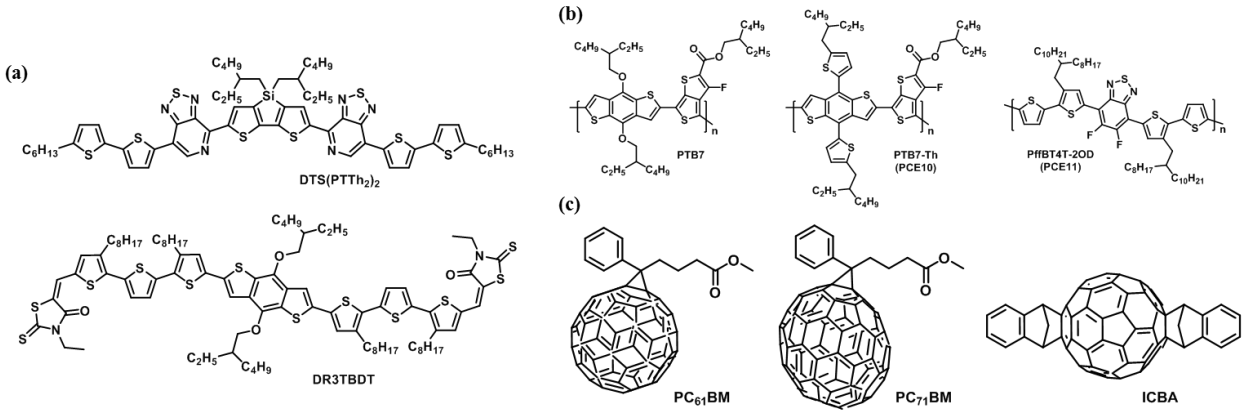

Figure 1-3. Chemical structures of (a) solution-processed small-molecule donors, (b) solution-processed polymeric donors, and (c) fullerene derivatives $PC_{61}BM$, $PC_{71}BM$ and ICBA.

Though fullerenes have been proven to be very efficient as a class of *n*-type semiconductors and acceptors for OPVs, there are two major drawbacks related to the nature of chemical properties of fullerenes, including weak optical absorption and lack of tunability on frontier orbital energy levels. Most fullerenes possess optical absorption limited within the range below 500 nm, which is far away from the wavelength region with maximum photon flux in solar spectrum (Figure 1-4). Also, the energy levels of chemically modified fullerene derivatives are dominated by the number of π-electrons on the fullerenes (Figure 1-5), no matter what kind of functional groups are attached onto the fullerenes through chemical modification.[16] What's worse, by introducing more functional groups onto the fullerene cage, the number of π-electrons is lessened and the absorption of modified fullerenes will be blue-shifted. The steric hindrance brought by these functional groups also interferes with the packing of modified fullerenes and reduce the charge carrier mobilities. As a result, the optical absorption and frontier orbital energy levels of fullerenes are limited only within a small range, which also limit the choice of suitable donors that may pair with fullerenes.

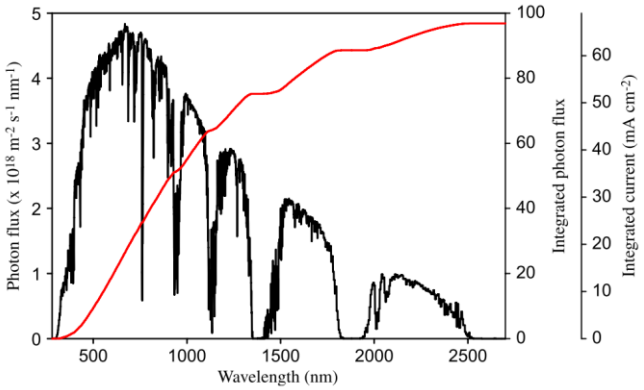

Figure 1-4. Photon flux and integrated photon flux as functions of wavelength at AM 1.5G (I =1000 W/m^2).[17]

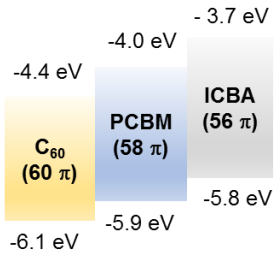

Figure 1-5. Energy levels of C_{60} and its derivatives.

To overcome the limitations of fullerenes, scientists have invested enormous efforts to develop different material systems as alternatives. In early to mid-2010s, one class of materials which received great attention was perylene diimide (PDI) and its derivatives. The optical absorption of PDIs can reach 550 nm, and is capable of extending to around 700 nm upon structural modification, which is a lot more red-shifted than fullerenes. However, most of PDI-based acceptors gave PCEs at around 6-8% (Figure 1-6),[18,19] which were not able to compete with the performance of fullerene-based photovoltaic devices. Moreover, structural modification of PDI derivatives can be problematic due to (1) bromination of PDI yields isomers which are extremely

difficult to separate and (2) structure of PDI only provides few positions accessible for chemical modification,[20] hindering further exploration of PDI-based acceptors.

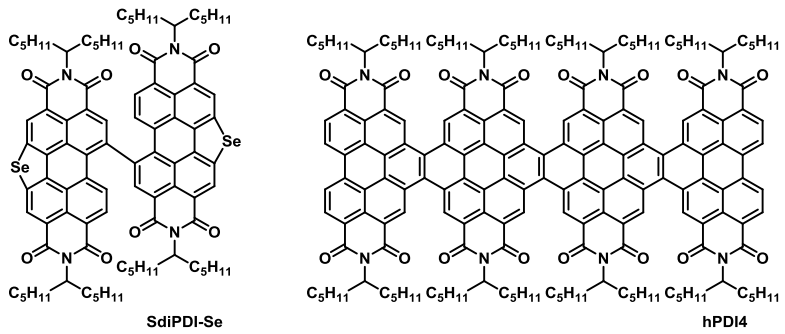

Figure 1-6. Chemical structures of PDI derivatives as acceptor materials.

Another class of acceptor materials that has been studied extensively is linear A-D-A type molecules, which are generally called as non-fullerene acceptors (NFAs). Organic semiconductors with A-D-A structural configuration have long been studied in the field of non-linear optics, organic light-emitting diodes, and even donor materials for OPVs. However, it was not until recently that people started to explore the potential of employing A-D-A type molecules as acceptors in OPVs. These A-D-A type NFAs are highly tunable in their optical and electrochemical properties through structural modification, offering a great opportunity to enhance the performance of OPVs. They have also shown great potential due to their good compatibility with polymer donors, efficient light harvesting to increase short circuit current density (J_{sc}), and relatively small energy loss to afford high open circuit voltage (V_{oc}) in OPVs.[21-41]

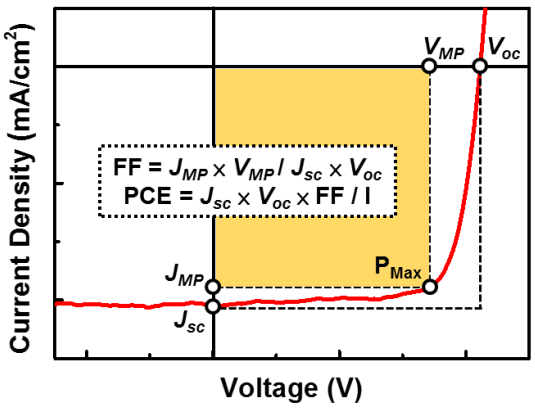

Figure 1-7. *J*-*V* curve of a photovoltaic device.

Starting from 2014, McCulloch *et al.* reported a series of A-D-A type NFAs derived from fluorene, indenofluorene (IDF) and indacenodithiophene (IDT) (Figure 1.8a). These materials demonstrated red-shifted light absorption up to 800 nm and gave PCEs over 6% when paired with P3HT.[39-41] In 2015, Zhan *et al.* reported ITIC as derived from ladder-type core 5,5,11,11-tetrakis(4-hexylphenyl)-dithieno[2,3-*d*:2',3'-*d'*]-s-indaceno[1,2-*b*:5,6-*b'*]dithiophene (IDTT) (Figure 1.8b), which is probably the most well-known A-D-A type NFA up-to-date. Photovoltaic devices based on binary BHJs of PTB7-Th:ITIC gave PCEs up to 6.8%, which was comparable with devices based on fullerene acceptors.[21]

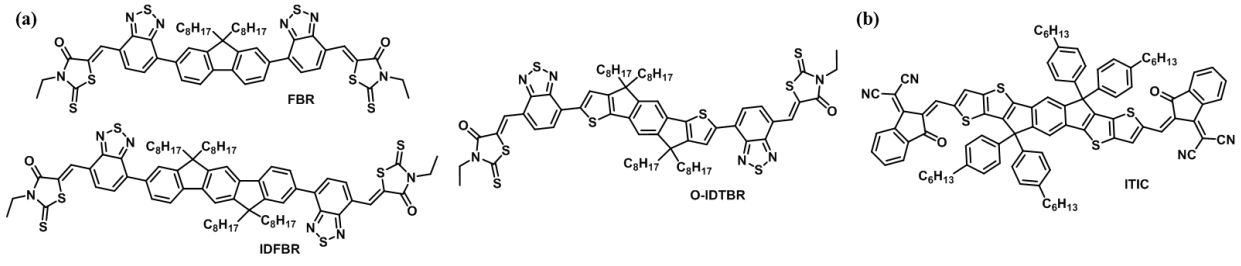

Figure 1-8. Chemical structures of (a) A-D-A type NFAs reported by McCulloch *et al.* and (b) ITIC.

Recently, PCEs surpassing 15 % have been reported on binary BHJs while pairing A-D-A type NFAs with large bandgap polymer donors, which have already been superior to fullerene-based counterparts.[42] Aside from polymer/NFA OPVs, all-small-molecule solar cells based on molecular donors and NFAs have also been reported to give PCEs up to 12%.[43] To further enhance the solar cell performance, several strategies have been explored based on the perspective of chemistry to design novel and efficient NFAs. Two of the most effective strategies, which are (1) bandgap engineering and (2) morphology control, are described in the latter of this chapter with corresponding examples.

1.2 Molecular Design Principles of A-D-A type NFAs

In photovoltaic devices based on binary BHJs, the J_{sc} of devices mainly correlate to the absorption of materials which is determined by the bandgap, namely the difference between the highest occupied molecular orbital (HOMO) and lowest unoccupied molecular orbital (LUMO) of the materials. The V_{oc} of devices mainly correlate to the relative bandgap alignment between the electron donor and electron acceptor pair. It is crucial that the electron donor and electron acceptor pair have well-matched bandgap to ensure photocurrent generation and mitigate energy loss (Fig. 1-9). The bandgap of A-D-A type NFAs, as well as the optical and electrochemical properties, can be tailored through adjusting the intramolecular donor-acceptor strength.

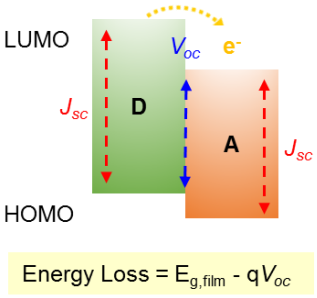

Figure 1-9. Bandgap alignment between donor and acceptor.

Aside from molecular properties, the intermolecular interactions between NFA:NFA molecules or donor:NFA blends also play an important role on the performance of solar cells. The compatibility between donor materials and NFAs can be tuned to achieve desirable active layer morphology to ensure efficient charge transport in devices. An ideal morphology at the donor:NFA interface is crucial to ensure efficient exciton dissociation and minimize trap-assisted recombination, which can enhance J_{sc} and FF of the devices and reduce energy loss.

1.2.1 *Bandgap Engineering: π-Conjugation Extension*

The bandgap of π-conjugated system can be reduced through increasing the conjugation length, as extended π-orbital overlap is provided for long-range π–electron delocalization. A growth in molar extinction coefficient often accompanies with the bandgap shrinkage, which is beneficial to the application as light absorbers for solar cells (Figure 1-10).[44-46] However, the disorder created by rotation of interannular single bonds in the π-conjugated system may interfere with the extension of π-orbital overlap and π-electron delocalization. As a consequence, there is a saturation point of conjugation length even in π-conjugation system with unlimited extension. This is known as

effective conjugation length, as defined by number of uninterrupted π-bonds at which the optical absorption onset reaches saturation in the conjugated system.

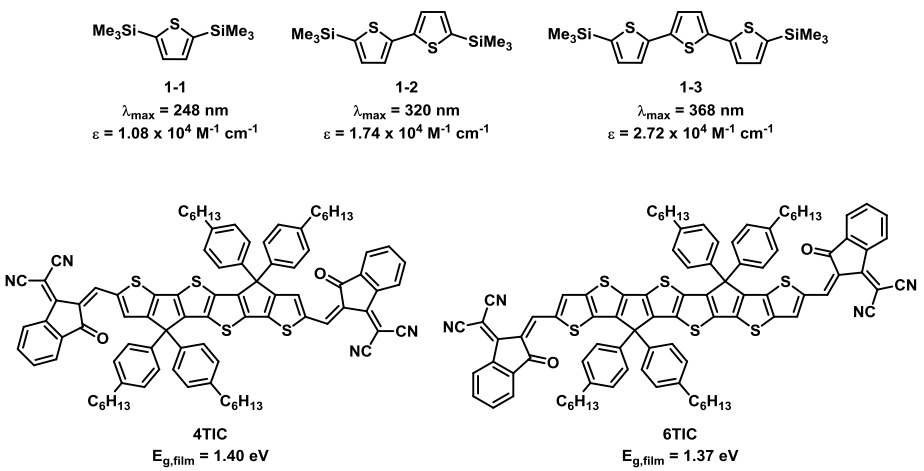

Figure 1-10. Examples demonstrating the effects of π-conjugation extension.

1.2.2 *Bandgap Engineering: Donor-Acceptor Push-Pull Effect*

Embedding electron-rich donor and electron-deficient acceptor moieties into conjugated systems facilitates π-electron delocalization by creating a push-pull intramolecular charge transfer from the donor toward the acceptor. Incorporation of strong donors will notably up-shift the HOMO and slightly up-shift the LUMO, while strong acceptors will notably down-shift the LUMO and slightly down-shift the HOMO of the material, and both serves the purpose of reducing bandgap. Through employing donors and acceptors with different push-pull strength into conjugated systems, the frontier orbital energy levels and the bandgap can be precisely tuned. This is an extremely powerful approach to engineer the bandgap. In A-D-A type NFAs, strongly push-pull donor-acceptor combinations have enabled light absorption up to 1000 nm (Figure 1-12),[47,48] which is superior to fullerene- and PDI-based acceptors.

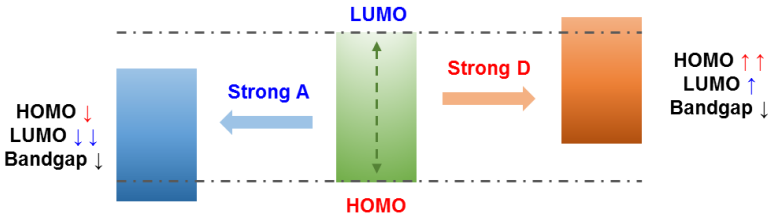

Figure 1-11. The shifting of HOMO/LUMO levels induced by donor and acceptor.

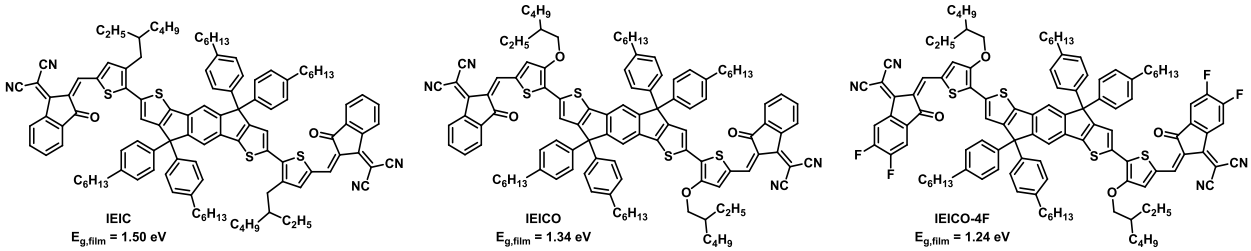

Figure 1-12. Examples demonstrating reduction of bandgap due to stronger donor-acceptor interactions.

1.2.3 *Bandgap Engineering: Structural Rigidification*

Most of the high-efficiency A-D-A type NFAs have a rigidified ladder-type core in the middle, sandwiched by two acceptor end groups on both sides. Rigidification by forming covalent bonds between π-conjugated units to co-planarize the molecular conformation is advantageous of mitigating the rotational disorder created by interannular single bonds between the adjacent cyclic conjugated moieties, lessening the reorganization energy while facilitating maximum π-orbital overlap and π-electron delocalization within the π-conjugated system, as well as extending the effective conjugation length. As a result, the bandgap of the π-conjugated system is reduced (Figure 1-13),[49,50] and the charge carrier mobilities can also be enhanced through rigidification due to the planarized molecular conformation and increased crystallinity. However, rigidification will

severely decrease the solubility of the molecules and requires side chains with appropriate lengths to be attached to the molecules to ensure adequate solubility and processability.

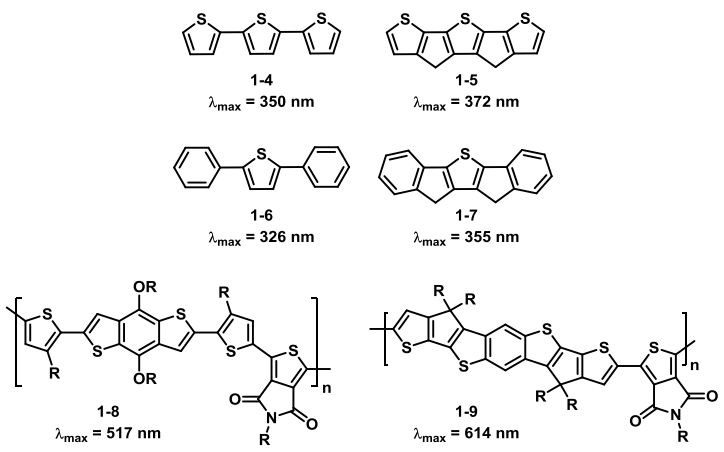

Figure 1-13. Examples demonstrating reduction of bandgap due to structural rigidification.

1.2.4 *Morphology Control: Side Chain Engineering*

The side chains attached onto the conjugated system, though may not directly involve with the delocalization of π-electrons, are also a key factor which affects the crystallinity and compatibility of the materials. The aggregation pattern of the materials is also strongly dependent on the type of side chains. In A-D-A type NFAs, the central ladder-type cores tends to form close packing due to π-orbital interactions between the planarized structures, which may lead to poor interactions between donor materials and NFAs and severe phase segregation at donor:NFA interfaces. In this regard, bulky side chains with cyclic aromatic phenyl or thienyl rings are often attached onto the ladder-type cores to reduce the strong self-aggregation.[25] In some cases, alkyl side chains with adequate length or branching may still serve the same purpose (Figure 1-14).[51] Nevertheless, the

synthesis of alkyl substituted ladder-type cores can be extremely difficult when using carbon as the bridging atom.

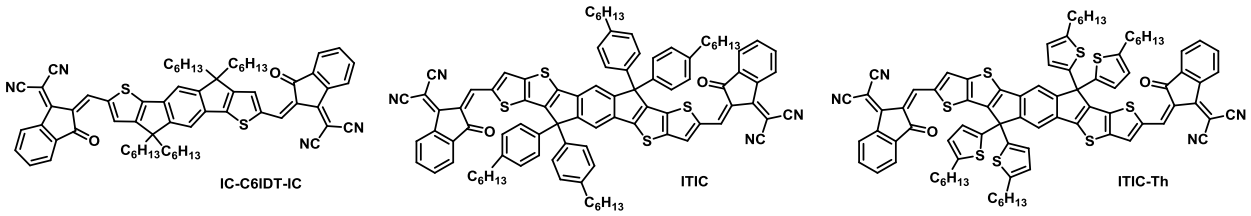

Figure 1-14. Examples illustrating side-chain engineering on NFAs.

1.2.5 *Morphology Control: Non-Covalent Interactions*

Introducing acceptor end groups which may induce non-covalent interactions onto A-D-A type NFAs is also capable of manipulating the morphology at donor:NFA interfaces, as well as enhancing electron mobility in the BHJ by forming electron-transporting channels through the communications of the electron-deficient acceptor end groups. Among literature, halogenation by introducing fluorine or chlorine atoms which provides strong dipole-dipole interactions is one of the most effective strategies,[37,38] while extending the π-conjugation of the end groups can also lead to stronger π-π interactions between the end groups (Figure 1-15).[52,53]

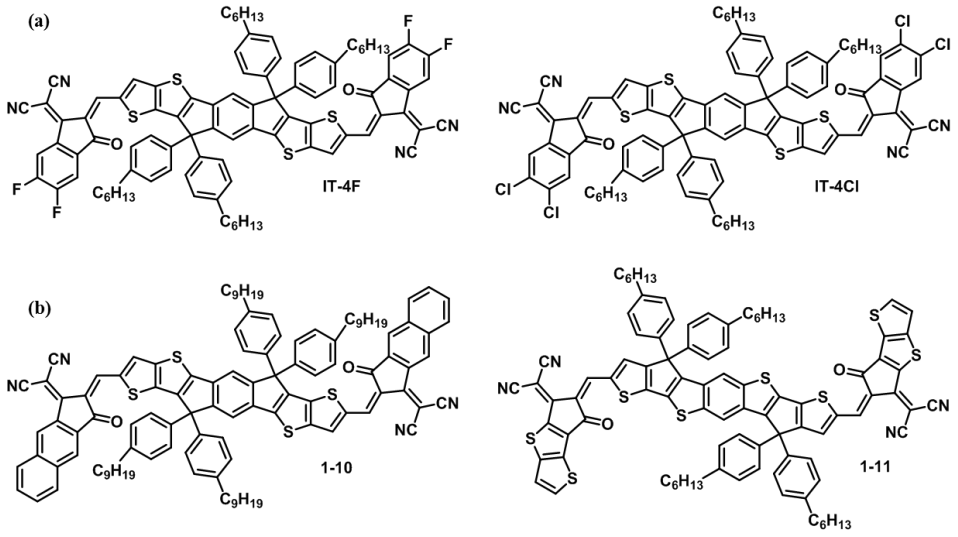

Figure 1-15. Examples illustrating introduction of non-covalent interactions on NFAs.

Beside structural modifications, it is noteworthy that the morphology of BHJ can also be tuned through multiple techniques during device fabrication, which includes thermal annealing, solvent vapor annealing,[43] and addition of solvent additives, *etc.* These techniques, however, needs to accommodate with the physical properties such as solubility and thermal stability of the materials, so that solar cells with high efficiency and long lifetime can be made.

1.3 CONCLUSION

In this chapter, a brief overview on the development of evolution of OPVs was provided. The principles of designing highly efficient A-D-A type NFAs summarized from the experience accumulated by tremendous amount of researchers over decades were also discussed with supporting examples. It is crucial that all these factors need to be considered while designing the materials to ensure preferable molecular properties and intermolecular interactions between

NFA:NFA molecules and donor:NFA blends, in hope of generating a molecular design strategy with clear rationale built from the structure-property relationships of materials.

1.4 REFERENCES

(1) Kearns, D.; Calvin, M. *Journal of Physical Chemistry* **1958**, *59*, 950.
(2) Delacote, G. M.; Fillard, J. P.; Marco, F. J. *Solid State Communications* **1964**, *2*, 373.
(3) Tang, C. W. *Applied Physics Letters* **1986**, *48*, 183.
(4) Sariciftci, N. S.; Smilowitz, L.; Heeger, A. J.; Wudl, F. *Synthetic Metals* **1993**, *59*, 333.
(5) Yu, G.; K., P.; Heeger, A. J. *Applied Physics Letters* **1994**, *64*, 3422.
(6) Hummelen, J. C.; Knight, B. W.; LePeq, F.; Wudl, F.; Yao, J.; Wilkins, C. L. *The Journal of Organic Chemistry* **1995**, *60*, 532.
(7) Yu, G.; Gao, J.; Hummelen, J. C.; Wudl, F.; Heeger, A. J. *Science* **1995**, *270*, 1789.
(8) Chen, Y. H.; Lin, L. Y.; Lu, C. W.; Lin, F.; Huang, Z. Y.; Lin, H. W.; Wang, P. H.; Liu, Y. H.; Wong, K. T.; Wen, J.; Miller, D. J.; Darling, S. B. *Journal of the American Chemical Society* **2012**, *134*, 13616.
(9) Steinmann, V.; Kronenberg, N. M.; Lenze, M. R.; Graf, S. M.; Hertel, D.; Meerholz, K.; Bürckstümmer, H.; Tulyakova, E. V.; Würthner, F. *Advanced Energy Materials* **2011**, *1*, 888.
(10) Fitzner, R.; Mena-Osteritz, E.; Mishra, A.; Schulz, G.; Reinold, E.; Weil, M.; Korner, C.; Ziehlke, H.; Elschner, C.; Leo, K.; Riede, M.; Pfeiffer, M.; Uhrich, C.; Bauerle, P. *Journal of the American Chemical Society* **2012**, *134*, 11064.
(11) Sun, Y.; Welch, G. C.; Leong, W. L.; Takacs, C. J.; Bazan, G. C.; Heeger, A. J. *Nature materials* **2011**, *11*, 44.
(12) Zhou, J.; Wan, X.; Liu, Y.; Zuo, Y.; Li, Z.; He, G.; Long, G.; Ni, W.; Li, C.; Su, X.; Chen, Y. *Journal of the American Chemical Society* **2012**, *134*, 16345.
(13) Liang, Y.; Feng, D.; Wu, Y.; Tsai, S.-T.; Li, G.; Ray, C.; Yu, L. *Journal of the American Chemical Society* **2009**, *131*, 7792.
(14) He, Z.; Xiao, B.; Liu, F.; Wu, H.; Yang, Y.; Xiao, S.; Wang, C.; Russell, T. P.; Cao, Y. *Nature Photonics* **2015**, *9*, 174.
(15) Liu, Y.; Zhao, J.; Li, Z.; Mu, C.; Ma, W.; Hu, H.; Jiang, K.; Lin, H.; Ade, H.; Yan, H. *Nature communications* **2014**, *5*, 5293.
(16) Matsuo, Y.; Kawai, J.; Inada, H.; Nakagawa, T.; Ota, H.; Otsubo, S.; Nakamura, E. *Advanced materials* **2013**, *25*, 6266.
(17) Smestad, G. P.; Krebs, F. C.; Lampert, C. M.; Granqvist, C. G.; Chopra, K. L.; Mathew, X.; Takakura, H. *Solar Energy Materials and Solar Cells* **2008**, *92*, 371.
(18) Zhong, Y.; Trinh, M. T.; Chen, R.; Purdum, G. E.; Khlyabich, P. P.; Sezen, M.; Oh, S.; Zhu, H.; Fowler, B.; Zhang, B.; Wang, W.; Nam, C. Y.; Sfeir, M. Y.; Black, C. T.; Steigerwald, M. L.; Loo, Y. L.; Ng, F.; Zhu, X. Y.; Nuckolls, C. *Nature communications* **2015**, *6*, 8242.
(19) Meng, D.; Sun, D.; Zhong, C.; Liu, T.; Fan, B.; Huo, L.; Li, Y.; Jiang, W.; Choi, H.; Kim, T.; Kim, J. Y.; Sun, Y.; Wang, Z.; Heeger, A. J. *Journal of the American Chemical Society* **2016**, *138*, 375.
(20) Rajasingh, P.; Cohen, R.; Shirman, E.; Shimon, L. J. W.; Rybtchinski, B. *Journal of Organic Chemistry* **2007**, *72*, 5973.
(21) Lin, Y.; Wang, J.; Zhang, Z. G.; Bai, H.; Li, Y.; Zhu, D.; Zhan, X. *Advanced materials* **2015**, *27*, 1170.
(22) Zhao, W.; Qian, D.; Zhang, S.; Li, S.; Inganas, O.; Gao, F.; Hou, J. *Advanced materials* **2016**, *28*, 4734.
(23) Yang, Y.; Zhang, Z. G.; Bin, H.; Chen, S.; Gao, L.; Xue, L.; Yang, C.; Li, Y. *Journal of the American Chemical Society* **2016**, *138*, 15011.
(24) Li, S.; Ye, L.; Zhao, W.; Zhang, S.; Mukherjee, S.; Ade, H.; Hou, J. *Advanced materials* **2016**, *28*, 9423.
(25) Lin, Y.; Zhao, F.; He, Q.; Huo, L.; Wu, Y.; Parker, T. C.; Ma, W.; Sun, Y.; Wang, C.; Zhu, D.; Heeger, A. J.; Marder, S. R.; Zhan, X. *Journal of the American Chemical Society* **2016**, *138*, 4955.
(26) Luo, Z.; Bin, H.; Liu, T.; Zhang, Z. G.; Yang, Y.; Zhong, C.; Qiu, B.; Li, G.; Gao, W.; Xie, D.; Wu, K.; Sun, Y.; Liu, F.; Li, Y.; Yang, C. *Advanced materials* **2018**, *30*.
(27) Cao, H.; Bauer, N.; Pang, C.; Rech, J.; You, W.; Rupar, P. A. *ACS Applied Energy Materials* **2018**, *1*, 7146.
(28) Yao, Z.; Liao, X.; Gao, K.; Lin, F.; Xu, X.; Shi, X.; Zuo, L.; Liu, F.; Chen, Y.; Jen, A. K. *Journal of the American Chemical Society* **2018**, *140*, 2054.
(29) Wang, Y.; Zhang, Y.; Qiu, N.; Feng, H.; Gao, H.; Kan, B.; Ma, Y.; Li, C.; Wan, X.; Chen, Y. *Advanced Energy Materials* **2018**, *8*, 1702870.
(30) Wang, C. K.; Jiang, B. H.; Su, Y. W.; Jeng, R. J.; Wang, Y. J.; Chen, C. P.; Wong, K. T. *ACS applied materials & interfaces* **2019**, *11*, 1125.
(31) Huang, C.; Liao, X.; Gao, K.; Zuo, L.; Lin, F.; Shi, X.; Li, C.-Z.; Liu, H.; Li, X.; Liu, F.; Chen, Y.; Chen, H.; Jen, A. K. Y. *Chemistry of Materials* **2018**, *30*, 5429.
(32) Hou, J.; Inganas, O.; Friend, R. H.; Gao, F. *Nature materials* **2018**, *17*, 119.
(33) Wadsworth, A.; Moser, M.; Marks, A.; Little, M. S.; Gasparini, N.; Brabec, C. J.; Baran, D.; McCulloch, I. *Chemical Society reviews* **2019**, *48*, 1596.
(34) Zhang, G.; Zhao, J.; Chow, P. C. Y.; Jiang, K.; Zhang, J.; Zhu, Z.; Zhang, J.; Huang, F.; Yan, H. *Chemical reviews* **2018**, *118*, 3447.
(35) Cheng, P.; Li, G.; Zhan, X.; Yang, Y. *Nature Photonics* **2018**, *12*, 131.
(36) Yan, C.; Barlow, S.; Wang, Z.; Yan, H.; Jen, A. K. Y.; Marder, S. R.; Zhan, X. *Nature Reviews Materials* **2018**, *3*.

(37) Zhao, W.; Li, S.; Yao, H.; Zhang, S.; Zhang, Y.; Yang, B.; Hou, J. *Journal of the American Chemical Society* **2017**, *139*, 7148.

(38) Zhang, H.; Yao, H.; Hou, J.; Zhu, J.; Zhang, J.; Li, W.; Yu, R.; Gao, B.; Zhang, S.; Hou, J. *Advanced materials* **2018**, *30*, e1800613.

(39) Holliday, S.; Ashraf, R. S.; Nielsen, C. B.; Kirkus, M.; Rohr, J. A.; Tan, C. H.; Collado-Fregoso, E.; Knall, A. C.; Durrant, J. R.; Nelson, J.; McCulloch, I. *Journal of the American Chemical Society* **2015**, *137*, 898.

(40) Holliday, S.; Ashraf, R. S.; Wadsworth, A.; Baran, D.; Yousaf, S. A.; Nielsen, C. B.; Tan, C. H.; Dimitrov, S. D.; Shang, Z.; Gasparini, N.; Alamoudi, M.; Laquai, F.; Brabec, C. J.; Salleo, A.; Durrant, J. R.; McCulloch, I. *Nature communications* **2016**, *7*, 11585.

(41) Baran, D.; Ashraf, R. S.; Hanifi, D. A.; Abdelsamie, M.; Gasparini, N.; Rohr, J. A.; Holliday, S.; Wadsworth, A.; Lockett, S.; Neophytou, M.; Emmott, C. J.; Nelson, J.; Brabec, C. J.; Amassian, A.; Salleo, A.; Kirchartz, T.; Durrant, J. R.; McCulloch, I. *Nature materials* **2017**, *16*, 363.

(42) Yuan, J.; Zhang, Y.; Zhou, L.; Zhang, G.; Yip, H.-L.; Lau, T.-K.; Lu, X.; Zhu, C.; Peng, H.; Johnson, P. A.; Leclerc, M.; Cao, Y.; Ulanski, J.; Li, Y.; Zou, Y. *Joule* **2019**, *3*, 1140.

(43) Gao, K.; Jo, S. B.; Shi, X.; Nian, L.; Zhang, M.; Kan, Y.; Lin, F.; Kan, B.; Xu, B.; Rong, Q.; Shui, L.; Liu, F.; Peng, X.; Zhou, G.; Cao, Y.; Jen, A. K. *Advanced materials* **2019**, *31*, e1807842.

(44) Tour, J. M.; Wu, R. *Macromolecules* **1992**, *25*, 1901.

(45) Shi, X.; Zuo, L.; Jo, S. B.; Gao, K.; Lin, F.; Liu, F.; Jen, A. K. Y. *Chemistry of Materials* **2017**, *29*, 8369.

(46) Shi, X.; Chen, J.; Gao, K.; Zuo, L.; Yao, Z.; Liu, F.; Tang, J.; Jen, A. K. Y. *Advanced Energy Materials* **2018**, *8*, 1702831.

(47) Yao, H.; Chen, Y.; Qin, Y.; Yu, R.; Cui, Y.; Yang, B.; Li, S.; Zhang, K.; Hou, J. *Advanced materials* **2016**, *28*, 8283.

(48) Yao, H.; Cui, Y.; Yu, R.; Gao, B.; Zhnag, H.; Hou, J. *Angewandte Chemie* **2017**, *56*, 3045.

(49) Roncali, J.; Thobie-Gautier, C. *Advanced materials* **1994**, *6*, 846.

(50) Chen, Y.-L.; Chang, C.-Y.; Cheng, Y.-J.; Hsu, C.-S. *Chemistry of Materials* **2012**, *24*, 3964.

(51) Lin, Y.; He, Q.; Zhao, F.; Huo, L.; Mai, J.; Lu, X.; Su, C. J.; Li, T.; Wang, J.; Zhu, J.; Sun, Y.; Wang, C.; Zhan, X. *Journal of the American Chemical Society* **2016**, *138*, 2973.

(52) Swick, S. M.; Zhu, W.; Matta, M.; Aldrich, T. J.; Harbuzaru, A.; Lopez Navarrete, J. T.; Ponce Ortiz, R.; Kohlstedt, K. L.; Schatz, G. C.; Facchetti, A.; Melkonyan, F. S.; Marks, T. J. *Proceedings of the National Academy of Sciences of the United States of America* **2018**, *115*, E8341.

(53) Chang, S.-L.; Cao, F.-Y.; Huang, W.-C.; Huang, P.-K.; Huang, K.-H.; Hsu, C.-S.; Cheng, Y.-J. *ACS Energy Letters* **2018**, *3*, 1722.

Chapter 2. INVESTIGATION ON THE EFFECT OF REGIO-SPECIFIC SELENIUM SUBSTITUTION IN NON-FULLERENE ACCEPTORS

2.1 INTRODUCTION

Substitution of chalcogen species from sulfur to selenium in the π-conjugation backbones can advantageously adjust both intrinsic optoelectronic properties and intermolecular interactions of the molecules.[1-9] The looser electron cloud delocalization around the more polarizable selenium atom enables stronger orbital overlap between selenium and the π-conjugated system, leading to a higher quinoid resonance character at ground state, which reduces the aromaticity and narrows the bandgap of selenophene.[10,11] The interaction between lone pairs on different selenium atoms is also stronger as they do not contribute to the aromaticity of π-conjugated system as much as the sulfur. As a result, intermolecular Se-Se interactions are stronger than S-S interactions, which is helpful to improve charge carrier mobilities.[12]

Introducing selenium into the molecular framework of NFAs has previously been reported by Liao *et al.* and gave PCEs over 8 % while paired with a large bandgap polymer J51.[13,14] Hou *et al.* also reported a selenophene-incorporated A-D-A type NFA, and demonstrated a high PCE of 13.32 %.[15] The authors claimed that the more polarizable selenium atom helps the red-shift of optical absorption and more efficient charge separation /transport in the polymer:NFA blends. However, in order to fully harness these advantages brought by selenium substitution, a more thorough study is necessary to reveal the explicit impacts on chemical, physical, and structural behaviors correlating to different chemical environments originated from regio-specific selenium substitution.

2.2 MOLECULAR DESIGN AND SYNTHESIS

Herein, we have systematically modulated selenium substitution based on 5,5,11,11-tetrakis(4-hexylphenyl)-dithieno[2,3-*d*:2',3'-*d'*]-s-indaceno[1,2-*b*:5,6-*b'*]dithiophene (**IDTT**). Two isomeric ladder-type electron-donating cores, 5,5,11,11-tetrakis(4-hexylphenyl)-diselenopheno[2,3-*d*:2',3'-*d'*]-s-indaceno[1,2-*b*:5,6-*b'*]dithiophene (**IDTS**) and 5,5,11,11-tetrakis(4-hexylphenyl)-dithieno[2,3-*d*:2',3'-*d'*]-s-indaceno[1,2-*b*:5,6-*b'*]diselenophene (**IDST),** were designed and synthesized to explore the regio-specific properties of selenium substitution (Figure 2-1).

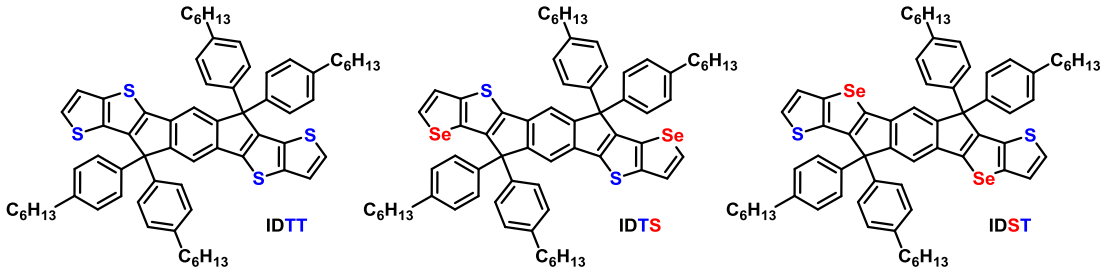

Figure 2-1. Chemical structures of **IDTT**, **IDTS** and **IDST**.

The asymmetric selenopheno[3,2-*b*]thiophene is the key to achieve our proposed structure. Although it has previously been utilized as a building block for polymeric materials on organic field effect transistors (OFETs),[16] a synthetic strategy to selectively functionalize this asymmetric molecule was not well established - the scope of reaction conditions is limited due to the distinct nature of selenopheno[3,2-*b*]thiophene. Commonly, generation of carbanions at the α-position of thiophene or selenophene derivatives can be achieved by lithium-proton exchange with ease. However, it is challenging to selectively lithiate the α-position of selenophene on selenopheno[3,2-

b]thiophene due to (1) the pK_a of α hydrogen of selenophene and thiophene is not distinct enough for a clean lithiation, and (2) the higher electrophilicity of selenium atom may lead to a higher tendency for selenophene to undergo ring-opening reaction upon treatment of strong base such as organolithium reagents, especially while there is a suitable leaving group at the β-position.[17,18] Multiple lithiation conditions were screened to selectively deprotonate the α-position of selenophene on selenopheno[3,2-*b*]thiophene, however it was found that this route was not an efficient approach (Table 2-1).

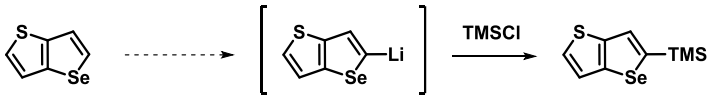

Trial	Reaction Condition			Result
	Solvent	Reagent	Temperature	
#1	THF (0.2 M)	1.00 eq. *n*-BuLi	-78 °C	Messy mixture containing 2- and 5-substituted products.
#2	THF (0.2 M)	1.00 eq. LDA	-78 °C	Mixture of 2- and 5-substituted and minor impurities.
#3	Et_2O (0.2 M)	1.00 eq. LDA	-78 °C	Mixture of unreacted starting material, 2- and 5-substituted and minor impurities.
#4	THF (0.2 M)	1.00 eq. LDA	-90 °C	Mixture of 2- and 5-substituted and minor impurities.

Table 2-1. Lithiation conditions tested on pristine selenopheno[3,2-*b*]thiophene.

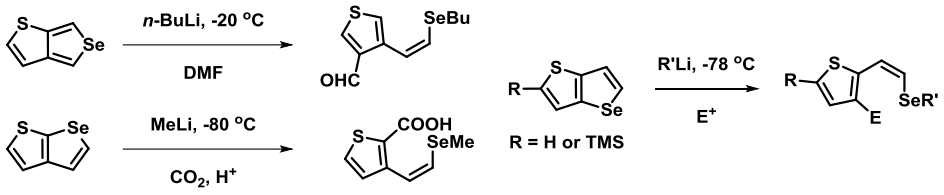

Figure 2-2. Ring-opening reaction of fused selenophene derivatives during lithiation.

An alternative route to avoid this issue is to conduct a lithium-bromine exchange, which possesses much higher reactivity, resulting in better selectivity and minimized side reactions at the α-position of selenophene rather than lithium-proton exchange. However, as from my attempts and as reported by Gol'dfarb *et al.*,[19] bromination of pristine selenopheno[3,2-*b*]thiophene under stoichiometric control is not plausible to yield 2-bromoselenopheno[3,2-*b*]thiophene in a scalable and efficient manner due to the similarity of α-directing effect of sulfur and selenium, which leads to small difference between the relative reactivity of electrophilic aromatic substitution of thiophene and selenophene.[16] A discreet synthetic approach to yield selectively functionalized selenopheno[3,2-*b*]thiophene efficiently is necessary to facilitate in-depth exploration on the properties of this unusual building block.

To begin with, I have developed a judicious route starting from bromination of selenopheno[3,2-*b*]thiophene-5-carboxylic acid (**2-1**) to yield 2-bromoselenopheno[3,2-*b*]thiophene-5-carboxylic acid (**2-2**).[16] Decarboxylation of **2-2** was carefully conducted under a mild condition to avoid carbon-bromine bond cleavage in dimethyl sulfoxide with acetic acid catalyzed by silver carbonate to give the key intermediate 2-bromoselenopheno[3,2-*b*]thiophene (**2-3**) at high yield under considerably large scale. Conventional decarboxylation conditions using elemental copper or oxidative copper chromite in quinolone were also tested, however these conditions were likely to result in multiple side reactions. Compound **2-3** was gradually converted to the two isomeric ladder-type cores, selenophene-exteriorized **IDTS** and selenophene-interiorized **IDST**. The synthesis of **IDTS** seemed to be more straightforward at this point, however it is noteworthy that in my first attempt of synthesizing **IDST**, I tried again to lithiate the α hydrogen of silyl-protected 2-trimethylsilylselenopheno[3,2-*b*]thiophene, but only again to yield ring-opened products as in my previous attempts of deprotonating pristine selenopheno[3,2-

b]thiophene. As a result, I protected the 2 position of selenopheno[3,2-*b*]thiophene with the less labile triisopropylsilyl (TIPS), and subsequently brominated the 5 position using *N*-bromosuccinimide followed by a second lithium halide exchange to yield the key stannylated intermediate **2-6** for synthesizing **IDST**.

The two isomeric cores, **IDTS** and **IDST**, were then formylated and condensed with 3-(1,1-dicyanomethylene)-indanone or 2-(5,6-difluoro-3-oxo-2,3-dihydro-1H-inden-1-ylidene)malononitrile to obtain the final products **SRID**/**TRID** and **SRID-4F** /**TRID-4F**, respectively (Scheme 2-1).

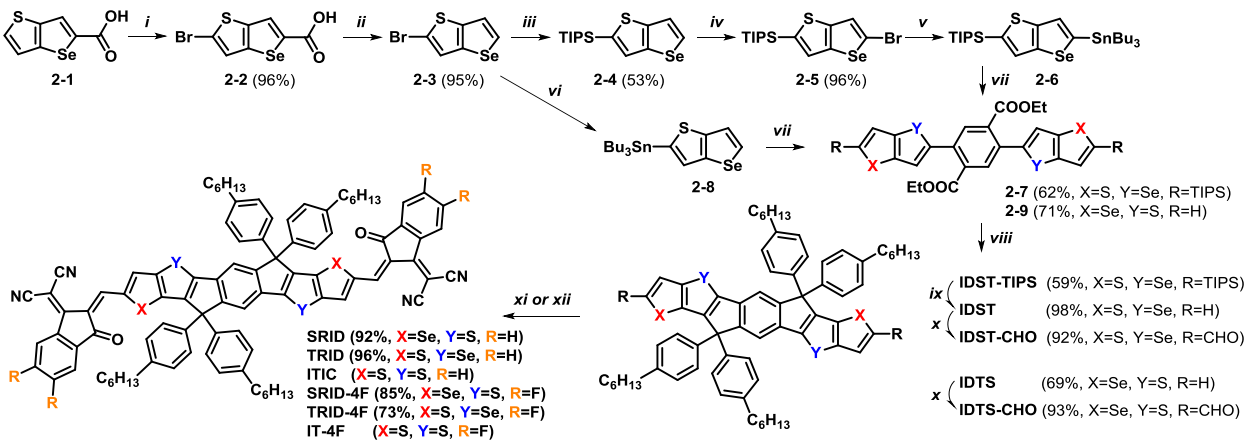

Reagents and conditions: i) *N*-bromosuccinimide, DMF, 0 ºC to r.t. *ii*) Ag_2CO_3, HOAc, DMSO. *iii*) *n*-BuLi, THF, -78 ºC; b) TIPSCl, -78 ºC to r.t. *iv*) *N*-bromosuccinimide, THF/DMF (v/v=3:1), 0 ºC to r.t. *v*) a) *n*-BuLi, THF, -78 ºC; b) Bu_3SnCl, -78 ºC to r.t. *vi*) a) *n*-BuLi, THF, -90 ºC; b) Bu_3SnCl, -90 ºC to r.t. *vii*) 2,5-dibromo-terephthalic acid diethyl ester, $PdCl_2(PPh_3)_2$, toluene, 110 ºC. *viii*) a) 4-hexyl-1-bromobenzene, *n*-BuLi, THF, -78 ºC to r.t. b) HOAc, $H_2SO_{4(conc.)}$, 80 ºC. *ix*) TBAF, THF, 0 ºC. *x*) DMF, $POCl_3$, 1,2-dichloroethane, 0 ºC to reflux. *xi*) 3-(1,1-dicyanomethylene)-indanone, β-alanine, 1,2-dichloroethane/isopropanol (v/v=3:2), 80 ºC. *xii*) 2-(5,6-difluoro-3-oxo-2,3-dihydro-1H-inden-1-ylidene)malononitrile, β-alanine, 1,2-dichloroethane/isopropanol (v/v=3:2), 80 ºC.

Scheme 2-1. Synthesis of **SRID**/**TRID** and **SRID-4F**/**TRID-4F**.

2.3 Optical and Electrochemical Properties

The optical properties of **IDTS**/**IDST**, **SRID**/**TRID**, and **SRID-4F**/**TRID-4F** were investigated using UV-Vis spectrometry. In solution, pristine cores **IDTS** and **IDST** show similar vibronic

structures and slightly red-shifted absorption (within 10 nm) comparing with **IDTT** (Figure 2-3), indicating that incorporation of selenophene with higher electron richness reduces the bandgap of the cores.

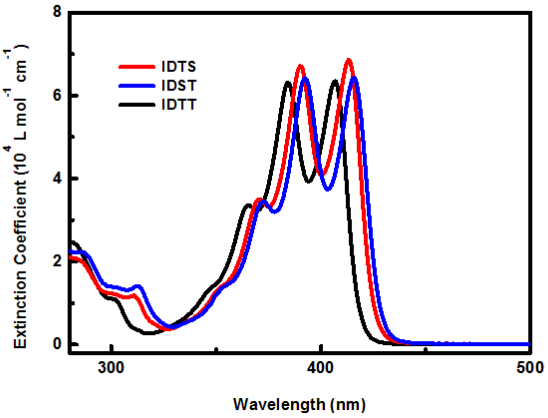

Figure 2-3. UV-Vis spectra of **IDTT**, **IDTS** and **IDST** in CH_2Cl_2.

While attached with strong electron-withdrawing indanone groups, both sets of **SRID**/**TRID** and **SRID-4F**/**TRID-4F** show strong absorption peaks in the range of 550 to 800 nm in diluted solution, while the absorption spectra of **SRID-4F**/**TRID-4F** are more red-shifted due to stronger intramolecular push-pull interaction (Figure 2-4a & 2-4c). In thin film, **SRID-4F**/**TRID-4F** show broadened absorption peaks and the absorption edges further shift to around 850 nm, which corresponds to 20-40 nm of red-shifting versus **IT-4F** and proves that **IDTS** and **IDST** are stronger electron donors than **IDTT** (Figure 2-4d). The thin film of **SRID**/**TRID** also show broadened absorption, however with less significant red-shifting of 10-20 nm versus the absorption edge of **ITIC** (Figure 2-4b). It is worth mentioning that **IDTS**-based NFAs possess more red-shifted absorption than **IDST**-based NFAs in both diluted solution and thin film, implying that the

intramolecular charge transfer between push-pull moieties in **IDTS**-based NFAs is more efficient, while there is not much difference between the electron richness of **IDTS** and **IDST**.

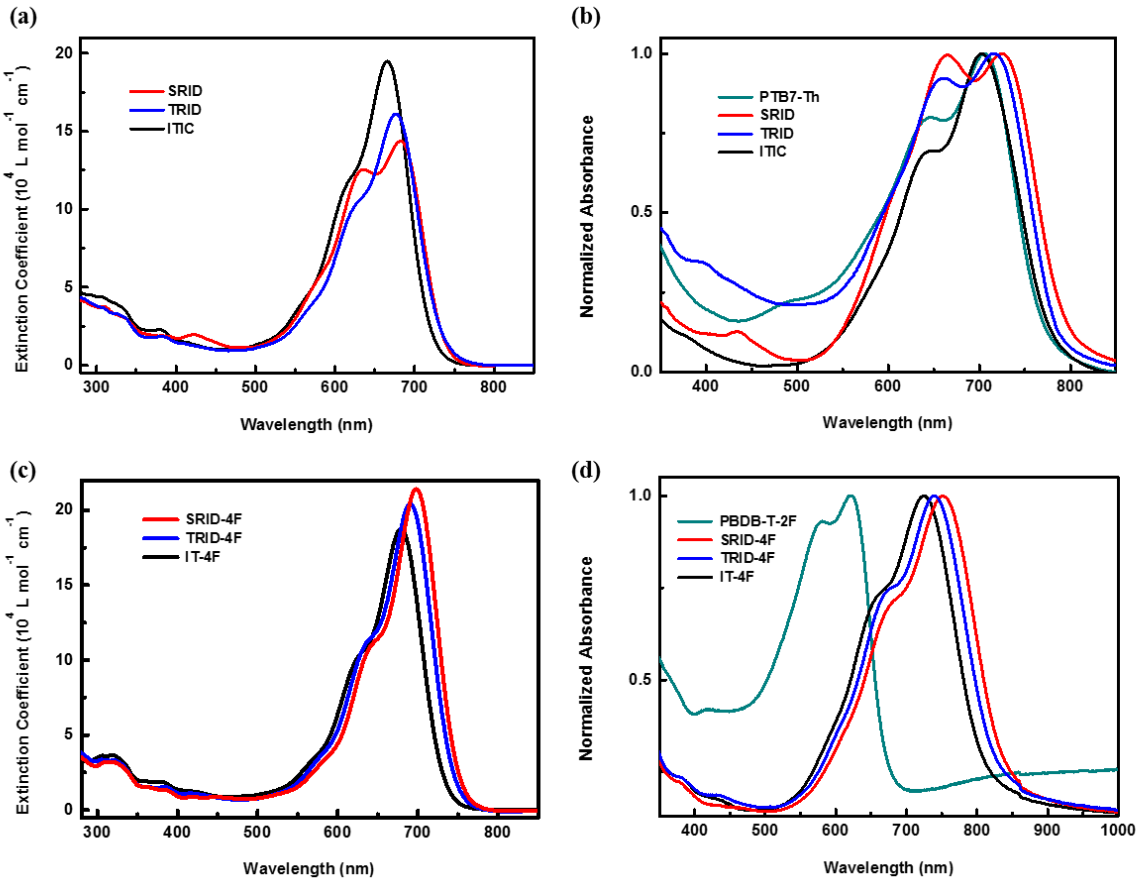

Figure 2-4. UV-Vis spectra of (a) **SRID**/**TRID**/**ITIC** in solution, (b) **SRID**/**TRID**/**ITIC** and PTB7-Th in thin film, (c) **SRID-4F**/**TRID-4F**/**IT-4F** in solution, and (d) **SRID-4F**/**TRID-4F**/**IT-4F** and PBDB-T-2F in thin film.

The frontier orbital energy levels of **SRID**/**TRID** and **SRID-4F**/**TRID-4F** were probed using cyclic voltammetry (CV) (Figure 2-5a & 2-5c). Both sets of **SRID**/**TRID** and **SRID-4F**/**TRID-4F** exhibit well-defined reversible oxidation waves corresponding to the oxidation of central electron-donating cores. In the cathodic potential regime, two irreversible reduction waves were observed

on all four materials, which could be attributed to the stepwise reduction on the electron-withdrawing indanone on different sides of the A-D-A molecule. Moreover, differential pulse voltammetry (DPV) was applied to clearly distinguish the electrochemical potential of the two very close reduction waves (Figure 2-4b & 2-4d).[20] Both CV and DPV measurements show that the ionization potentials (IP, corresponding to HOMO) and electron affinities (EA, corresponding to LUMO) of **SRID**/**TRID** are similar, as well as those of **SRID-4F**/**TRID-4F**. The IP/EA values of **SRID**/**TRID** are -5.49/-3.76 and -5.48/-3.75 eV, and -5.52/-3.90 eV for both **SRID-4F**/**TRID-4F**, as derived from the redox half potentials obtained in CV measurement (Table 2-2).[21]

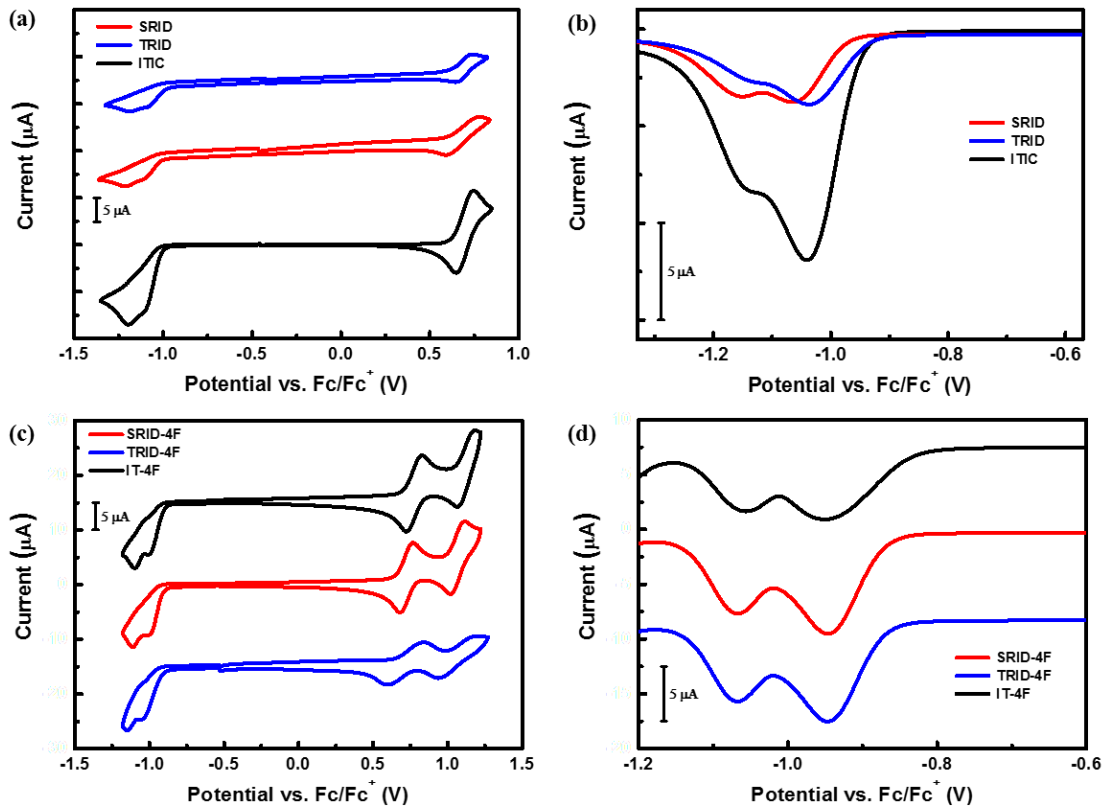

Figure 2-5. (a) CV and (b) DPV characteristics of **SRID**/**TRID**/**ITIC**, and (c) CV and (d) DPV characteristics of **SRID-4F**/**TRID-4F**/**IT-4F**.

It is very interesting to find out that the electrochemical bandgap of **SRID**/**TRID** ($E_{g,CV}$ = 1.73 eV for both) and **SRID-4F**/**TRID-4F** ($E_{g,CV}$ = 1.62 eV for both) are similar, respectively. However, the optical bandgap of **IDTS**-based NFAs ($E_{g,film}$ = 1.56 eV for **SRID** and 1.44 eV for **SRID-4F**) are larger than those of **IDST**-based NFAs ($E_{g,film}$ = 1.58 eV for **TRID** and 1.48 eV for **TRID-4F**) (Table 2-2). This phenomenon can be attributed to the structural difference between selenophene-exteriorized **IDTS** and selenophene-interiorized **IDST**. Although these two isomeric cores have similar electron richness, **IDTS** may have better communication with the electron-withdrawing indanone units then **IDST**, as the more polarizable and electron-donating selenophene is located outward on its side. The larger dipole moment between the push-pull moieties in **SRID** and **SRID-4F** results in efficient charge transfer and more red-shifted absorption in both thin film and diluted solution. It is also noteworthy that **SRID** and **SRID-4F** are the first examples among literature to demonstrate a selenophene-vinyl bridge-acceptor configuration where selenophene is directly fused onto the donor moiety.

	$\lambda_{max,\ soln}$[a] (nm)	ε[a] (10^4 L mol^{-1} cm^{-1})	$\lambda_{max,\ film}$[b] (nm)	λ_{edge}[c] (nm)	$E_{g,\ film}$[d] (eV)	IP[e] (eV)	EA[e] (eV)	$E_{g,\ CV}$[f] (eV)
SRID	682	14.4	725	795	1.56	-5.49	-3.76	1.73
TRID	677	16.1	716	787	1.58	-5.48	-3.75	1.73
ITIC	666	19.5	703	778	1.59	-5.50	-3.76	1.74
SRID-4F	698	21.4	752	862	1.44	-5.52	-3.90	1.62
TRID-4F	691	20.4	740	836	1.48	-5.52	-3.90	1.62
IT-4F	679	18.8	723	820	1.51	-5.57	-3.89	1.68

[a] Measured in CH_2Cl_2 solution (1×10^{-6} M). [b] Spin-cast thin film. [c] Optical bandgap estimated from thin-film absorption. [d] Calculated from the absorption edge of thin-film spectra. [e] Cyclic voltammetry (CV) was measured in CH_2Cl_2 solution with 0.1 M NBu_4PF_6 as supporting electrolyte. Sample concentration was 0.01 M for the measurements. All potentials were recorded using Fc/Fc^+ as an external reference, which was referenced at -4.80 eV below vacuum level. [f] Electrochemical bandgap estimated from the redox half potentials of CV measurement.

Table 2-2. Summary of optical and electrochemical properties of **SRID**/**TRID**/**ITIC** and **SRID-4F**/**TRID-4F**/**IT-4F**.

2.4 Device Characteristics and Morphological Study of SRID/TRID

2.4.1 *Photovoltaic Characteristics*

SRID/**TRID** were paired with PTB7-Th as the donor for fabrication of photovoltaic devices with configuration of ITO/ZnO/PTB7-Th:**NFAs**/MoO_3/Ag. The optimal donor/acceptor ratio was found to be 1:1.5 for both **SRID**/**TRID**, and 1:1.25 for PTB7-Th:**ITIC** reference devices. Despite highly overlapped optical absorption of PTB7-Th with the NFAs, devices based on PTB7-Th:**TRID** delivered a V_{oc} of 0.84 V, a J_{sc} of 16.01 mA/cm^2, a FF of 0.61, and thus a PCE of 8.17 %, which is superior to the 7.28% PCE of devices based on PTB7-Th:**ITIC**. To further boost the performance, 1,8-diiodooctane (DIO) was applied as an additive. However, it was found that the PTB7-Th:**TRID** BHJ is extremely additive-sensitive, as a tiny ratio of DIO additive at 0.25 v/v % could slightly enhance the PCE to 8.60 %, then unfavorably lowered the PCEs while increasing the ratio of DIO (Table 2-3). On the other hand, devices of PTB7-Th:**SRID** delivered a V_{oc} of 0.85 V, a J_{sc} of 16.50 mA/cm^2, a FF of 0.59, and thus a PCE of 8.21 %. The PCE of **SRID**-based devices was dramatically boosted to 9.10 % by adding 1 v/v % DIO, as the FF was greatly benefited from the additive to reach a value of 0.65 (Table 2-3). The different response of **SRID**/**TRID** to DIO additive could be an indirect evidence corresponding to discrepancy between solid-state microstructure of these two isomeric molecules. It is also noteworthy that the external quantum efficiency (EQE) spectra of optimized PTB7-Th:**SRID** cells achieved a maximum EQE close to 80 % through 600-700 nm (Figure 2-6), and the V_{oc} of **SRID**-based devices is the highest among all three NFAs regardless of the higher HOMO of **SRID**, implying the energy loss (defined as $E_{g,film} - qV_{oc}$) is reduced in this system.

	D:A raio	Processing condition	V_{oc} (V)	J_{sc} (mA/cm^2)	FF	PCE (%)
PTB7-Th: **SRID**	1:1	CB	0.84	14.29	0.39	4.61
	1:1.5	CB	0.85	16.50	0.59	8.21
	1:2	CB	0.85	15.32	0.56	7.29
	1:1.5	CB+0.5% DIO	0.85	16.13	0.62	8.50
	1:1.5	**CB+1% DIO**	**0.85**	**16.45**	**0.65**	**9.10**
	1:1.5	CB+3% DIO	0.86	15.29	0.55	7.23
PTB7-Th: **TRID**	1:1	CB	0.82	16.02	0.50	6.56
	1:1.5	CB	0.84	16.01	0.61	8.17
	1:2	CB	0.84	14.79	0.56	6.96
	1:1.5	**CB+0.25% DIO**	**0.83**	**16.18**	**0.64**	**8.60**
	1:1.5	CB+0.5% DIO	0.83	15.37	0.60	7.65
	1:1.5	CB+1% DIO	0.84	14.79	0.53	6.58
PTB7-Th: **ITIC**	1:1.25	CB	0.83	15.18	0.57	7.28

Table 2-3. Device optimization parameters for PTB7-Th:**SRID**/**TRID**/**ITIC**.

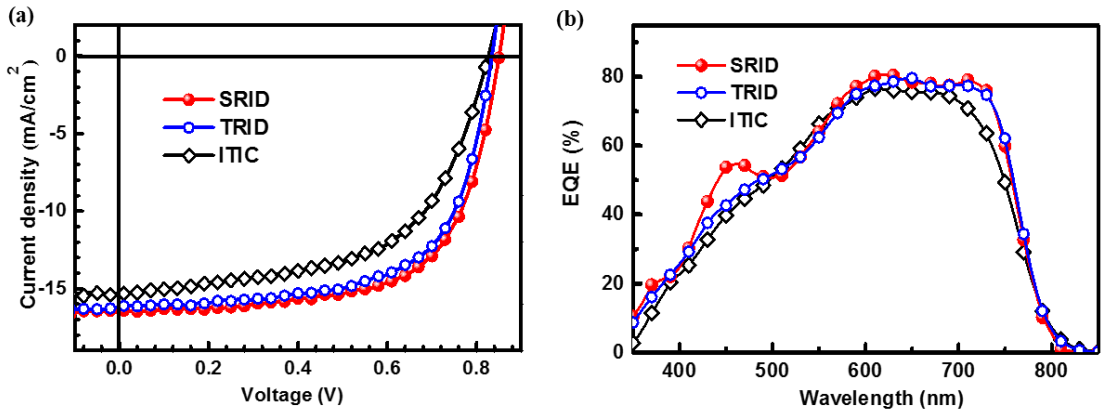

Figure 2-6. (a) *J*-*V* characteristics and (b) EQE spectra of optimized PTB7-Th:**SRID**/**TRID**/**ITIC** devices.

2.4.2 *Charge Transport Characteristics*

The electron mobility (μ_e) of **SRID**/**TRID** were probed by *n*-channel OFETs based on a device configuration of Si/SiO_2/BCB/**NFAs**/Ca/Ag. **SRID** possesses μ_e up to 0.0177 $cm^2V^{-1}S^{-1}$, which is the five times higher than that of **TRID** (μ_e = 3.35×10^{-3} $cm^2V^{-1}S^{-1}$) and close to the electron

mobility of PCBM.[22] This result indicates stronger and more regular intermolecular interactions between **SRID** molecules under solid state, which is beneficial to charge transporting. Moreover, charge transporting behaviour of blended PTB7-Th:**SRID** and PTB7-Th:**TRID** films were analyzed using space-charge-limited current (SCLC) method. The hole/electron mobilities (μ_h/μ_e) were found to be $4.3\times10^{-4}/3.8\times10^{-4}$ and $3.1\times10^{-4}/2.1\times10^{-4}$ $cm^2V^{-1}S^{-1}$ for devices based on PTB7-Th:**SRID** and PTB7-Th:**TRID**, respectively. The higher μ_h/μ_e ratio of PTB7-Th:**TRID** is an indirect evidence that the *p*-type polymer plays the major role of charge transporting in the blend. A more balanced μ_h/μ_e ratio of 1.13 in PTB7-Th:**SRID** film suggests both *n*-type and *p*-type materials contribute equally in terms of charge transporting, and the higher μ_e of PTB7-Th:**SRID** film also echoes with the higher μ_e of **SRID** measured from OFETs, indicating that **SRID** may have better interconnectivity between different domains which improves the charge transporting ability. Although Langevin recombination raised from higher mobility could be expected, significantly enhanced mobility and balanced μ_h/μ_e ratio in PTB7-Th:**SRID** film may ensure effective charge extraction thus reducing bimolecular recombination in the active layer.[23,24] The SCLC characteristics also highly correspond with the photovoltaic performance as **SRID**-based devices showed highest J_{sc} and FF, which may result from favourable interactions between NFA and polymer.

2.4.3 *GIWAXS Characteristics*

To further explore the discrepancy between the solid-state microstructure of neat and BHJ films of **SRID**/**TRID** in detail, the technique of grazing-incidence wide-angle X-ray scattering (GIWAXS) was employed. The neat **SRID** film showed high crystallinity and strong molecular orientation, in agreement with a Bragg scattering peak with very strong intensity at $q = 0.35$ Å $^{-1}$ in

the in-plane direction corresponding to a lamellar packing distance of 17.9 Å, and another at q = 1.70 $Å^{-1}$ in the out-of-plane direction corresponding to a π-π interaction distance of 3.7 Å, indicating that **SRID** is face-on oriented (Figure 2-7a). Moreover, it is of great excitement that **SRID** showed the ability to induce the formation of highly oriented PTB7-Th:**SRID** film, which was not observed in the cases of **TRID** (Figure 2-7b & 2-7d). The strong scattering peak at q = 0.52 $Å^{-1}$ in the out-of-plane direction appeared neither in neat film of **SRID** nor PTB7-Th,[25] indicative of the fact that **SRID** formed highly ordered lamellar microstructure with the polymer, while similar scattering pattern was not observed in PTB7-Th:**TRID**. Although the π-π distance of PTB7-Th:**SRID** is slightly larger than that of PTB7-Th:**TRID**, the highly regular microstructure ensures efficient charge separation and transportation in the active layer. Besides, high crystallinity of **SRID** was found not causing severe phase separation in PTB7-Th:**SRID** film, as the smooth surface topology was identified by tapping-mode atomic force microscopy measurement. This is also responsive to the argument derived from SCLC mobility characteristics that **SRID** is forming well interconnected nanocrystalline domains when blended with PTB7-Th. The GIWAXS measurements also explained why PTB7-Th:**SRID** and PTB7-Th:**TRID** responded differently to DIO additive. We anticipated that the morphology of PTB7-Th:**TRID** films could be easily affected by the addition of DIO due to low crystallinity. Contrarily, addition of DIO was more advantageous to PTB7-Th:**SRID** films upon enhancing the interconnectivity between nanocrystalline domains of **SRID** in active layer due to the highly crystalline nature of **SRID**.

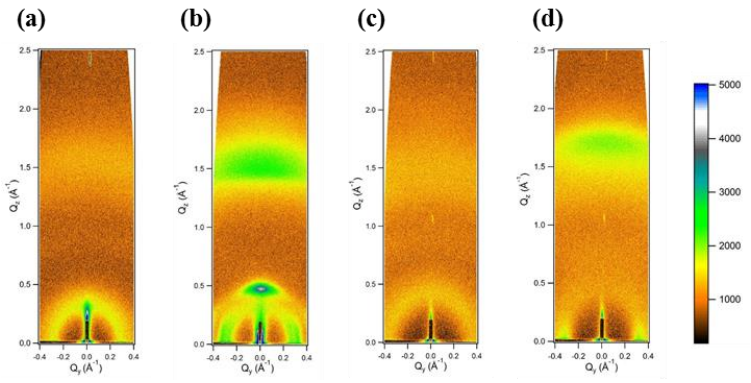

Figure 2-7. GIWAXS patterns of (a) **SRID**, (b) PTB7-Th:**SRID**, (c) **TRID** and (d) PTB7-Th:**TRID** thin films.

2.5 Device Characteristics and Morphological Study of SRID-4F/TRID-4F

2.5.1 *Photovoltaic Characteristics*

SRID-4F/**TRID-4F** were paired with PBDB-T-2F polymeric donor to investigate the effect of selenium substitution on photovoltaic performance, with a device configuration of ITO/PEDOT:PSS/PBDB-T-2F:**NFAs**/Bis-C_{60}/Ag. PBDB-T-2F possesses highly complementary optical absorption with the NFAs within visible light and near infrared range. The optimal donor/acceptor ratios were found to be 1:1 for both **SRID-4F** and **IT-4F**, and 1:1.5 on **TRID-4F**.[26] Devices based on PBDB-T-2F:**SRID-4F** delivered a V_{oc} of 0.846 V, a J_{sc} of 20.21 mA/cm^2, a fill factor of 0.752, and thus a PCE of 13.05 %, which is the highest performance among all three NFAs. The remarkably high J_{sc} can be ascribed to the red-shifted absorption of **SRID-4F**, which is supported by an EQE curve extended to 850 nm. Although devices based on PBDB-T-2F:**TRID-4F** also delivered fairly high PCE of 12.33% with a higher V_{oc} of 0.890 V and a similar fill factor of 0.750, the J_{sc} of 18.45 mA/cm^2 is somehow lower due to the optical absorption of **TRID-4F** in

the near infrared range is not as efficient as that of **SRID-4F**. Notably, compared to the **IT-4F**, it is also clearly observed that selenium substitution can effectively reduce the energy loss. The energy loss for **IT-4F**-based device was calculated as 0.650 eV, but dramatically dropped to 0.593 eV on **SRID-4F**/**TRID-4F**-based devices. The reduced energy loss can be originated from the change of CT energy due to improved interfacial morphologies at donor/acceptor interfaces, and reduced non-ideal charge recombination loss, including both radiative and non-radiative pathways. Obviously, the molecular behaviors changed by regio-specific selenium substitution indeed affect the photovoltaic performance in a positive manner.

	D:A raio	**Processing condition**	V_{oc} **(V)**	J_{sc} **(mA/cm^2)**	**FF**	**PCE (%)**
PBDB-T-2F: **SRID-4F**	2:1	CB	0.863	19.15	0.723	11.95
	1:1.5	CB	0.872	18.81	0.746	12.24
	1:1.5	CB+0.25% DIO	0.823	20.42	0.749	12.58
	1:1.5	CB+0.25% DIO Annealed at 100 ºC	0.844	20.25	0.737	12.58
	1:1	**CB+0.25% DIO Annealed at 100 ºC**	**0.846**	**20.51**	**0.752**	**13.05**
	1:1	CB+0.25% DIO Annealed at 100 ºC Thicker film ~ 150 nm	0.823	8.83	0.586	8.83
PBDB-T-2F: **TRID-4F**	2:1	CB	0.880	18.11	0.706	11.24
	1:1.5	CB	0.891	17.59	0.734	11.50
	1:1.5	CB+0.25% DIO	0.867	18.04	0.746	11.68
	1:1.5	**CB+0.25% DIO Annealed at 100 ºC**	**0.888**	**18.42**	**0.747**	**12.33**
	1:1	CB+0.25% DIO Annealed at 100 ºC	0.890	17.25	0.750	11.52
	1:1	CB+0.25% DIO Annealed at 100 ºC Thicker film ~ 150 nm	0.869	18.59	0.742	11.98
	1:1	CB+0.25% DIO Annealed at 100 ºC Thicker film ~ 200 nm	0.871	18.62	0.669	10.85
PBDB-T-2F: **IT-4F**	1:1	CB+0.25% DIO Annealed at 100 ºC	0.862	19.18	0.764	12.63

Table 2-4. Device optimization parameters for PTB7-Th:**SRID-4F**/**TRID-4F**/**IT-4F**.

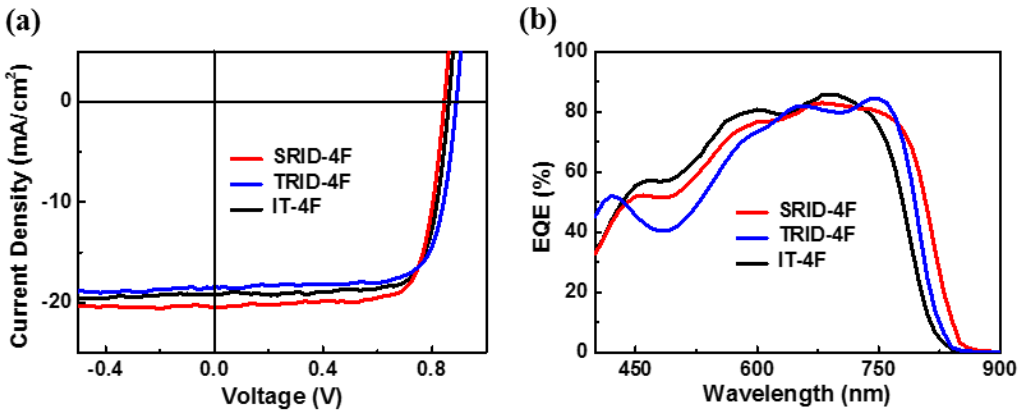

Figure 2-8. (a) *J-V* characteristics and (b) EQE spectra of optimized PBDB-T-2F:**SRID-4F**/**TRID-4F**/**IT-4F** devices.

2.5.2 *Charge Transport Characteristics*

To gain more insight into the charge transporting behavior of the materials, charge carrier mobilities in PBDB-T-2F:**NFA** blended films were analyzed using SCLC method. The electron and hole mobilities in PBDB-T-2F:**SRID-4F** and PBDB-T-2F:**TRID-4F** were generally increased compared with PBDB-T-2F:**IT-4F** due to incorporation of selenium.[12-15] The ratio of hole mobility over electron mobility (μ_h/μ_e) of PBDB-T-2F:**SRID-4F**/**TRID-4F**/**IT-4F** was calculated to be 0.92 ($2.15\times10^{-4}/1.98\times10^{-4}$ $cm^2V^{-1}S^{-1}$), 0.65 ($2.65\times10^{-4}/1.72\times10^{-4}$ $cm^2V^{-1}S^{-1}$) and 1.07 ($1.51\times10^{-4}/1.61\times10^{-4}$ $cm^2V^{-1}S^{-1}$), respectively. The dependence of V_{oc} and J_{sc} on light intensity was also measured to clarify the charge recombination mechanism in devices. The α values of devices based on PBDB-T-2F:**SRID-4F**/**TRID-4F**/**IT-4F** derived from the equation $J_{sc} \propto P^{\alpha}$ were found to be similar, indicating similar charge recombination behavior at short circuit condition for all devices (Figure 2-9a). However, the dependence of V_{oc} on light intensity of **SRID-4F**-based devices yields a much smaller slope (1.72 kT/q) than that of **TRID-4F**/**IT-4F**-based devices (1.92 and 1.98 kT/q, respectively), which is evidential that the recombination pathway is less dependent on trap-assisted

recombination in **SRID-4F**-based devices (Figure 2-9b). As a result, the higher J_{sc} in **SRID-4F**-based devices may be benefited not only from the broader optical absorption of **SRID-4F**, but also efficient charge transporting behavior in PBDB-T-2F:**SRID-4F** blended film.

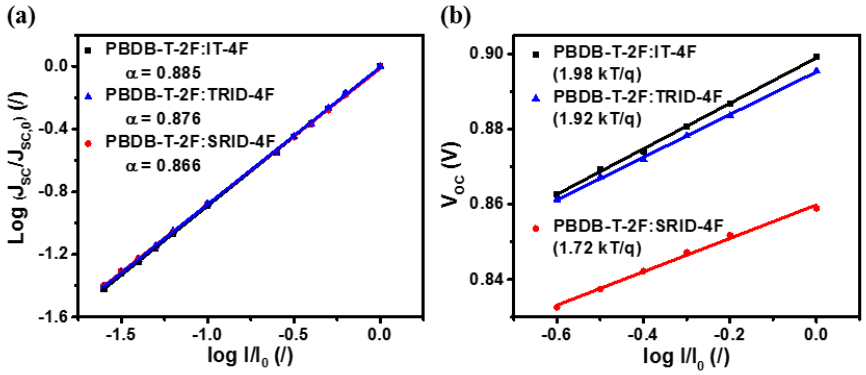

Figure 2-9. Light-intensity dependent (a) J_{sc} and (b) V_{oc} curves of devices based on PBDB-T-2F:**SRID-4F**/**TRID-4F**/**IT-4F**.

2.5.3 *GIWAXS and RSoXS Characteristics*

Grazing-incidence wide-angle X-ray scattering (GIWAXS) was used to investigate the solid-state molecular packing of neat NFA films. 2D GIWAXS profiles, together with in-plane and out-of-plane line cuts, and the corresponding parameters including the value of crystal coherence length (CCL) calculated by Scherrer equation were demonstrated (Figure 2-10 and Table 2-5).[27] All three NFAs showed a preferential face-on orientation in thin films, which is beneficial for vertical charge transport. **IT-4F** thin film displayed a broad (100) diffraction toward the in-plane direction at 0.38 $Å^{-1}$, and a sharper signal in the out-of-plane direction at 1.75 $Å^{-1}$ corresponding to π-π stacking with a *d*-spacing of 3.4 Å. A sharp peak also emerged along the in-plane direction at 0.45 $Å^{-1}$, which can be attributed to the diffraction of crystal plane along backbone direction, indicating relatively disordered packing along the in-plane direction, namely, lamellar structure disorder.[28,29]

In **SRID-4F** thin film, there existed a (100) diffraction in the in-plane direction at 0.37 $Å^{-1}$ and a (010) diffraction at 1.84 $Å^{-1}$. It can be clearly observed that **SRID-4F** favors to stack in a face-on fashion in thin film and the position of (010) diffraction shifted to 1.84 $Å^{-1}$, which correlated to a smaller (010) *d*-spacing of 3.4 Å. Obviously, the closer π-π stacking in **SRID-4F** thin-film is beneficial for more efficient charge transport, which echoes with the red-shifted optical absorption and higher charge carrier mobilities obtained from SCLC measurement.[30] Such a scattering pattern implies a simple but relatively ordered packing manner which is contributive to the high J_{sc} and relatively good FF of **SRID-4F**–based devices. **TRID-4F** presented a preferential face-on orientation as well, but the incorporation of selenium significantly changed the self-organization of molecules in thin film. The (100) peak toward in-plane direction shifted to 0.33 $Å^{-1}$, and the (010) diffraction toward out-of-plane direction moved to 1.61 $Å^{-1}$ which corresponds to the largest *d*-spacing of 3.9 Å among all three NFAs, indicating a looser stacking mode which might originate from the introduction of a larger selenium atom compared to sulfur. Moreover, the relatively loose packing manner upraises the disorder in the thin film, which was evidenced by the emergence of several new peaks with low intensity in the out-of-plane direction, indicating a more complicated and less ordered packing manner. The 2D GIWAXS profiles of **SRID-4F**, **TRID-4F** and **IT-4F** highly suggest that **SRID-4F** possesses more ordered nanostructures, due to not only the larger dipole between central electron-donating **IDTS** core and electron-withdrawing indanones, but possibly the stronger intramolecular Se-O interaction between the softer, outward-located selenium atom with the carbonyl group of the indanone. In **TRID-4F**, the inward-located selenium atom cannot interact with the indanone, thus the less strong S-O interaction dominates the interaction between **IDST** and indanones, which goes the same way in **IT-4F** as the existence of selenium is lacking.[31]

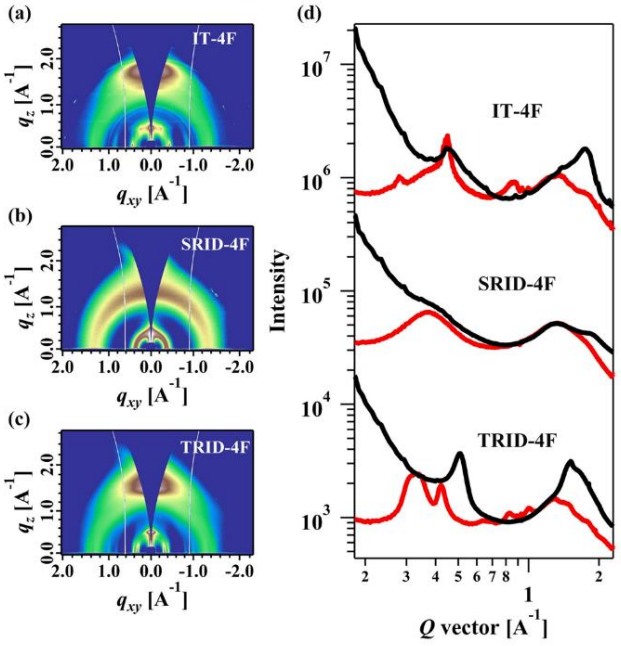

Figure 2-10. The 2D GIWAXS profiles of neat films of (a) **IT-4F**, (b) **SRID-4F**, and (c) **TRID-4F**. (d) In-plane (red line) and out-of-plane (black line) line-cut profile of GIWAXS patterns.

To understand the active layer morphology and gain more insight into the interaction between donor polymer and NFAs, PBDB-T-2F:**NFA** blended films was studied using GIWAXS and resonant soft X-ray scattering (RSoXS) (Figure 2-11). In the 2D GIWAXS profiles, it was clearly observed that the features of the blends were dominated by PBDB-T-2F donor polymer, and the characteristic diffraction peaks from NFAs were mitigated, indicating that the crystallization of NFAs were suppressed when mixed with PBDB-T-2F. However, we were able to extract some important parameters of (100) and (010) diffraction peaks through multi-peak fitting (Figure 2-11 c). It is noteworthy that smallest *d*-spacing was found in PBDB-T-2F:**SRID-4F** blend, which is indicative of a tighter packing pattern. The increased CCL and diffraction peak area also supports that the existence of **SRID-4F** significantly improved the crystallinity of **PBDB-T-2F**. The (010)

peak showed similar trend, which is consistent with the SCLC measurement that PBDB-T-2F:**SRID-4F** blend possesses the highest hole mobility.

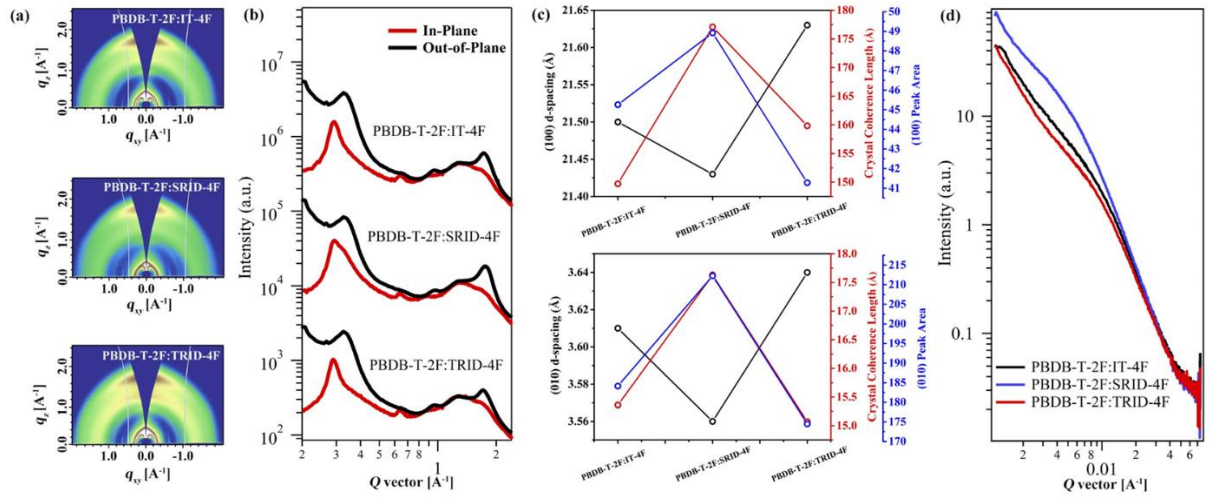

Figure 2-11. (a) The 2D GIWAXS profiles of blended PBDB-T-2F:**IT-4F**/**SRID-4F**/**TRID-4F** films. (b) In-plane (red line) and out-of-plane (black line) line-cut profiles of GIWAXS patterns. (c) *d*-Spacing, crystal coherence length and peak area of different blends. (d) RSoXS profiles of PBDB-T-2F:**IT-4F** (black line)/**SRID-4F** (blue line)/**TRID-4F** (red line) blends.

Neat Film	**Peak**	**Position (Å $^{-1}$)**	**FWHM (Å $^{-1}$)**	***d*-spacing (Å)**	**CCL (Å)**
PBDB-T-2F	100	0.29	0.079	21.66	71.58
	010	1.70	0.470	3.69	12.03
IT-4F	100	0.38	0.096	16.53	58.90
	010	1.75	0.294	3.59	19.23
SRID-4F	100	0.37	0.201	16.98	28.13
	010	1.84	0.602	3.41	9.40
TRID-4F	100	0.33	0.041	19.03	137.92
	010	1.61	0.620	3.90	9.12

Blend	**Peak**	**Position (Å $^{-1}$)**	**FWHM (Å $^{-1}$)**	**Area**	***d*-spacing (Å)**	**CCL (Å)**
PBDB-T-2F:**IT-4F**	100	0.292	0.0378	45.26	21.50	149.72
	010	3.61	0.3681	184.14	3.61	15.36
PBDB-T-2F:**SRID-4F**	100	0.293	0.0319	48.92	21.43	177.08
	010	3.56	0.3207	212.25	3.56	17.63
PBDB-T-2F:**TRID-4F**	100	0.290	0.0354	41.28	21.63	159.84
	010	3.64	0.3752	174.48	3.64	15.07

Table 2-5. Summary of GIWAXS characteristics of neat **NFAs**, PBDB-T-2F and blends.

Phase separation of the blends was further studied by RSoXS. The RSoXS scattering profiles of PBDB-T-2F:**NFA** blended films at an optimized photon energy of 284.2 eV were summarized (Figure 2-11d). In PBDB-T-2F:**IT-4F** blend, a shoulder at the position of 0.01 $Å^{-1}$ was observed, which corresponds to a center-to-center distance of 62.8 nm. The blend of PBDB-T-2F:**TRID-4F** gave a similar scattering pattern with slightly decreased intensity, indicating higher miscibility between donor/acceptor. A more distinct peak at 0.006 $Å^{-1}$, corresponding to a center-to-center distance of 105 nm, emerged in PBDB-T-2F:**SRID-4F** blend. This is likely due to the increased crystallinity of PBDB-T-2F in the blend, which echoes with the higher intensity of scattering pattern as the crystallization in the blend is stronger. The length scale of phase separation and ordered nanostructures in PBDB-T-2F:**SRID-4F** blend may lead to efficient exciton dissociation and charge transporting properties, guaranteeing better photovoltaic performance on devices based on PBDB-T-2F:**SRID-4F**.

2.6 X-RAY CRYSTALLOGRAPHY STUDY ON SINGLE CRYSTALS

To extensively study the regio-specific properties of selenium substitution correlating to intra- and intermolecular interactions under solid state, single crystals of **SRID**/**TRID** and **SRID-4F**/**TRID-4F** were analyzed using single-crystal X-ray diffraction to reveal the discrepancy between molecular geometry induced by regio-specific selenium substitution. The single crystals of **ITIC** and **IT-4F** were also grown and studied for a comprehensive comparison.

2.6.1 *Single Crystal Structure of SRID*

SRID shows only one single conformation in the single crystal, with a D-A dihedral angle of 3.60° and a Se-O distance of 2.683 Å, which is within the sum of Van der Waals radii of selenium (1.90 Å) and oxygen (1.52 Å). Adjacent **SRID** molecules communicate through the stacking of indanone end groups to form a zig-zag 1D chain (Figure 2-12c), and the interchain communications are dominated by the interaction between cyano groups and hydrogens (Figure 2-12d).

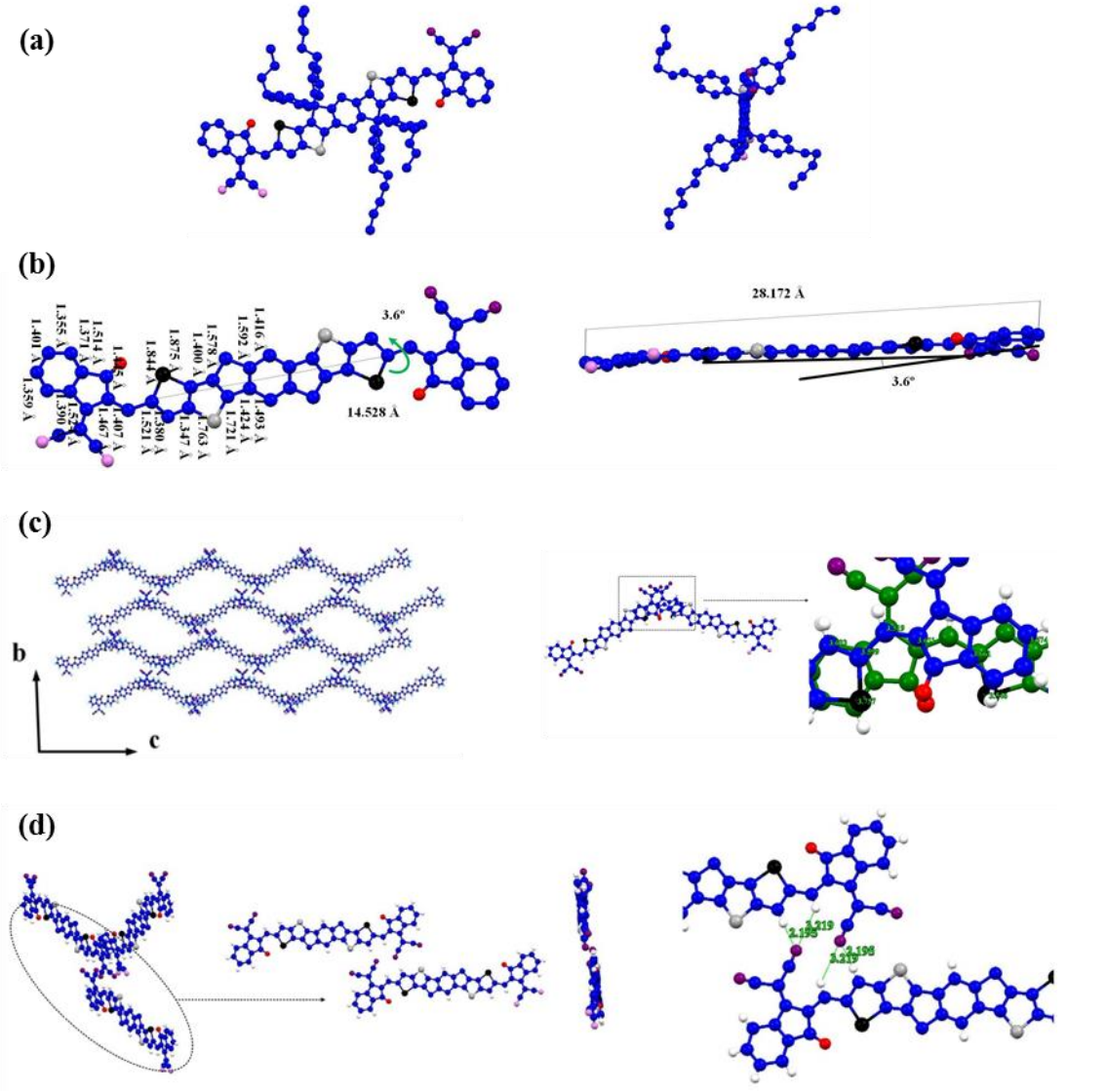

Figure 2-12. (a) Single-molecule conformation of **SRID**. (b) Zig-zag 1D chains of **SRID** viewed along *a*-axis. (c) Interaction between indanones. (d) Interchain interactions. Side chains were omitted for clearance.

2.6.2 *Single Crystal Structure of TRID*

TRID presents two different molecular conformations in the single crystal, (1) a D-A dihedral angle of 2.79^{o} and a S-O distance of 2.769 Å (labelled in blue), and (2) a D-A dihedral angle of 18.13^{o} with no S-O interaction (labelled in green) (Figure 2-13a). Formation of zig-zag 1D chains can be observed in the crystal structure, which is also induced by the interactions between indanone end groups on adjacent blue and green molecules (Figure 2-13c). Interchain communications in **TRID** single crystal are as well dominated by interaction between cyano groups and hydrogens (Figure 2-13d).

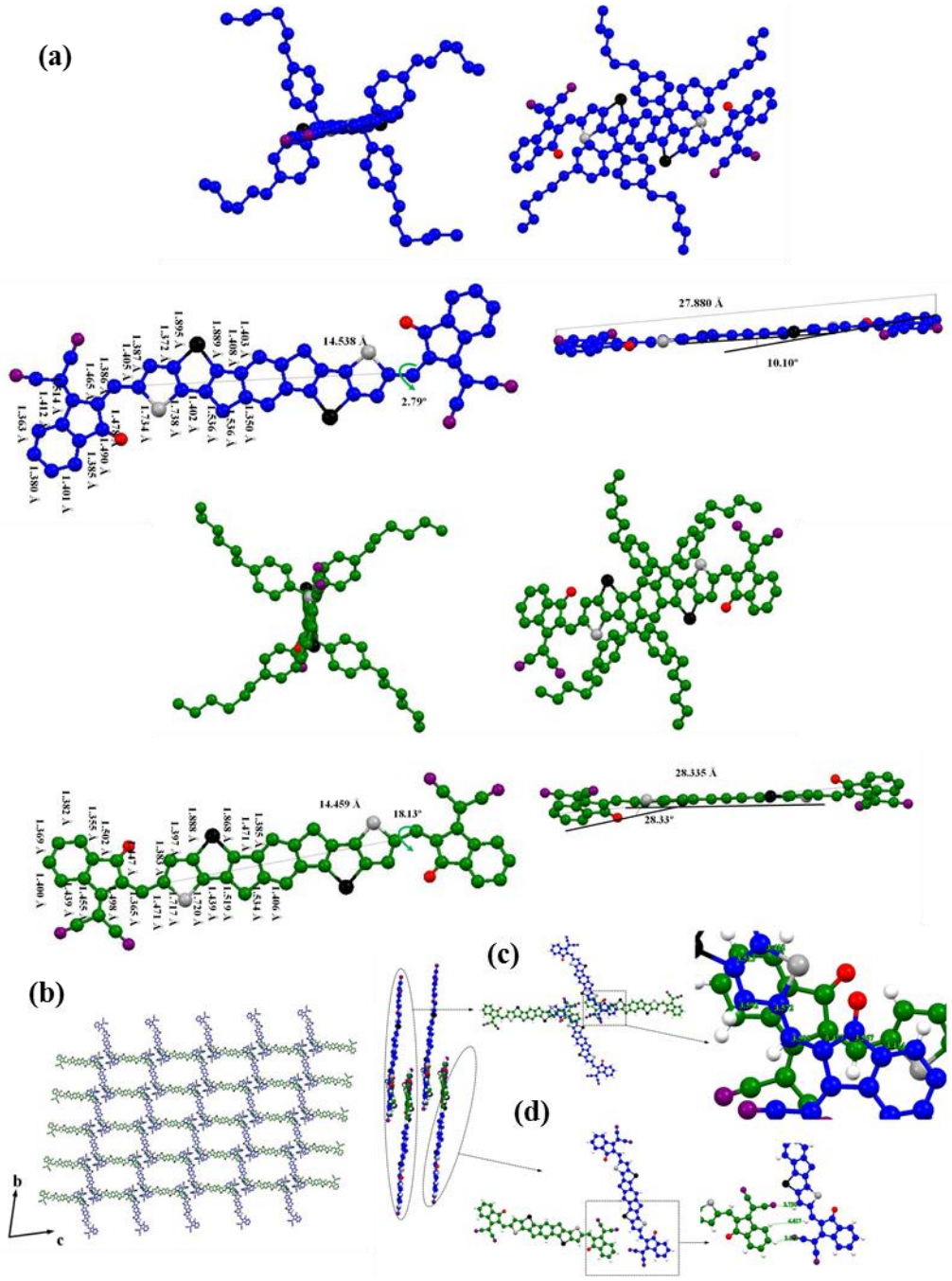

Figure 2-13. (a) Single-molecule conformation of **TRID**. (b) Zig-zag 1D chains of **TRID** viewed along *a*-axis. (c) Interaction between indanones. (d) Interchain interactions. Side chains were omitted for clearance.

The single crystal structures of **SRID**/**TRID** unambiguously illustrate the interaction between chalcogen atom in the central electron-donating core and the oxygen atom on carbonyl group of indanone is the key to "lock" the molecular geometry, giving rise to a more planar conformation without covalent confinement.[31] The stronger Se-O interaction in **SRID** leads to a higher coplanarity of the molecule, which also results in more regular and dense packing pattern. The stronger intermolecular communications in **SRID** is desirable for through-space charge hopping, which echoes with the electron mobility measured from *n*-channel OFETs.

2.6.3 *Single Crystal Structure of ITIC*

ITIC possesses only one conformation in the single crystal, with a D-A dihedral angle of 5.35º and a S-O distance of 2.659 Å, and exhibits a highly twisted S-shape geometry (Figure 2-14a). Two types of zig-zag 1D chains with same geometry but different directions (labelled in green and blue, respectively) are formed through end group interactions similar with **SRID**/**TRID** (Figure 2-14c), however these chains form interdigitating network in the crystal (Figure 2-14b), as the interchain communications are contributed by S-H interactions between the central **IDTT** cores at the intersection of two different 1D chains (Figure 2-14d).

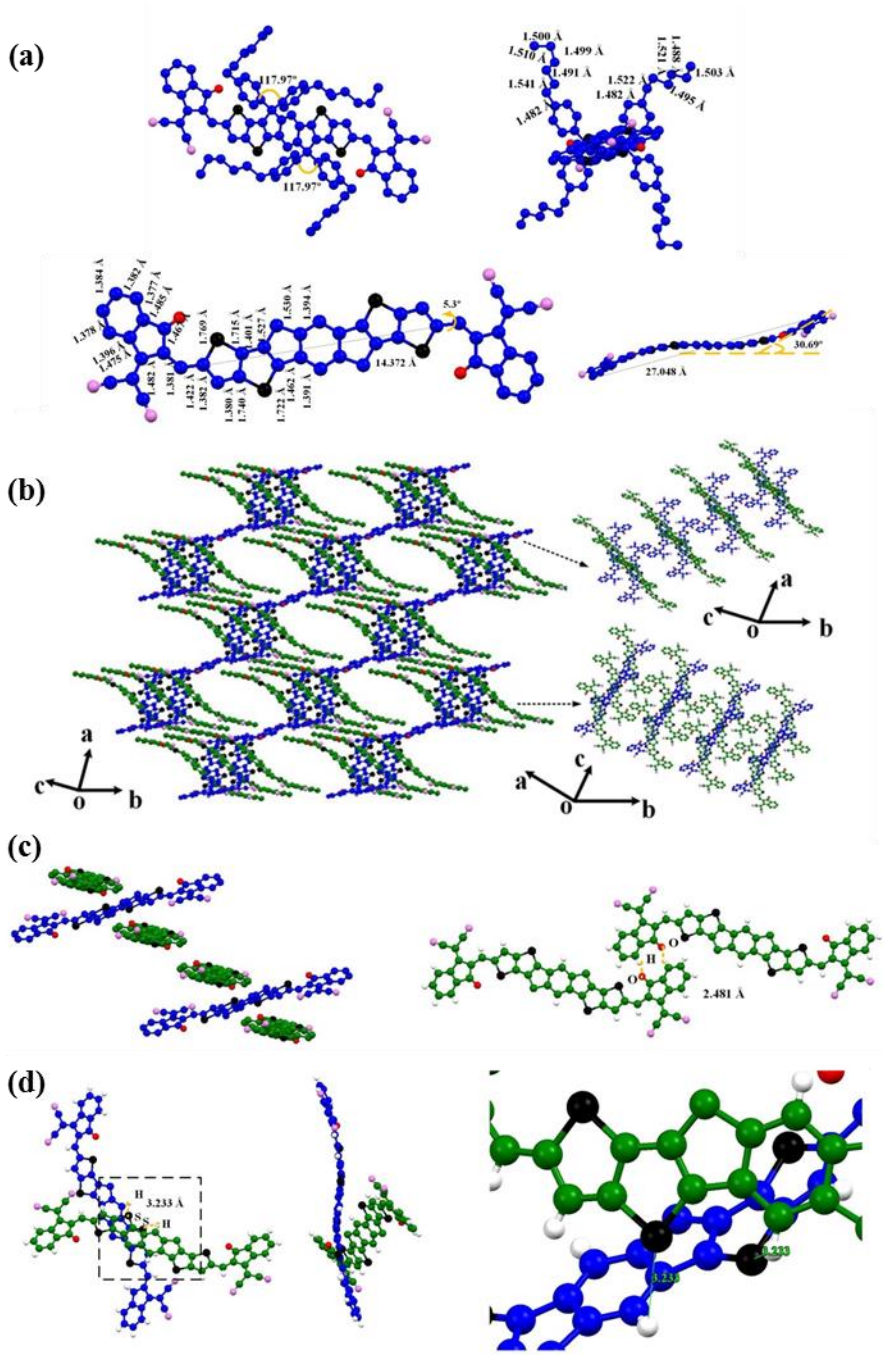

Figure 2-14. (a) Single-molecule conformation of **ITIC**. (b) Zig-zag 1D chains of **ITIC**. (c) Interaction between indanones. (d) Interchain interactions. Side chains were omitted for clearance.

2.6.4 *Single Crystal Structure of SRID-4F*

Similar to **SRID**, **SRID-4F** also gives only one conformation in the single crystal, with a small D-A dihedral angle of 2.13º and a Se-O distance of 2.674 Å (Figure 2-15a), and demonstrates a highly ordered layer-by-layer packing pattern induced by the end group interactions, however a slightly large distance of around 7 Å between the layers is observed due to the bulky side chains on **IDTS** cores (Figure 2-15c). The ordered packing pattern of **SRID-4F** echoes with the high crystallinity of **SRID-4F** films observed from GIWAXS measurements.

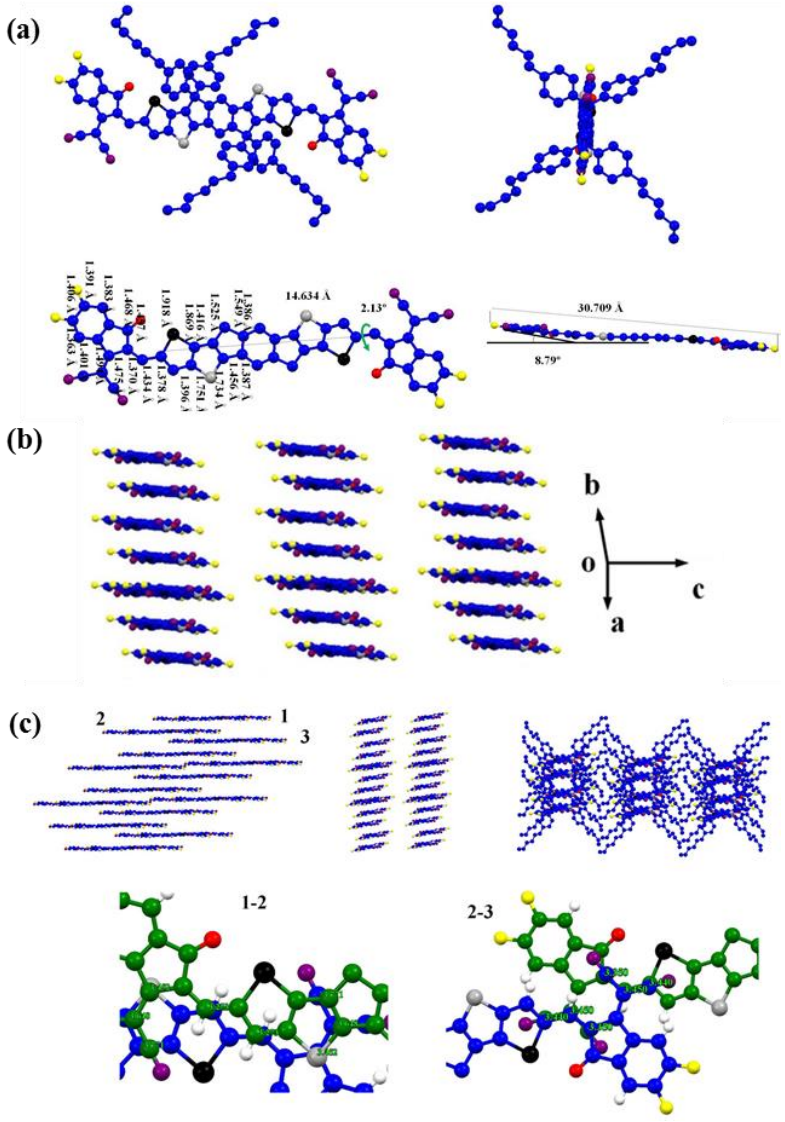

Figure 2-15. (a) Single-molecule conformation of **SRID-4F**. (b) Layer-by-layer packing of **SRID-4F**. (c) Interalayer interactions. Side chains were omitted for clearance.

2.6.5 *Single Crystal Structure of TRID-4F*

The single crystal structure of **TRID-4F** shows less ordered geometry, giving three conformations including (1) a D-A dihedral angle of 2.13° and a S-O distance of 2.583 Å (labelled in green), (2) a D-A dihedral angle of 4.90° and a S-O distance of 2.653 Å (labelled in blue), and (3) a D-A dihedral angle of 8.59° and a S-O distance of 2.733 Å (labelled in yellow) (Figure 2-16). The complexity of packing pattern in the crystal is arisen from the existence of multiple molecular conformations. A green molecule is centro-symmetrically sandwiched by a pair of blue molecules and another pair of yellow molecules to form a basic unit through π-π stacking (Figure 2-17b), which repeatedly extends through sharing the blue and yellow molecules with adjacent basic units.

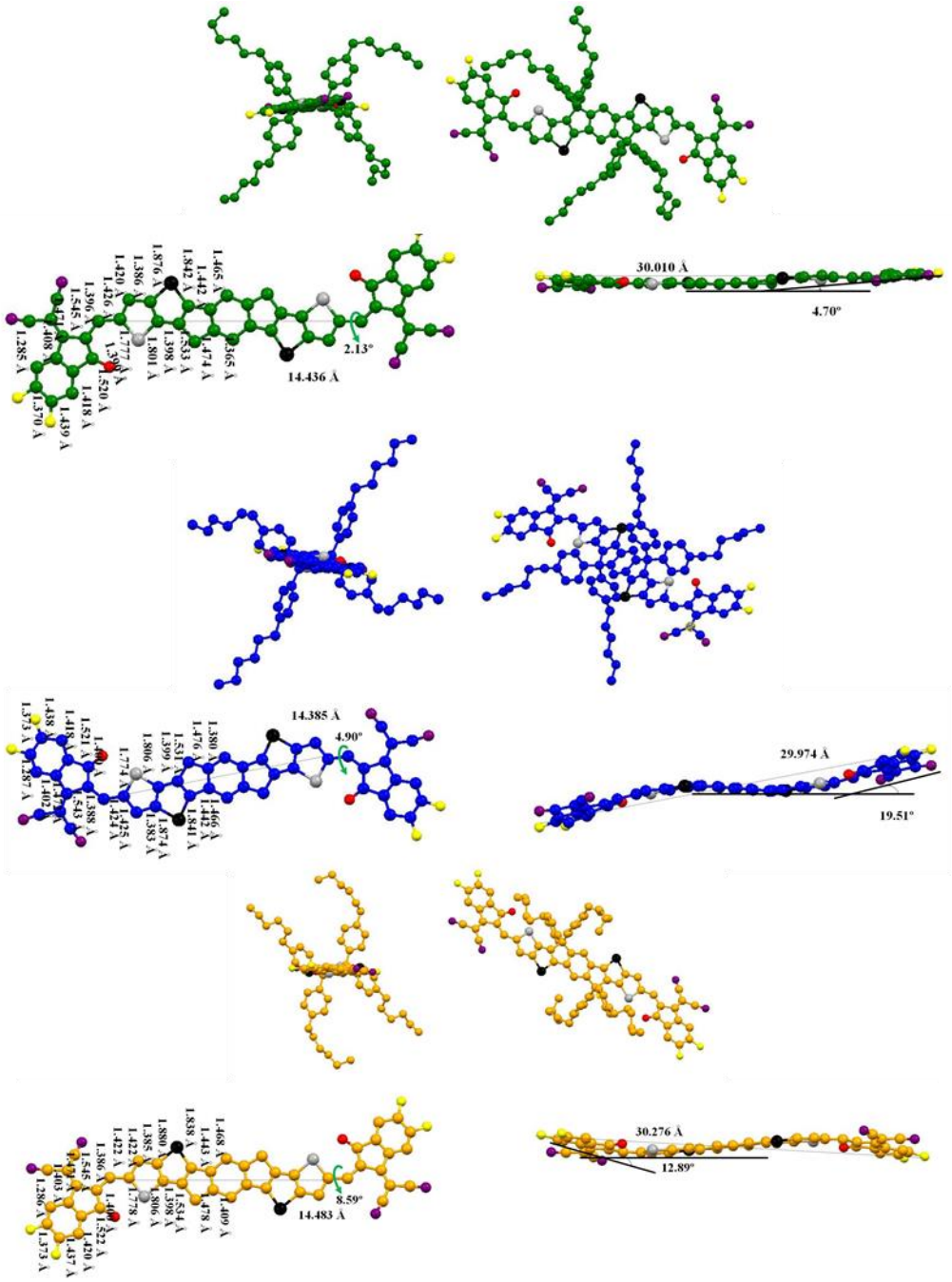

Figure 2-16. Three different conformations of **TRID-4F**.

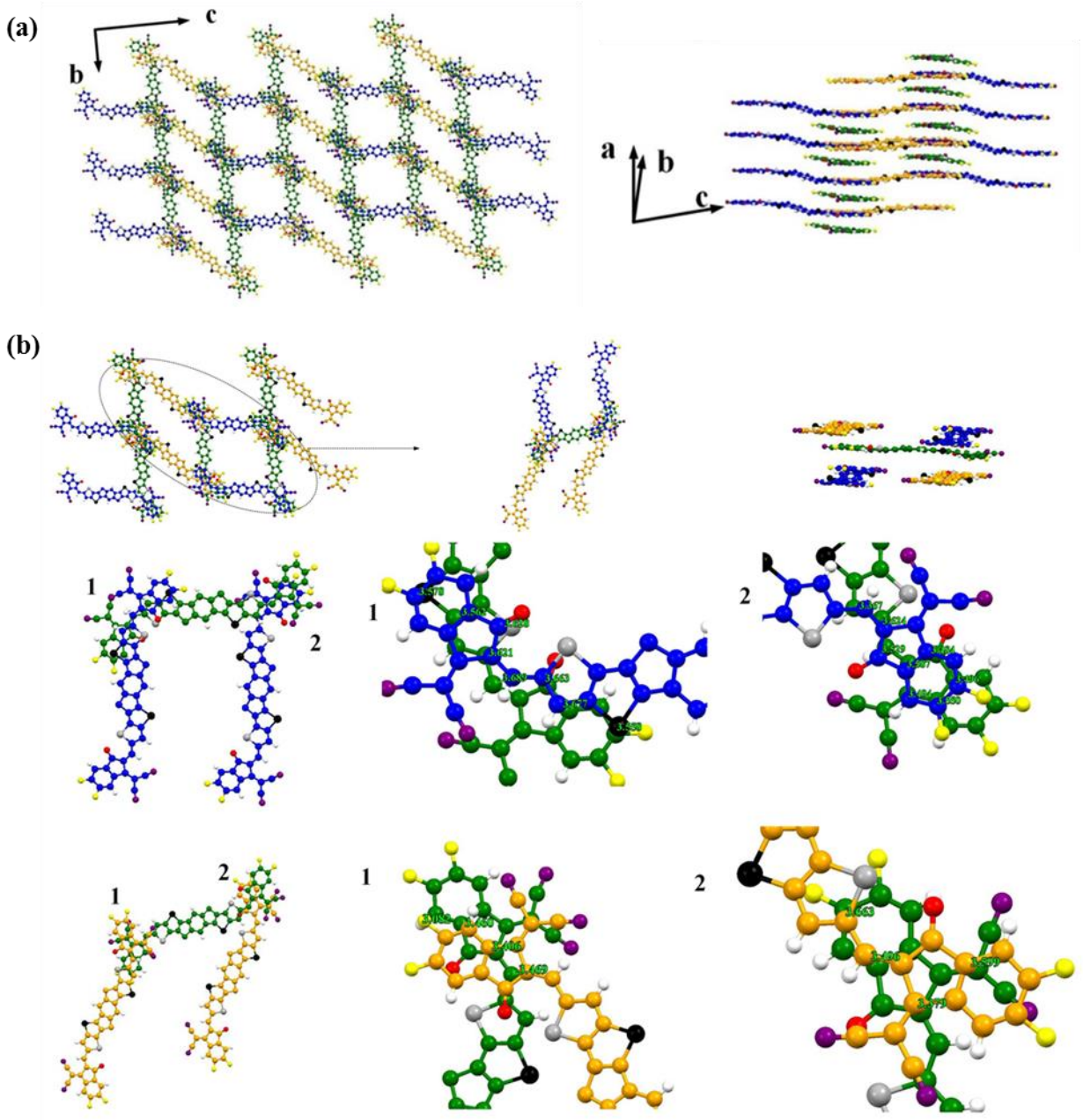

Figure 2-17. (a) Packing of **TRID-4F** viewed along *a*-axis and *b*-axis. (b) The basic unit of packing and interchain interactions. Side chains were omitted for clearance.

2.6.6 *Single Crystal Structure of IT-4F*

IT-4F possesses two conformations in the single crystal, including (1) a D-A dihedral angle of 4.16^{o} and a S-O distance of 2.686 Å (labelled in blue), and (2) a D-A dihedral angle of 11.33^{o} and

a S-O distance of 2.764 Å (labelled in green) (Figure 2-18a). One blue **IT-4F** molecule is sandwiched between two green **IT-4F** molecules to form a "brick" (Figure 2-18c). The bricks stack to form channels relying on (1) the π-π stacking between the green molecules in adjacent bricks along *b*-axis, and (2) O-H and CN-H interactions between indanone end group on adjacent blue molecules in *ac* plane (Figure 2-18b).

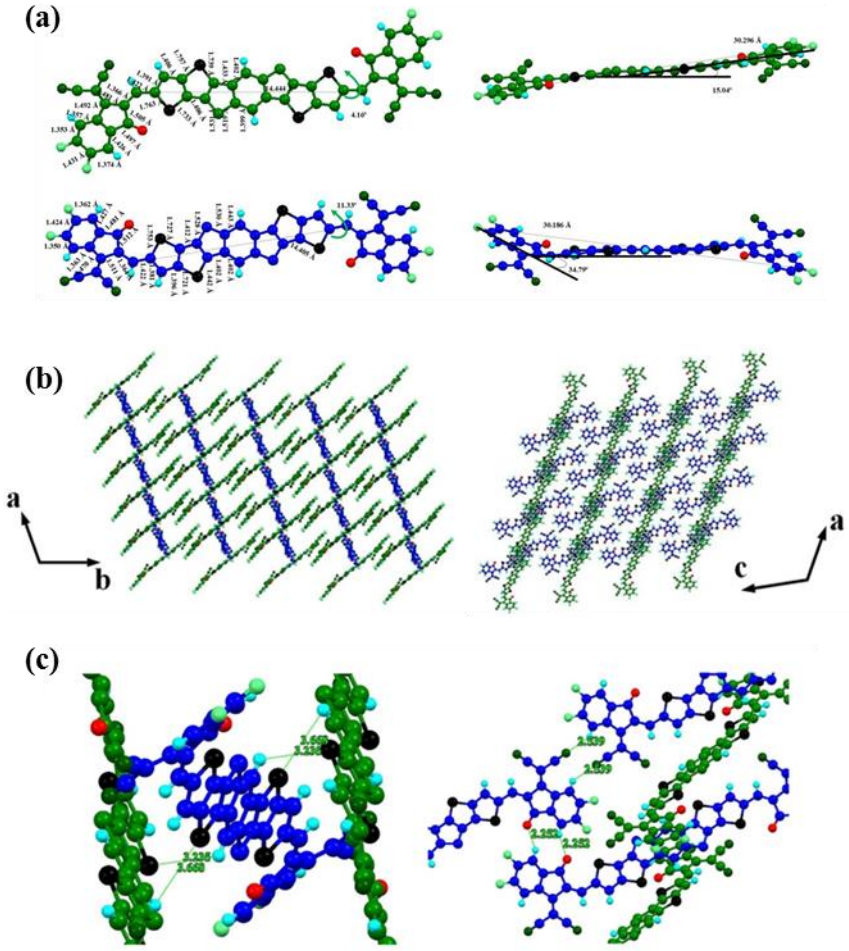

Figure 2-18. (a) Single-molecule conformations of **IT-4F**. (b) Packing of **IT-4F** viewed along *c*-axis and *b*-axis. (c) Interactions within the "brick" and interchain interactions. Side chains were omitted for clearance.

2.7 CONCLUSION

In this chapter, a pair of isomeric ladder-type cores, **IDTS** and **IDST**, as well as NFAs derived from these cores, **SRID**/**TRID** and **SRID-4F**/**TRID-4F**, were synthesized through a judiciously designed route with atomically precise selenium substitution for systematical investigation on the effect of selenium substitution in A-D-A type NFAs. Comparison between these materials reveals that the different interactions raised by selenium atom in **SRID**/**TRID** and **SRID-4F**/**TRID-4F** indeed affect the intra- and intermolecular interactions of the materials in terms of optical and electrochemical properties, as well as photovoltaic performances.

The single crystals of **SRID**/**TRID**, **SRID-4F**/**TRID-4F**, and reference materials **ITIC/IT-4F** were grown and analyzed using single-crystal X-ray diffraction. Aside from understanding the structural information of the materials, different molecular conformations and packing patterns induced by regio-specific selenium substitution can also create different charge transport channels under solid state. The single crystal study will be coupled with morphological study with extensive GIWAXS simulations and thin-film GIWAXS measurements build up correlations between single crystal structures and film morphologies, as well as computational study on charge transfer integral, for a comprehensive study on the charge transporting mechanism of these materials.

2.8 EXPERIMENTAL DETAILS

General Methods. Unless otherwise stated, all chemicals and reagents were used as received from commercial sources (Sigma-Aldrich, Matrix Scientific, Combi-Blocks) without further purification. Solvents for chemical synthesis were purified by distillation under nitrogen. All chemical reactions were carried out under protection of argon or nitrogen atmosphere. Compound

2-1 was prepared according to literature procedures.[16] PBDB-T-2F was purchased from 1-Material. The ^{1}H and ^{13}C NMR spectra were recorded on a Bruker AV500 spectrometer using $CDCl_3$, d_6-DMSO or C_6D_6 as solvents. Mass spectrometry was performed on Bruker APEX III 47e Fourier Transform mass spectrometer. The UV-Vis spectra were recorded on a Varian Cary 5000 UV-Vis-NIR Spectrophotometer. Cyclic voltammetry and differential pulse voltammetry were measured on a CH Instruments CHI660E Electrochemical Analyzer/Workstation using a conventional three-electrode cell with a glassy carbon working electrode, Pt wire counter-electrode, and Ag/AgCl reference electrode at a scan rate of 50 mV/s using 0.1 M tetrabutylammonium hexafluorophosphate ($TBAPF_6$) in CH_2Cl_2 as the electrolyte and referenced to the $FeCp_2/FeCp_2^+$ redox couple.

Preparation of 2 M solution of lithium diisopropylamide (LDA) in THF. A 3-neck round-bottom-flask was flame-dried under vacuum, cooled to room temperature, refilled with argon, and was added dry THF and diisopropylamine (1.05 eq) which was freshly distilled from KOH under dry nitrogen. The volume of THF was calculated to give a reagent concentration of ca. 2 M. The mixture was cooled to 0 ^{o}C, and n-BuLi (2.5 M in hexanes, 1.00 eq) was dropwise added to give a slightly cloudy solution was a pale color of yellow. The mixture was then stirred at 0 ^{o}C for 30 mins, then raised to room temperature and stirred for another 30 mins to give the desired LDA solution, which was immediately used after cooled to appropriate temperature.

Material Synthesis.

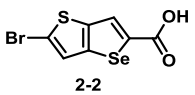

2-2

*Synthesis of 2-bromoselenopheno[3,2-b]thiophene-5-carboxylic acid (**2-2**).* To a stirring solution of selenopheno[3,2-*b*]thiophene-5-carboxylic acid (**2-1**) (21.3 g, 92.0 mmol) in DMF (200 mL) was dropwise added a solution of *N*-bromosuccinimide (16.8 g, 94.0 mmol) in DMF (80 mL) through an addition funnel under the absence of light at 0 ^{o}C. The reaction mixture was stirred overnight and slowly warmed to room temperature, and then poured into a mixture of ice and water. The precipitate was collected by filtration, and consecutively washed with water, methanol and acetone to afford **2-2** as a white solid (27.3 g, 96%). ^{1}H NMR (d_6-DMSO, 500 MHz) δ 8.27 (s, 1H), 7.70 (s, 1H); ^{13}C NMR (d_6-DMSO, 125 MHz) δ 164.37, 142.55, 140.12, 139.37, 128.19, 126.73, 116.68; GC-MS (*m/z*) Calcd for $C_7H_3{}^{79}BrO_2SSe$ 309.8, found 309.8; calcd for $C_7H_3{}^{81}BrO_2SSe$ 311.8, found 311.8.

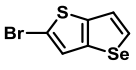

2-3

*Synthesis of 2-bromoselenopheno[3,2-b]thiophene (**2-3**).* Compound **2-2** (31.0 g, 100.0 mmol) was dissolved in DMSO (150 mL), followed by the addition of acetic acid (572 μL, 10.0 mmol) and catalytic amount of silver carbonate (1.38 g, 5.0 mmol). The mixture was the heated to 120 ^{o}C for 1 day, and then quenched with 1 N $HCl_{(aq)}$. The precipitate was removed by filtration through a celite pad and the filtrate was extracted with water and CH_2Cl_2. The combined extracts were washed with brine, dried over anhydrous $MgSO_4$, and then filtered. The solvent was removed by rotary evaporation, and the crude product was purified by column chromatography on silica gel with hexanes as eluent to afford **2-3** as an off-white solid (25.2 g, 95%). The product is unstable upon long-term storage under room temperature. ^{1}H NMR ($CDCl_3$, 500 MHz) δ 7.99 (d, J = 5.0 Hz, 1H), 7.41 (d, J = 5.0 Hz, 1H), 7.30 (s, 1H); ^{13}C NMR ($CDCl_3$, 125 MHz) δ 141.13, 137.37,

130.06, 125.10, 121.52, 113.14; GC-MS (*m/z*) Calcd for $C_6H_3{}^{79}BrSSe$ 265.8, found 265.9; calcd for $C_6H_3{}^{81}BrSSe$ 267.8, found 267.9.

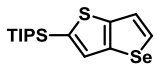

2-4

*Synthesis of 2-triisopropylsilylselenopheno[3,2-b]thiophene (**2-4**).* To a stirring solution of **2-3** (11.4 g, 43.0 mmol) in 160 mL anhydrous diethyl ether was dropwise added *n*-BuLi (2.5 M in hexanes, 17.2 mL, 43.0 mmol) at -78 ^oC under the protection of argon. The reaction mixture was stirred at -78 ^oC for 1 hour, followed by the addition of triisopropylsilyl chloride (11.2 mL, 47.3 mmol) in one portion, and then slowly warmed to room temperature, finally quenched with water and extracted with hexanes. The combined extracts were washed with brine, dried over anhydrous $MgSO_4$, and then filtered. The solvent was removed by rotary evaporation to obtain the crude product, which was then purified by column chromatography on silica gel with hexanes as eluent to afford **2-4** as a pale yellow solid (7.80 g, 53%). ^1H NMR ($CDCl_3$, 500 MHz) δ 7.96 (d, *J* = 5.0 Hz, 1H), 7.51 (d, *J* = 5.0 Hz, 1H), 7.43 (s, 1H), 1.38 (septet, *J* = 5.0 Hz, 3H), 1.15 (d, *J* = 5.0 Hz, 18H); ^{13}C NMR ($CDCl_3$, 125 MHz) δ 146.27, 140.27, 137.49, 130.88, 130.10, 121.81, 18.61, 11.86; GC-MS (*m/z*) Calcd for $C_{15}H_{24}SSeSi$ 344.1, found 344.1.

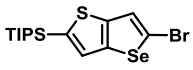

2-5

*Synthesis of 5-bromo-2-triisopropylsilylselenopheno[3,2-b]thiophene (**2-5**).* To a solution of **2-4** (8.59 g, 25.0 mmol) in THF (75 mL) was added a solution of *N*-bromosuccinimide (4.68 g, 26.3 mmol) in 25 mL DMF through an addition funnel under the absence of light at 0 ^oC. The reaction mixture was stirred overnight and slowly warmed to room temperature, poured into a mixture of

ice and water, and then extracted with CH_2Cl_2. The combined extracts were washed with brine, dried over anhydrous $MgSO_4$, and then filtered. The solvent was removed by rotary evaporation to yield afford **2-5** as a yellow solid (10.1 g, 96%). ^{1}H NMR ($CDCl_3$, 500 MHz) δ 7.50 (s, 1H), 7.32 (s, 1H), 1.36 (septet, *J* = 5.0 Hz, 3H), 1.13 (d, *J* = 5.0 Hz, 18H); ^{13}C NMR ($CDCl_3$, 125 MHz) δ 143.96, 140.57, 136.43, 129.47, 124.83, 115.19, 18.58, 11.84; GC-MS (*m/z*) Calcd for $C_{15}H_{23}{}^{79}BrSSeSi$ 422.0, found 422.0; calcd for $C_{15}H_{23}{}^{81}BrSSeSi$ 424.0, found 424.0.

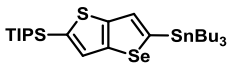

2-6

*Synthesis of 5-tributylstannyl-2-triisopropylsilylselenopheno[3,2-b]thiophene (**2-6**).* To a stirring solution of **2-5** (10.6 g, 25.0 mmol) in 125 mL anhydrous diethyl ether was dropwise added *n*-BuLi (2.5 M in hexanes, 10.0 mL, 25.0 mmol) at -78 ^{o}C under the protection of argon. The reaction mixture was stirred at -78 ^{o}C for 1 hour, followed by the addition of tributyltin chloride (7.46 mL, 27.5 mmol) in one portion, and then slowly warmed to room temperature, finally quenched with water and extracted with hexanes. The combined extracts were washed with brine, dried over anhydrous $MgSO_4$, and then filtered. The solvent was removed by rotary evaporation to obtain **2-6** as a yellow oil. The stannylated compound was used without further purification.

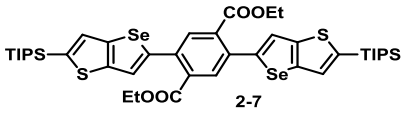

2-7

*Synthesis of 2,5-di(2-triisopropylsilylselenopheno[3,2-b]thiophen-5-yl)terephthalic acid diethyl ester (**2-7**).* To a two-neck flask was added **2-6** (15.8 g, 25.0 mmol), 2,5-dibromo-terephthalic acid diethyl ester (4.56 g, 12.0 mmol), $PdCl_2(PPh_3)_2$ (505 mg, 6 mol%) and anhydrous toluene (50 mL)

under an argon atmosphere. The reaction mixture was then heated at 110 ^{o}C for 1 day. The solvent was removed by rotary evaporation, and the crude product was purified by column chromatography on silica gel with hexanes/CH_2Cl_2 (v/v = 1:2) as eluent to afford **2-7** as a pale yellow solid (6.70 g, 62%). ^{1}H NMR ($CDCl_3$, 500 MHz) δ 7.86 (s, 1H), 7.44 (s, 1H), 7.43 (s, 1H), 4.27 (quartet, *J* = 5.0 Hz, 4H), 1.39 (septet, *J* = 5.0 Hz, 3H), 1.16 (t, *J* = 5.0 Hz, 6H), 1.15 (d, *J* = 5.0 Hz, 18H); ^{13}C NMR ($CDCl_3$, 125 MHz) δ 167.39, 146.14, 145.82, 141.15, 137.62, 135.76, 133.66, 131.98, 130.09, 121.50, 61.76, 18.60, 13.79, 11.88; MS (*m/z*, MALDI) Calcd for $C_{42}H_{58}O_4S_2Se_2Si_2$ 906.16, found 906.12.

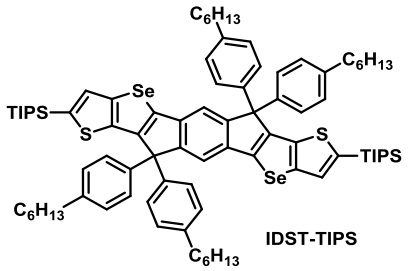

IDST-TIPS

*Synthesis of 3,9-bis(triisopropylsilyl)-5,5,11,11-tetrakis(4-hexylphenyl)-dithieno[2,3-d:2',3'-d']-s-indaceno[1,2-b:5,6-b']diselenophene (**IDST-TIPS**).* To a solution of 4-hexyl-1-bromobenzene (3.57 g, 14.8 mmol) in anhydrous THF (60 mL) was added *n*-BuLi (2.5 M in hexanes, 5.92 mL, 14.8 mmol) at -78 ^{o}C under the protection of argon. After being kept at -78 ^{o}C for 1 hour, a solution of **2-7** (3.08 g, 3.40 mmol) in anhydrous THF (35 mL) was added dropwise. The reaction mixture was then stirred at -78 ^{o}C for 3 hours, warmed to room temperature, poured into water and extracted with CH_2Cl_2. The combined extracts were washed with brine, dried over anhydrous $MgSO_4$, and then filtered. The solvent was removed by rotary evaporation to yield a dark oil, which was mixed with acetic acid (80 mL) and 3 drops of $H_2SO_{4(conc.)}$ and heated at 80 ^{o}C for 1 hour. The reaction mixture was then added water and again extracted with CH_2Cl_2. The combined extracts

were washed with brine, dried over anhydrous $MgSO_4$, and then filtered. After removing the volatile species by rotary evaporation, the crude product was obtained as a dark oil and further purified by column chromatography on silica gel with hexanes/CH_2Cl_2 (v/v = 19:1) as eluent to afford **IDST-TIPS** as a light yellow solid (2.85 g, 59%). ^{1}H NMR (C_6D_6, 500 MHz) δ 7.97 (s, 2H), 7.54 (d, *J* = 10.0 Hz, 8H), 7.12 (s, 2H), 6.93 (d, *J* = 10.0 Hz, 8H), 2.36 (t, *J* = 5.0 Hz, 8H), 1.39 (quintet, *J* = 5.0 Hz, 8H), 1.21-1.13 (m, 32H), 1.02 (d, *J* = 5.0 Hz, 36H), 0.85 (t, *J* = 5.0 Hz, 12H); ^{13}C NMR (C_6D_6, 125 MHz) δ 154.64, 148.83, 145.61, 142.74, 141.94, 140.76, 140.72, 139.50, 136.68, 131.21, 128.99, 128.94, 117.48, 65.26, 35.88, 32.03, 31.52, 29.39, 22.92, 18.78, 14.28, 12.11; MS (*m/z*, MALDI) Calcd for $C_{86}H_{114}S_2Se_2Si_2$ 1462.62, found 1462.71.

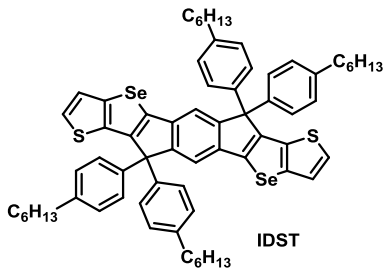

IDST

*Synthesis of 5,5,11,11-tetrakis(4-hexylphenyl)-dithieno[2,3-d:2',3'-d']-s-indaceno[1,2-b:5,6-b']diselenophene (**IDST**).* To a solution of **IDST-TIPS** (2.85 g, 2.00 mmol) in anhydrous THF was dropwise added TBAF (1 M in THF, 6.00 mL, 6.00 mmol) under the absence of light at 0 °C. The reaction mixture was kept at 0 °C for 30 minutes, and was then added ethanol. The precipitate was collected by filtration to afford **IDST** as a light yellow solid (2.18 g, 98%). ^{1}H NMR (C_6D_6, 500 MHz) δ 7.92 (s, 2H), 7.48 (d, *J* = 10.0 Hz, 8H), 6.93 (d, *J* = 10.0 Hz, 8H), 6.76 (d, *J* = 5.0 Hz, 2H), 6.66 (d, *J* = 5.0 Hz, 2H), 2.39 (t, *J* = 5.0 Hz, 8H), 1.41 (quintet, *J* = 5.0 Hz, 8H), 1.21-1.13 (m, 24H), 0.84 (t, *J* = 5.0 Hz, 12H); ^{13}C NMR (C_6D_6, 125 MHz) δ 154.60, 149.09, 144.85, 141.97,

140.91, 140.62, 139.30, 135.42, 129.03, 128.88, 126.43, 123.25, 117.35, 65.14, 35.92, 32.03, 31.55, 29.42, 22.91, 14.27; MS (*m/z*, MALDI) Calcd for $C_{68}H_{74}S_2Se_2$ 1114.36, found 1114.42.

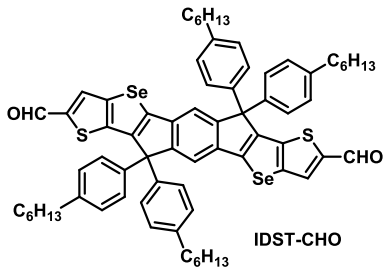

*Synthesis of 5,5,11,11-tetrakis(4-hexylphenyl)-dithieno[2,3-d:2',3'-d']-s-indaceno[1,2-b:5,6-b']diselenophene-3,9-dicarbaldehyde (**IDST-CHO**).* To a solution of **IDST** (1.11 g, 1.00 mmol) in anhydrous 1,2-dichloroethane (40 mL) was added anhydrous DMF (4.65 mL, 60.0 mmol) under the protection of argon. The reaction mixture was then cooled with an ice bath, followed by slow addition of $POCl_3$ (0.56 mL, 6.00 mmol). After being kept at 0 ^oC for 10 minutes, the reaction mixture was heated to reflux for one day, cooled to room temperature, poured into water and extracted with CH_2Cl_2. The combined extracts were washed with brine, dried over anhydrous $MgSO_4$, and then filtered. The solvent was removed by rotary evaporation to yield the crude product, which was then purified by column chromatography on silica gel with hexanes/CH_2Cl_2 (v/v = 1:2) as eluent to afford **IDST-CHO** as a dark yellow solid (1.08 g, 92%). ^1H NMR ($CDCl_3$, 500 MHz) δ 9.88 (s, 2H), 7.95 (s, 2H), 7.56 (s, 2H), 7.16 (d, *J* = 10.0 Hz, 8H), 7.11 (d, *J* = 10.0 Hz, 8H), 2.57 (t, *J* = 5.0 Hz, 8H), 1.59 (quintet, *J* = 5.0 Hz, 8H), 1.35-1.27 (m, 24H), 0.87 (t, *J* = 5.0 Hz, 12H); ^{13}C NMR ($CDCl_3$, 125 MHz) δ 182.54, 154.57, 151.19, 148.51, 143.93, 142.30, 141.92, 140.28, 138.84, 138.82, 132.24, 128.74, 128.67, 128.06, 127.85, 117.99, 64.33, 43.40, 35.56, 31.67, 31.17, 29.11, 22.54, 14.02; MS (*m/z*, MALDI) Calcd for $C_{70}H_{74}O_2S_2Se_2$ 1170.35, found 1170.42.

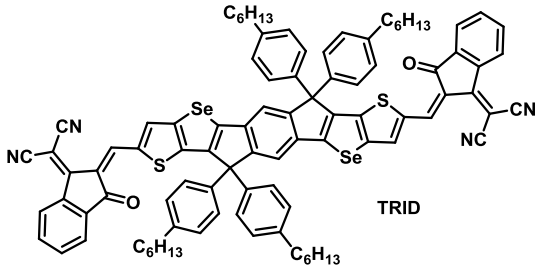

TRID

*Synthesis of 3,9-bis(2-methylene-(3-(1,1-dicyanomethylene)-indanone))- 5,5,11,11-tetrakis(4-hexylphenyl)-dithieno[2,3-d:2',3'-d']-s-indaceno[1,2-b:5,6-b']diselenophene (**TRID**).* To a solution of **IDST-CHO** (292 mg, 0.25 mmol) and 3-(1,1-dicyanomethylene)-indanone (194 mg, 1.00 mmol) in 1,2-dichloroethane (15 mL) and isopropanol (10 mL) was added a few clusters of β-alanine. The reaction mixture was then heated overnight at 80 ^{o}C. After cooling to room temperature, the volatile species were removed by rotary evaporation. The crude product was then purified by column chromatography on silica gel with hexanes/CH_2Cl_2 (v/v = 1:3) as eluent to afford **TRID** as a dark solid (365 mg, 96%). ^{1}H NMR ($CDCl_3$, 500 MHz) δ 8.83 (s, 2H), 8.66 (d, *J* = 10.0 Hz, 2H), 8.25 (s, 2H), 7.90 (d, *J* = 10.0 Hz, 2H), 7.72 (m, 4H), 7.59 (s, 2H), 7.24 (d, *J* = 10.0 Hz, 8H), 7.15 (d, *J* = 10.0 Hz, 8H), 2.57 (t, *d* = 5.0 Hz, 8H), 1.60 (quintet, *d* = 5.0 Hz, 8H), 1.36-1.26 (m, 24H), 0.86 (t, *J* = 5.0 Hz, 12H); ^{13}C NMR ($CDCl_3$, 125 MHz) δ 187.94, 160.41, 155.52, 154.67, 149.60, 148.93, 142.49, 142.20, 140.01, 139.36, 139.25, 138.62, 137.80, 136.91, 135.05, 134.35, 128.82, 128.08, 125.25, 123.71, 122.86, 118.52, 114.63, 114.56, 69.30, 64.45, 35.59, 31.67, 31.16, 29.16, 22.55, 14.02; MS (*m/z*, MALDI) Calcd for $C_{94}H_{82}N_4O_2S_2Se_2$ 1522.42, found 1522.38.

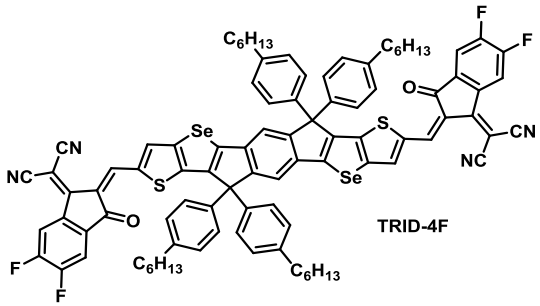

TRID-4F

*Synthesis of 3,9-bis(2-methylene-(3-(1,1-dicyanomethylene)-5,6-difluoroindanone))- 5,5,11,11-tetrakis(4-hexylphenyl)-dithieno[2,3-d:2',3'-d']-s-indaceno[1,2-b:5,6-b']diselenophene (**TRID-4F**).* To a solution of **IDST-CHO** (117 mg, 0.10 mmol) and 2-(5,6-difluoro-3-oxo-2,3-dihydro-1H-inden-1-ylidene)malononitrile (69 mg, 0.30 mmol) in 1,2-dichloroethane (10 mL) and isopropanol (5 mL) was added a grain of β-alanine. The reaction mixture was then heated overnight at 80 °C. After cooling to room temperature, the volatile species were removed by rotary evaporation. The crude product was then purified by column chromatography on silica gel with hexanes/CH_2Cl_2 (v/v = 1:3) as eluent to afford **TRID-4F** as a dark solid (117 mg, 73%). ^{1}H NMR ($CDCl_3$, 500 MHz) δ 8.82 (s, 2H), 8.53 (quartet, *J* = 5.0 Hz, 2H), 8.28 (s, 2H), 7.68 (t, *J* = 5.0 Hz, 2H), 7.59 (s, 2H), 7.21 (d, *J* = 10.0 Hz, 8H), 7.14 (d, *J* = 10.0 Hz, 8H), 2.57 (t, *J* = 5.0 Hz, 8H), 1.57 (quintet, *J* = 5.0 Hz, 8H), 1.36-1.28 (m, 24H), 0.86 (t, *J* = 5.0 Hz, 12H); ^{13}C NMR ($CDCl_3$, 125 MHz) δ 185.63, 158.32, 155.67, 155.51, 149.65, 149.58, 142.59, 138.46, 138.04, 128.90, 128.85, 128.03, 121.85, 118.67, 115.03, 114.85, 114.24, 114.13, 112.72, 112.57, 69.76, 64.41, 35.59, 31.68, 31.19, 29.15, 22.56, 14.04; MS (*m/z*, MALDI) Calcd for $C_{94}H_{78}F_4N_4O_2S_2Se_2$ 1594.38, found 1594.34.

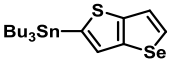

2-8

*Synthesis of 2-tributylstannylselenopheno[3,2-b]thiophene (**2-8**).* To a stirring solution of **2-3** (3.19 g, 12.0 mmol) in 60 mL anhydrous THF was dropwise added *n*-BuLi (2.5 M in hexanes, 4.80 mL, 12.0 mmol) at -95 ^{o}C in a hexanes/liquid nitrogen bath under the protection of argon. The reaction mixture was stirred at -78 ^{o}C for 1 hour, followed by the addition of tributyltin chloride (3.58 mL, 13.2 mmol) in one portion, and then slowly warmed to room temperature, finally quenched with water and extracted with hexanes. The combined extracts were washed with brine, dried over anhydrous $MgSO_4$, and then filtered. The solvent was removed by rotary evaporation to obtain **2-8** as a yellow oil. The stannylated compound was used without further purification.

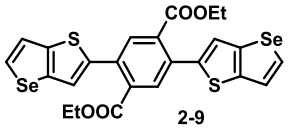

2-9

*Synthesis of 2,5-di(selenopheno[3,2-b]thiophen-2-yl)terephthalic acid diethyl ester (**2-9**).* To a two-neck flask was added **2-8** (5.71 g, 12 mmol), 2,5-dibromo-terephthalic acid diethyl ester (2.07 g, 5.45 mmol), $PdCl_2(PPh_3)_2$ (230 mg, 6 mol%) and anhydrous toluene (25 mL) under an argon atmosphere. The reaction mixture was then heated at 110 ^{o}C for 1 day. The solvent was removed by rotary evaporation, and the crude product was purified by column chromatography on silica gel with hexanes/CH_2Cl_2 (v/v = 1:1) as eluent to afford **2-9** as a yellow solid (2.30 g, 71%). ^{1}H NMR ($CDCl_3$, 500 MHz) δ 7.99 (d, *J* = 5.0 Hz, 2H), 7.89 (s, 2H), 7.51 (d, *J* = 5.0 Hz, 2H), 7.34 (s, 2H), 4.25 (quartet, *J* = 5.0 Hz, 4H), 1.14 (t, *J* = 5.0 Hz, 6H); ^{13}C NMR ($CDCl_3$, 125 MHz) δ 167.43, 141.70, 141.58, 138.72, 134.06, 133.58, 131.99, 130.76, 122.44, 122.02, 61.75, 13.81; MS (*m/z*, MALDI) Calcd for $C_{24}H_8O_4S_2Se_2$ 593.89, found 593.87.

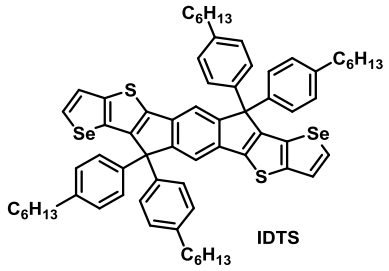

IDTS

*Synthesis of 5,5,11,11-tetrakis(4-hexylphenyl)-diselenopheno[2,3-d:2',3'-d']-s-indaceno[1,2-b:5,6-b']dithiophene (**IDTS**).* To a solution of 4-hexyl-1-bromobenzene (4.05 g, 16.8 mmol) in anhydrous THF (70 mL) was added *n*-BuLi (2.5 M in hexanes, 6.72 mL, 16.8 mmol) at -78 ^{o}C under the protection of argon. After being kept at -78 ^{o}C for 1 hour, a solution of **2-9** (2.07 g, 3.50 mmol) in anhydrous THF (35 mL) was added dropwise. The reaction mixture was then stirred at -78 ^{o}C for 3 hours, warmed to room temperature, poured into water and extracted with CH_2Cl_2. The combined extracts were washed with brine, dried over anhydrous $MgSO_4$, and then filtered. The solvent was removed by rotary evaporation to yield a dark yellow solid, which was mixed with acetic acid (80 mL) and 3 drops of $H_2SO_{4(conc.)}$ and heated at 80 ^{o}C for 1 hour. Water was then added to the reaction mixture and the solid was collected by filtration. The crude product was then purified by column chromatography on silica gel with hexanes/CH_2Cl_2 (v/v = 1:3) as eluent to afford **IDTS** as a light yellow solid (2.67 g, 69%). ^{1}H NMR (C_6D_6, 500 MHz) δ 7.99 (s, 2H), 7.43 (d, *J* = 10.0 Hz, 8H), 7.21 (d, *J* = 5.0 Hz, 2H), 7.00 (d, *J* = 5.0 Hz, 2H), 6.94 (d, *J* = 10.0 Hz, 8H), 2.39 (t, *J* = 5.0 Hz, 8H), 1.43 (quintet, *J* = 5.0 Hz, 8H), 1.21-1.13 (m, 24H), 0.84 (t, *J* = 5.0 Hz, 12H); ^{13}C NMR (C_6D_6, 125 MHz) δ 154.95, 150.41, 143.44, 143.12, 141.96, 140.95, 136.96, 134.25, 130.35, 129.08, 128.68, 122.94, 117.41, 63.94, 35.91, 32.03, 31.56, 29.41, 22.92, 14.27; MS (*m/z*, MALDI) Calcd for $C_{68}H_{74}S_2Se_2$ 1114.36, found 1114.41.

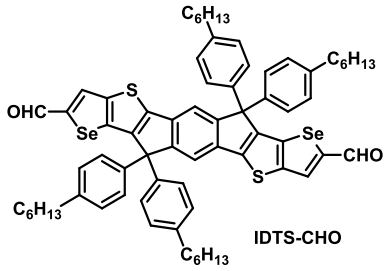

*Synthesis of 5,5,11,11-tetrakis(4-hexylphenyl)-diselenopheno[2,3-d:2',3'-d']-s-indaceno[1,2-b:5,6-b']dithiophene-3,9-dicarbaldehyde (**IDTS-CHO**).* To a solution of **IDTS** (1.11 g, 1.00 mmol) in anhydrous 1,2-dichloroethane (40 mL) was added anhydrous DMF (4.65 mL, 60.0 mmol) under the protection of argon. The reaction mixture was then cooled with an ice bath, followed by slow addition of $POCl_3$ (0.56 mL, 6.00 mmol). After being kept at 0 ^oC for 10 minutes, the reaction mixture was heated to reflux for one day, cooled to room temperature, poured into water and extracted with CH_2Cl_2. The combined extracts were washed with brine, dried over anhydrous $MgSO_4$, and then filtered. The solvent was removed by rotary evaporation to yield the crude product, which was then purified by column chromatography on silica gel with hexanes/CH_2Cl_2 (v/v = 1:2) as eluent to afford **IDTS-CHO** as a dark yellow solid (1.09 g, 93%). ^1H NMR ($CDCl_3$, 500 MHz) δ 9.78 (s, 2H), 8.17 (s, 2H), 7.64 (s, 2H), 7.15 (d, *J* = 10.0 Hz, 8H), 7.11 (d, *J* = 10.0 Hz, 8H), 2.56 (t, *J* = 5.0 Hz, 8H), 1.58 (quintet, *J* = 5.0 Hz, 8H), 1.36-1.27 (m, 24H), 0.87 (t, *J* = 5.0 Hz, 12H); ^{13}C NMR ($CDCl_3$, 125 MHz) δ 183.70, 154.98, 150.22, 148.83, 148.72, 142.61, 142.35, 140.16, 139.24, 136.44, 132.57, 128.75, 127.86, 118.04, 63.18, 35.56, 31.67, 31.18, 29.10, 22.55, 14.02; MS (*m/z*, MALDI) Calcd for $C_{70}H_{74}O_2S_2Se_2$ 1170.35, found 1170.41.

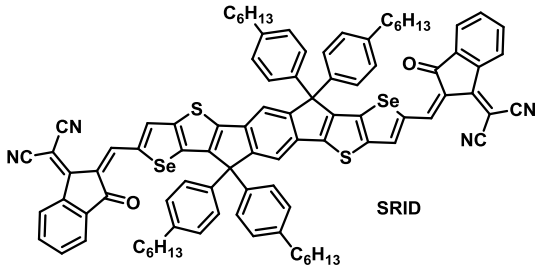

*Synthesis of 3,9-bis(2-methylene-(3-(1,1-dicyanomethylene)-indanone))-5,5,11,11-tetrakis(4-hexylphenyl)-diselenopheno[2,3-d:2',3'-d']-s-indaceno[1,2-b:5,6-b']dithiophene (**SRID**).* To a solution of **IDTS-CHO** (292 mg, 0.25 mmol) and 3-(1,1-dicyanomethylene)-indanone (194 mg, 1.00 mmol) in 1,2-dichloroethane (15 mL) and isopropanol (10 mL) was added a few clusters of β-alanine. The reaction mixture was then heated overnight at 80 ^{o}C. After cooling to room temperature, the volatile species were removed by rotary evaporation. The crude product was then purified by column chromatography on silica gel with hexanes/CH_2Cl_2 (v/v = 1:3) as eluent to afford **SRID** as a dark solid (350 mg, 92%). ^{1}H NMR ($CDCl_3$, 500 MHz) δ 9.02 (s, 2H), 8.67 (d, *J* = 5.0 Hz, 2H), 8.24 (s, 2H), 7.88 (d, *J* = 5.0 Hz, 2H), 7.72 (m, 4H), 7.68 (s, 2H), 7.21 (d, *J* = 10.0 Hz, 8H), 7.15 (d, *J* = 10.0 Hz, 8H), 2.57 (t, *d* = 5.0 Hz, 8H), 1.60 (quintet, *d* = 5.0 Hz, 8H), 1.37-1.27 (m, 24H), 0.86 (t, *J* = 5.0 Hz, 12H); ^{13}C NMR ($CDCl_3$, 125 MHz) δ 188.99, 160.04, 156.14, 152.74, 151.75, 150.27, 144.82, 142.48, 141.30, 141.22, 140.45, 140.02, 139.02, 137.04, 136.76, 135.20, 134.34, 128.87, 127.92, 125.32, 123.66, 121.61, 118.69, 114.59, 69.32, 63.22, 35.58, 31.68, 31.20, 29.13, 22.55, 14.03; MS (m/z, MALDI) Calcd for $C_{94}H_{82}N_4O_2S_2Se_2$ 1522.42, found 1522.36.

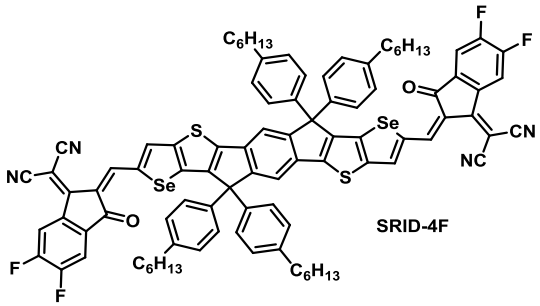

*Synthesis of 3,9-bis(2-methylene-(3-(1,1-dicyanomethylene)-5,6-difluoroindanone))-5,5,11,11-tetrakis(4-hexylphenyl)-diselenopheno[2,3-d:2',3'-d']-s-indaceno[1,2-b:5,6-b']dithiophene (**SRID-4F**).* To a solution of **IDTS-CHO** (117 mg, 0.10 mmol) and 2-(5,6-difluoro-3-oxo-2,3-dihydro-1H-inden-1-ylidene)malononitrile (69 mg, 0.30 mmol) in 1,2-dichloroethane (10 mL) and isopropanol (5 mL) was added a grain of β-alanine. The reaction mixture was then heated overnight at 80 °C. After cooling to room temperature, the volatile species were removed by rotary evaporation. The crude product was then purified by column chromatography on silica gel with hexanes/CH_2Cl_2 (v/v = 1:3) as eluent to afford **SRID-4F** as a dark solid (135 mg, 85%). ^{1}H NMR ($CDCl_3$, 500 MHz) δ 9.01 (s, 2H), 8.53 (quartet, *J* = 5.0 Hz, 2H), 8.27 (s, 2H), 7.69 (s, 2H), 7.66 (t, *J* = 5.0 Hz, 2H), 7.19 (d, *J* = 10.0 Hz, 8H), 7.14 (d, *J* = 10.0 Hz, 8H), 2.57 (t, *J* = 5.0 Hz, 8H), 1.60 (quintet, *J* = 5.0 Hz, 8H), 1.34-1.27 (m, 24H), 0.86 (t, *J* = 5.0 Hz, 12H); ^{13}C NMR ($CDCl_3$, 125 MHz) δ 186.64, 157.94, 156.26, 153.54, 151.76, 150.84, 145.10, 142.48, 141.51, 141.25, 140.98, 138.84, 137.11, 136.62, 134.31, 128.89, 127.84, 120.63, 118.84, 114.20, 114.14, 112.63, 112.49, 69.75, 63.16, 35.56, 31.67, 31.23, 29.13, 22.56, 14.06; MS (*m/z*, MALDI) Calcd for $C_{94}H_{78}F_4N_4O_2S_2Se_2$ 1594.38, found 1594.41.

Fabrication of OFETs for SRID/TRID. Field-effect transistors were fabricated through the top-contact and bottom-gate geometry, with a $p^{++}Si/SiO_2$/BCB/NFA/Ca/Ag structure. Heavily doped *p*-type silicon <100> substrates with a 300 nm thermal oxide layer were purchased from Montco

Silicon Technologies INC. After cleaning the substrate, the oxide layer was passivated with a thin divinyltetramethyldisiloxane-bis(benzocyclobutene) (BCB) layer. NFA thin films were spin-coated from its chloroform solution. Interdigitated source and drain electrodes (W = 1000 μm, L = 20 μm) were defined by evaporating a thin Ag layer (50 nm) through a shadow mask from the resistively heated Mo boat at 10^{-7} Torr. OFET characterization was carried out in a N_2–filled glovebox using an Agilent 4155B semiconductor parameter S6 analyzer. The field-effect mobility, μ_{FET} was calculated from the linear fit of $(I_{ds})_{1/2}$ vs V_{gs} in the saturation regime. The threshold voltage (V_t) was estimated as the x intercept of the linear section of the plot of $(I_{ds})_{1/2}$ vs V_{gs}.

Fabrication of PTB7-Th:SRID/TRID/ITIC solar cell devices. ITO-coated glass substrates (15 Ω sq^{-1}) were cleaned ultrasonically with detergent, deionized water, acetone, and isopropyl alcohol in sequence for 15 min each. Then, the ITO-coated glass substrates were treated with oxygen plasma for 15 min. A ZnO precursor solution was spin-coated onto pre-cleaned ITO-coated glass substrates at 4000 rpm for 60 s and annealed at 200 ℃ for 1 h in air to complete the thin layer of ZnO (ca. 20 nm). The ZnO precursor solution was prepared by dissolving zinc acetate dehydrate $C_4H_6O_4Zn{\cdot}2(H_2O)$ (99.5%, Merck,1 g) and ethanolamine (98% Acros, 0.28 g) in 2-methoxyethanol ($CH_3OCH_2CH_2OH$, Aldrich, 98%, 10 mL) under stirring for hydrolysis reaction and aging. The active layers were obtained by spin-coating the active layer solution that was filtered with a PTFE filter (0.45 μm) atop the thin layer of ETL. The optimal BHJ active layer films (100-110 nm) were fabricated from donor/acceptor solution with different ratios and solvents. For the films fabricated from solution with additive 1,8-diiodooctane (DIO), the films were stored in the vacuum for at least 1 h. Subsequently, the anode of each device, MoO_3/Ag (8 nm/150 nm),

was thermally evaporated at a pressure of about 10^{-7} torr. The area of each device was 3.14 mm^2 defined by a shadow mask.

Fabrication of PBDB-T-2F:SRID-4F/TRID-4F/IT-4F solar cell devices. Patterned ITO glass substrates were cleaned in an ultrasonic bath sequentially with detergent, deionized water, acetone and isopropanol. The substrates were then blown-dried and treated with air plasma for 10 mins, after which PEDOT:PSS (*CLEVIOS*™ P VP AI 4083) was immediately spin-coated. The substrates coated with PEDOT:PSS were annealed at 150 ºC for 15 mins before transferred into glove box (N_2) for deposition of active layer. Precursor solutions of active layers composed of PBDB-T-2F (donor, D) and **IT-4F**, **SRID-4F**, **TRID-4F** (acceptors, A) in chlorobenzene solution were deposited onto these PEDOT:PSS-coated substrates *via* spin-coating. Optimization of devices included exploring influence of different D:A ratios, addition of DIO, spin-coating speed and annealing conditions. On top of active layer, Bis-C_{60} salt (2 mg/mL in methanol) was spin-coated at 3000 rpm.[32] Finally, 120 nm Ag electrode was deposited *via* thermal evaporation under a base vacuum of $2*10^{-6}$ Torr at a rate of 0.2 nm/s. The *J-V* characteristics of devices under an AM 1.5 G illumination of 100 mW cm^{-2} were measured by using a Keithley 2400 source-measure unit in a nitrogen-filled glove box. The AM 1.5 G illumination was simulated by using an Oriel 300 W Solar Simulator and calibrated by using a silicon photodiode with a protective KG5 filter calibrated by the National Renewable Energy Laboratory (NREL). The EQE system uses a lock-in amplifier (Stanford Research Systems SR830) to record the short-circuit current under chopped monochromatic light.

Fabrication of SCLC devices. For PTB7-Th:**SRID**/**TRID**/**ITIC**, hole-only devices were fabricated with the configuration of ITO/PEDOT:PSS/BHJ/MoO_3 (8 nm)/Ag (150 nm) and electron-only devices were fabricated with the configuration of ITO/ZnO/BHJ/Ca (20 nm)/Ag (150 nm). For PBDB-T-2F:**SRID-4F**/**TRID-4F**/**IT-4F**, hole-only devices were fabricated with the configuration of ITO/PEDOT:PSS/Active layer/MoO_3/Ag and electron-only devices were fabricated with the configuration of ITO/ZnO/Active layer/Bis-C_{60}/Ag. The devices with different active layers were prepared following the optimized condition as described for photovoltaic devices. The ZnO layer for electron-only device was deposited *via* a sol-gel process as reported.[33] The MoO_3 layer for the hole-only device was deposited *via* thermal evaporation.

GIWAXS measurement for SRID/TRID neat films and BHJ films. GIWAXS measurements were conducted with Anton Paar SAXSess instrument. The wavelength of the X-ray (Cu Kα) was 1.54 Å . The films or were spin-coated on the Si substrates with 1.5 cm × 1.5 cm size. They were aligned and tilted with a 0.19° angle by using pin diode. The 2D scattering patterns were recorded on wide-angle image plates for 15 h. The reduction of the GIWAXS data was within the framework of Distorted Wave Born Approximation (DWBA), which enables the analytical treatment of the scattering intensity. Custom IGOR Pro reduction macros were utilized to convert pixel positions on each raw scattering image to intensity versus Q_y and Q_z with respect to the sample reference plane. All the scattering intensity was normalized to scattering time.

GIWAXS and RSoXS measurements for SRID-4F/TRID-4F/IT-4F neat films and BHJ films. GIWAXS and RSoXS samples were fabricated by depositing neat NFAs or blends on a silicon substrate coated with PEDOT:PSS. The D:A ratio of the blends are identical with the optimal

photovoltaic devices. GIWAXS measurement was carried out at beamline 7.3.3 Lawrence Berkeley National Lab (LBNL). The sample was put inside a helium chamber, and Pilatus 2M detector was used to collect the signal. GIWAXS raw data were analyzed using Nika software package and peak information was assessed by Gaussian fitting. RSoXS was performed at beamline 11.0.1.2 Lawrence Berkeley National Lab. Thin films was flowed and transferred onto Si_3N_4 substrate and experiment was done in transition mode.

2.9 REFERENCES

(1) Liang, Z.; Li, M.; Zhang, X.; Wang, Q.; Jiang, Y.; Tian, H.; Geng, Y. *Journal of Materials Chemistry A* **2018**, *6*, 8059.
(2) Wan, S. S.; Chang, C.; Wang, J. L.; Yuan, G. Z.; Wu, Q.; Zhang, M.; Li, Y. *Solar RRL* **2018**, 1800250.
(3) Meng, D.; Sun, D.; Zhong, C.; Liu, T.; Fan, B.; Huo, L.; Li, Y.; Jiang, W.; Choi, H.; Kim, T.; Kim, J. Y.; Sun, Y.; Wang, Z.; Heeger, A. J. *Journal of the American Chemical Society* **2016**, *138*, 375.
(4) Liang, T.; Xiao, L.; Liu, C.; Gao, K.; Qin, H.; Cao, Y.; Peng, X. *Organic Electronics* **2016**, *29*, 127.
(5) Cao, F.-Y.; Tseng, C.-C.; Lin, F.-Y.; Chen, Y.; Yan, H.; Cheng, Y.-J. *Chemistry of Materials* **2017**, *29*, 10045.
(6) Tsai, C.-E.; Yu, R.-H.; Lin, F.-J.; Lai, Y.-Y.; Hsu, J.-Y.; Cheng, S.-W.; Hsu, C.-S.; Cheng, Y.-J. *Chemistry of Materials* **2016**, *28*, 5121.
(7) Pao, Y.-C.; Yang, C.-T.; Lai, Y.-Y.; Huang, W.-C.; Hsu, C.-S.; Cheng, Y.-J. *Polymer Chemistry* **2016**, *7*, 4654.
(8) Lai, Y.-Y.; Chang, H.-H.; Lai, Y.-Y.; Liang, W.-W.; Tsai, C.-E.; Cheng, Y.-J. *Macromolecules* **2015**, *48*, 6994.
(9) Pao, Y. C.; Chen, Y. L.; Chen, Y. T.; Cheng, S. W.; Lai, Y. Y.; Huang, W. C.; Cheng, Y. J. *Organic letters* **2014**, *16*, 5724.
(10) Fringuelli, F.; Marino, G.; Taticchi, A. *Journal of the Chemical Society, Perkin Transactions 2* **1974**, 689.
(11) Patra, A.; Bendikov, M. *J. Mater. Chem.* **2010**, *20*, 422.
(12) Kang, I.; An, T. K.; Hong, J. A.; Yun, H. J.; Kim, R.; Chung, D. S.; Park, C. E.; Kim, Y. H.; Kwon, S. K. *Advanced materials* **2013**, *25*, 524.
(13) Li, Y.; Qian, D.; Zhong, L.; Lin, J.-D.; Jiang, Z.-Q.; Zhang, Z.-G.; Zhang, Z.; Li, Y.; Liao, L.-S.; Zhang, F. *Nano Energy* **2016**, *27*, 430.
(14) Li, Y.; Zhong, L.; Wu, F.-P.; Yuan, Y.; Bin, H.-J.; Jiang, Z.-Q.; Zhang, Z.; Zhang, Z.-G.; Li, Y.; Liao, L.-S. *Energy & Environmental Science* **2016**, *9*, 3429.
(15) Wang, J.-L.; Liu, K.-K.; Hong, L.; Ge, G.-Y.; Zhang, C.; Hou, J. *ACS Energy Letters* **2018**, *3*, 2967.
(16) Mishra, S. P.; Javier, A. E.; Zhang, R.; Liu, J.; Belot, J. A.; Osaka, I.; McCullough, R. D. *J. Mater. Chem.* **2011**, *21*, 1551.
(17) Iteke, F. B.; Christiaens, L.; Renson, M. *Tetrahedron* **1976**, *32*, 589.
(18) Konar, A. *Chemica Scripta* **1983**, *22*, 177.
(19) Litvinov, V. P.; Konyaeva, P.; Gol'dfarb, Y. L. *Bulletin of the Academy of Sciences of the USSR, Division of Chemical Science* **1974**, *23*, 1493.
(20) Lin, L.-Y.; Lu, C.-W.; Huang, W.-C.; Chen, Y.-H.; Lin, H.-W.; Wong, K.-T. *Organic letters* **2011**, *13*, 4962.
(21) Bredas, J.-L. *Mater. Horiz.* **2014**, *1*, 17.
(22) Schroeder, B. C.; Li, Z.; Brady, M. A.; Faria, G. C.; Ashraf, R. S.; Takacs, C. J.; Cowart, J. S.; Duong, D. T.; Chiu, K. H.; Tan, C. H.; Cabral, J. T.; Salleo, A.; Chabinyc, M. L.; Durrant, J. R.; McCulloch, I. *Angewandte Chemie* **2014**, *53*, 12870.
(23) Maurano, A.; Shuttle, C. G.; Hamilton, R.; Ballantyne, A. M.; Nelson, J.; Zhang, W.; Heeney, M.; Durrant, J. R. *The Journal of Physical Chemistry C* **2011**, *115*, 5947.
(24) Bartesaghi, D.; Perez Idel, C.; Kniepert, J.; Roland, S.; Turbiez, M.; Neher, D.; Koster, L. J. *Nature communications* **2015**, *6*, 7083.
(25) Singh, R.; Lee, J.; Kim, M.; Keivanidis, P. E.; Cho, K. *Journal of Materials Chemistry A* **2017**, *5*, 210.
(26) Zhang, H.; Yao, H.; Hou, J.; Zhu, J.; Zhang, J.; Li, W.; Yu, R.; Gao, B.; Zhang, S.; Hou, J. *Advanced materials* **2018**, *30*, e1800613.
(27) Liu, F.; Gu, Y.; Shen, X.; Ferdous, S.; Wang, H.-W.; Russell, T. P. *Progress in Polymer Science* **2013**, *38*, 1990.
(28) Liu, X.; Nian, L.; Gao, K.; Zhang, L.; Qing, L.; Wang, Z.; Ying, L.; Xie, Z.; Ma, Y.; Cao, Y.; Liu, F.; Chen, J. *Journal of Materials Chemistry A* **2017**, *5*, 17619.
(29) Huang, J.; Tang, Y.; Gao, K.; Liu, F.; Guo, H.; Russell, T. P.; Yang, T.; Liang, Y.; Cheng, X.; Guo, X. *Macromolecules* **2016**, *50*, 137.
(30) Gao, K.; Miao, J.; Xiao, L.; Deng, W.; Kan, Y.; Liang, T.; Wang, C.; Huang, F.; Peng, J.; Cao, Y.; Liu, F.; Russell, T. P.; Wu, H.; Peng, X. *Advanced materials* **2016**, *28*, 4727.
(31) Turbiez, M.; Frere, P.; Leriche, P.; Mercier, N.; Roncali, J. *Chemical communications* **2005**, 1161.

(32) Li, C.-Z.; Chueh, C.-C.; Yip, H.-L.; O'Malley, K. M.; Chen, W.-C.; Jen, A. K. Y. *Journal of Materials Chemistry* **2012**, *22*, 8574.

(33) Sun, Y.; Seo, J. H.; Takacs, C. J.; Seifter, J.; Heeger, A. J. *Advanced materials* **2011**, *23*, 1679.

Chapter 3. INTRODUCTION OF 6-ALKYLSELENOPHENO[3,2-*B*]THIOPHENE AS A BUILDING BLOCK FOR NON-FULLERENE ACCEPTORS

3.1 INTRODUCTION

In the previous chapter, the effects of regio-specific selenium substitution on A-D-A type NFAs were investigated and discussed. Aside from the as-expected photocurrent enhancement, interestingly it was found that energy loss has been reduced in binary OPVs based on selenium-substituted NFAs. In order to provide a more comprehensive material system to rationally study this phenomenon, as well as further reducing the energy loss, in this chapter, a series of NFAs derived from state-of-the-art high-performance materials has been designed and synthesized by introducing a novel building block, 6-alkylselenopheno[3,2-*b*]thiophene (Figure 3-1) which is a side-chain engineered derivative of selenopheno[3,2-*b*]thiophene.

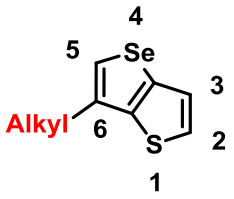

Figure 3-1. Chemical structure of 6-alkylselenopheno[3,2-*b*]thiophene.

Side chain engineering has long been an effective strategy to tune the solubility and crystallinity of organic functional materials, as mentioned in Chapter 1. However it was not until lately that researchers started to attach linear alkyl chains onto the β positions of central donor core in A-D-A type NFAs (Figure 3-2). This strategy has not only changed the solubility and

crystallinity of the material, but also led to reduced energy loss up to 50-60 meV in binary OPVs, which is a result of (1) favorable molecular conformation with less structural disorder induced by the steric hindrance of side chains and (2) enhanced compatibility between donor materials and NFAs, as claimed by Tang, Chen *et al.*[1,2] Moreover, in early 2019, a new series of high-performance NFAs based on π-extended thiadiazole central donor cores (BTP) was reported (Figure 3-2c).[3-5] These NFAs also have long, linear undecyl chains attached at the β positions on their central donor cores, which were used to reduce the high crystallinity of BTP derivatives to improve the compatibility of NFAs with donor materials.[6-8] However, the introduction of side chains at this specific position of NFAs may lead to slightly blue-shifted optical absorption.

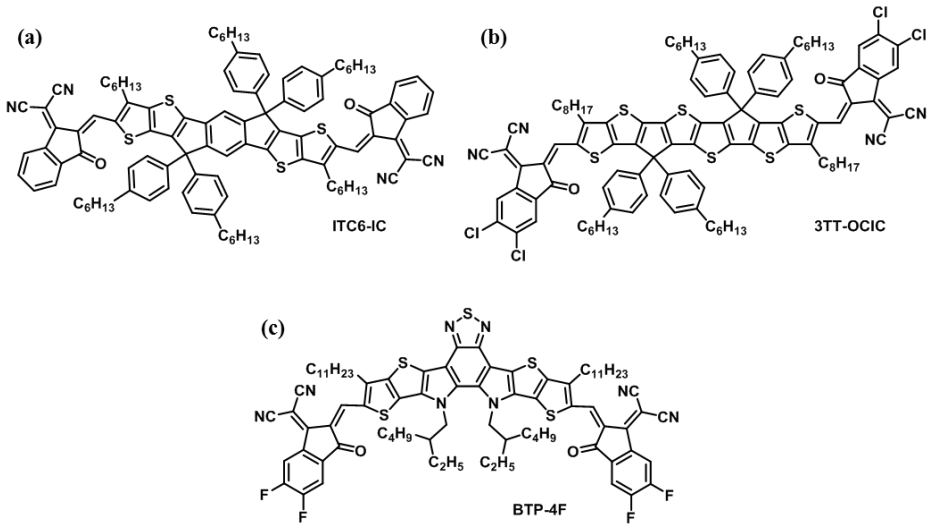

Figure 3-2. Chemical structures of (a) ITC6-IC, (b) 3TT-OCIC and (c) BTP-4F.

3.2 Molecular Design and Synthesis

The idea to use 6-alkylselenopheno[3,2-*b*]thiophene as a building block instead of 3-alkylselenopheno[3,2-*b*]thiophene is for the purpose of preventing the possible negative impacts

which may lead to loss on J_{sc} accompanying with alkylation at β position on the central donor core of NFAs, including (1) blue-shifted optical absorptions and (2) reduced crystallinity of the material. In the previous study on **IDTS** and **IDST**-based NFAs, it was found that the selenophene-exteriorized **SRID** and **SRID-4F** delivered higher photocurrent due to more red-shifted optical absorption, while both systems showed comparable performance in terms of reducing energy loss. The crystallinity of **SRID** and **SRID-4F** are also higher due to more ordered molecular conformations originated from the Se-O interaction as revealed from X-ray single-crystal analysis, while **TRID** and **TRID-4F** both possess mixed molecular conformations under solid state. After all these factors were taken into consideration, 6-alkylselenopheno[3,2-*b*]thiophene was synthesized as the precursor in order to give selenophene-exteriorized central donor cores. In this way, J_{sc} can only be minimally compromised while V_{oc} is enhanced.

The synthetic approach of 6-alkylselenopheno[3,2-*b*]thiophene is somehow similar with the widely reported 3-alkylthieno[3,2-*b*]thiophene,[9] however as the chemistry tends to get complicated when selenophenes are involved, some of the reaction conditions needed to be modified drastically in order to give the desired products. At first, the Friedel-Crafts acylation between ethyl 2-(thiophen-3-ylselanyl)acetate (**3-1**) and heptanoyl chloride was conducted using tin (IV) chloride as an efficient Lewis acid to give ethyl [2-(hexylthiophen-3-yl)selanyl]acetate (**3-2**), while aluminum (III) chloride and titanium (IV) chloride both led to messy reactions. Cyclization of **3-2** to yield the ester intermediate of 6-hexylselenopheno[3,2-*b*]thiophene was found to be unfeasible after several trials employing different conditions. The stronger bases hydrolyzed the starting material to give a non-reactive carboxylate by-product, and the weaker bases failed to deprotonate the α hydrogen of the selanyl acetate to provide a nucleophile for the cyclization reaction. Alternatively, I decided to skip through the ester intermediate and synthesize 6-

hexylselenopheno[3,2-*b*]thiophene-5-carboxylic acid (**3-3**) in a one-pot reaction using excessive amount of sodium ethoxide as base.[10] The competition between hydrolysis and deprotonation/cyclization was still observed, however the intermediate **3-3** was still managed to be obtained at an acceptable yield, and further underwent silver-catalyzed decarboxylation to give the key intermediates, 6-hexylselenopheno[3,2-*b*]thiophene (**3-4**).

Metalation of alkylated selenopheno[3,2-*b*]thiophene **3-4** turned out to be extremely problematic. In order to selectively deprotonate the α hydrogen on thiophene, multiple attempts were made using different combinations of bases/solvents/temperatures. It was anticipated that the alkyl substituent at 6 position of selenopheno[3,2-*b*]thiophene can (1) reduce the acidity of α hydrogen of selenophene due to inductive effect and (2) provide steric hindrance to enhance the regioselectivity of metalation while using bulky bases, both of which are helpful in terms of selectively deprotonating the α hydrogen on thiophene side.[11] However, the high electron richness of 6-alkylselenopheno[3,2-*b*]thiophene makes it unstable upon treatment with strong base and the metalation reaction is extremely hard to control (Table 3-1). Finally, with a base/solvent/temperature combination of LDA/THF/-40 ^{o}C, a very clean and efficient reaction was finally achieved and the stannylated key intermediate (**3-5**) was obtained in quantitative yields. Compound **3-5** was then gradually converted to ladder-type cores **C6IDTS** and **C6Se6T**, respectively, over several steps (Scheme 3-1). It is noteworthy that the bromination-decarboxylation strategy employed on selenopheno[3,2-*b*]thiophene-5-carboxylic acid in Chapter 2 did not work for the alkylated analogues, as the bromination of 6-hexylselenopheno[3,2-*b*]thiophene-5-carboxylic acid using *N*-bromosuccinimide gave a messy mixture.

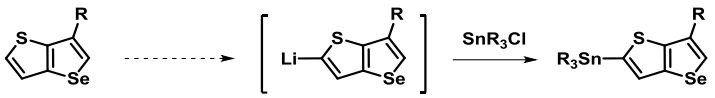

Trial	Reaction Condition			Result
	Solvent	Reagent	Temperature	
#1	THF (0.2 M)	1.00 eq. *n*-BuLi	-78 °C	Messy mixture with very minor desired product.
#2	THF (0.2 M)	1.00 eq. TMPMgCl·LiCl	0 °C	Mixture of minor unreacted starting material, product (~1:1) and impurities.
#3	THF (0.2 M)	1.00 eq. TMPMgCl·LiCl	20 °C	Messy mixture.
#4	Et_2O (0.2 M)	1.00 eq. LDA	-78 °C	Unreacted starting material : product ~1:2
#5	Et_2O (0.2 M)	1.00 eq. LDA	-40 °C	Unreacted starting material : product ~1:3
#6	THF (0.2 M)	1.00 eq. LDA	-40 °C	Clean product.

Table 3-1. Metalation conditions tested on 6-hexylselenopheno[3,2-*b*]thiophene.

3.3 Non-Fullerene Acceptors Based on Ladder-Type Cores Fused with 6-Hexylselenopheno[3,2-*b*]thiophene

NFAs based on **C6IDTS** and **C6Se6T** were synthesized through Vilsmeier-Haack formylation followed by condensation with 2-(5,6-difluoro-3-oxo-2,3-dihydro-1H-inden-1-ylidene)malononitrile to obtain the final products, **C6SRID-4F** and **C6Se6I-4F**, respectively (Scheme 3-1). A non-alkylated derivative of **C6Se6I-4F**, abbreviated as **Se6I-4F** (Figure 3-3), was also synthesized according to similar manner reported in Chapter 2 for comprehensive comparison.[12] It is noteworthy that both **C6-Se6T** and **Se6T** are not stable under storage, which may be due to the strong electron-donating nature of these ladder-type cores.

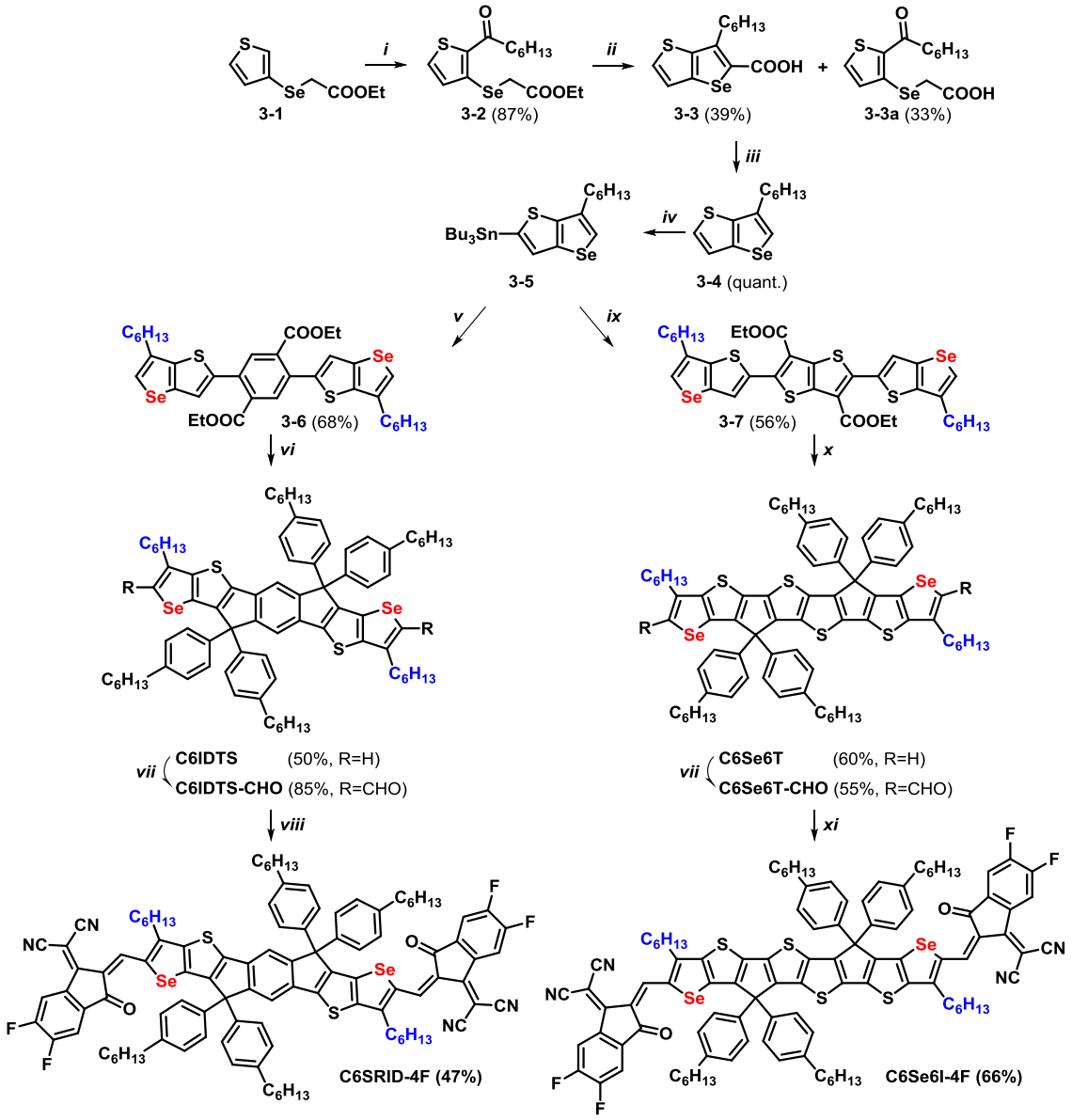

Reagents and conditions: i) Heptanoyl chloride, $SnCl_4$, toluene, -10 °C to r.t. *ii*) NaOEt, EtOH, r.t. then 80 °C. *iii*) Ag_2CO_3, HOAc, DMSO, 120 °C *iv*) a) LDA, THF, -40 oC; b) Bu_3SnCl, -40 °C to r.t. *v*) 2,5-dibromo-terephthalic acid diethyl ester, $PdCl_2(PPh_3)_2$, toluene, 110 °C. *vi*) a) 4-hexyl-1-bromobenzene, *n*-BuLi, THF, -78 °C to r.t. b) Amberlyst 15, toluene, 80 °C. *vii*) DMF, $POCl_3$, 1,2-dichloroethane, 0 °C to reflux. *viii*) 2-(5,6-difluoro-3-oxo-2,3-dihydro-1H-inden-1-ylidene)malononitrile, β-alanine, 1,2-dichloroethane/isopropanol (v/v=3:2), 80 °C. *ix*) 2,5-dichlorothieno[3,2-*b*]thiophene-3,6-dicarboxylic acid diethyl ester, $Pd(PPh_3)_4$, toluene, 110 °C. *x*) a) 4-hexyl-1-bromobenzene, Mg, THF, r.t. to reflux. b) Amberlyst 15, toluene, 80 °C. *xi*) 2-(5,6-difluoro-3-oxo-2,3-dihydro-1H-inden-1-ylidene)malononitrile, pyridine, $CHCl_3$.

Scheme 3-1. Synthesis of **C6SRID-4F** and **C6Se6I-4F**.

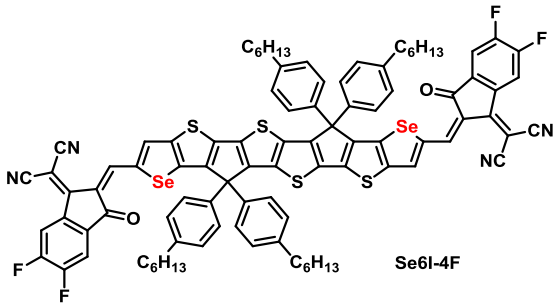

Figure 3-3. Chemical structure of **Se6I-4F**.

3.3.1 *Optical and Electrochemical Properties*

The optical properties of **C6SRID-4F** and **C6Se6I-4F** were probed using UV-Vis spectrometry for comparison with non-alkylated **SRID-4F** and **Se6I-4F**, respectively (Figure 3-4). In diluted solution, both **C6SRID-4F** and **C6Se6I-4F** show slightly red-shifted absorption and higher extinction coefficient, which can be due to stronger intramolecular charge transfer as alkyl possesses a slightly electron-donating nature. However, the shoulder peaks of **C6SRID-4F** (~650 nm) and **C6Se6I-4F** (~730 nm) show slightly suppressed intensity relative to the main peaks, implying that incorporation of alkyl chains may lead to less ordered microstructures as less well-defined vibronic peaks are shown.[13] Similar trend becomes more obvious in the thin-film absorption profiles. The peak height of 0-1 transition of both **C6SRID-4F** and **C6Se6I-4F** are reduced when the absorption intensity is normalized by the peak height of 0-0 transition, respectively. What's more, **C6SRID-4F** and **C6Se6I-4F** both exhibit blue-shifted absorption under solid state comparing with **SRID-4F** and **Se6I-4F**, respectively, which could be due to reduced order in terms of packing or aggregation.

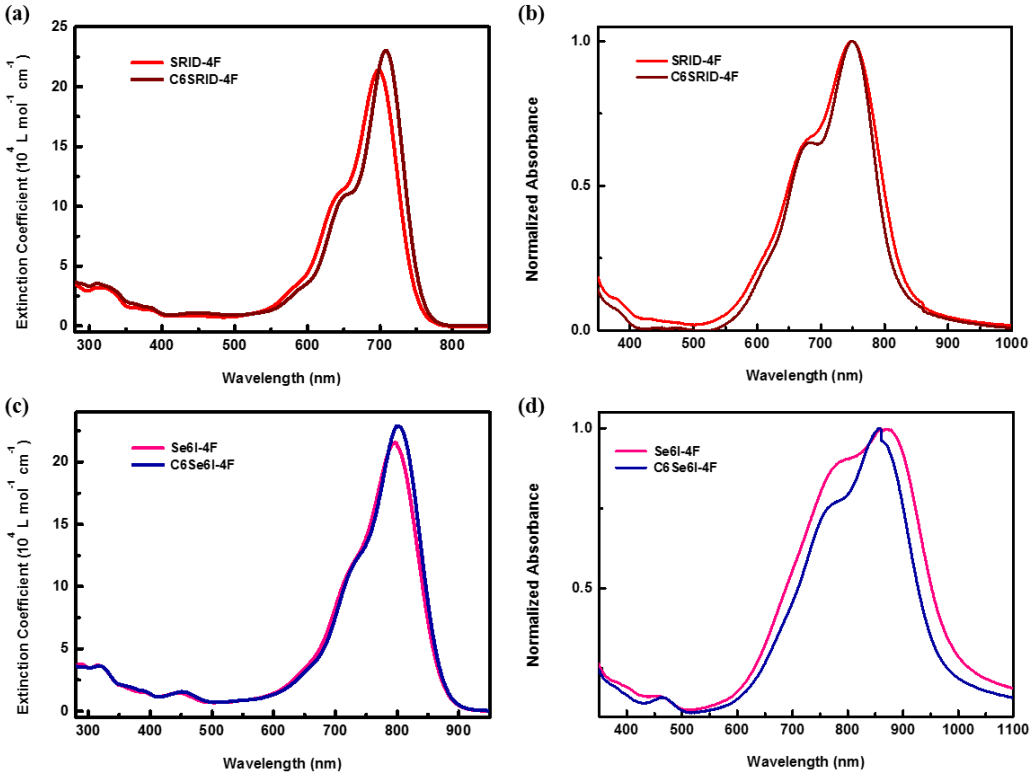

Figure 3-4. UV-Vis spectra of **SRID-4F** and **C6SRID-4F** in (a) solution and (b) thin film, and **Se6I-4F** and **C6Se6I-4F** in (c) solution and (d) thin film.

The frontier orbital energy levels of **C6SRID-4F** and **C6Se6I-4F** were investigated using cyclic voltammetry (CV) (Figure 3-5). Both **C6SRID-4F** and **C6Se6I-4F** give quasi-reversible oxidation waves, while the oxidation waves of **SRID-4F** and **Se6I-4F** show higher reversibility. As oxidation waves correspond to the oxidation of central electron-donating cores, the incorporation of alkyl chains may sterically hinder the electrochemically active cores and interfere with charge transfer, which leads to oxidation waves with lower reversibility. In the cathodic potential regime, two irreversible to quasi-reversible reduction waves were observed on both **C6SRID-4F** and **C6Se6I-4F**, similar as other A-D-A-type molecules. The ionization potentials (IP, corresponding to HOMO) and electron affinities (EA, corresponding to LUMO) of **C6SRID-**

4F and **C6Se6I-4F** were determined as -5.54/-3.90 and -5.26/-3.89 eV, respectively, as derived from the redox half potentials obtained in CV measurement (Table 3-2). Both **C6SRID-4F** and **C6Se6I-4F** show slightly down-shifted HOMO level and larger bandgap comparing to **SRID-4F** and **Se6I-4F**, respectively.

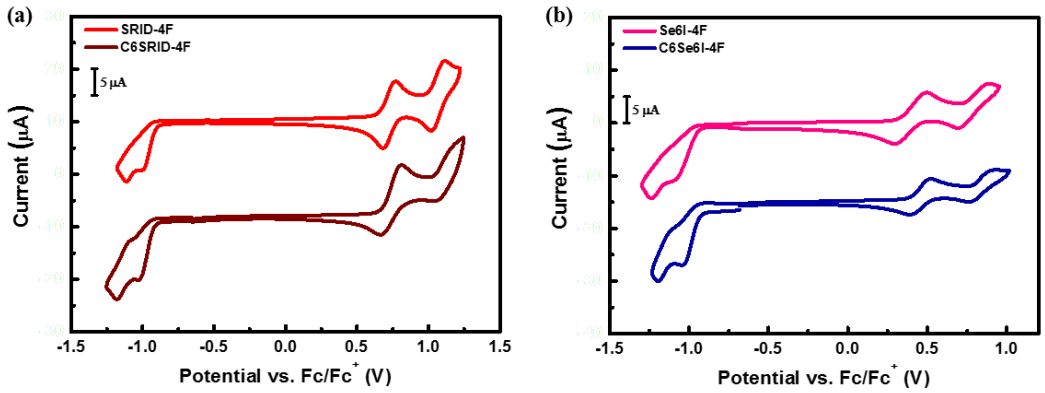

Figure 3-5. CV characteristics of (a) **SRID-4F** and **C6SRID-4F**, and (b) **Se6I-4F** and **C6Se6I-4F**.

	$\lambda_{max,\ soln}$[a] (nm)	ε[a] (10^4 L mol^{-1} cm^{-1})	$\lambda_{max,\ film}$[b] (nm)	λ_{edge}[c] (nm)	$E_{g,\ film}$[d] (eV)	IP[e] (eV)	EA[e] (eV)	$E_{g,\ CV}$[f] (eV)
SRID-4F	698	21.4	752	862	1.44	-5.52	-3.90	1.62
C6SRID-4F	708	23.0	751	852	1.46	-5.54	-3.90	1.64
Se6I-4F	797	21.6	873	992	1.25	-5.20	-3.87	1.33
C6Se6I-4F	802	22.9	859	967	1.28	-5.26	-3.89	1.37

[a] Measured in CH_2Cl_2 solution (1×10^{-6} M). [b] Spin-cast thin film. [c] Optical bandgap estimated from thin-film absorption. [d] Calculated from the absorption edge of thin-film spectra. [e] Cyclic voltammetry (CV) was measured in CH_2Cl_2 solution with 0.1 M NBu_4PF_6 as supporting electrolyte. Sample concentration was 0.01 M for the measurements. All potentials were recorded using Fc/Fc^+ as an external reference, which was referenced at -4.80 eV below vacuum level. [f] Electrochemical bandgap estimated from the redox half potentials of CV measurement.

Table 3-2. Summary of optical and electrochemical properties of **SRID-4F**, **C6SRID-4F**, **Se6I-4F** and **C6Se6I-4F**.

3.3.2 *Photovoltaic Characteristics*

The photovoltaic performance of **C6SRID-4F** and **C6Se6I-4F** were investigated pairing with PBDB-T-2F as donor, with a device configuration of ITO/PEDOT:PSS/PBDB-T-2F:**NFAs**/Bis-C_{60}/Ag. The optimal donor/acceptor ratios were found to be 1:1 for both **C6SRID-4F** and **C6Se6I-4F**, which were also the same for **SRID-4F** and **Se6I-4F** (Table 3-3).

Photovoltaic devices based on PBDB-T-2F:**C6SRID-4F** delivered a V_{oc} of 0.879 V, a J_{sc} of 20.70 mA/cm^2, a fill factor of 0.747, and a PCE of 13.59 %, which is slightly higher than the 13.05% PCE delivered from devices based on PBDB-T-2F:**SRID-4F**. With the introduction of side chain, the V_{oc} was increased by around 0.03 V, while the J_{sc} did not suffer from blue-shifted absorption of **C6SRID-4F**. On the other hand, devices based on PBDB-T-2F:**C6Se6I-4F** delivered a PCE of 11.37% with a V_{oc} of 0.833 V, a J_{sc} of 22.64 mA/cm^2, and a fill factor of 0.603. Although the V_{oc} was amazingly increased by 0.08 V comparing to devices based on PBDB-T-2F:**Se6I-4F** (V_{oc} = 0.749 V, J_{sc} = 24.33 mA/cm^2, FF = 0.657, PCE = 11.98 %), such gain on V_{oc} did not compensate the loss on J_{sc} and FF.

	V_{oc} (V)	J_{sc} (mA/cm^2)	FF	PCE (%)
PBDB-T-2F: **SRID-4F**[a]	0.846	20.21	0.752	13.05
PBDB-T-2F: **C6SRID-4F**[a]	0.879	20.70	0.747	13.59
PBDB-T-2F: **Se6I-4F**[a]	0.749	24.33	0.657	11.98
PBDB-T-2F: **C6Se6I-4F**[a]	0.833	22.64	0.603	11.37

[a] 1:1 in CB + 0.25 % DIO, annealed at 100 °C.

Table 3-3. The optimized photovoltaic parameters of devices.

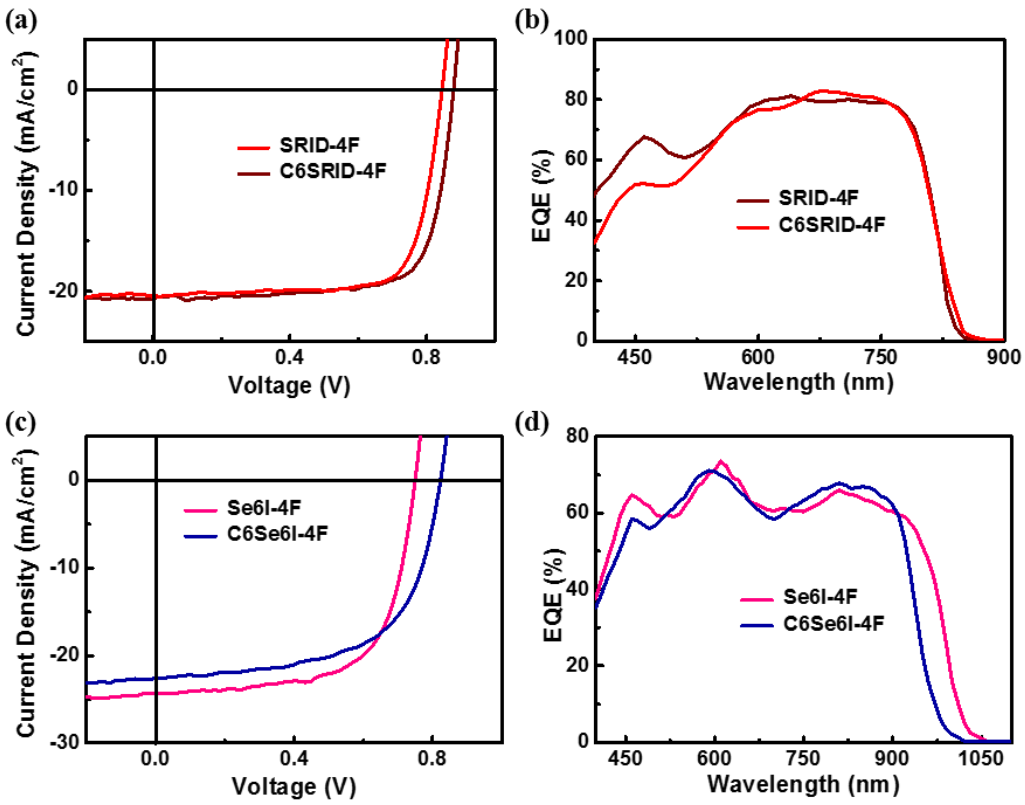

Figure 3-6. (a) *J*-*V* characteristics and (b) EQE spectra of optimized PBDB-T-2F:**SRID-4F**/**C6SRID-4F** devices, and (c) *J*-*V* characteristics and (d) EQE spectra of optimized PBDB-T-2F:**Se6I-4F**/**C6Se6I-4F** devices

3.4 Non-Fullerene Acceptors Based on π-Extended Thiadiazole Cores Fused with 6-Undecylselenopheno[3,2-*b*]thiophene

It is also of our great interest to study the effect of selenium substitution on other high-efficiency NFA systems, as we found that selenium substitution not only benefits the optical absorption, but also reduces the energy loss in the previous study in Chapter 2.[14,15] As a feasible approach to synthesize 6-hexylselenopheno[3,2-*b*]thiophene has been developed, 6-undecylselenopheno[3,2-*b*]thiophene was also synthesized through a similar manner using lauroyl chloride as the precursor, followed by stannylation and converted to the selenium-substituted π-extended thiadiazole core,

EHBSP, and subsequently **EHSBR-4F** as the NFA final product. However, it was found that the low solubility and high crystallinity of **EHSBR-4F** led to severe phase segregation while blended with donor polymers. To solve this issue, a derivative with longer *N*-substituted branching alkyl chains, **BOBSP**, was synthesized and converted to **BOSBR-4F**. A chlorinated NFA derivative, **BOSBR-4Cl**, was also synthesized with the expectation of extending the optical absorption of NFA into more red-shifted region (Scheme 3-2).

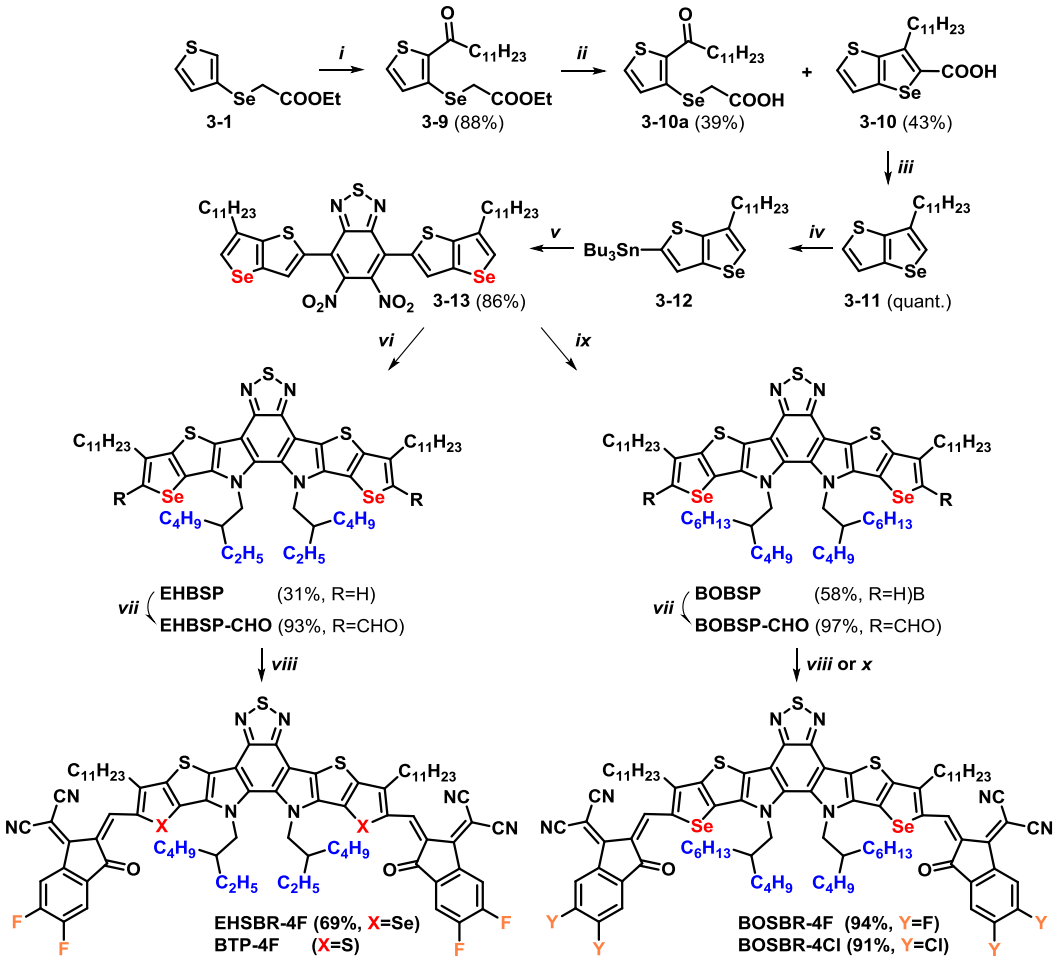

Reagents and conditions: i) Lauroyl chloride, $SnCl_4$, toluene, -10 °C to r.t. *ii*) NaOEt, EtOH, r.t. then 80 °C. *iii*) Ag_2CO_3, HOAc, DMSO, 120 °C *iv*) a) LDA, THF, -40 oC; b) Bu_3SnCl, -40 °C to r.t. *v*) 4,7-dibromo-5,6-dinitro[2,1,3]benzothiadiazole, $Pd_2(dba)_3$, P(*o*-tol)$_3$, toluene, r.t. *vi*) a) $P(OEt)_3$, *o*-DCB, 180 °C; b) 2-ethylhexyl bromide, K_2CO_3, KI, DMF, 90 °C. *vii*) DMF, $POCl_3$, 1,2-dichloroethane, 0 °C to reflux. *viii)* 2-(5,6-difluoro-3-oxo-2,3-dihydro-1H-inden-1-ylidene)malononitrile, pyridine, $CHCl_3$. *ix)* a) $P(OEt)_3$, *o*-DCB, 180 °C; b) 2-butyloctyl iodide, NaOH, DMF, 70 °C. *x)* 2-(5,6-dichloro-3-oxo-2,3-dihydro-1H-inden-1-ylidene)malononitrile, pyridine, $CHCl_3$.

Scheme 3-2. Synthesis of **EHSBR-4F**, **BOSBR-4F** and **BOSBR-4Cl**.

3.4.1 *Optical and Electrochemical Properties*

The optical properties of **EHSBR-4F**, **BOSBR-4F** and **BOSBR-4Cl** were probed using UV-Vis spectrometry. In diluted solution, the absorption edge of **EHSBR-4F** and **BOSBR-4F** both shows ~30 nm red-shift to ~820 nm comparing to **BTP-4F**, as the absorption edge of **BOSBR-4Cl** further shifts to ~840 nm. In thin film, regardless of the absorption edge of the materials are similar, the absorption profile of **BOSBR-4F** clearly interestingly shows vibronic structure with a shoulder peak emerging at ~750 nm. This is a direct evidence that the packing of **BOSBR-4F** in thin film is not affected by incorporation of the longer *N*-substituted side chains on **BOBSP** core. **BOSBR-4Cl** also shows similar absorption profile to **BOSBR-4F** with marginal red-shifting.

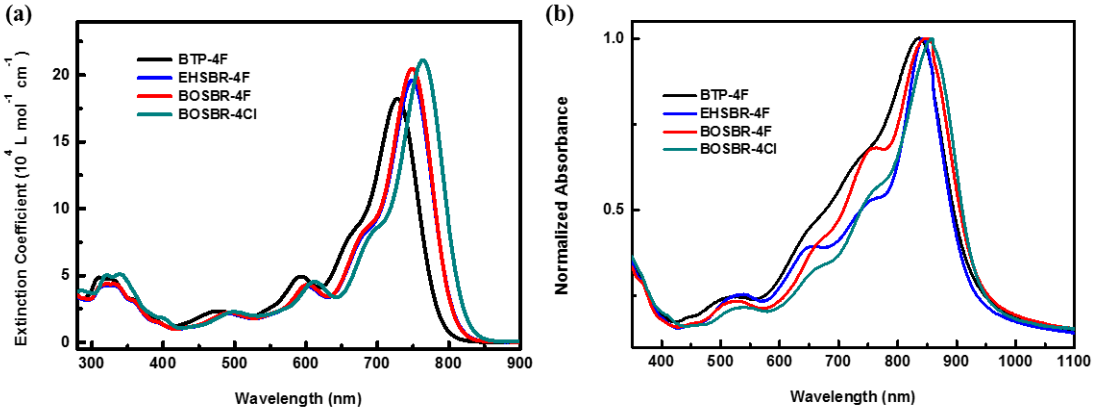

Figure 3-7. UV-Vis spectra of **BTP-4F**, **EHSBR-4F**, **BOSBR-4F** and **BOSBR-4Cl** in (a) solution and (b) thin film.

The frontier orbital energy levels of **EHSBR-4F**, **BOSBR-4F** and **BOSBR-4Cl**, along with **BTP-4F**, were investigated using cyclic voltammetry (CV) in chloroform solution, due to the

inadequate solubility of **EHSBR-4F**, **BOSBR-4Cl** and **BTP-4F** in dichloromethane (Figure 3-8). The voltammetry profiles of the materials are similar. The IPs and EAs of **EHSBR-4F**, **BOSBR-4F**, **BOSBR-4Cl** and **BTP-4F** were determined as -5.59/-3.96, -5.59/-3.97, -5.63/-4.01 and -5.60/-3.94 eV, respectively, as derived from the redox half potentials obtained in CV measurement (Table 3-4). The bandgap of the materials are reduced by selenium substitution mainly through down-shifting the LUMOs, and the introduction of stronger electron-withdrawing end groups on **BOSBR-4Cl** further down-shifts the HOMO/LUMO energy levels.

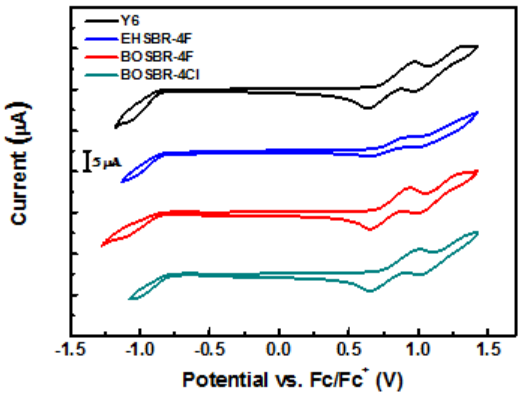

Figure 3-8. CV characteristics of **BTP-4F**, **EHSBR-4F**, **BOSBR-4F** and **BOSBR-4Cl**.

	$\lambda_{max,\ soln}$[a] (nm)	ε[a] (10^4 L mol^{-1} cm^{-1})	$\lambda_{max,\ film}$[b] (nm)	λ_{edge}[c] (nm)	$E_{g,\ film}$[d] (eV)	IP[e] (eV)	EA[e] (eV)	$E_{g,\ CV}$[f] (eV)
BTP-4F	728	18.2	839	945	1.31	-5.60	-3.94	1.66
EHSBR-4F	749	19.6	842	934	1.33	-5.59	-3.96	1.63
BOSBR-4F	749	20.5	849	958	1.29	-5.59	-3.97	1.62
BOSBR-4Cl	764	21.1	856	962	1.29	-5.63	-4.01	1.62

[a] Measured in CH_2Cl_2 solution (1×10^{-6} M). [b] Spin-cast thin film. [c] Optical bandgap estimated from thin-film absorption. [d] Calculated from the absorption edge of thin-film spectra. [e] Cyclic voltammetry (CV) was measured in $CHCl_3$ solution with 0.1 M NBu_4PF_6 as supporting electrolyte. Sample concentration was 0.01 M for the measurements. All potentials were recorded using Fc/Fc^+ as an external reference, which was referenced at -4.80 eV below vacuum level. [f] Electrochemical bandgap estimated from the redox half potentials of CV measurement.

Table 3-4. Summary of optical and electrochemical properties of **BTP-4F**, **EHSBR-4F**, **BOSBR-4F** and **BOSBR-4Cl**.

3.4.2 *Photovoltaic Characteristics*

Photovoltaic devices were fabricated with binary BHJs based on PBDB-T-2F as donor with the NFAs, with a device configuration of ITO/PEDOT:PSS/PBDB-T-2F:**NFAs**/Bis-C_{60}/Ag. The optimal donor/acceptor ratios were determined as 1:1.25 for all four NFAs, **EHSBR-4F**, **BOSBR-4F**, **BOSBR-4Cl** and **BTP-4F**.

Devices based on PBDB-T-2F:**EHSBR-4F** delivered a V_{oc} of 0.869 V, a J_{sc} of 18.34 mA/cm^2, a fill factor of 0.684, and a lower PCE of 10.90 %, due to the severe phase segregation and incompatibility between donor:NFA arisen from the low solubility of **EHSBR-4F**. The NFAs with longer *N*-substituted side chains gave much better performance, as devices based on PBDB-T-2F:**BOSBR-4F** delivered a V_{oc} of 0.836 V, a J_{sc} of 25.28 mA/cm^2, a fill factor of 0.749, and a PCE of 15.82 %, and devices based on PBDB-T-2F:**BOSBR-4Cl** delivered a V_{oc} of 0.828 V, a J_{sc} of 25.69 mA/cm^2, a fill factor of 0.741, and a PCE of 15.77 %, which were both superior to the reference PBDB-T-2F:**BTP-4F** system. Although the thin-film absorption profiles did not show notable red-shifting, the EQE curve of PBDB-T-2F:**BOSBR-4F** and PBDB-T-2F:**BOSBR-4Cl** both showed an extension of ~40 nm and gave higher J_{sc} than that of PBDB-T-2F:**BTP-4F**. The higher V_{oc} and fill factor values also indicated that the proper compatibility was established between donor:NFAs, although the impact of reducing energy loss through selenium substitution was not obvious. It was also found that chlorination only gave marginal growth in terms of photovoltaic performance on this material system.

	V_{oc} (V)	J_{sc} (mA/cm^2)	FF	PCE (%)
PBDB-T-2F: **BTP-4F**[a]	0.822	24.56	0.720	14.53

PBDB-T-2F: **EHSBR-4F**[a]	0.869	18.34	0.684	10.90
PBDB-T-2F: **BOSBR-4F**[a]	0.836	25.28	0.749	15.82
PBDB-T-2F: **BOSBR-4Cl**[a]	0.828	25.69	0.741	15.77

[a] 1:1.25 in CB + 0.25 % DIO, annealed at 100 °C.

Table 3-5. The optimized photovoltaic parameters of devices.

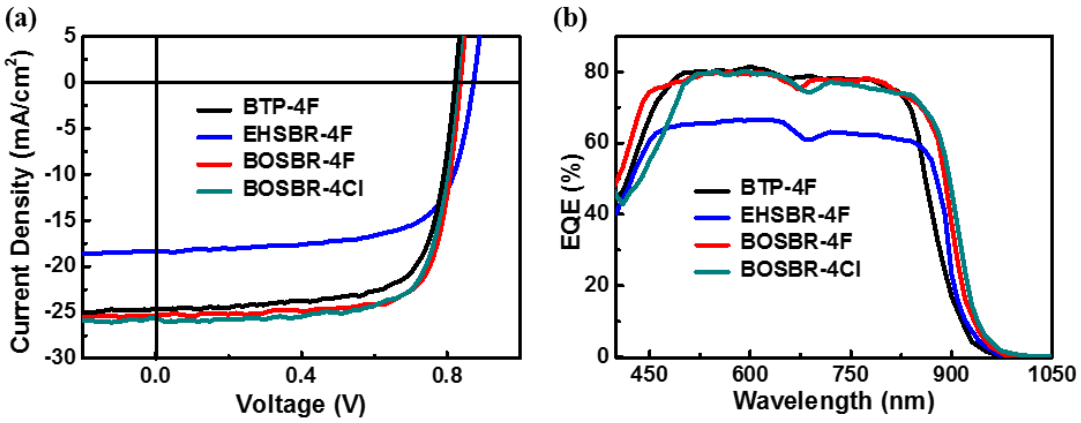

Figure 3-9. (a) *J-V* characteristics and (b) EQE spectra of optimized PBDB-T-2F:**BTP-4F**/**EHSBR-4F**/**BOSBR-4F**/**BOSBR-4Cl** devices,

3.4.3 *X-ray Crystallography Study on Single Crystals*

Single crystals of **BTP-4F** and **BOSBR-4F** were grown and analyzed using single-crystal X-ray diffraction to investigate the structure of these NFAs derived from π-extended thiadiazole cores, in the hope of revealing the difference in terms of molecular geometries and charge transfer pathways between different high-efficiency NFA material systems.

BTP-4F possesses one type of conformation in the single crystal, with an asymmetric molecular geometry due to the twisted structure of BTP-4F. The D-A dihedral angles on different sides of the molecule are not the same, which are 25.37° and 0.76°, corresponding to different S-O distances of 2.620 Å and 2.640 Å, respectively (Figure 3-10a). Adjacent **BTP-4F** molecules

dimerize in a tail-to-tail manner, and form wavy zig-zag 1D chains between dimers through π-π interactions of indanone end groups (Figure 3-10b & 3-10c).

Among literature, single crystal structures of several smaller π-extended thiadiazole cores with shorter side chains were reported. In many cases, it was found that these cores tends to form head-to-head dimers through the S-N interactions between the thiadiazole rings on adjacent molecules.[16-18] However, In **BTP-4F**, this specific type of interaction is interrupted by the introduction of long, branching side chains. No distinct interchain communication can either be found as the 1D chains are surrounded by the bulky side chains.

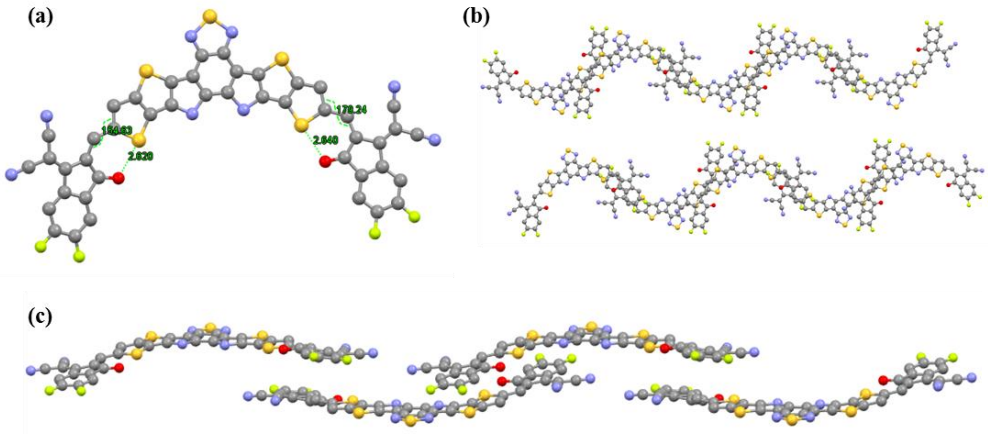

Figure 3-10. (a) Single-molecule conformation of **BTP-4F**. (b) Zig-zag 1D chains with large interchain distance of **BTP-4F**. (c) Zig-zag 1D chain formation. Side chains were omitted for clearance.

BOSBR-4F presents two different types of molecular conformation in the single crystal, both of which possesses asymmetric molecular geometry, including (1) D-A dihedral angles of 5.69° on both sides, however with different Se-O distances of 2.651 Å and 2.661 Å (labelled in blue), and (2) D-A dihedral angles of 0.79° and 3.78°, corresponding to different Se-O distances of 2.701 Å and 2.636 Å, respectively (labelled in green) (Figure 3-11a). Dimers are formed by two adjacent

blue and green molecules through π-π interactions of indanone end groups (Figure 3-11(b), circled in yellow) and N-S interactions among thiadiazoles (Figure 3-11(b), circled in red). Although multiple conformations have been observed, the stronger intermolecular interactions give rise to highly ordered packing between dimers to form a very nice 3D network, regardless of the incorporation of longer 2-butyloctyl branching side chains. The dimers pack along *a*-axis to form a column through π-π interactions of indanone groups, and the communication between different columns are dominated by the π-π interactions of exposed indanone groups.

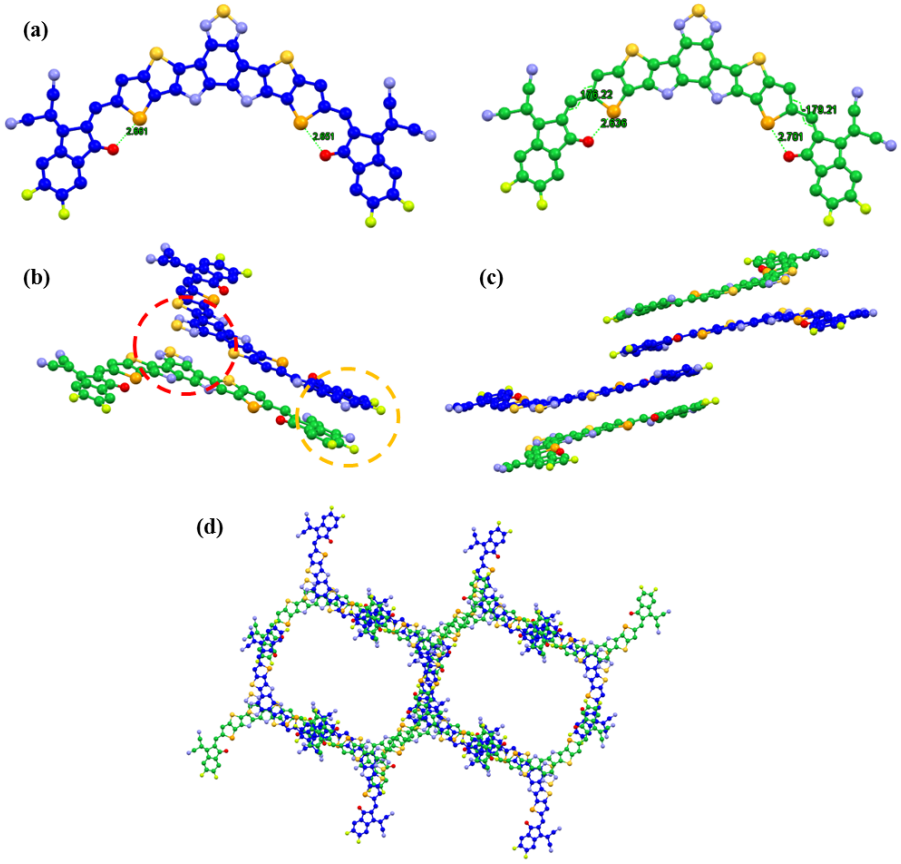

Figure 3-11. (a) Two conformations of **BOSBR-4F**. (b) Dimer formation in **BOSBR-4F**. (c) Stacking of dimers viewed along *b*-axis. (d) Packing viewed along *a*-axis.

3.5 CONCLUSION

In this chapter, 6-alkylselenopheno[3,2-*b*]thiophene was developed as a new building block for NFAs, which is capable of simultaneously providing accessibility to two important features including (1) regio-specific selenium substitution which may enhance optical absorption and reduce energy loss, and (2) β-alkylation on central donor cores which can reduce energy loss. Multiple derivatives based on state-of-the-art high-performance NFAs were synthesized employing 6-alkylselenopheno[3,2-*b*]thiophene as a precursor to incorporate the aforementioned features.

While trying to examine if selenium substitution coupled with β-alkylation on central donor cores could be a universal strategy to enhance the photovoltaic performance of the materials, it was found that different material systems respond in slightly different manners. **C6SRID-4F**-based devices showed better performance than **SRID-4F**-based devices upon incorporation of the alkyl chain, however devices based on **C6Se6I-4F** did not outperform those based on **Se6I-4F**, as the enhancement of V_{oc} did not compensate the loss on J_{sc} and FF. If combined with further investigation into the difference between morphologies, these two material systems can be good candidates to systematically study the different pathways of energy loss in different materials.

Structural modification including selenium substitution, *N*-alkyl modulation, and incorporation of stronger electron-withdrawing end groups on **BTP-4F** turned out to give very promising results. The mechanism of charge transport and energy loss reduction of **BOSBR-4F** and **BOSBR-4Cl** will be studied with the aid of further analysis on single crystal structures and morphological study.

3.6 EXPERIMENTAL DETAILS

General Methods. Unless otherwise stated, all chemicals and reagents were used as received from commercial sources (Sigma-Aldrich, Matrix Scientific, Combi-Blocks) without further purification. Solvents for chemical synthesis were purified by distillation under nitrogen. All chemical reactions were carried out under protection of argon or nitrogen atmosphere. Compound **3-1** and 2-butyloctyl iodide were prepared according to literature procedures.[19,20] PBDB-T-2F was purchased from 1-Material. The ^{1}H and ^{13}C NMR spectra were recorded on a Bruker AV500 spectrometer using $CDCl_3$, d_6-DMSO or C_6D_6 as solvents. Mass spectrometry was performed on Bruker APEX III 47e Fourier Transform mass spectrometer. The UV-Vis spectra were recorded on a Varian Cary 5000 UV-Vis-NIR Spectrophotometer. Cyclic voltammetry and differential pulse voltammetry were measured on a CH Instruments CHI660E Electrochemical Analyzer/Workstation using a conventional three-electrode cell with a glassy carbon working electrode, Pt wire counter-electrode, and Ag/AgCl reference electrode at a scan rate of 50 mV/s using 0.1 M tetrabutylammonium hexafluorophosphate ($TBAPF_6$) in CH_2Cl_2 or $CHCl_3$ as the electrolyte and referenced to the $FeCp_2/FeCp_2^+$ redox couple.

Preparation of 2 M solution of lithium diisopropylamide (LDA) in THF. A 3-neck round-bottom-flask was flame-dried under vacuum, cooled to room temperature, refilled with argon, and was added dry THF and diisopropylamine (1.05 eq, freshly distilled from KOH). The volume of THF was calculated to give a reagent concentration of ca. 2 M. The mixture was cooled to 0 ^{o}C, and n-BuLi (2.5 M in hexanes, 1.00 eq) was dropwise added to give a slightly cloudy solution was a pale color of yellow. The mixture was then stirred at 0 ^{o}C for 30 mins, then raised to room

temperature and stirred for another 30 mins to give the desired LDA solution, which was immediately used after cooled to appropriate temperature.

Preparation of 1.3 M solution of isopropylmagnesium chloride lithium chloride complex (*i*PrMgCl·LiCl) in THF. A 3-neck round-bottom-flask was flame-dried under vacuum, cooled to room temperature, refilled with argon, and was added anhydrous THF, LiCl (1.02 eq, previously flame-dried under vacuum) and magnesium turnings (1.02 eq, activated by washing with saturated $NH_4Cl_{(aq)}$). The volume of THF was calculated to give a reagent concentration of ca. 1.3 M. A few drops of 1,2-dibromoethane was added, and then 2-chloropropane (1.00 eq) was added dropwise. The mixture was heated with an oil bath to maintain gentle reflux during the addition of 2-chloropropane. After the addition, the mixture was refluxed for another 6 hours and then cooled to room temperature and left settled. The supernatant was cannulated to another flame-dried flask to remove the residual magnesium and give the desired *i*PrMgCl·LiCl solution.

Preparation of 1.3 M solution of 2,2,6,6-tetramethylpiperidinylmagnesium chloride lithium chloride complex (TMPMgCl·LiCl) in THF. To a solution of 1.3 M *i*PrMgCl·LiCl in THF (1.00 eq) was added 2,2,6,6-tetramethylpiperidine (1.02 eq, freshly distilled from CaH_2) under an argon atmosphere. Evolution of propane gas was observed during the addition. The solution was stirred at room temperature for two days until completion of reaction to give a solution of TMPMgCl·LiCl at ca. 1.3 M.

Material synthesis.

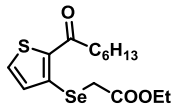

3-2

*Synthesis of ethyl [2-(heptanoylthiophen-3-yl)selanyl]acetate (**3-2**).* To a stirred solution of ethyl 2-(thiophen-3-ylselanyl)acetate (**3-1**, 12.5 g, 50.0 mmol) and heptanoyl chloride (8.52 mL, 55.0 mmol) in dry toluene (50 mL) was dropwise added a solution of tin(IV) chloride (6.13 mL, 52.5 mmol) in dry toluene (25 mL) at -10 ^{o}C under an argon atmosphere. The mixture was kept at -10 ^{o}C for 30 minutes, and then stirred at room temperature overnight. The reaction was quenched by addition of 10% HCl in aqueous solution and extracted with CH_2Cl_2. The combined extracts were washed with brine, dried over anhydrous $MgSO_4$, and then filtered. The solvent was removed by rotary evaporation to give the crude product as a brown oil, which was further purified by column chromatography on silica gel with hexanes/CH_2Cl_2 (v/v = 2:1) as eluent to afford **3-2** as a yellow oil (15.7 g, 87%). ^{1}H NMR ($CDCl_3$, 500 MHz) δ 7.54 (d, *J* = 5.0 Hz, 1H), 7.36 (d, *J* = 5.0 Hz, 1H), 4.16 (q, *J* = 5.0 Hz, 2H), 3.56 (s, 2H), 2.79 (t, *J* = 5.0 Hz, 2H), 1.73 (quintet, *J* = 5.0 Hz, 2H), 1.37-1.27 (m, 6H), 1.24 (t, *J* = 5.0 Hz, 3H), 0.87 (t, *J* = 5.0 Hz, 3H); ^{13}C NMR ($CDCl_3$, 125 MHz) δ 193.10, 171.08, 138.50, 132.21, 131.21, 128.71, 61.42, 40.52, 31.52, 28.90, 25.56, 24.55, 22.42, 14.00, 13.96; GC-MS (*m/z*) Calcd for $C_{15}H_{22}O_3SSe$ 362.05, found 362.07.

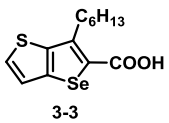

3-3

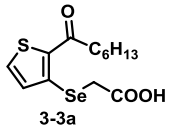

3-3a

*Synthesis of 6-hexylselenopheno[3,2-b]thiophene-5-carboxylic acid (**3-3**).* At room temperature, a solution of **3-2** (15.1 g, 35.0 mmol) in absolute ethanol (35 mL) was dropwise added into a solution of NaOEt, which was freshly prepared from sodium (2.41 g, 105 mmol) and absolute ethanol (70 mL), under an argon atmosphere to form a thick yellow slurry. The mixture was then refluxed

overnight, after which the solvents were removed by rotary evaporation. The residue was dissolved in water and acidified with 10% HCl in aqueous solution, followed by extraction using ethyl acetate. The combined extracts were washed with brine, dried over anhydrous $MgSO_4$, and then filtered. The solvent was removed by rotary evaporation to give the crude product as a brown solid, which was further purified by column chromatography on silica gel with CH_2Cl_2 as eluent to afford **3-3** as a white solid (5.29 g, 39%). A portion of **3-2** hydrolyzed before forming the desired cyclized product during the reaction, giving [2-(heptanoylthiophen-3-yl)selanyl]acetic acid (**3-3a**), which was recovered using ethyl acetate/CH_2Cl_2 (v/v = 1:3) as eluent, also as a white solid (4.60 g, 33%). ^{1}H NMR (d_6-DMSO, 500 MHz) δ 7.85 (d, *J* = 5.0 Hz, 1H), 7.52 (d, *J* = 5.0 Hz, 1H), 3.08 (t, *J* = 5.0 Hz, 2H), 1.64 (quintet, *J* = 5.0 Hz, 2H), 1.33-1.25 (m, 8H), 0.84 (t, *J* = 5.0 Hz, 3H); ^{13}C NMR (d_6-DMSO, 125 MHz) δ 164.90, 143.88, 142.67, 139.63, 131.79, 130.67, 124.13, 30.86, 29.71, 28.66, 28.53, 21.92, 13.85.; GC-MS (*m/z*) Calcd for $C_{13}H_{16}O_2SSe$ 316.00, found 316.05.

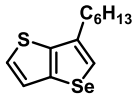

3-4

*Synthesis of 6-hexylselenopheno[3,2-b]thiophene (**3-4**).* A mixture of **3-3** (3.15 g, 10.0 mmol) and silver carbonate (110 mg, 0.40 mmol) in DMSO (15 mL) was added acetic acid (46 μL, 0.80 mmol), followed by heating at 120 ^{o}C overnight. The reaction mixture was then cooled to room temperature and passed through a celite pad to remove the inorganic residues. The celite pad was rinsed with diethyl ether for several times, and the combined filtrates were extracted with water. The combined extracts were washed with brine, dried over anhydrous $MgSO_4$, and then filtered. The solvent was removed by rotary evaporation to give the crude product as a light brown oil, which was further purified by column chromatography on silica gel with hexanes as eluent to

afford **3-4** as a colorless oil (2.71 g, quant.). ^{1}H NMR ($CDCl_3$, 500 MHz) δ 7.53 (s, 1H), 7.34 (m, 2H), 2.73 (t, *J* = 5.0 Hz, 2H), 1.79 (quintet, *J* = 5.0 Hz, 2H), 1.44-1.35 (m, 8H), 0.93 (t, *J* = 5.0 Hz, 3H); ^{13}C NMR ($CDCl_3$, 125 MHz) δ 141.91, 137.27, 136.91, 125.93, 123.89, 122.98, 31.59, 31.55, 29.04, 28.38, 22.57, 14.06.; GC-MS (*m/z*) Calcd for $C_{12}H_{16}SSe$ 272.01, found 272.05.

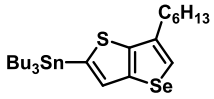

3-5

*Synthesis of 6-hexyl-2-tributylstannylselenopheno[3,2-b]thiophene (**3-5**).* To a stirred solution of **3-4** (2.71 g, 10.0 mmol) in dry THF (40 mL) was added LDA (11.0 mmol), which was freshly prepared from diisopropylamine (1.63 mL, 11.6 mmol) and *n*-BuLi (2.5 M in hexanes, 4.40 mL, 11.0 mmol) in dry THF (5.5 mL), at -40 ^{o}C (dry ice/ACN) under an argon atmosphere. After stirring at -40 ^{o}C for 1 hour, tributyltin chloride (3.26 mL, 12 mmol) was added in one portion under -40 ^{o}C. The reaction mixture was slowly warmed to room temperature overnight, quenched by addition of water and extracted with hexanes. The combined extracts were washed with brine, dried over anhydrous $MgSO_4$, and then filtered. The solvent was removed by rotary evaporation to give the stannylated compound **3-5** as a light yellow oil, which was used without further purification.

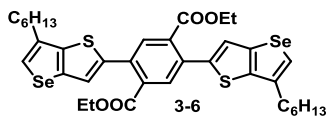

3-6

*Synthesis of 2,5-di(6-hexylselenopheno[3,2-b]thiophen-2-yl)terephthalic acid diethyl ester (**3-6**).* To a two-neck flask was added **3-5** (2.80 g, 5.00 mmol), 2,5-dibromo-terephthalic acid diethyl ester (760 mg, 2.00 mmol), $PdCl_2(PPh_3)_2$ (56 mg, 4 mol%) and anhydrous toluene (10 mL) under

an argon atmosphere. The reaction mixture was then heated at 110 ^{o}C for 1 day to give a light yellow solution. The solvent was removed by rotary evaporation, and the crude product was purified by column chromatography on silica gel with hexanes/CH_2Cl_2 (v/v = 2:1) as eluent to afford **3-6** as a yellow solid (1.03 g, 68 %). ^{1}H NMR ($CDCl_3$, 500 MHz) δ 7.88 (s, 2H), 7.53 (s, 2H), 7.32 (s, 2H), 4.25 (q, *J* = 5.0 Hz,, 4H), 2.71 (t, *J* = 5.0 Hz, 4H), 1.77 (quintet, *J* = 5.0 Hz, 4H), 1.41-1.32 (m, 16H), 1.14 (t, *J* = 5.0 Hz, 6H), 0.90 (t, *J* = 5.0 Hz, 3H); ^{13}C NMR ($CDCl_3$, 125 MHz) δ 167.63, 142.54, 140.78, 137.45, 137.07, 134.00, 133.53, 131.90, 124.32, 122.93, 61.77, 31.61, 31.55, 29.03, 28.43, 22.58, 14.07, 13.83.; MS (*m/z*, MALDI) Calcd for $C_{36}H_{42}O_4S_2Se_2$ 762.09, found 762.11.

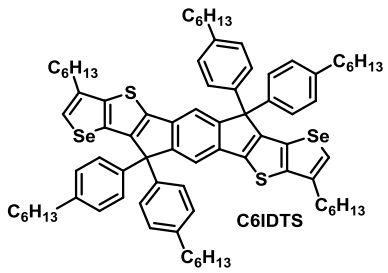

*Synthesis of 2,8-dihexyl-5,5,11,11-tetrakis(4-hexylphenyl)-diselenopheno[2,3-d:2',3'-d']-s-indaceno[1,2-b:5,6-b']dithiophene (**C6IDTS**).* To a solution of 4-hexyl-1-bromobenzene (1.00 g, 4.16 mmol) in anhydrous THF (20 mL) was added *n*-BuLi (2.5 M in hexanes, 1.58 mL, 3.96 mmol) at -78 ^{o}C under the protection of argon. After stirring at -78 ^{o}C for 1 hour, a solution of **3-6** (685 mg, 0.90 mmol) in anhydrous THF (9 mL) was added dropwise. The reaction mixture was then stirred at -78 ^{o}C for 3 hours, warmed to room temperature, poured into water and extracted with hexanse. The combined extracts were washed with brine, dried over anhydrous $MgSO_4$, and then filtered. The solvent was removed by rotary evaporation to yield a dark yellow oil, which was dissolved in anhydrous toluene (15 mL), followed by addition of amberlyst 15 (574 mg, ~3 meq)

and heated at 80 °C for 1 hour. The volatile species were removed by rotary evaporation, and the crude product was obtained as a dark yellow oil and further purified by column chromatography on silica gel with hexanes/CH_2Cl_2 (v/v = 8:1) as eluent to afford **C6IDTS** as a bright yellow solid (575 mg, 50%). ^{1}H NMR (C_6D_6, 500 MHz) δ 8.00 (s, 2H), 7.49 (d, *J* = 5.0 Hz, 8H), 6.96 (d, *J* = 5.0 Hz, 8H), 2.49 (t, *J* = 5.0 Hz, 4H), 2.40 (t, *J* = 5.0 Hz, 8H), 1.60 (m, 4H), 1.43 (m, 8H), 1.21-1.15 (m, 36H), 0.85 (m, 18H); ^{13}C NMR (C_6D_6, 125 MHz) δ 154.79, 150.79, 144.35, 142.03, 141.92, 141.16, 137.75, 136.91, 133.21, 129.07, 128.73, 124.39, 117.34, 64.04, 35.93, 32.04, 31.99, 31.62, 31.38, 29.43, 28.94, 22.93, 14.31.; MS (*m/z*, MALDI) Calcd for $C_{80}H_{98}S_2Se_2$ 1282.54, found 1282.39.

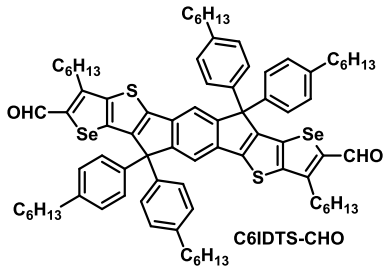

*Synthesis of 2,8-dihexyl-5,5,11,11-tetrakis(4-hexylphenyl)-diselenopheno[2,3-d:2',3'-d']-s-indaceno[1,2-b:5,6-b']dithiophene-3,9-dicarbaldehyde (**C6IDTS-CHO**).* To a solution of **C6IDTS** (385 mg, 0.30 mmol) in anhydrous 1,2-dichloroethane (15 mL) was added anhydrous DMF (372 μL, 4.80 mmol) under the protection of argon. The reaction mixture was then cooled with an ice bath, followed by slow addition of $POCl_3$ (337 μL, 3.60 mmol). After being kept at 0 °C for 10 minutes, the reaction mixture was heated to reflux for one day, cooled to room temperature, quenched with saturated aqueous solution of sodium acetate and extracted with CH_2Cl_2. The combined extracts were washed with brine, dried over anhydrous $MgSO_4$, and then filtered. The solvent was removed by rotary evaporation to yield the crude product, which was

then purified by column chromatography on silica gel with hexanes/CH_2Cl_2 (v/v = 1:3) as eluent to afford **C6IDTS-CHO** as a yellowish orange solid (340 mg, 85%). ^{1}H NMR ($CDCl_3$, 500 MHz) δ 9.92 (s, 2H), 7.61 (s, 2H), 7.11 (m, 16H), 3.06 (t, *J* = 5.0 Hz, 4H), 2.56 (t, *J* = 5.0 Hz, 8H), 1.80 (m, 4H), 1.58 (m, 8H), 1.42-1.28 (m, 36H), 0.88 (m, 18H); ^{13}C NMR ($CDCl_3$, 125 MHz) δ 182.56, 154.77, 150.37, 148.12, 147.34, 145.07, 142.23, 139.39, 138.81, 136.29, 128.67, 127.85, 117.95, 63.20, 35.55, 31.67, 31.47, 31.21, 30.49, 29.46, 29.28, 29.11, 22.55, 22.48, 14.05, 14.03.; MS (*m/z*, MALDI) Calcd for $C_{82}H_{98}O_2S_2Se_2$ 1338.53, found 1338.56.

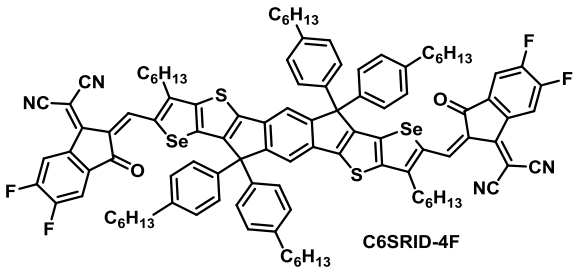

*Synthesis of 3,9-bis(2-methylene-(3-(1,1-dicyanomethylene)-5,6-difluoroindanone))-2,8-dihexyl-5,5,11,11-tetrakis(4-hexylphenyl)-diselenopheno[2,3-d:2',3'-d']-s-indaceno[1,2-b:5,6-b']dithiophene (**C6SRID-4F**).* To a solution of **C6IDTS-CHO** (161 mg, 0.12 mmol) and 2-(5,6-difluoro-3-oxo-2,3-dihydro-1H-inden-1-ylidene)malononitrile (69 mg, 0.30 mmol) in 1,2-dichloroethane (12 mL) and ethanol (6 mL) was added a grain of β-alanine. The reaction mixture was then heated overnight at 80 °C. After cooling to room temperature, the volatile species were removed by rotary evaporation. The crude product was then purified by column chromatography on silica gel with hexanes/CH_2Cl_2 (v/v = 3:2) as eluent to afford **C6SRID-4F** as a black solid (100 mg, 47%). ^{1}H NMR ($CDCl_3$, 500 MHz) δ 9.14 (s, 2H), 8.53 (m, 2H), 7.68 (s, 2H), 7.63 (t, *J* = 5.0 Hz, 2H), 7.17 (m, 16H), 3.14 (t, *J* = 5.0 Hz, 4H), 2.57 (t, *J* = 5.0 Hz, 8H), 1.76 (m, 4H), 1.60-1.28 (m, 56H), 0.87 (m, 18H); ^{13}C NMR ($CDCl_3$, 125 MHz) δ 186.61, 158.87, 156.23, 156.19, 155.37,

153.29, 152.00, 148.00, 147.94, 142.55, 138.95, 137.93, 137.03, 136.49, 136.43, 135.63, 134.38, 128.86, 127.87, 119.43, 118.84, 114.89, 114.54, 112.32, 99.97, 68.61, 63.34, 35.58, 31.68, 31.56, 31.41, 31.23, 29.51, 29.14, 22.56, 22.47, 14.05.; MS (m/z, MALDI) Calcd for $C_{106}H_{102}F_4N_4O_2S_2Se_2$ 1762.57, found 1762.56.

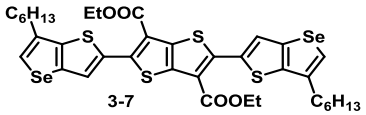

*Synthesis of 2,5-di(6-hexylselenopheno[3,2-b]thiophen-2-yl)thieno[3,2-b]thiophene-3,6-dicarboxylic acid diethyl ester (**3-7**).* To a two-neck flask was added **3-5** (2.80 g, 5.00 mmol), 2,5-dichlorothieno[3,2-*b*]thiophene-3,6-dicarboxylic acid diethyl ester (706 mg, 2.00 mmol), $Pd(PPh_3)_4$ (185 mg, 8 mol%) and anhydrous toluene (10 mL) under an argon atmosphere. The reaction mixture was then heated at 110 ^oC for 1 day to give a bright yellow solution. The solvent was removed by rotary evaporation, and the crude product was purified by column chromatography on silica gel with hexanes/CH_2Cl_2 (v/v = 3:1) as eluent to afford **3-7** as a bright yellow solid (921 mg, 56 %). ^1H NMR ($CDCl_3$, 500 MHz) δ 7.88 (s, 2H), 7.59 (s, 2H), 4.43 (q, *J* = 5.0 Hz, 4H), 2.72 (t, *J* = 5.0 Hz, 4H), 1.78 (quintet, *J* = 5.0 Hz, 4H), 1.45-1.33 (m, 16H), 0.90 (t, *J* = 5.0 Hz, 6H); ^{13}C NMR ($CDCl_3$, 125 MHz) δ 161.78, 146.60, 144.11, 137.45, 137.14, 134.21, 125.80, 119.50, 99.98, 61.43, 31.60, 31.48, 29.05, 28.43, 22.60, 14.30, 14.07.; MS (*m/z*, MALDI) Calcd for $C_{36}H_{40}O_4S_4Se_2$ 824.01, found 823.97.

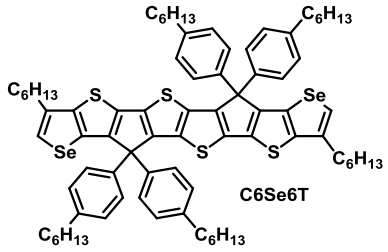

*Synthesis of 2,8-dihexyl-5,5,11,11-tetrakis(4-hexylphenyl)thieno[2',3':4,5]thieno[3,2-]thieno[2'''',3'''':4''',5''']-thieno[2''',3''':4'',5'']cyclopentadieno[2'',3'':4',5']thieno[2',3':4,5]thieno[2,3-d]cyclopentadiene (**C6Se6T**).* To a flame-dried two-neck flask was added magnesium turnings (61 mg, 2.50 mmol) and anhydrous THF (5 mL), followed by slow addition of 4-hexyl-1-bromobenzene (615 mg, 2.55 mmol). The reaction mixture was heated to reflux for 1 hour after the addition to give the Grignard reagent. After cooling to room temperature, the Grignard reagent was cannulated to a solution of **3-7** (411 mg, 0.50 mmol) in anhydrous THF (5 mL) at 0 ^{o}C. The reaction mixture was then refluxed overnight, cooled to room temperature, quenched by addition of saturated aqueous solution of ammonium chloride and extracted with hexanes. The combined extracts were washed with brine, dried over anhydrous $MgSO_4$, and then filtered. The solvent was removed by rotary evaporation to yield a dark yellow oil, which was dissolved in anhydrous toluene (10 mL), followed by addition of amberlyst 15 (320 mg, ~3 meq) and heated at 80 ^{o}C for 1 hour. The volatile species were removed by rotary evaporation, and the crude product was obtained as a dark yellow oil and purified by flash column chromatography on silica gel with hexanes/CH_2Cl_2 (v/v = 10:1) as eluent to afford **C6Se6T** as a yellow sticky oil (403 mg, 60%), which was used immediately without further purification. **C6Se6T** is not stable under storage, and the ^{1}H NMR, ^{13}C NMR and MS spectra were not collected due to the instability of the compound.

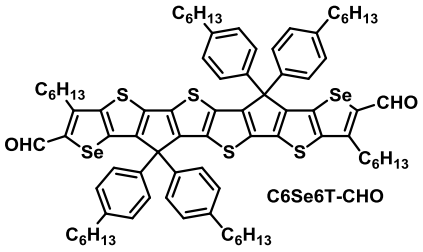

*Synthesis of 2,8-dihexyl-5,5,11,11-tetrakis(4-hexylphenyl)thieno[2',3':4,5]thieno[3,2-]thieno[2'''',3'''':4''',5''']-thieno[2''',3''':4'',5'']cyclopentadieno[2'',3'':4',5']thieno[2',3':4,5]thieno[2,3-d]cyclopentadiene-3,9-dicarbaldehyde (**C6Se6T-CHO**).* To a solution of **C6Se6T** (403 mg, 0.30 mmol) in anhydrous 1,2-dichloroethane (15 mL) was added anhydrous DMF (372 μL, 4.80 mmol) under the protection of argon. The reaction mixture was then cooled with an ice bath, followed by slow addition of $POCl_3$ (337 μL, 3.60 mmol). After being kept at 0 ^oC for 10 minutes, the reaction mixture was heated at 60 ^oC overnight, cooled to room temperature, quenched with saturated aqueous solution of sodium acetate and extracted with CH_2Cl_2. The combined extracts were washed with brine, dried over anhydrous $MgSO_4$, and then filtered. The solvent was removed by rotary evaporation to yield the crude product, which was then purified by column chromatography on silica gel with hexanes/CH_2Cl_2 (v/v = 1:2) as eluent to afford **C6Se6T-CHO** as a reddish orange solid (230 mg, 55%). ^1H NMR ($CDCl_3$, 500 MHz) δ 9.91 (s, 2H), 7.12 (m, 16H), 3.04 (t, *J* = 5.0 Hz, 4H), 2.55 (t, *J* = 5.0 Hz, 8H), 1.79 (quintet, *J* = 5.0 Hz, 4H), 1.59-1.53 (m, 8H), 1.42-1.23 (m, 36H), 0.88 (t, *J* = 5.0 Hz, 18H); ^{13}C NMR ($CDCl_3$, 125 MHz) δ 182.24, 151.18, 150.69, 148.09, 143.61, 143.39, 142.63, 141.21, 138.73, 138.11, 137.31, 136.46, 128.94, 127.73, 62.44, 35.59, 31.65, 31.45, 31.14, 30.52, 29.40, 29.28, 29.12, 22.54, 22.49, 14.04.; MS (*m/z*, MALDI) Calcd for $C_{82}H_{96}O_2S_4Se_2$ 1400.46, found 1400.29.

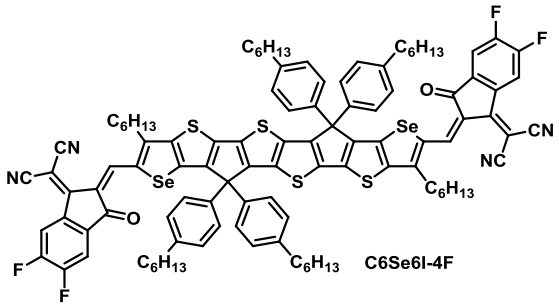

*Synthesis of 3,9-bis(2-methylene-(3-(1,1-dicyanomethylene)-5,6-difluoroindanone))-2,8-dihexyl-5,5,11,11-tetrakis(4-hexylphenyl)thieno[2',3':4,5]thieno[3,2-]thieno[2'''',3'''':4''',5''']-thieno[2''',3''':4'',5'']cyclopentadieno[2'',3'':4',5']thieno[2',3':4,5]thieno[2,3-d]cyclopentadiene (**C6Se6I-4F**).* To a solution of **C6Se6T-CHO** (140 mg, 0.10 mmol) and 2-(5,6-difluoro-3-oxo-2,3-dihydro-1H-inden-1-ylidene)malononitrile (92 mg, 0.40 mmol) in chloroform (10 mL) was added pyridine (0.20 mL). The reaction mixture was then kept at room temperature until the completion of the reaction (ca. 1 day), after which the volatile species were removed by rotary evaporation. The crude product was then purified by column chromatography on silica gel with hexanes/CH_2Cl_2 (v/v = 3:2) as eluent to afford **C6Se6I-4F** as a black solid (120 mg, 66%). ^{1}H NMR ($CDCl_3$, 500 MHz) δ 9.10 (s, 2H), 8.52 (quartet, *J* = 5.0 Hz, 2H), 7.66 (t, *J* = 5.0 Hz, 2H), 7.17 (m, 16H), 3.09 (t, *J* = 5.0 Hz, 4H), 2.55 (t, *J* = 5.0 Hz, 8H), 1.76-1.26 (m, 48H), 0.86 (m, 18H); ^{13}C NMR ($CDCl_3$, 125 MHz) δ 186.67, 158.79, 156.02, 155.24, 153.46, 148.47, 147.77, 147.10, 143.00, 139.93, 138.35, 137.37, 136.76, 135.07, 134.30, 129.16, 127.72, 118.74, 115.11, 115.00, 114.95, 114.74, 112.33, 112.18, 67.85, 62.56, 35.60, 31.64, 31.54, 31.35, 31.16, 29.50, 29.14, 22.54, 22.47, 14.03.; MS (m/z, MALDI) Calcd for $C_{106}H_{100}F_4N_4O_2S_4Se_2$ 1824.50, found 1594.41.

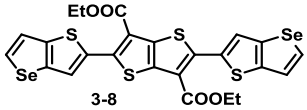

*Synthesis of 2,5-di(selenopheno[3,2-b]thiophen-2-yl)thieno[3,2-b]thiophene-3,6-dicarboxylic acid diethyl ester (**3-8**).* To a two-neck flask was added **2-8** (1.62 g, 3.40 mmol), 2,5-dichlorothieno[3,2-*b*]thiophene-3,6-dicarboxylic acid diethyl ester (565 mg, 1.60 mmol), $Pd(PPh_3)_4$ (148 mg, 8 mol%) and anhydrous toluene (8 mL) under an argon atmosphere. The reaction mixture was then heated at 110 ^oC for 1 day. After cooling to room temperature, cold acetone was added to the reaction mixture, followed by filtration to collect **3-8** as a dark orange solid (1.03 g, 98%), which was used without further purification. ^1H NMR and ^{13}C NMR were not collected due to the poor solubility of the compound in various solvents. MS (*m/z*, MALDI) Calcd for $C_{24}H_{16}O_4S_4Se_2$ 655.83, found 655.71.

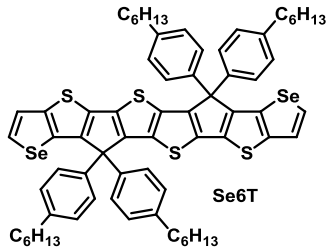

Se6T

*Synthesis of 5,5,11,11-tetrakis(4-hexylphenyl)thieno[2',3':4,5]thieno[3,2-]thieno[2'''',3'''':4''',5''']-thieno[2''',3''':4'',5'']cyclopentadieno[2'',3'':4',5']thieno[2',3':4,5]thieno[2,3-d]cyclopentadiene (**Se6T**).* To a flame-dried two-neck flask was added magnesium turnings (199 mg, 8.20 mmol) and anhydrous THF (16 mL), followed by slow addition of 4-hexyl-1-bromobenzene (1.93 mg, 8.00 mmol). The reaction mixture was heated to reflux for 1 hour after the addition to give the Grignard reagent. After cooling to room temperature, the Grignard reagent was cannulated to a suspension of **3-8** (1.05 mg, 1.60 mmol) in anhydrous THF (8 mL) at 0 ^oC. The reaction mixture was then refluxed overnight, cooled to room temperature, quenched by addition of saturated aqueous solution of ammonium chloride and extracted with hexanes. The

combined extracts were washed with brine, dried over anhydrous $MgSO_4$, and then filtered. The solvent was removed by rotary evaporation to yield a dark yellow oil, which was dissolved in anhydrous toluene (25 mL), followed by addition of amberlyst 15 (1.02 g, ~3 meq) and heated at 80 ^oC for 1 hour. The volatile species were removed by rotary evaporation, and the crude product was obtained as a dark yellow oil and purified by flash column chromatography on silica gel with hexanes/CH_2Cl_2 (v/v = 1:5) as eluent to afford **Se6T** as a dark yellow solid (510 mg, 27%), which was used immediately without further purification. **Se6T** is not stable under storage, and the ^1H NMR, ^{13}C NMR and MS spectra were not collected due to the instability of the compound.

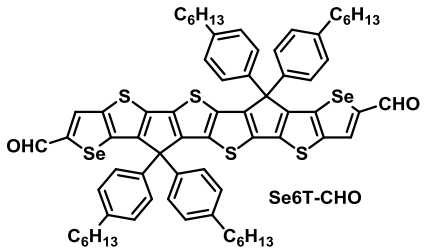

*Synthesis of 5,5,11,11-tetrakis(4-hexylphenyl)thieno[2',3':4,5]thieno[3,2-]thieno[2''',3''':4''',5''']-thieno[2''',3''':4'',5'']cyclopentadieno[2'',3'':4',5']thieno[2',3':4,5]thieno[2,3-d]cyclopentadiene-3,9-dicarbaldehyde (**Se6T-CHO**).* To a solution of **Se6T** (353 mg, 0.30 mmol) in anhydrous 1,2-dichloroethane (15 mL) was added anhydrous DMF (372 μL, 4.80 mmol) under the protection of argon. The reaction mixture was then cooled with an ice bath, followed by slow addition of $POCl_3$ (337 μL, 3.60 mmol). After being kept at 0 ^oC for 10 minutes, the reaction mixture was heated at 60 ^oC for 5 hours, cooled to room temperature, quenched with saturated aqueous solution of sodium acetate and extracted with CH_2Cl_2. The combined extracts were washed with brine, dried over anhydrous $MgSO_4$, and then filtered. The solvent was removed by

rotary evaporation to yield the crude product, which was then purified by column chromatography on silica gel with hexanes/CH_2Cl_2 (v/v = 2:3) as eluent to afford **Se6T-CHO** as a reddish orange solid (290 mg, 79%). ^{1}H NMR ($CDCl_3$, 500 MHz) δ 9.76 (s, 2H), 8.14 (s, 2H), 7.12 (m, 16H), 2.55 (t, *J* = 5.0 Hz, 8H), 1.57 (m, 8H), 1.33-1.28 (m, 24H), 0.86 (t, *J* = 5.0 Hz, 12H); ^{13}C NMR ($CDCl_3$, 125 MHz) δ 183.50, 150.84, 147.50, 144.91, 142.73, 141.16, 140.03, 138.23, 137.16, 136.47, 132.56, 129.01, 127.67, 62.35, 35.58, 31.64, 31.14, 29.10, 22.54, 14.04.; MS (*m/z*, MALDI) Calcd for $C_{70}H_{72}O_2S_4Se_2$ 1232.27, found 1232.27.

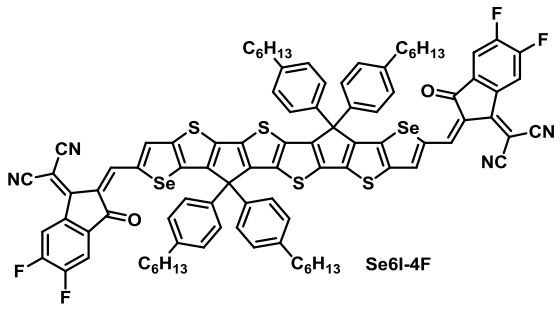

*Synthesis of 3,9-bis(2-methylene-(3-(1,1-dicyanomethylene)-5,6-difluoroindanone))-5,5,11,11-tetrakis(4-hexylphenyl)thieno[2',3':4,5]thieno[3,2-]thieno[2'''',3'''':4''',5''']-thieno[2''',3''':4'',5'']cyclopentadieno[2'',3'':4',5']thieno[2',3':4,5]thieno[2,3-d]cyclopentadiene (**Se6I-4F**).* To a solution of **Se6T-CHO** (197 mg, 0.16 mmol) and 2-(5,6-difluoro-3-oxo-2,3-dihydro-1H-inden-1-ylidene)malononitrile (147 mg, 0.64 mmol) in chloroform (16 mL) was added pyridine (0.32 mL). The reaction mixture was then kept at room temperature until the completion of the reaction (ca. 1 day), after which the volatile species were removed by rotary evaporation. The crude product was then purified by column chromatography on silica gel with hexanes/CH_2Cl_2 (v/v = 2:3) as eluent to afford **Se6T-4F** as a black solid (230 mg, 87%). ^{1}H NMR ($CDCl_3$, 500 MHz) δ 8.95 (s, 2H), 8.48 (quartet, *J* = 5.0 Hz, 2H), 8.12 (s, 2H), 7.63 (t, *J* = 5.0 Hz, 2H), 7.18 (s, 16H), 2.57 (t, *J* = 5.0 Hz, 8H), 1.59 (quintet, *J* = 5.0 Hz, 8H),

1.34-1.27 (m, 24H), 0.85 (t, *J* = 5.0 Hz, 12H); ^{13}C NMR ($CDCl_3$, 125 MHz) δ 186.70, 157.81, 155.51, 153.39, 153.16, 152.67, 150.68, 150.01, 144.24, 143.06, 141.05, 140.93, 140.05, 138.27, 136.70, 134.21, 129.23, 127.70, 119.91, 114.98, 114.34, 112.49, 112.34, 69.02, 62.40, 35.60, 31.65, 31.18, 29.12, 22.54, 14.04.; MS (m/z, MALDI) Calcd for $C_{94}H_{76}F_4N_4O_2S_4Se_2$ 1656.31, found 1656.24.

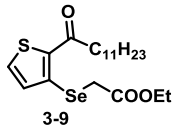

3-9

*Synthesis of ethyl [2-(lauroylthiophen-3-yl)selanyl]acetate. (**3-9**)* To a stirred solution of ethyl 2-(thiophen-3-ylselanyl)acetate (**3-1**, 15.0 g, 60.0 mmol) and lauroyl chloride (15.3 mL, 66.0 mmol) in dry toluene (60 mL) was dropwise added a solution of tin(IV) chloride (7.34 mL, 63.0 mmol) in dry toluene (30 mL) at -10 ^{o}C. The mixture was kept at -10 ^{o}C for 30 minutes, and then stirred at room temperature overnight. The reaction was quenched by addition of 10% HCl in aqueous solution and extracted with CH_2Cl_2. The combined extracts were washed with brine, dried over anhydrous $MgSO_4$, and then filtered. The solvent was removed by rotary evaporation to give the crude product as a brown oil, which was further purified by column chromatography on silica gel with hexanes/CH_2Cl_2 (v/v = 2:1) as eluent to afford **3-9** as a yellow oil (22.7 g, 88%), which slowly solidified under prolonged storage. ^{1}H NMR ($CDCl_3$, 500 MHz) δ 7.54 (d, *J* = 5.0 Hz, 1H), 7.35 (d, *J* = 5.0 Hz, 1H), 4.16 (q, *J* = 5.0 Hz, 2H), 3.56 (s, 2H), 2.79 (t, *J* = 5.0 Hz, 2H), 1.73 (quintet, *J* = 5.0 Hz, 2H), 1.35-1.22 (m, 19H), 0.86 (t, *J* = 5.0 Hz, 3H); ^{13}C NMR ($CDCl_3$, 125 MHz) δ 193.09, 171.06, 138.50, 132.21, 131.19, 128.71, 61.40, 40.52, 31.84, 29.54, 29.38, 29.34, 29.25, 29.24, 25.56, 24.60, 22.61, 14.03, 14.00; GC-MS (*m/z*) Calcd for $C_{20}H_{32}O_3SSe$ 432.12, found 432.08.

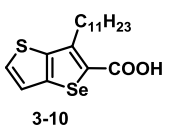

3-10

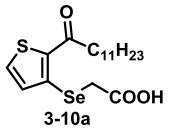

3-10a

*Synthesis of 6-undecylselenopheno[3,2-b]thiophene-5-carboxylic acid (**3-10**).* At room temperature, a solution of **3-9** (23.5 g, 35.0 mmol) in absolute ethanol (65 mL) was dropwise added into a solution of NaOEt, which was freshly prepared from sodium (4.48 g, 195 mmol) and absolute ethanol (130 mL), under an argon atmosphere to form a thick yellow slurry. The mixture was then refluxed overnight, after which the solvents were removed by rotary evaporation. The residue was dissolved in water and acidified with 10% HCl in aqueous solution, followed by extraction using ethyl acetate. The combined extracts were washed with brine, dried over anhydrous $MgSO_4$, and then filtered. The solvent was removed by rotary evaporation to give the crude product as a brown solid, which was further purified by column chromatography on silica gel with CH_2Cl_2 as eluent to afford **3-10** as a white solid (8.72 g, 43%). A portion of **3-9** hydrolyzed before forming the desired cyclized product during the reaction, giving [2-(lauroylthiophen-3-yl)selanyl]acetic acid (**3-10a**), which was recovered using ethyl acetate/CH_2Cl_2 (v/v = 1:3) as eluent, also as a white solid (8.35 g, 39%). ^{1}H NMR (*d*$_6$-DMSO, 500 MHz) δ 7.84 (d, *J* = 5.0 Hz, 1H), 7.52 (d, *J* = 5.0 Hz, 1H), 3.08 (t, *J* = 5.0 Hz, 2H), 1.64 (quintet, *J* = 5.0 Hz, 2H), 1.31-1.21 (m, 16H), 0.84 (t, *J* = 5.0 Hz, 3H); ^{13}C NMR (*d*$_6$-DMSO, 125 MHz) δ 164.88, 143.91, 142.67, 139.65, 131.70, 130.65, 124.12, 31.24, 29.71, 28.94, 28.85, 28.82, 28.65, 28.64, 22.05, 13.90.; GC-MS (*m/z*) Calcd for $C_{18}H_{26}O_2SSe$ 386.08, found 386.09.

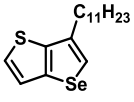

3-11

*Synthesis of 6-undecylselenopheno[3,2-b]thiophene (**3-11**).* A mixture of **3-10** (3.85 g, 10.0 mmol) and silver carbonate (110 mg, 0.40 mmol) in DMSO (15 mL) was added acetic acid (46 μL, 0.80 mmol), and then heated at 120 ^{o}C overnight. The reaction mixture was then cooled to room temperature and passed through a celite pad to remove the inorganic residues. The celite pad was rinsed with diethyl ether for several times, and the combined filtrates were extracted with water. The combined extracts were washed with brine, dried over anhydrous $MgSO_4$, and then filtered. The solvent was removed by rotary evaporation to give the crude product as a light brown oil, which was further purified by column chromatography on silica gel with hexanes as eluent to afford **3-11** as a colorless oil (3.41 g, quant.). ^{1}H NMR ($CDCl_3$, 500 MHz) δ 7.51 (s, 1H), 7.33 (m, 2H), 2.71 (t, *J* = 5.0 Hz, 2H), 1.77 (quintet, *J* = 5.0 Hz, 2H), 1.40-1.28 (m, 16H), 0.90 (t, *J* = 5.0 Hz, 3H); ^{13}C NMR ($CDCl_3$, 125 MHz) δ 141.93, 137.28, 136.95, 125.95, 123.89, 123.00, 31.91, 31.56, 29.65, 29.62, 29.56, 29.40, 29.38, 29.33, 28.42, 22.68, 14.10; GC-MS (*m/z*) Calcd for $C_{17}H_{26}SSe$ 342.09, found 342.10.

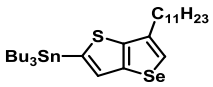

3-12

*Synthesis of 6-undecyl-2-tributylstannylselenopheno[3,2-b]thiophene (**3-12**).* To a stirred solution of **3-11** (3.41 g, 10.0 mmol) in dry THF (40 mL) was added LDA (11.0 mmol), which was freshly prepared from diisopropylamine (1.63 mL, 11.6 mmol) and *n*-BuLi (2.5 M in hexanes, 4.40 mL, 11.0 mmol) in dry THF (5.5 mL), at -40 ^{o}C (dry ice/ACN) under an argon atmosphere. After stirring at -40 ^{o}C for 1 hour, tributyltin chloride (3.26 mL, 12.0 mmol) was added in one portion under -40 ^{o}C. The reaction mixture was slowly warmed to room temperature overnight, quenched by addition of water and extracted with hexanes. The combined extracts were washed with brine,

dried over anhydrous $MgSO_4$, and then filtered. The solvent was removed by rotary evaporation to give the stannylated compound **3-12** as a light yellow oil, which was used without further purification.

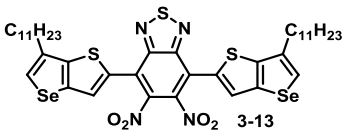

*Synthesis of 5,6-dinitro-4,7-bis(6-undecylselenopheno[3,2-b]thiophen-2-yl)benzo[c]-[1,2,5]thiadiazole (**3-13**).* A mixture of **3-12** (2.84 g, 4.50 mmol), 4,7-dibromo-5,6-dinitro[2,1,3] benzothiadiazole (787 mg, 2.05 mmol), $Pd_2(dba)_3$ (18 mg, 1 mol%) and tri(*o*-tolyl)phosphine (49 mg, 8 mol%) in dry toluene (10 mL) was stirred under protection of argon at room temperature for 3 days. The solvents were then removed by rotary evaporation, and the residue was subjected onto a silica gel column then eluted with hexanes/CH_2Cl_2 (v/v = 4:1) to afford **3-13** as a dark red solid (1.60 g, 86%). ^{1}H NMR ($CDCl_3$, 500 MHz) δ 7.75 (s, 2H), 7.71 (s, 2H), 2.75 (t, *J* = 5.0 Hz, 4H), 1.79 (quintet, *J* = 5.0 Hz, 4H), 1.42-1.27 (m, 32H), 0.88 (t, *J* = 5.0 Hz, 6H); ^{13}C NMR ($CDCl_3$, 125 MHz) δ 152.20, 146.69, 141.70, 137.80, 137.09, 129.55, 127.84, 127.07, 121.13, 31.90, 31.41, 29.65, 29.62, 29.56, 29.38, 29.33, 28.38, 22.67, 14.09; MS (m/z, MALDI) Calcd for $C_{40}H_{50}N_4O_2S_3Se_2$ 906.13, found 906.09.

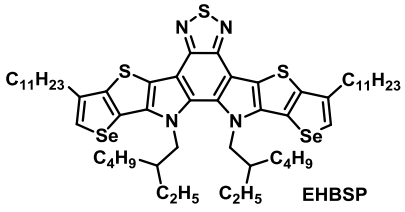

*Synthesis of 12,13-bis(2-ethylhexyl)-3,9-diundecyl-diselenopheno[2'',3'':4',5']thieno[2',3':4,5] pyrrolo[3,2-e:2',3'-g][2,1,3]benzothiadiazole (**EHBSP**).* To a solution of **3-13** (633 mg, 0.70

mmol) in degassed 1,2-dicholorobenzene (3.5 mL) was added freshly distilled $P(OEt)_3$ (2.40 mL, 14.0 mmol) under protection of argon. The reaction mixture was then refluxed overnight, cooled to room temperarture and precipitated with cold methanol. The crude product was collected by filtration as a bright orange solid, which was then dissolved in anhydrous DMF (7 mL) and added 2-ethylhexyl bromide (744 μL, 4.2 mmol), potassium iodide (46 mg, 0.28 mmol) and potassium carbonate (774 mg, 5.6 mmol) under an argon atmosphere. The reaction mixture was then heated at 90 ^oC for 1 day, quenched by addition of water and extracted with CH_2Cl_2. The combined extracts were washed with brine, dried over anhydrous $MgSO_4$, and then filtered. The solvent was removed by rotary evaporation to give the crude product as a brown oil, which was further purified by column chromatography on silica gel with hexanes/CH_2Cl_2 (v/v = 5:1) as eluent to afford **EHBSP** as an orange oil (230 mg, 31%). ^1H NMR (C_6D_6, 500 MHz) δ 7.16 (s, 2H, overlapped with C_6D_6), 4.71 (m, 4H), 2.62 (t, J = 5.0 Hz, 4H), 2.19 (m, 2H), 1.73 (m, 4H), 1.43-1.28 (m, 32H), 0.94-0.85 (m, 22H), 0.60-0.49 (m, 12H); ^{13}C NMR (C_6D_6, 125 MHz) δ 148.32, 144.41, 141.10, 139.18, 132.63, 123.28, 122.50, 122.35, 112.48, 55.13, 40.45, 32.37, 31.30, 30.23, 30.14, 30.05, 29.98, 29.85, 29.77, 29.05, 28.01, 27.93, 23.48, 23.14, 23.03, 14.39, 13.92, 10.14, 10.06; MS (m/z, MALDI) Calcd for $C_{56}H_{82}N_4S_3Se_2$ 1066.40, found 1066.36.

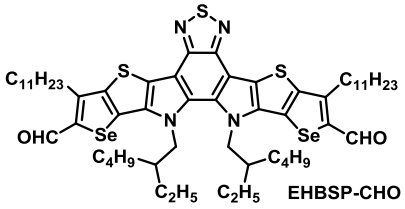

*Synthesis of 12,13-bis(2-ethylhexyl)-3,9-diundecyl-diselenopheno[2'',3'':4',5']thieno[2',3':4,5] pyrrolo[3,2-e:2',3'-g][2,1,3]benzothiadiazole-2,10-dicarbaldehyde (**EHBSP-CHO**).* To a solution of **EHBSP** (223 mg, 0.21 mmol) in anhydrous 1,2-dichloroethane (6 mL) was added

anhydrous DMF (260 μL, 3.36 mmol) under the protection of argon. The reaction mixture was then cooled with an ice bath, followed by slow addition of $POCl_3$ (236 μL, 2.52 mmol). After being kept at 0 ^oC for 10 minutes, the reaction mixture was heated at 80 ^oC overnight, cooled to room temperature, quenched with saturated aqueous solution of sodium acetate and extracted with CH_2Cl_2. The combined extracts were washed with brine, dried over anhydrous $MgSO_4$, and then filtered. The solvent was removed by rotary evaporation to yield the crude product, which was then purified by column chromatography on silica gel with hexanes/CH_2Cl_2 (v/v = 2:3) as eluent to afford **EHBSP-CHO** as a reddish orange solid (220 mg, 93%). ^1H NMR ($CDCl_3$, 500 MHz) δ 10.04 (s, 2H), 4.60 (m, 4H), 3.18 (t, *J* = 5.0 Hz, 4H), 2.02-1.90 (m, 6H), 1.49-1.26 (m, 32H), 1.05-0.85 (m, 22H), 0.67-0.58 (m, 12H); ^{13}C NMR ($CDCl_3$, 125 MHz) δ 182.42, 149.21, 147.59, 144.51, 141.10, 140.49, 133.21, 128.37, 126.54, 112.10, 55.02, 40.21, 31.88, 30.67, 29.69, 29.60, 29.58, 29.49, 29.35, 29.30, 27.58, 23.13, 22.66, 14.08, 13.63, 10.05; MS (*m/z*, MALDI) Calcd for $C_{58}H_{82}O_2S_3Se_2$ 1122.39, found 1122.26.

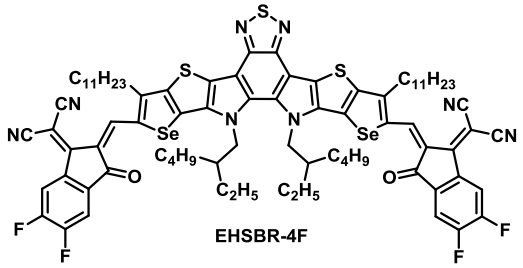

*Synthesis of 2,10-bis(2-methylene-(3-(1,1-dicyanomethylene)-5,6-difluoroindanone))- 12,13-bis(2-ethylhexyl)-3,9-diundecyl-diselenopheno[2'',3'':4',5']thieno[2',3':4,5]pyrrolo[3,2-e:2', 3'-g][2,1,3]benzothiadiazole (**EHSBR-4F**).* To a solution of **EHBSP-CHO** (157 mg, 0.14 mmol) and 2-(5,6-difluoro-3-oxo-2,3-dihydro-1H-inden-1-ylidene)malononitrile (129 mg, 0.56 mmol) in 1,2-dichloroethane (14 mL) and ethanol (7 mL) was added a grain of β-alanine. The reaction

mixture was then heated overnight at 80 ^{o}C. After cooling to room temperature, the volatile species were removed by rotary evaporation. The crude product was then purified by column chromatography on silica gel with hexanes/$CHCl_3$ (v/v = 3:1) as eluent to afford **EHSBR-4F** as a black solid (150 mg, 69%). ^{1}H NMR ($CDCl_3$, 500 MHz) δ 9.21 (s, 2H), 8.50 (quartet, *J* = 5.0 Hz, 2H), 7.71 (t, *J* = 5.0 Hz, 2H), 4.74 (m, 4H), 3.22 (t, *J* = 5.0 Hz, 4H), 2.17 (m, 2H), 1.85 (m, 4H), 1.51 (m, 4H), 1.36-0.95 (m, 44H), 0.86 (t, *J* = 5.0 Hz, 6H), 0.78 (t, *J* = 5.0 Hz, 6H), 0.67 (t, *J* = 5.0 Hz, 6H); ^{13}C NMR ($CDCl_3$, 125 MHz) δ 186.92, 158.53, 156.94, 153.47, 153.30, 153.24, 147.53, 142.02, 137.72, 137.58, 136.58, 134.37, 134.06, 129.74, 119.15, 115.05, 114.91, 114.50, 113.62, 112.56, 112.41, 68.61, 55.69, 40.26, 31.90, 31.55, 31.31, 29.91, 29.69, 29.62, 29.61, 29.50, 29.46, 29.32, 27.69, 23.29, 22.76, 22.66, 14.08, 13.70, 10.32; MS (m/z, MALDI) Calcd for $C_{82}H_{86}F_4N_8O_2S_3Se_2$ 1546.43, found 1546.75.

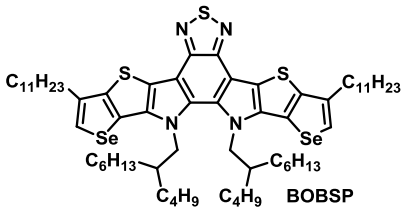

*Synthesis of 12,13-bis(2-butyloctyl)-3,9-diundecyl-diselenopheno[2'',3'':4',5']thieno[2',3':4,5] pyrrolo[3,2-e:2',3'-g][2,1,3]benzothiadiazole (**BOBSP**).* To a solution of **3-13** (723 mg, 0.80 mmol) in degassed 1,2-dicholorobenzene (4 mL) was added freshly distilled $P(OEt)_3$ (2.74 mL, 16.0 mmol) under protection of argon. The reaction mixture was then refluxed overnight, cooled to room temperarture and precipitated with cold methanol. The crude product was collected by filtration as a bright orange solid, which was then dissolved in anhydrous DMF (16 mL) and added 2-butyloctyl iodide (1.42 g, 4.80 mmol) and freshly ground sodium hydroxide (256 mg, 6.40 mmol) under an argon atmosphere. The reaction mixture was then heated at 70 ^{o}C for 1 day, quenched by

addition of water and extracted with CH_2Cl_2. The combined extracts were washed with brine, dried over anhydrous $MgSO_4$, and then filtered. The solvent was removed by rotary evaporation to give the crude product as an orange oil, which was further purified by column chromatography on silica gel with hexanes/CH_2Cl_2 (v/v = 8:1) as eluent to afford **BOBSP** as a yellowish orange solid (545 mg, 58 %). ^{1}H NMR (C_6D_6, 500 MHz) δ 7.15 (s, 2H, overlapped with C_6D_6), 4.76 (m, 4H), 2.63 (t, *J* = 5.0 Hz, 4H), 2.28 (m, 2H), 1.74 (m, 4H), 1.31-1.29 (m, 32H), 1.04-0.61 (m, 50H); ^{13}C NMR (C_6D_6, 125 MHz) δ 148.31, 144.44, 139.15, 132.86, 123.45, 122.36, 112.52, 55.28, 39.23, 32.36, 32.03, 31.29, 30.13, 30.04, 29.84, 29.76, 29.06, 23.14, 22.90, 14.38, 14.27, 13.98; MS (m/z, MALDI) Calcd for $C_{64}H_{98}N_4S_3Se_2$ 1178.53, found 1178.32.

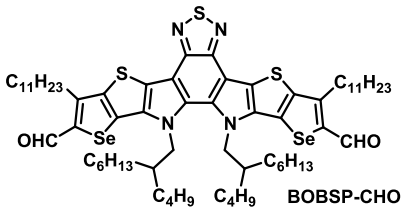

*Synthesis of 12,13-bis(2-butyloctyl)-3,9-diundecyl-diselenopheno[2'',3'':4',5']thieno[2',3':4,5] pyrrolo[3,2-e:2',3'-g][2,1,3]benzothiadiazole-2,10-dicarbaldehyde (**BOBSP-CHO**).* To a solution of **BOBSP** (471 mg, 0.40 mmol) in anhydrous 1,2-dichloroethane (12 mL) was added anhydrous DMF (496 μL, 6.40 mmol) under the protection of argon. The reaction mixture was then cooled with an ice bath, followed by slow addition of $POCl_3$ (449 μL, 4.80 mmol). After being kept at 0 ^{o}C for 10 minutes, the reaction mixture was heated at 80 ^{o}C overnight, cooled to room temperature, quenched with saturated aqueous solution of sodium acetate and extracted with CH_2Cl_2. The combined extracts were washed with brine, dried over anhydrous $MgSO_4$, and then filtered. The solvent was removed by rotary evaporation to yield the crude product, which was then purified by column chromatography on silica gel with hexanes/CH_2Cl_2 (v/v = 4:3) as eluent

to afford **BOBSP-CHO** as a reddish orange solid (480 mg, 97%). ^{1}H NMR ($CDCl_3$, 500 MHz) δ 10.04 (s, 2H), 4.59 (m, 4H), 3.19 (t, *J* = 5.0 Hz, 4H), 2.04 (m, 2H), 1.93 (m, 4H), 1.31-1.29 (m, 32H), 1.04-0.61 (m, 38H), 0.67-0.68 (m, 12H); ^{13}C NMR ($CDCl_3$, 125 MHz) δ182.42, 149.21, 147.54, 144.55, 141.10, 140.50, 133.44, 128.41, 126.74, 112.12, 55.14, 38.99, 31.89, 31.50, 30.68, 30.41, 30.26, 29.70, 29.61, 29.58, 29.50, 29.36, 29.30, 28.01, 25.01, 22.73, 22.66, 22.42, 22.39, 14.08, 13.91, 13.69, 13.65; MS (*m/z*, MALDI) Calcd for $C_{66}H_{98}N_4O_2S_3Se_2$ 1234.52, found 1234.64.

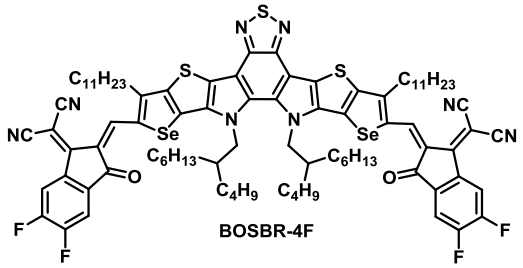

*Synthesis of 2,10-bis(2-methylene-(3-(1,1-dicyanomethylene)-5,6-difluoroindanone))- 12,13-bis(2-butyloctyl)-3,9-diundecyl-diselenopheno[2'',3'':4',5']thieno[2',3':4,5]pyrrolo[3,2-e:2',3'-g][2,1,3]benzothiadiazole (**BOSBR-4F**).* To a solution of **BOBSP-CHO** (222 mg, 0.18 mmol) and 2-(5,6-difluoro-3-oxo-2,3-dihydro-1H-inden-1-ylidene)malononitrile (166 mg, 0.72 mmol) in chloroform (18 mL) was added pyridine (0.36 mL). The reaction mixture was then kept at room temperature until the completion of the reaction (ca. 1 day), after which the volatile species were removed by rotary evaporation. The crude product was then purified by column chromatography on silica gel with hexanes/CH_2Cl_2 (v/v = 4:3) as eluent to afford **BOSBR-4F** as a black solid (280 mg, 94%). ^{1}H NMR ($CDCl_3$, 500 MHz) δ 9.24 (s, 2H), 8.53 (quartet, *J* = 5.0 Hz, 2H), 7.70 (t, *J* = 5.0 Hz, 2H), 4.72 (m, 4H), 3.23 (t, *J* = 5.0 Hz, 4H), 2.19 (m, 2H), 1.85 (m, 4H), 1.52 (m, 4H), 1.36-0.85 (m, 66H), 0.71-0.64 (m, 12H); ^{13}C NMR ($CDCl_3$, 125 MHz) δ 186.86, 158.59, 156.87, 155.37, 153.29, 147.53, 147.42, 141.91, 137.76, 137.62, 136.52, 134.33, 134.08, 130.00, 119.14,

114.92, 114.53, 113.56, 112.36, 68.61, 55.78, 39.02, 31.90, 31.57, 31.53, 31.30, 30.45, 30.36, 29.92, 29.64, 29.61, 29.50, 29.47, 29.33, 28.04, 27.89, 25.45, 25.30, 22.78, 22.74, 22.67, 22.45, 14.09, 13.98, 13.74, 13.71; MS (m/z, MALDI) Calcd for $C_{90}H_{102}F_4N_8O_2S_3Se_2$ 1658.56, found 1658.95.

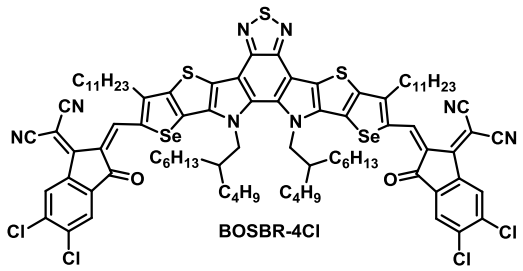

*Synthesis of 2,10-bis(2-methylene-(3-(1,1-dicyanomethylene)-5,6-dichloroindanone))- 12,13-bis(2-butyloctyl)-3,9-diundecyl-diselenopheno[2'',3'':4',5']thieno[2',3':4,5]pyrrolo[3,2-e:2',3'-g][2,1,3]benzothiadiazole (**BOSBR-4Cl**).* To a solution of **BOBSP-CHO** (173 mg, 0.14 mmol) and 2-(5,6-dichloro-3-oxo-2,3-dihydro-1H-inden-1-ylidene)malononitrile (147 mg, 0.56 mmol) in chloroform (14 mL) was added pyridine (0.28 mL). The reaction mixture was then kept at room temperature until the completion of the reaction (ca. 1 day), after which the volatile species were removed by rotary evaporation. The crude product was then purified by column chromatography on silica gel with hexanes/$CHCl_3$ (v/v = 2:1) as eluent to afford **BOSBR-4Cl** as a black solid (220 mg, 91%). ^{1}H NMR ($CDCl_3$, 500 MHz) δ 9.21 (s, 2H), 8.70 (s, 2H), 7.95 (s, 2H), 4.74 (m, 4H), 3.20 (m, 4H), 2.22 (m, 2H), 1.84 (m, 4H), 1.51 (m, 4H), 1.35-0.85 (m, 66H), 0.72-0.66 (m, 12H); ^{13}C NMR ($CDCl_3$, 125 MHz) δ 186.93, 179.15, 158.42, 158.38, 147.65, 147.55, 147.51, 139.57, 139.07, 138.61, 135.93, 134.50, 130.27, 126.86, 124.91, 115.03, 114.53, 99.98, 55.87, 39.07, 31.90, 31.55, 31.31, 30.49, 30.40, 29.92, 29.64, 29.61, 29.50, 29.47, 29.40, 29.32, 28.05, 27.93, 25.53,

25.40, 22.76, 22.66, 22.46, 14.08, 13.99, 13.75, 13.73; MS (m/z, MALDI) Calcd for $C_{90}H_{102}Cl_4N_8O_2S_3Se_2$ 1722.44, found 1722.44.

Fabrication of solar cell devices. Patterned ITO glass substrates were cleaned in an ultrasonic bath sequentially with detergent, deionized water, acetone and isopropanol. The substrates were then blown-dried and treated with air plasma for 10 mins, after which PEDOT:PSS (*CLEVIOS*™ P VP AI 4083) was immediately spin-coated. The substrates coated with PEDOT:PSS were annealed at 150 ^oC for 15 mins before transferred into glove box (N_2) for deposition of active layer. Precursor solutions of active layers composed of PBDB-T-2F (donor, D) and **NFAs** (acceptors, A) in chlorobenzene solution were deposited onto these PEDOT:PSS-coated substrates *via* spin-coating. Optimization of devices included exploring influence of different D:A ratios, addition of DIO, spin-coating speed and annealing conditions. On top of active layer, Bis-C_{60} salt (2 mg/mL in methanol) was spin-coated at 3000 rpm. Finally, 120 nm Ag electrode was deposited *via* thermal evaporation under a base vacuum of $2*10^{-6}$ Torr at a rate of 0.2 nm/s. The *J-V* characteristics of devices under an AM 1.5 G illumination of 100 mW cm^{-2} were measured by using a Keithley 2400 source-measure unit in a nitrogen-filled glove box. The AM 1.5 G illumination was simulated by using an Oriel 300 W Solar Simulator and calibrated by using a silicon photodiode with a protective KG5 filter calibrated by the National Renewable Energy Laboratory (NREL). The EQE system uses a lock-in amplifier (Stanford Research Systems SR830) to record the short-circuit current under chopped monochromatic light.

3.7 REFERENCES

(1) Zhang, Z.; Yu, J.; Yin, X.; Hu, Z.; Jiang, Y.; Sun, J.; Zhou, J.; Zhang, F.; Russell, T. P.; Liu, F.; Tang, W. *Advanced Functional Materials* **2018**, *28*, 1705095.

(2) Gao, H. H.; Sun, Y.; Cai, Y.; Wan, X.; Meng, L.; Ke, X.; Li, S.; Zhang, Y.; Xia, R.; Zheng, N.; Xie, Z.; Li, C.; Zhang, M.; Yip, H. L.; Cao, Y.; Chen, Y. *Advanced Energy Materials* **2019**, *9*, 1901024.
(3) Yuan, J.; Zhang, Y.; Zhou, L.; Zhang, G.; Yip, H.-L.; Lau, T.-K.; Lu, X.; Zhu, C.; Peng, H.; Johnson, P. A.; Leclerc, M.; Cao, Y.; Ulanski, J.; Li, Y.; Zou, Y. *Joule* **2019**, *3*, 1140.
(4) Cui, Y.; Yao, H.; Zhang, J.; Zhang, T.; Wang, Y.; Hong, L.; Xian, K.; Xu, B.; Zhang, S.; Peng, J.; Wei, Z.; Gao, F.; Hou, J. *Nature communications* **2019**, *10*, 2515.
(5) Hong, L.; Yao, H.; Wu, Z.; Cui, Y.; Zhang, T.; Xu, Y.; Yu, R.; Liao, Q.; Gao, B.; Xian, K.; Woo, H. Y.; Ge, Z.; Hou, J. *Advanced materials* **2019**, e1903441.
(6) Feng, L.; Yuan, J.; Zhang, Z.; Peng, H.; Zhang, Z. G.; Xu, S.; Liu, Y.; Li, Y.; Zou, Y. *ACS applied materials & interfaces* **2017**, *9*, 31985.
(7) Cheng, Y.-J.; Ho, Y.-J.; Chen, C.-H.; Kao, W.-S.; Wu, C.-E.; Hsu, S.-L.; Hsu, C.-S. *Macromolecules* **2012**, *45*, 2690.
(8) Ye, X.; Zhao, X.; Li, Q.; Ma, Y.; Song, W.; Quan, Y.-Y.; Wang, Z.; Wang, M.; Huang, Z.-S. *Dyes and Pigments* **2019**, *164*, 407.
(9) Bruce, P. G.; Freunberger, S. A.; Hardwick, L. J.; Tarascon, J. M. *Nature materials* **2011**, *11*, 19.
(10) Kim, H.; Lee, J.; Ahn, H.; Kim, O.; Park, M. J. *Nature communications* **2015**, *6*, 7278.
(11) Kunz, T.; Knochel, P. *Chemistry - A European Journal* **2011**, *17*, 866.
(12) Shi, X.; Liao, X.; Gao, K.; Zuo, L.; Chen, J.; Zhao, J.; Liu, F.; Chen, Y.; Jen, A. K. Y. *Advanced Functional Materials* **2018**, *28*, 1802324.
(13) Coffin, R. C.; Peet, J.; Rogers, J.; Bazan, G. C. *Nature chemistry* **2009**, *1*, 657.
(14) Liao, X.; Shi, X.; Zhang, M.; Gao, K.; Zuo, L.; Liu, F.; Chen, Y.; Jen, A. K. *Chemical communications* **2019**, *55*, 8258.
(15) Lin, F.; Zuo, L.; Gao, K.; Zhang, M.; Jo, S. B.; Liu, F.; Jen, A. K. Y. *Chemistry of Materials* **2019**, *31*, 6770.
(16) Kato, S.; Furuya, T.; Kobayashi, A.; Nitani, M.; Ie, Y.; Aso, Y.; Yoshihara, T.; Tobita, S.; Nakamura, Y. *The Journal of organic chemistry* **2012**, *77*, 7595.
(17) Kato, S.; Furuya, T.; Nitani, M.; Hasebe, N.; Ie, Y.; Aso, Y.; Yoshihara, T.; Tobita, S.; Nakamura, Y. *Chemistry - A European Journal* **2015**, *21*, 3115.
(18) Ghosh, S.; Das, S.; Kumar, N. R.; Agrawal, A. R.; Zade, S. S. *New Journal of Chemistry* **2017**, *41*, 11568.
(19) Mishra, S. P.; Javier, A. E.; Zhang, R.; Liu, J.; Belot, J. A.; Osaka, I.; McCullough, R. D. *J. Mater. Chem.* **2011**, *21*, 1551.
(20) Kim, D. J.; Je, S. H.; Sampath, S.; Choi, J. W.; Coskun, A. *RSC Advances* **2012**, *2*, 7968.

Chapter 4. DESIGN AND SYNTHESIS OF ORGANIC FUNCTIONAL MATERIALS FOR ENERGY STORAGE

4.1 INTRODUCTION

In the previous chapters, the design and synthesis of efficient materials for solar energy conversion were demonstrated. In this chapter, the role that organic functional materials play in the field of energy storage research, specifically sulfur cathode in Li-S batteries, will be discussed.

The reaction of lithium with elemental sulfur to form Li_2S produces a theoretical gravimetric specific capacity of 1673 mAh/g within the range of 1.5~2.4 V vs Li/Li^+. When matched with a metallic lithium anode possessing a theoretical gravimetric specific capacity of 3860 mAh/g, the combined Li-S redox couple can deliver a much higher energy density than that of graphite-lithium metal oxide used in current lithium ion battery industry. This combination is highly attractive for electric vehicles and large-scale electrochemical energy storage systems.[1]

However, a commercially-viable Li-S battery has remained elusive due to multiple technical challenges. Many of them stem from the formation of lithium polysulfide (Li_2S_x, $3 \leq x \leq 8$) during multi-step redox process between elemental sulfur and Li_2S. These polysulfide species are highly soluble in organic electrolytes, and tend to escape into the electrolyte during discharge, leading to low coloumbic efficiency due to the loss of active material and self-discharge.[2] When the battery is recharged, polysulfide travels with the lithium flux toward anode and react with the lithium metal. This process is known as “shuttle effect” and results in passivation of the lithium anode. Moreover, differences in forward and backward reaction mechanism also cause voltage hysteresis during battery operation.

Aside from the high solubility of polysulfide in organic electrolytes, the highly insulating nature of sulfur derivatives also necessitates the use of a large amount of conductive carbon additives in the electrode composite to achieve suitable conductivity. Moreover, because the overall reaction is accompanied by a large volume change, this electrode composite matrix is prone to cracking, leading to battery failure due to loss of conductive network between components. Finally, on the anode side, lithium metal tends to form dendrites upon repeated stripping and plating, which puncture the cell separator and cause internal shorting.[3] While rendering the battery useless, such situation may even cause fires and explosions in the worst case.

4.2 Multifunctional Polyelectrolyte Gel for Li-S Batteries

The Li-S battery is a very complicated system, and the kinetics in batteries change quickly during different stages of operation. To design efficient organic functional materials for Li-S batteries, the aforementioned issues must be addressed from several aspects.

(1) Physical trapping of polysulfide: Polysulfide is highly soluble in conventional ether-based electrolytes, which can be replaced by electrolytes with low polysulfide solubility such as ionic liquids to suppress polysulfide dissolution.[4,5] On the other hand, using mesoporous carbon as the host material of sulfur to trap the polysulfide has also been proven to be an efficient approach to elongate the cycle life of batteries.[6]

(2) Chemical trapping of polysulfide: Incorporating functional groups which interact with polysulfide through non-covalent interactions or even forms chemical bonding with polysulfide is also a feasible strategy.[4] Chemical modification on the surface of mesoporous carbon,[7,8] as well as incorporating chemical cross-linkers into the electrode,[9,10] are both capable of improving the cycling stability and even rate performance of the batteries.

(3) Conductivity: Due to the insulating nature of elemental sulfur and polysulfide, the supportive materials in the electrode must create a network with adequate ionic and electrical conductivities to facilitate the redox reactions of sulfur species. The electrical conductivity can be enhanced through using conductive host materials such as mesoporous carbons, or by addition of conductive additives in the electrode composite.[2,10] The ionic conductivity is mainly determined by the electrolytes. Higher conductivities lead to better rate performance and capacity retention.

(4) Redox mediators: Introducing redox-active or electrochemically active functional groups onto sulfur host materials or other supportive electrode materials can facilitate the exchange of charges between different species,[7,8,11,12] this speeding up the charge/discharge rate.

(5) Suppression of lithium dendrite formation: Poly(ethylene oxide) derivatives, crown ethers and ionic liquids are known to mitigate the hot spots on lithium metal surface which induce the formation of lithium dendrites, and helps to form a smooth, uniform surface during stripping and plating.[13,14]

(6) Mechanical strength: The charge/discharge process of electrodes always accompanies with change of volume, as lithium flux moves in and out of the electrode. This is a common issue among most of high-capacity electrodes, as the electrodes can crack the conductive network within the electrode can no longer be maintained. Introduction of self-healing functional groups onto supportive materials in the electrode can notably enhance the stability and lifetime of the battery.[15,16]

It is extremely difficult to combine all the desirable properties into one single material, but more feasible to gather these properties from different materials to make a multi-component material system, which is the multifunctional polyelectrolyte gel that our group has been working

on over the past few years. The polyelectrolyte gel is composed of three main features, including (i) glyme-based solvate ionic liquid (LiG_4TFSI), (ii) a chemically cross-linked branched polymethacrylates network with oligo(ethylene oxide) and ionomer pendant groups, and (iii) a physically cross-linked, self-healing polymer composite utilizing the interaction between naphthalene diimide (NDI) pendant groups on linear polymethacrylates and pyrene dopants.[17-19] This system possesses sufficient ionic conductivity, mechanical strength, and ability to retain polysulfide near cathode which are required to build a safe and efficient Li-S battery.

In this project, my work has mainly been focused on the design and synthesis of the polymers with NDI pendant groups for the composite. A series of linear polymethacrylates with NDI pendant groups and different side chains, abbreviated as **PENDI**, were rationally designed, synthesized and fully characterized (Figure 4-1).The properties of these polymers were mainly tuned through side-chain engineering to control the ionic conductivity, as well as the capability of forming physically cross-linked network with pyrene dopants and the self-healing properties of the composite.

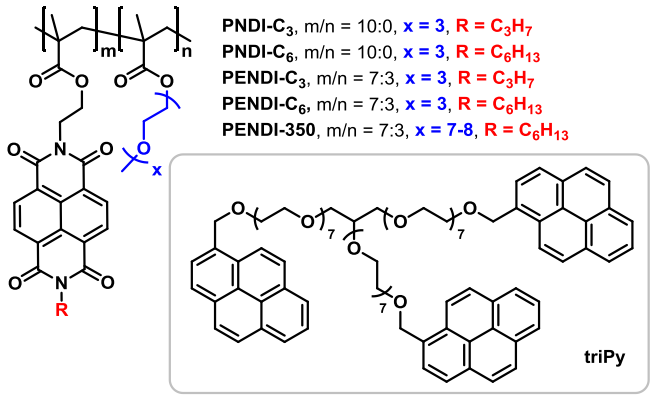

Figure 4-1. Chemical structures of **PENDI** family and **triPy** cross-linker.

4.2.1 *Design and Synthesis of PENDI Polymers*

The interaction between electron-rich pyrene and electron-deficient NDI results in formation of pyrene-NDI charge-transfer complexes, which possess binding energy within the range of -10 ~ -20 kJ/mol at room temperature. Colquhoun *et al.* have reported polymer composites prepared from two polymers composed of pyrene and NDI units, respectively, to be elastic and self-healable due to reversible π-π stacking interactions.[17-19] This material system not only provides mechanical toughness which is necessary for building up the electrode, but also the self-healing ability can be tuned temperature-dependently within the operating temperature range of a lithium-based battery. Moreover, NDI is able to trap polysulfide chains through electrostatic interactions.[20] The reduction potential of NDI derivatives is also reported to sit in between the operating potential range of a sulfur cathode, which makes NDI an electrochemically active intermediate to assist the conversion between Li_2S and polysulfide.[21,22]

Conjugated polymers based on NDI derivatives have been extensively studies. However, instead of making conjugated polymers, **PENDI** polymers were constructed through polymethacrylate backbones which possess better scalability and reproducibility, as radical-initiated polymerization reactions are more controllable then metal-catalyzed polycondensation reactions.

Polymethacrylates with NDI pendant groups were prepared from asymmetric NDI monomers using 2,2'-azobis(2-methylpropionitrile) (AIBN) as a radical initiator.[23] Instead of using branching side chains, linear aliphatic chains were attached onto NDI units to aid with solubility, as well as avoid interfering with the interactions between pyrene and NDI. The properties of these polymers were modulated through side-chain engineering. Four polymers with different side chain combination were synthesized for preliminary comparison (Scheme 4-1), including two

homopolymers **PNDI-C$_3$** and **PNDI-C$_6$**, and two copolymers **PENDI-C$_3$** and **PENDI-C$_6$** composed of 7:3 ratio of NDI/triethylene glycol monomethyl ether to ensure sandwich-type interaction between pyrene-NDI.

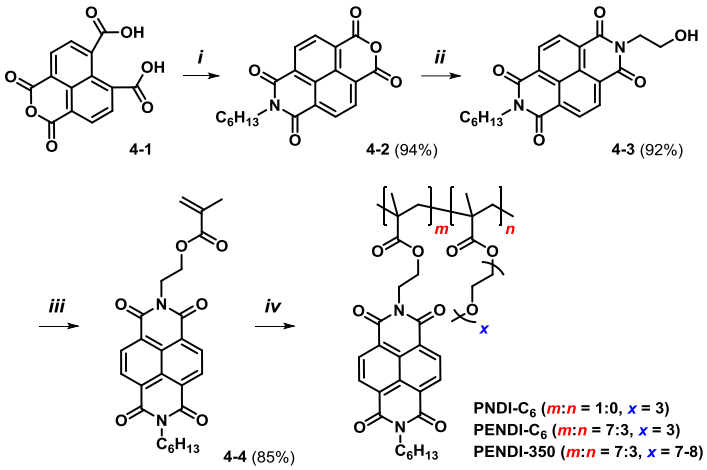

Reagents and conditions: i) a) 1-Hexylamine, H_2O, 0 °C, then refluxed; b) 10% $HCl_{(aq)}$, 0 °C; c) THF/$HCl_{(conc.)}$, (v/v=1:2). *ii)* Ethanolamine, EtOH, 80 °C. *iii)* Methacryloyl chloride, Et_3N, DCM/THF (v/v=1:1), 40 °C. *iv)* Triethylene glycol methyl ether methacrylate (TEGMA) or polyethylene glycol methyl ether methacrylate (PEG350MA), AIBN, THF, 70 °C.

Scheme 4-1. Synthetic routes of **PNDI-C6**, **PENDI-C6** and **PENDI-350**.

	M_n (kDa)	PDI[a]	E_{red} (eV)[b]
PNDI-C$_3$	10.9	1.11	-3.76
PNDI-C$_6$	145.2	1.43	-3.77
PENDI-C$_3$	42.7	1.13	-3.73
PENDI-C$_6$	122.5	1.43	-3.74
PENDI-350	19.2	2.67	-3.74

[a] PDI = M_w/M_n. [b] Cyclic voltammetry measured in THF solution with 0.1 M NBu_4PF_6 as supporting electrolyte. Sample concentration was 0.01 M based on NDI units. All potentials were recorded versus Fc/Fc^+ as an external reference.

Table 4-1. Molecular weight distribution and electrochemistry characteristics of polymers.

4.2.2 *Study of Temperature-Dependent Self-Healing Behaviors*

Homopolymer **PNDI-C$_3$** and **PNDI-C$_6$** were found to be poorly processable due to strong self-aggregation and failed to form smooth, homogeneous films. The incorporation of triethylene glycol side chains favorably enhance the solubility and processability of polymers, and the effect on addition of pyrene dopant (**triPy**) was investigated using copolymer **PENDI-C$_3$** (Figure 4-2). While pristine **PENDI-C$_3$** gives a brittle film which slowly cracks upon evaporation of solvents, blended **PENDI-C$_3$**:**triPy** (1:1 pyrene:NDI molar ratio, **PP-C$_3$**) gives a smooth film with a deep red color originated from the formation of pyrene-NDI charge-transfer complex. The binding energy between pyrene-NDI in the composite was calculated to be -12.44 kJ/mol.

Self-healing behavior of **PENDI-C$_3$**:**triPy** was successfully demonstrated by thermally annealing a broken film at 60 ˚C for 4 hours. Furthermore, the temperature-dependent self-healing behavior was investigated using the combination **PENDI-C$_6$**:**triPy** (1:1 pyrene:NDI molar ratio, **PP-C$_6$**), as longer and slightly bulkier side chain (hexyl vs. propyl) on NDI units reduces the interaction strength between pyrene-NDI, thus lowering the self-healing temperature to a closer value matching with the operating temperature range of a lithium-based battery. This phenomenon also echoes with the lower glass transition temperature (T_g = 113 ^{o}C) of **PENDI-C$_6$** versus **PENDI-C$_3$** (T_g = 168 ^{o}C), which indicates the polymers chains of **PENDI-C$_6$** have higher mobility. **PP-C$_6$** was cured by thermal treatment at 40 ˚C for 4 hours, while **PP-C$_3$** failed to heal after heating at 40 ˚C for 24 hours (**Fig. 6**). The binding energy between pyrene-NDI in **PP-C$_6$** composite was calculated to be -9.43 kJ/mol.

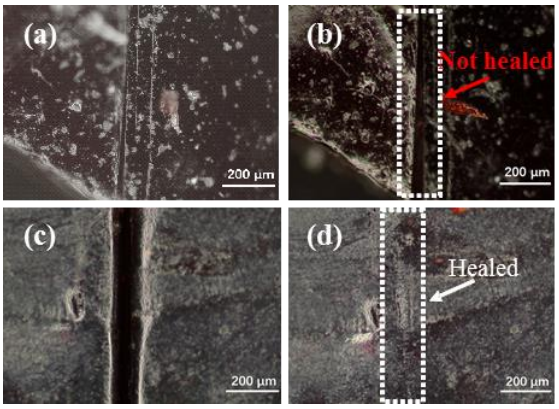

Figure 4-2. OM image of composite films **PP-C$_3$** (a) damaged and (b) cured at 40 ℃ for 24 hours, and **PP-C$_6$** (c) damaged and (d) cured at 40 ℃ for 4 hours.

4.2.3 *Ionic Conductivity and Battery Performance*

The ionic conductivity of **PP-C$_6$** composite, doped with LiTFSI at a 5% molar ratio versus ethylene oxide units, was determined to be 3.95×10^{-7} S/cm under room temperature with electrochemical impedance spectroscopy (EIS) measurement. To further enhance the ionic conductivity, a new polymer with longer oligoethylene glycol side chains, **PENDI-350**, was designed and synthesized.[24] Composite based on **PENDI-350**:**triPy** (1:1 pyrene:NDI molar ratio, **PP-350**) gave marginally higher lithium ion conductivity of 4.50×10^{-7} S/cm under room temperature, however this composite showed better stretchability and lower self-healing temperature compared to **PP-C$_6$**.

A composite of **PENDI-350**:**triPy** with modified formula (1:3 pyrene:NDI molar ratio, **PP'-350**) was incorporated into coin cells to preliminarily assess the capability of employing this material system into Li-S batteries. Sulfur cathodes were fabricated with a formulation containing 75 wt% sulfur-infused mesoporous carbon (MJ430, 50 wt% sulfur content), 20 wt% polymer binders (PVDF or **PP'-350**), 5 wt% Super P carbon as conductive additive and 30 μL electrolyte

(1 M LiTFSI in DOL/DME (v/v = 1:1), with 1 wt% $LiNO_3$). The sulfur content of the electrode was calculated to be ~0.9 mg/cm^2. Cells based on **PP'-350** showed much better capacity retention under a slow C rate of C/20, giving a capacity 400 mAh/g higher than that of PVDF-based cells after 100 cycles (Figure 4-3a). The rate performance of the cells was also tested. To our excitement, **PP'-350**-based cells showed excellent capability under a fairly high rate of 1C (Figure 4-3b). The performance in terms of capacity retention of **PP'-350**-based devices cycled under 1C was also amazing, giving 98 % capacity retention after 100 cycles, while PVDF-based cells were only able to retain 77% of its original capacity (Figure 4-3c). These extremely inspiring results have proven that **PP'-350** can be a very efficient material to build high-performance Li-S batteries.

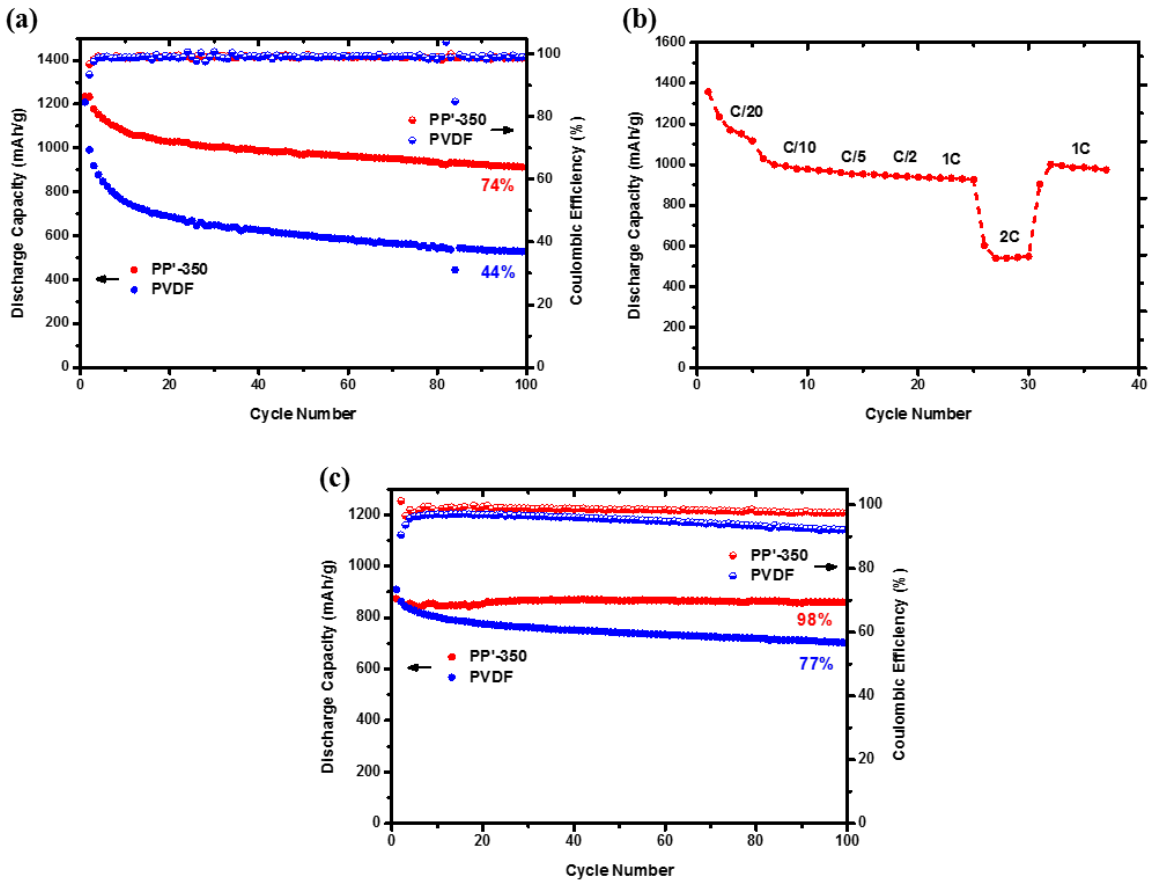

Figure 4-3. (a) Cycling performance and coulombic efficiency of cells employing PVDF and **PP'-350** as binder at C/20. (b) Cycling performance of **PP'-350**-based cells under different C rates. (c) Cycling performance and coulombic efficiency of cells employing PVDF and **PP'-350** as binder at 1C.

4.3 CONCLUSION

In this chapter, a brief overview on current issues in Li-S batteries has been provided. To address these issues, a multifunctional polyelectrolyte gel with multiple components has been designed. The design, synthesis, characterization of **PENDI** polymers, and composites based on cross-linking different **PENDI** derivatives and pyrene dopants have been discussed. Among these composites, **PP-350** has demonstrated proper ionic conductivity, self-healing ability, and mechanical strength. Preliminary test of Li-S batteries employing **PP'-350** as a binder in the sulfur cathode gave highly inspiring performance in terms of cycling rate and capacity retention. These polymers and composites will be further employed into the polyelectrolyte gel for sulfur cathode fabrication, and the mechanism of performance enhancement will be investigated.

4.4 EXPERIMENTAL DETAILS

General Methods. Unless otherwise stated, all chemicals and reagents were used as received from commercial sources (Sigma-Aldrich, Matrix Scientific, Combi-Blocks) without further purification. Solvents for chemical synthesis were purified by distillation under nitrogen. All chemical reactions were carried out under protection of argon or nitrogen atmosphere. Compound **triPy** and **PEG350MA** were prepared according to literature procedures. [19,25] The ^{1}H and ^{13}C NMR spectra were recorded on a Bruker AV500 spectrometer using $CDCl_3$ or d_6-DMSO as solvents.

Mass spectrometry was performed on Bruker APEX III 47e Fourier Transform mass spectrometer. The UV-Vis spectra were recorded on a Varian Cary 5000 UV-Vis-NIR Spectrophotometer. Cyclic voltammetry was measured on a CH Instruments CHI660E Electrochemical Analyzer/Workstation using a conventional three-electrode cell with a glassy carbon working electrode, Pt wire counter-electrode, and Ag/AgCl reference electrode at a scan rate of 50 mV/s using 0.1 M tetrabutylammonium hexafluorophosphate ($TBAPF_6$) in THF as the electrolyte and referenced to the $FeCp_2/FeCp_2^+$ redox couple. The molecular weight and PDI of the polymers were analyzed by gel permeation chromatography on a Shimadzu LC-20AD with RID-20A detector using polystyrene as standards. Differential scanning calorimetry was performed on a Shimadzu DSC-60 differential scanning calorimeter.

Material synthesis.

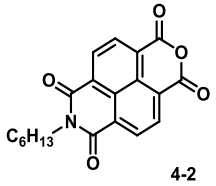

4-2

*Synthesis of N-hexyl-1,4,5,8-naphthalenetetracarboxy-1,8-monoanhydride-4,5-monoimide (**4-2**).* To a stirred suspension of **4-1** (5.72 g, 20.0 mmol) in DI water (300 mL) was dropwise added n-hexylamine (12.1 g, 120 mmol) through an addition funnel at 0 ^oC during which the solution turned clear. The reaction mixture was stirred overnight and slowly allowed to warm up to room temperature, then refluxed for 2 hours and again cooled to 0 ^oC followed by the addition of 10% $HCl_{(aq)}$ (100 mL). The precipitate was collected by filtration, and washed with water and ice-cold methanol, which was then refluxed in a mixture of $HCl_{(conc.)}$ (40 mL) and THF (20 mL). The suspension was again filtered, and the solid collected was washed consecutively with water,

methanol and ice-cold acetone to afford **4-2** as a pale yellow solid (6.61 g, 94%). ^{1}H NMR (*d*$_6$-DMSO, 500 MHz) δ 8.67 (m, 4H), 4.03 (t, *J* = 7.5 Hz, 2H), 1.65 (m, 2H), 1.29–1.36 (m, 6H), 0.87 (t, *J* = 7.5 Hz, 3H); ^{13}C NMR (*d*$_6$-DMSO, 125 MHz) δ 162.31, 158.66, 131.82, 130.39, 128.43, 127.08, 126.07, 123.67, 39.02, 30.93, 27.25, 26.15, 21.95, 13.89; HRMS (*m/z*, ESI) calcd for $C_{20}H_{17}NO_5$ 351.1107, found 351.1116.

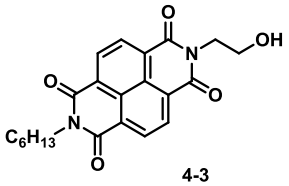

4-3

*Synthesis of N-hexyl-N'-(2-hydroxyethyl)-1,4,5,8-naphthalenetetracarboxydiimide (**4-3**).* To a stirring suspension of **4-2** (5.27 g, 15.0 mmol) in ethanol (150 mL) was dropwise added ethanolamine (1.10 g, 18 mmol) through an addition funnel at room temperature. The reaction mixture was then refluxed and stirred overnight. The precipitate was collected by filtration and washed with ice-cold methanol to afford **4-3** as a pale yellow solid (5.44 g, 92%). ^{1}H NMR (*d*$_6$-DMSO, 500 MHz) δ 8.53 (m, 4H), 4.83 (t, *J* = 5 Hz, 2H), 4.13 (t, *J* = 5 Hz, 2H), 4.00 (t, *J* = 7.5 Hz, 2H), 3.64 (m, 2H), 1.63 (m, 2H), 1.30–1.36 (m, 6H), 0.87 (t, *J* = 7.5 Hz, 3H); ^{13}C NMR (*d*$_6$-DMSO, 125 MHz) δ 162.28, 162.15, 130.11, 130.08, 125.95, 125.84, 125.74, 57.56, 42.06, 30.68, 27.10, 25.93, 21.69, 13.58; HRMS (*m/z*, ESI) calcd for $C_{22}H_{23}N_2O_5$ 395.1607, found 395.1618.

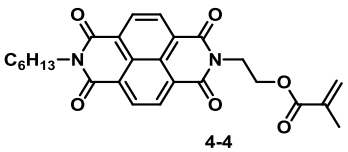

4-4

*Synthesis of N-hexyl-N'-(2-[methacryloyl]ethyl)-1,4,5,8-naphthalene tetracarboxydiimide (**4-4**).* To a stirring suspension of **4-3** (5.52 g, 14.0 mmol) in a mixed solvent of THF (70 mL) and DCM

(70 mL), with trace amount of 4-methoxyphenol, was added distilled Et_3N (1.56 g, 15.4 mmol) and then cooled to 0 °C, after which freshly distilled methacryloyl chloride (1.61 g, 15.4 mmol) was added dropwise. The reaction mixture was gently heated to 40 °C and stirred overnight. After cooling to room temperature, the mixture was poured into cold methanol. The precipitate was collected by filtration then washed with ice-cold methanol to afford **4-4** as a pale yellow solid (5.56 g, 85%). ^{1}H NMR (d_6-DMSO, 500 MHz) δ 8.74 (m, 4H), 6.02 (s, 1H), 5.51 (s, 1H), 4.57 (t, J = 5 Hz, 2H), 4.50 (t, J = 5 Hz, 2H), 4.18 (t, J = 6.5 Hz, 2H), 1.84 (s, 3H), 1.74 (m, 2H), 1.33–1.44 (m, 6H), 0.89 (t, J = 6.5 Hz, 3H); ^{13}C NMR (d_6-DMSO, 125 MHz) δ 167.18, 162.84, 162.70, 135.87, 130.91, 126.81, 126.29, 125.96, 61.75, 40.97, 39.47, 31.45, 27.98, 26.69, 22.50, 18.19, 14.00; HRMS (*m/z*, ESI) calcd for $C_{26}H_{27}N_2O_6$ 463.1869, found 463.1876.

General procedure of synthesis of PENDI polymers. To a mixture of methacrylate monomers (2 mmol) and AIBN (4 mg, 1.2 mol%) in a sealed flask was added THF (3 mL). The reaction mixture was degassed through 3 freeze-pump-thaw cycles and heated under 70 °C for one day with vigorous stirring. After cooling to room temperature, the mixture was poured into cold methanol. The precipitate was collected by filtration and washed with methanol and diethyl ether to give the desired polymers.

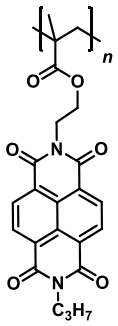

PNDI-C_3

Synthesis of poly(N-ethyl-N'-propyl-1,4,5,8-naphthalenetetracarboxydiimidyl methacrylate) ***(PNDI-C$_3$).*** Following the general procedure, polymerization of *N*-propyl-*N*'-(2-[methacryloyl]ethyl)-1,4,5,8-naphthalene tetracarboxydiimide (841 mg, 2.0 mmol) gave **PNDI-C$_3$** as a greyish green solid (760 mg, 90%). GPC (M_n = 10.9 kDa, PDI = 1.11).

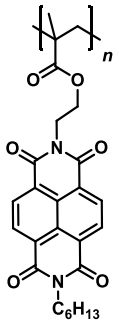

PNDI-C$_6$

Synthesis of poly(N-ethyl-N'-hexyl-1,4,5,8-naphthalenetetracarboxydiimidyl methacrylate) ***(PNDI-C$_6$).*** Following the general procedure, polymerization of **4-4** (925 mg, 2.0 mmol) gave **PNDI-C$_6$** as a light pink solid (780 mg, 84%). GPC (M_n = 145.2 kDa, PDI = 1.43).

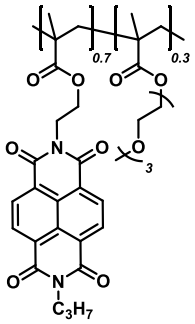

PENDI-C$_3$

Synthesis of poly(N-ethyl-N'-propyl-1,4,5,8-naphthalenetetracarboxydiimidyl methacrylate-co-triethylene glycol methyl ether methacrylate) ***(PENDI-C$_3$).*** Following the general procedure, polymerization of *N*-propyl-*N*'-(2-[methacryloyl]ethyl)-1,4,5,8-naphthalene tetracarboxydiimide

(589 mg, 1.4 mmol) and triethylene glycol methyl ether methacrylate (139 mg, 0.6 mmol) gave **PENDI-C$_3$** as a pale green solid (650 mg, 89%). GPC (M_n = 42.7 kDa, PDI = 1.13).

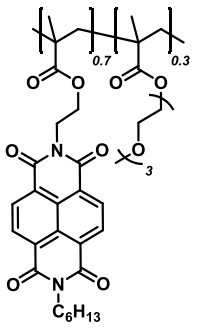

PENDI-C$_6$

*Synthesis of poly(N-ethyl-N'-hexyl-1,4,5,8-naphthalenetetracarboxydiimidyl methacrylate-co-triethylene glycol methyl ether methacrylate) (**PENDI-C$_6$**).* Following the general procedure, polymerization of **4-4** (647 mg, 1.4 mmol) and triethylene glycol methyl ether methacrylate (139 mg, 0.6 mmol) gave **PENDI-C$_6$** as a white solid (730 mg, 93%). GPC (M_n = 122.5 kDa, PDI = 1.43).

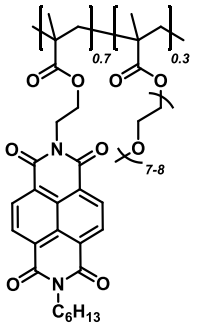

PENDI-350

*Synthesis of poly(N-ethyl-N'-hexyl-1,4,5,8-naphthalenetetracarboxydiimidyl methacrylate-co-polyethylene glycol 350 methyl ether methacrylate) (**PENDI-350**).* Following the general procedure, polymerization of **4-4** (647 mg, 1.4 mmol) and polyethylene glycol 350 methyl ether

methacrylate (251 mg, 0.6 mmol) gave **PENDI-350** as a white solid (820 mg, 91%). GPC (M_n = 19.2 kDa, PDI = 2.67).

Cell fabrication and test. The carbon-sulfur composite was prepared by melt-infiltration of a mixture of MJ430 carbon (Porous Carbon CNovel™; Toyo Tanso USA, INC.) and sulfur at a weight ratio of 3:7 at 155 ^{o}C for 24 h in a sealed vacuum tube. The carbon-sulfur composite was then mixed with Super P (EnerG2) as conductive additive and **PP'-350** as binder, at a weight ratio of 75:5:20, in *N*-methyl-2-pyrrolidone (NMP, Sigma-Aldrich) to give a slurry, which was cast on a C-coated Al foil current collector (MTI Corp.) and dried overnight at 60 ^{o}C under vacuum. 2032 coin-type cells were assembled using lithium metal (250 μm, Alfa Aesar) as the anode, polypropylene (PP) Celgard2500 (Celgard, LLC Corp.) as the separator, and 1 M LiTFSI (Sigma-Aldrich) and 1 wt% LiNO3 (Alfa Aesar) in DOL/DME (Sigma-Aldrich, v/v = 1:1) as the electrolyte for each cell. The electrochemical performances of the cells were evaluated at room temperature in a voltage window of 1.9–2.8 V vs. Li^{+}/Li at various C-rates using a battery tester (BT-2043, Arbin).

Spectroscopic characterization. Electrochemical impedance spectroscopy (EIS) was performed using an AMETEK VersaSTAT4 potentiostat/galvanostat in the frequency range of 10-2 to 106 Hz by applying a 5 mV ac oscillation. The ionic conductivity of the sample was derived from the EIS measurement.

4.5 REFERENCES

(1) Bruce, P. G.; Freunberger, S. A.; Hardwick, L. J.; Tarascon, J. M. *Nature materials* **2011**, *11*, 19.
(2) Kang, W.; Deng, N.; Ju, J.; Li, Q.; Wu, D.; Ma, X.; Li, L.; Naebe, M.; Cheng, B. *Nanoscale* **2016**, *8*, 16541.

(3) Tikekar, M. D.; Choudhury, S.; Tu, Z.; Archer, L. A. *Nature Energy* **2016**, *1*, 16114.
(4) Pang, Q.; Liang, X.; Kwok, C. Y.; Nazar, L. F. *Nature Energy* **2016**, *1*, 16132.
(5) Scheers, J.; Fantini, S.; Johansson, P. *Journal of Power Sources* **2014**, *255*, 204.
(6) Ji, X.; Lee, K. T.; Nazar, L. F. *Nature materials* **2009**, *8*, 500.
(7) Kim, J. H.; Kim, T.; Jeong, Y. C.; Lee, K.; Park, K. T.; Yang, S. J.; Park, C. R. *Advanced Energy Materials* **2015**, *5*, 1500268.
(8) Li, Y.; Murphy, I. A.; Chen, Y.; Lin, F.; Wang, X.; Wang, S.; Hubble, D.; Jang, S.-H.; Muller, K. T.; Wang, C.; Jen, A. K. Y.; Yang, J. *Journal of Materials Chemistry A* **2019**, *7*, 13372.
(9) Chung, W. J.; Griebel, J. J.; Kim, E. T.; Yoon, H.; Simmonds, A. G.; Ji, H. J.; Dirlam, P. T.; Glass, R. S.; Wie, J. J.; Nguyen, N. A.; Guralnick, B. W.; Park, J.; Somogyi, A.; Theato, P.; Mackay, M. E.; Sung, Y. E.; Char, K.; Pyun, J. *Nature chemistry* **2013**, *5*, 518.
(10) Kim, H.; Lee, J.; Ahn, H.; Kim, O.; Park, M. J. *Nature communications* **2015**, *6*, 7278.
(11) Sun, Z.; Zhang, J.; Yin, L.; Hu, G.; Fang, R.; Cheng, H. M.; Li, F. *Nature communications* **2017**, *8*, 14627.
(12) Zhu, L.; Li, C.; Ren, W.; Qin, M.; Xu, L. *New Journal of Chemistry* **2018**, *42*, 5109.
(13) Lu, Y.; Korf, K.; Kambe, Y.; Tu, Z.; Archer, L. A. *Angewandte Chemie* **2014**, *53*, 488.
(14) Yang, Y. B.; Liu, Y. X.; Song, Z.; Zhou, Y. H.; Zhan, H. *ACS applied materials & interfaces* **2017**, *9*, 38950.
(15) Magasinski, A.; Zdyrko, B.; Kovalenko, I.; Hertzberg, B.; Burtovyy, R.; Huebner, C. F.; Fuller, T. F.; Luzinov, I.; Yushin, G. *ACS applied materials & interfaces* **2010**, *2*, 3004.
(16) Kwon, T. W.; Jeong, Y. K.; Lee, I.; Kim, T. S.; Choi, J. W.; Coskun, A. *Advanced materials* **2014**, *26*, 7979.
(17) Burattini, S.; Colquhoun, H. M.; Fox, J. D.; Friedmann, D.; Greenland, B. W.; Harris, P. J.; Hayes, W.; Mackay, M. E.; Rowan, S. J. *Chemical communications* **2009**, 6717.
(18) S., B.; Greenland, B. W.; H., M. D.; Weng, W.; Seppala, J.; Colquhoun, H. M.; Hayes, W.; Mackay, M. E.; Hamley, I. W.; Rowan, S. J. *Journal of the American Chemical Society* **2010**, *132*, 12051.
(19) Hart, L. R.; Hunter, J. H.; Nguyen, N. A.; Harries, J. L.; Greenland, B. W.; Mackay, M. E.; Colquhoun, H. M.; Hayes, W. *Polym. Chem.* **2014**, *5*, 3680.
(20) Gu, P. Y.; Zhao, Y.; Xie, J.; Binte Ali, N.; Nie, L.; Xu, Z. J.; Zhang, Q. *ACS applied materials & interfaces* **2016**, *8*, 7464.
(21) Kim, D. J.; Je, S. H.; Sampath, S.; Choi, J. W.; Coskun, A. *RSC Advances* **2012**, *2*, 7968.
(22) Häupler, B.; Wild, A.; Schubert, U. S. *Advanced Energy Materials* **2015**, *5*, 1402034.
(23) Takahashi, M.; Ui, M.; Inuzuka, T.; Sengoku, T.; Yoda, H. *Tetrahedron* **2014**, *70*, 9175.
(24) Golodnitsky, D.; Strauss, E.; Peled, E.; Greenbaum, S. *Journal of The Electrochemical Society* **2015**, *162*, A2551.
(25) Jones, M. W.; Gibson, M. I.; Mantovani, G.; Haddleton, D. M. *Polymer Chemistry* **2011**, *2*, 572.

BIBLIOGRAPHY

[1] Kearns, D.; Calvin, M. *Journal of Physical Chemistry* **1958**, *59*, 950.

[2] Delacote, G. M.; Fillard, J. P.; Marco, F. J. *Solid State Communications* **1964**, *2*, 373.

[3] Tang, C. W. *Applied Physics Letters* **1986**, *48*, 183.

[4] Sariciftci, N. S.; Smilowitz, L.; Heeger, A. J.; Wudl, F. *Synthetic Metals* **1993**, *59*, 333.

[5] Yu, G.; K., P.; Heeger, A. J. *Applied Physics Letters* **1994**, *64*, 3422.

[6] Hummelen, J. C.; Knight, B. W.; LePeq, F.; Wudl, F.; Yao, J.; Wilkins, C. L. *The Journal of Organic Chemistry* **1995**, *60*, 532.

[7] Yu, G.; Gao, J.; Hummelen, J. C.; Wudl, F.; Heeger, A. J. *Science* **1995**, *270*, 1789.

[8] Chen, Y. H.; Lin, L. Y.; Lu, C. W.; Lin, F.; Huang, Z. Y.; Lin, H. W.; Wang, P. H.; Liu, Y. H.; Wong, K. T.; Wen, J.; Miller, D. J.; Darling, S. B. *Journal of the American Chemical Society* **2012**, *134*, 13616.

[9] Steinmann, V.; Kronenberg, N. M.; Lenze, M. R.; Graf, S. M.; Hertel, D.; Meerholz, K.; Bürckstümmer, H.; Tulyakova, E. V.; Würthner, F. *Advanced Energy Materials* **2011**, *1*, 888.

[10] Fitzner, R.; Mena-Osteritz, E.; Mishra, A.; Schulz, G.; Reinold, E.; Weil, M.; Korner, C.; Ziehlke, H.; Elschner, C.; Leo, K.; Riede, M.; Pfeiffer, M.; Uhrich, C.; Bauerle, P. *Journal of the American Chemical Society* **2012**, *134*, 11064.

[11] Sun, Y.; Welch, G. C.; Leong, W. L.; Takacs, C. J.; Bazan, G. C.; Heeger, A. J. *Nature materials* **2011**, *11*, 44.

[12] Zhou, J.; Wan, X.; Liu, Y.; Zuo, Y.; Li, Z.; He, G.; Long, G.; Ni, W.; Li, C.; Su, X.; Chen, Y. *Journal of the American Chemical Society* **2012**, *134*, 16345.

[13] Liang, Y.; Feng, D.; Wu, Y.; Tsai, S.-T.; Li, G.; Ray, C.; Yu, L. *Journal of the American Chemical Society* **2009**, *131*, 7792.

[14] He, Z.; Xiao, B.; Liu, F.; Wu, H.; Yang, Y.; Xiao, S.; Wang, C.; Russell, T. P.; Cao, Y. *Nature Photonics* **2015**, *9*, 174.

[15] Liu, Y.; Zhao, J.; Li, Z.; Mu, C.; Ma, W.; Hu, H.; Jiang, K.; Lin, H.; Ade, H.; Yan, H. *Nature communications* **2014**, *5*, 5293.

[16] Matsuo, Y.; Kawai, J.; Inada, H.; Nakagawa, T.; Ota, H.; Otsubo, S.; Nakamura, E. *Advanced materials* **2013**, *25*, 6266.

[17] Smestad, G. P.; Krebs, F. C.; Lampert, C. M.; Granqvist, C. G.; Chopra, K. L.; Mathew, X.; Takakura, H. *Solar Energy Materials and Solar Cells* **2008**, *92*, 371.

[18] Zhong, Y.; Trinh, M. T.; Chen, R.; Purdum, G. E.; Khlyabich, P. P.; Sezen, M.; Oh, S.; Zhu, H.; Fowler, B.; Zhang, B.; Wang, W.; Nam, C. Y.; Sfeir, M. Y.; Black, C. T.; Steigerwald, M. L.; Loo, Y. L.; Ng, F.; Zhu, X. Y.; Nuckolls, C. *Nature communications* **2015**, *6*, 8242.

[19] Meng, D.; Sun, D.; Zhong, C.; Liu, T.; Fan, B.; Huo, L.; Li, Y.; Jiang, W.; Choi, H.; Kim, T.; Kim, J. Y.; Sun, Y.; Wang, Z.; Heeger, A. J. *Journal of the American Chemical Society* **2016**, *138*, 375.

[20] Rajasingh, P.; Cohen, R.; Shirman, E.; Shimon, L. J. W.; Rybtchinski, B. *Journal of Organic Chemistry* **2007**, *72*, 5973.

[21] Lin, Y.; Wang, J.; Zhang, Z. G.; Bai, H.; Li, Y.; Zhu, D.; Zhan, X. *Advanced materials* **2015**, *27*, 1170.

[22] Zhao, W.; Qian, D.; Zhang, S.; Li, S.; Inganas, O.; Gao, F.; Hou, J. *Advanced materials* **2016**, *28*, 4734.

[23] Yang, Y.; Zhang, Z. G.; Bin, H.; Chen, S.; Gao, L.; Xue, L.; Yang, C.; Li, Y. *Journal of the American Chemical Society* **2016**, *138*, 15011.

[24] Li, S.; Ye, L.; Zhao, W.; Zhang, S.; Mukherjee, S.; Ade, H.; Hou, J. *Advanced materials* **2016**, *28*, 9423.

[25] Lin, Y.; Zhao, F.; He, Q.; Huo, L.; Wu, Y.; Parker, T. C.; Ma, W.; Sun, Y.; Wang, C.; Zhu, D.; Heeger, A. J.; Marder, S. R.; Zhan, X. *Journal of the American Chemical Society* **2016**, *138*, 4955.

[26] Luo, Z.; Bin, H.; Liu, T.; Zhang, Z. G.; Yang, Y.; Zhong, C.; Qiu, B.; Li, G.; Gao, W.; Xie, D.; Wu, K.; Sun, Y.; Liu, F.; Li, Y.; Yang, C. *Advanced materials* **2018**, *30*.

[27] Cao, H.; Bauer, N.; Pang, C.; Rech, J.; You, W.; Rupar, P. A. *ACS Applied Energy Materials* **2018**, *1*, 7146.

[28] Yao, Z.; Liao, X.; Gao, K.; Lin, F.; Xu, X.; Shi, X.; Zuo, L.; Liu, F.; Chen, Y.; Jen, A. K. *Journal of the American Chemical Society* **2018**, *140*, 2054.

[29] Wang, Y.; Zhang, Y.; Qiu, N.; Feng, H.; Gao, H.; Kan, B.; Ma, Y.; Li, C.; Wan, X.; Chen, Y. *Advanced Energy Materials* **2018**, *8*, 1702870.

[30] Wang, C. K.; Jiang, B. H.; Su, Y. W.; Jeng, R. J.; Wang, Y. J.; Chen, C. P.; Wong, K. T. *ACS applied materials & interfaces* **2019**, *11*, 1125.

[31] Huang, C.; Liao, X.; Gao, K.; Zuo, L.; Lin, F.; Shi, X.; Li, C.-Z.; Liu, H.; Li, X.; Liu, F.; Chen, Y.; Chen, H.; Jen, A. K. Y. *Chemistry of Materials* **2018**, *30*, 5429.

[32] Hou, J.; Inganas, O.; Friend, R. H.; Gao, F. *Nature materials* **2018**, *17*, 119.

[33] Wadsworth, A.; Moser, M.; Marks, A.; Little, M. S.; Gasparini, N.; Brabec, C. J.; Baran, D.; McCulloch, I. *Chemical Society reviews* **2019**, *48*, 1596.

[34] Zhang, G.; Zhao, J.; Chow, P. C. Y.; Jiang, K.; Zhang, J.; Zhu, Z.; Zhang, J.; Huang, F.; Yan, H. *Chemical reviews* **2018**, *118*, 3447.

[35] Cheng, P.; Li, G.; Zhan, X.; Yang, Y. *Nature Photonics* **2018**, *12*, 131.

[36] Yan, C.; Barlow, S.; Wang, Z.; Yan, H.; Jen, A. K. Y.; Marder, S. R.; Zhan, X. *Nature Reviews Materials* **2018**, *3*.

[37] Zhao, W.; Li, S.; Yao, H.; Zhang, S.; Zhang, Y.; Yang, B.; Hou, J. *Journal of the American Chemical Society* **2017**, *139*, 7148.

[38] Zhang, H.; Yao, H.; Hou, J.; Zhu, J.; Zhang, J.; Li, W.; Yu, R.; Gao, B.; Zhang, S.; Hou, J. *Advanced materials* **2018**, *30*, e1800613.

[39] Holliday, S.; Ashraf, R. S.; Nielsen, C. B.; Kirkus, M.; Rohr, J. A.; Tan, C. H.; Collado-Fregoso, E.; Knall, A. C.; Durrant, J. R.; Nelson, J.; McCulloch, I. *Journal of the American Chemical Society* **2015**, *137*, 898.

[40] Holliday, S.; Ashraf, R. S.; Wadsworth, A.; Baran, D.; Yousaf, S. A.; Nielsen, C. B.; Tan, C. H.; Dimitrov, S. D.; Shang, Z.; Gasparini, N.; Alamoudi, M.; Laquai, F.; Brabec, C. J.; Salleo, A.; Durrant, J. R.; McCulloch, I. *Nature communications* **2016**, *7*, 11585.

[41] Baran, D.; Ashraf, R. S.; Hanifi, D. A.; Abdelsamie, M.; Gasparini, N.; Rohr, J. A.; Holliday, S.; Wadsworth, A.; Lockett, S.; Neophytou, M.; Emmott, C. J.; Nelson, J.; Brabec, C. J.; Amassian, A.; Salleo, A.; Kirchartz, T.; Durrant, J. R.; McCulloch, I. *Nature materials* **2017**, *16*, 363.

[42] Yuan, J.; Zhang, Y.; Zhou, L.; Zhang, G.; Yip, H.-L.; Lau, T.-K.; Lu, X.; Zhu, C.; Peng, H.; Johnson, P. A.; Leclerc, M.; Cao, Y.; Ulanski, J.; Li, Y.; Zou, Y. *Joule* **2019**, *3*, 1140.

[43] Gao, K.; Jo, S. B.; Shi, X.; Nian, L.; Zhang, M.; Kan, Y.; Lin, F.; Kan, B.; Xu, B.; Rong, Q.; Shui, L.; Liu, F.; Peng, X.; Zhou, G.; Cao, Y.; Jen, A. K. *Advanced materials* **2019**, *31*, e1807842.

[44] Tour, J. M.; Wu, R. *Macromolecules* **1992**, *25*, 1901.

[45] Shi, X.; Zuo, L.; Jo, S. B.; Gao, K.; Lin, F.; Liu, F.; Jen, A. K. Y. *Chemistry of Materials* **2017**, *29*, 8369.

[46] Shi, X.; Chen, J.; Gao, K.; Zuo, L.; Yao, Z.; Liu, F.; Tang, J.; Jen, A. K. Y. *Advanced Energy Materials* **2018**, *8*, 1702831.

[47] Yao, H.; Chen, Y.; Qin, Y.; Yu, R.; Cui, Y.; Yang, B.; Li, S.; Zhang, K.; Hou, J. *Advanced materials* **2016**, *28*, 8283.

[48] Yao, H.; Cui, Y.; Yu, R.; Gao, B.; Zhnag, H.; Hou, J. *Angewandte Chemie* **2017**, *56*, 3045.

[49] Roncali, J.; Thobie-Gautier, C. *Advanced materials* **1994**, *6*, 846.

[50] Chen, Y.-L.; Chang, C.-Y.; Cheng, Y.-J.; Hsu, C.-S. *Chemistry of Materials* **2012**, *24*, 3964.

[51] Lin, Y.; He, Q.; Zhao, F.; Huo, L.; Mai, J.; Lu, X.; Su, C. J.; Li, T.; Wang, J.; Zhu, J.; Sun, Y.; Wang, C.; Zhan, X. *Journal of the American Chemical Society* **2016**, *138*, 2973.

[52] Swick, S. M.; Zhu, W.; Matta, M.; Aldrich, T. J.; Harbuzaru, A.; Lopez Navarrete, J. T.; Ponce Ortiz, R.; Kohlstedt, K. L.; Schatz, G. C.; Facchetti, A.; Melkonyan, F. S.; Marks, T. J. *Proceedings of the National Academy of Sciences of the United States of America* **2018**, *115*, E8341.

[53] Chang, S.-L.; Cao, F.-Y.; Huang, W.-C.; Huang, P.-K.; Huang, K.-H.; Hsu, C.-S.; Cheng, Y.-J. *ACS Energy Letters* **2018**, *3*, 1722.

[54] Liang, Z.; Li, M.; Zhang, X.; Wang, Q.; Jiang, Y.; Tian, H.; Geng, Y. *Journal of Materials Chemistry A* **2018**, *6*, 8059.

[55] Wan, S. S.; Chang, C.; Wang, J. L.; Yuan, G. Z.; Wu, Q.; Zhang, M.; Li, Y. *Solar RRL* **2018**, 1800250.

[56] Meng, D.; Sun, D.; Zhong, C.; Liu, T.; Fan, B.; Huo, L.; Li, Y.; Jiang, W.; Choi, H.; Kim, T.; Kim, J. Y.; Sun, Y.; Wang, Z.; Heeger, A. J. *Journal of the American Chemical Society* **2016**, *138*, 375.

[57] Liang, T.; Xiao, L.; Liu, C.; Gao, K.; Qin, H.; Cao, Y.; Peng, X. *Organic Electronics* **2016**, *29*, 127.

[58] Cao, F.-Y.; Tseng, C.-C.; Lin, F.-Y.; Chen, Y.; Yan, H.; Cheng, Y.-J. *Chemistry of Materials* **2017**, *29*, 10045.

[59] Tsai, C.-E.; Yu, R.-H.; Lin, F.-J.; Lai, Y.-Y.; Hsu, J.-Y.; Cheng, S.-W.; Hsu, C.-S.; Cheng, Y.-J. *Chemistry of Materials* **2016**, *28*, 5121.

[60] Pao, Y.-C.; Yang, C.-T.; Lai, Y.-Y.; Huang, W.-C.; Hsu, C.-S.; Cheng, Y.-J. *Polymer Chemistry* **2016**, *7*, 4654.

[61] Lai, Y.-Y.; Chang, H.-H.; Lai, Y.-Y.; Liang, W.-W.; Tsai, C.-E.; Cheng, Y.-J. *Macromolecules* **2015**, *48*, 6994.

[62] Pao, Y. C.; Chen, Y. L.; Chen, Y. T.; Cheng, S. W.; Lai, Y. Y.; Huang, W. C.; Cheng, Y. J. *Organic letters* **2014**, *16*, 5724.

[63] Fringuelli, F.; Marino, G.; Taticchi, A. *Journal of the Chemical Society, Perkin Transactions 2* **1974**, 689.

[64] Patra, A.; Bendikov, M. *J. Mater. Chem.* **2010**, *20*, 422.

[65] Kang, I.; An, T. K.; Hong, J. A.; Yun, H. J.; Kim, R.; Chung, D. S.; Park, C. E.; Kim, Y. H.; Kwon, S. K. *Advanced materials* **2013**, *25*, 524.

[66] Li, Y.; Qian, D.; Zhong, L.; Lin, J.-D.; Jiang, Z.-Q.; Zhang, Z.-G.; Zhang, Z.; Li, Y.; Liao, L.-S.; Zhang, F. *Nano Energy* **2016**, *27*, 430.

[67] Li, Y.; Zhong, L.; Wu, F.-P.; Yuan, Y.; Bin, H.-J.; Jiang, Z.-Q.; Zhang, Z.; Zhang, Z.-G.; Li, Y.; Liao, L.-S. *Energy & Environmental Science* **2016**, *9*, 3429.

[68] Wang, J.-L.; Liu, K.-K.; Hong, L.; Ge, G.-Y.; Zhang, C.; Hou, J. *ACS Energy Letters* **2018**, *3*, 2967.

[69] Mishra, S. P.; Javier, A. E.; Zhang, R.; Liu, J.; Belot, J. A.; Osaka, I.; McCullough, R. D. *J. Mater. Chem.* **2011**, *21*, 1551.

[70] Iteke, F. B.; Christiaens, L.; Renson, M. *Tetrahedron* **1976**, *32*, 589.

[71] Konar, A. *Chemica Scripta* **1983**, *22*, 177.

[72] Litvinov, V. P.; Konyaeva, P.; Gol'dfarb, Y. L. *Bulletin of the Academy of Sciences of the USSR, Division of Chemical Science* **1974**, *23*, 1493.

[73] Lin, L.-Y.; Lu, C.-W.; Huang, W.-C.; Chen, Y.-H.; Lin, H.-W.; Wong, K.-T. *Organic letters* **2011**, *13*, 4962.

[74] Bredas, J.-L. *Mater. Horiz.* **2014**, *1*, 17.

[75] Schroeder, B. C.; Li, Z.; Brady, M. A.; Faria, G. C.; Ashraf, R. S.; Takacs, C. J.; Cowart, J. S.; Duong, D. T.; Chiu, K. H.; Tan, C. H.; Cabral, J. T.; Salleo, A.; Chabinyc, M. L.; Durrant, J. R.; McCulloch, I. *Angewandte Chemie* **2014**, *53*, 12870.

[76] Maurano, A.; Shuttle, C. G.; Hamilton, R.; Ballantyne, A. M.; Nelson, J.; Zhang, W.; Heeney, M.; Durrant, J. R. *The Journal of Physical Chemistry C* **2011**, *115*, 5947.

[77] Bartesaghi, D.; Perez Idel, C.; Kniepert, J.; Roland, S.; Turbiez, M.; Neher, D.; Koster, L. J. *Nature communications* **2015**, *6*, 7083.

[78] Singh, R.; Lee, J.; Kim, M.; Keivanidis, P. E.; Cho, K. *Journal of Materials Chemistry A* **2017**, *5*, 210.

[79] Liu, F.; Gu, Y.; Shen, X.; Ferdous, S.; Wang, H.-W.; Russell, T. P. *Progress in Polymer Science* **2013**, *38*, 1990.

[80] Liu, X.; Nian, L.; Gao, K.; Zhang, L.; Qing, L.; Wang, Z.; Ying, L.; Xie, Z.; Ma, Y.; Cao, Y.; Liu, F.; Chen, J. *Journal of Materials Chemistry A* **2017**, *5*, 17619.

[81] Huang, J.; Tang, Y.; Gao, K.; Liu, F.; Guo, H.; Russell, T. P.; Yang, T.; Liang, Y.; Cheng, X.; Guo, X. *Macromolecules* **2016**, *50*, 137.

[82] Gao, K.; Miao, J.; Xiao, L.; Deng, W.; Kan, Y.; Liang, T.; Wang, C.; Huang, F.; Peng, J.; Cao, Y.; Liu, F.; Russell, T. P.; Wu, H.; Peng, X. *Advanced materials* **2016**, *28*, 4727.

[83] Turbiez, M.; Frere, P.; Leriche, P.; Mercier, N.; Roncali, J. *Chemical communications* **2005**, 1161.

[84] Li, C.-Z.; Chueh, C.-C.; Yip, H.-L.; O'Malley, K. M.; Chen, W.-C.; Jen, A. K. Y. *Journal of Materials Chemistry* **2012**, *22*, 8574.

[85] Sun, Y.; Seo, J. H.; Takacs, C. J.; Seifter, J.; Heeger, A. J. *Advanced materials* **2011**, *23*, 1679.

[86] Zhang, Z.; Yu, J.; Yin, X.; Hu, Z.; Jiang, Y.; Sun, J.; Zhou, J.; Zhang, F.; Russell, T. P.; Liu, F.; Tang, W. *Advanced Functional Materials* **2018**, *28*, 1705095.

[87] Gao, H. H.; Sun, Y.; Cai, Y.; Wan, X.; Meng, L.; Ke, X.; Li, S.; Zhang, Y.; Xia, R.; Zheng, N.; Xie, Z.; Li, C.; Zhang, M.; Yip, H. L.; Cao, Y.; Chen, Y. *Advanced Energy Materials* **2019**, *9*, 1901024.

[88] Cui, Y.; Yao, H.; Zhang, J.; Zhang, T.; Wang, Y.; Hong, L.; Xian, K.; Xu, B.; Zhang, S.; Peng, J.; Wei, Z.; Gao, F.; Hou, J. *Nature communications* **2019**, *10*, 2515.

[89] Hong, L.; Yao, H.; Wu, Z.; Cui, Y.; Zhang, T.; Xu, Y.; Yu, R.; Liao, Q.; Gao, B.; Xian, K.; Woo, H. Y.; Ge, Z.; Hou, J. *Advanced materials* **2019**, e1903441.

[90] Feng, L.; Yuan, J.; Zhang, Z.; Peng, H.; Zhang, Z. G.; Xu, S.; Liu, Y.; Li, Y.; Zou, Y. *ACS applied materials & interfaces* **2017**, *9*, 31985.

[91] Cheng, Y.-J.; Ho, Y.-J.; Chen, C.-H.; Kao, W.-S.; Wu, C.-E.; Hsu, S.-L.; Hsu, C.-S. *Macromolecules* **2012**, *45*, 2690.

[92] Ye, X.; Zhao, X.; Li, Q.; Ma, Y.; Song, W.; Quan, Y.-Y.; Wang, Z.; Wang, M.; Huang, Z.-S. *Dyes and Pigments* **2019**, *164*, 407.

[93] Bruce, P. G.; Freunberger, S. A.; Hardwick, L. J.; Tarascon, J. M. *Nature materials* **2011**, *11*, 19.

[94] Kim, H.; Lee, J.; Ahn, H.; Kim, O.; Park, M. J. *Nature communications* **2015**, *6*, 7278.

[95] Kunz, T.; Knochel, P. *Chemistry - A European Journal* **2011**, *17*, 866.

[96] Shi, X.; Liao, X.; Gao, K.; Zuo, L.; Chen, J.; Zhao, J.; Liu, F.; Chen, Y.; Jen, A. K. Y. *Advanced Functional Materials* **2018**, *28*, 1802324.

[97] Coffin, R. C.; Peet, J.; Rogers, J.; Bazan, G. C. *Nature chemistry* **2009**, *1*, 657.

[98] Liao, X.; Shi, X.; Zhang, M.; Gao, K.; Zuo, L.; Liu, F.; Chen, Y.; Jen, A. K. *Chemical communications* **2019**, *55*, 8258.

[99] Lin, F.; Zuo, L.; Gao, K.; Zhang, M.; Jo, S. B.; Liu, F.; Jen, A. K. Y. *Chemistry of Materials* **2019**, *31*, 6770.

[100] Kato, S.; Furuya, T.; Kobayashi, A.; Nitani, M.; Ie, Y.; Aso, Y.; Yoshihara, T.; Tobita, S.; Nakamura, Y. *The Journal of organic chemistry* **2012**, *77*, 7595.

[101] Kato, S.; Furuya, T.; Nitani, M.; Hasebe, N.; Ie, Y.; Aso, Y.; Yoshihara, T.; Tobita, S.; Nakamura, Y. *Chemistry - A European Journal* **2015**, *21*, 3115.

[102] Ghosh, S.; Das, S.; Kumar, N. R.; Agrawal, A. R.; Zade, S. S. *New Journal of Chemistry* **2017**, *41*, 11568.

[103] Kim, D. J.; Je, S. H.; Sampath, S.; Choi, J. W.; Coskun, A. *RSC Advances* **2012**, *2*, 7968.

[104] Bruce, P. G.; Freunberger, S. A.; Hardwick, L. J.; Tarascon, J. M. *Nature materials* **2011**, *11*, 19.

[105] Kang, W.; Deng, N.; Ju, J.; Li, Q.; Wu, D.; Ma, X.; Li, L.; Naebe, M.; Cheng, B. *Nanoscale* **2016**, *8*, 16541.

[106] Tikekar, M. D.; Choudhury, S.; Tu, Z.; Archer, L. A. *Nature Energy* **2016**, *1*, 16114.

[107] Pang, Q.; Liang, X.; Kwok, C. Y.; Nazar, L. F. *Nature Energy* **2016**, *1*, 16132.

[108] Scheers, J.; Fantini, S.; Johansson, P. *Journal of Power Sources* **2014**, *255*, 204.

[109] Ji, X.; Lee, K. T.; Nazar, L. F. *Nature materials* **2009**, *8*, 500.

[110] Kim, J. H.; Kim, T.; Jeong, Y. C.; Lee, K.; Park, K. T.; Yang, S. J.; Park, C. R. *Advanced Energy Materials* **2015**, *5*, 1500268.

[111] Li, Y.; Murphy, I. A.; Chen, Y.; Lin, F.; Wang, X.; Wang, S.; Hubble, D.; Jang, S.-H.; Muller, K. T.; Wang, C.; Jen, A. K. Y.; Yang, J. *Journal of Materials Chemistry A* **2019**, *7*, 13372.

[112] Chung, W. J.; Griebel, J. J.; Kim, E. T.; Yoon, H.; Simmonds, A. G.; Ji, H. J.; Dirlam, P. T.; Glass, R. S.; Wie, J. J.; Nguyen, N. A.; Guralnick, B. W.; Park, J.; Somogyi, A.; Theato, P.; Mackay, M. E.; Sung, Y. E.; Char, K.; Pyun, J. *Nature chemistry* **2013**, *5*, 518.

[113] Kim, H.; Lee, J.; Ahn, H.; Kim, O.; Park, M. J. *Nature communications* **2015**, *6*, 7278.

[114] Sun, Z.; Zhang, J.; Yin, L.; Hu, G.; Fang, R.; Cheng, H. M.; Li, F. *Nature communications* **2017**, *8*, 14627.

[115] Zhu, L.; Li, C.; Ren, W.; Qin, M.; Xu, L. *New Journal of Chemistry* **2018**, *42*, 5109.

[116] Lu, Y.; Korf, K.; Kambe, Y.; Tu, Z.; Archer, L. A. *Angewandte Chemie* **2014**, *53*, 488.

[117] Yang, Y. B.; Liu, Y. X.; Song, Z.; Zhou, Y. H.; Zhan, H. *ACS applied materials & interfaces* **2017**, *9*, 38950.

[118] Magasinski, A.; Zdyrko, B.; Kovalenko, I.; Hertzberg, B.; Burtovyy, R.; Huebner, C. F.; Fuller, T. F.; Luzinov, I.; Yushin, G. *ACS applied materials & interfaces* **2010**, *2*, 3004.

[119] Kwon, T. W.; Jeong, Y. K.; Lee, I.; Kim, T. S.; Choi, J. W.; Coskun, A. *Advanced materials* **2014**, *26*, 7979.

[120] Burattini, S.; Colquhoun, H. M.; Fox, J. D.; Friedmann, D.; Greenland, B. W.; Harris, P. J.; Hayes, W.; Mackay, M. E.; Rowan, S. J. *Chemical communications* **2009**, 6717.

[121] S., B.; Greenland, B. W.; H., M. D.; Weng, W.; Seppala, J.; Colquhoun, H. M.; Hayes, W.; Mackay, M. E.; Hamley, I. W.; Rowan, S. J. *Journal of the American Chemical Society* **2010**, *132*, 12051.

[122] Hart, L. R.; Hunter, J. H.; Nguyen, N. A.; Harries, J. L.; Greenland, B. W.; Mackay, M. E.; Colquhoun, H. M.; Hayes, W. *Polym. Chem.* **2014**, *5*, 3680.

[123] Gu, P. Y.; Zhao, Y.; Xie, J.; Binte Ali, N.; Nie, L.; Xu, Z. J.; Zhang, Q. *ACS applied materials & interfaces* **2016**, *8*, 7464.

[124] Kim, D. J.; Je, S. H.; Sampath, S.; Choi, J. W.; Coskun, A. *RSC Advances* **2012**, *2*, 7968.

[125] Häupler, B.; Wild, A.; Schubert, U. S. *Advanced Energy Materials* **2015**, *5*, 1402034.

[126] Takahashi, M.; Ui, M.; Inuzuka, T.; Sengoku, T.; Yoda, H. *Tetrahedron* **2014**, *70*, 9175.

[127] Golodnitsky, D.; Strauss, E.; Peled, E.; Greenbaum, S. *Journal of The Electrochemical Society* **2015**, *162*, A2551.

[128] Jones, M. W.; Gibson, M. I.; Mantovani, G.; Haddleton, D. M. *Polymer Chemistry* **2011**, *2*, 572.

APPENDIX A: ^{1}H AND ^{13}C NMR SPECTRA

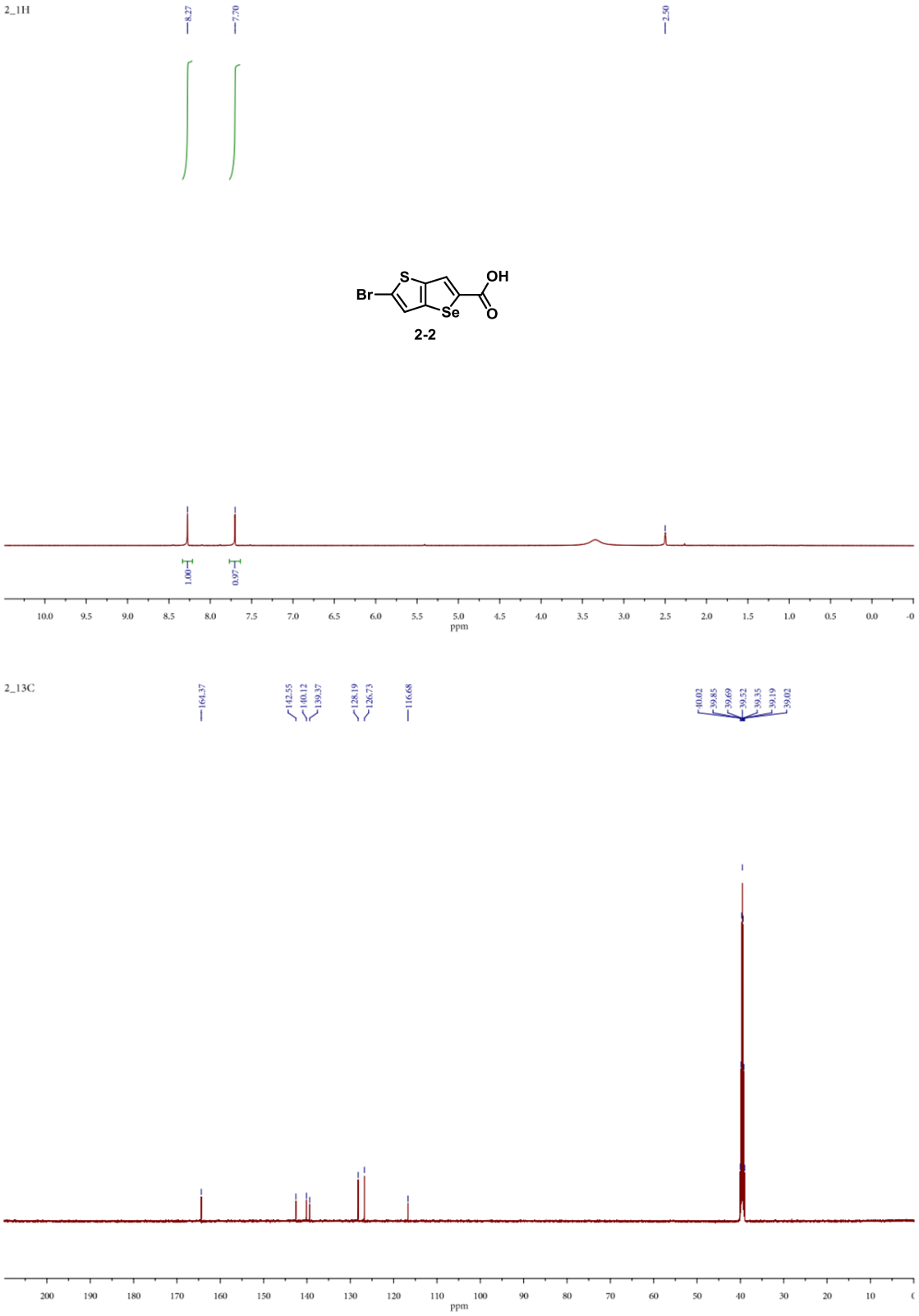

Figure A-1. ^{1}H and ^{13}C NMR spectra of compound **2-2**.

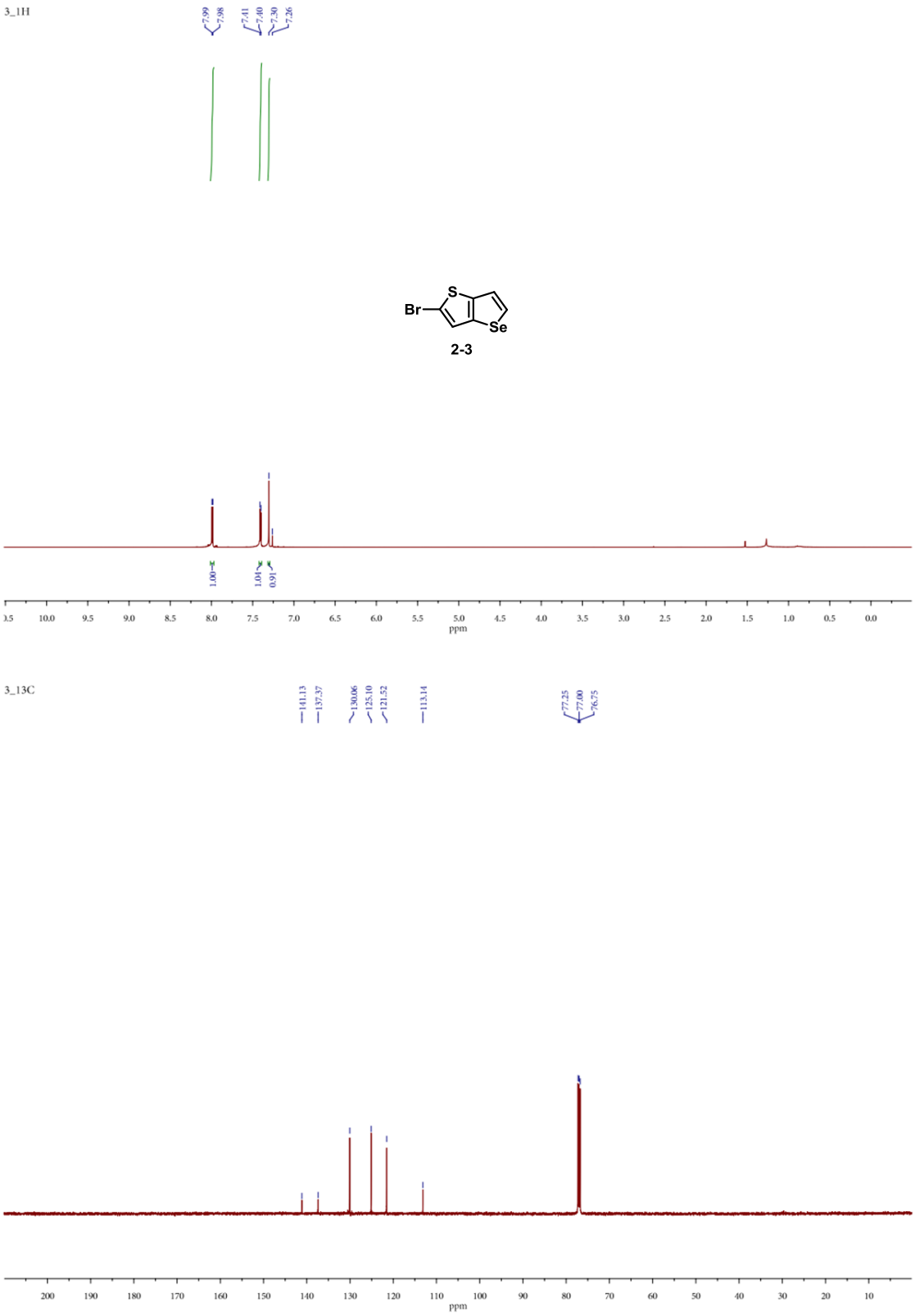

Figure A-2. ^{1}H and ^{13}C NMR spectra of compound **2-3**.

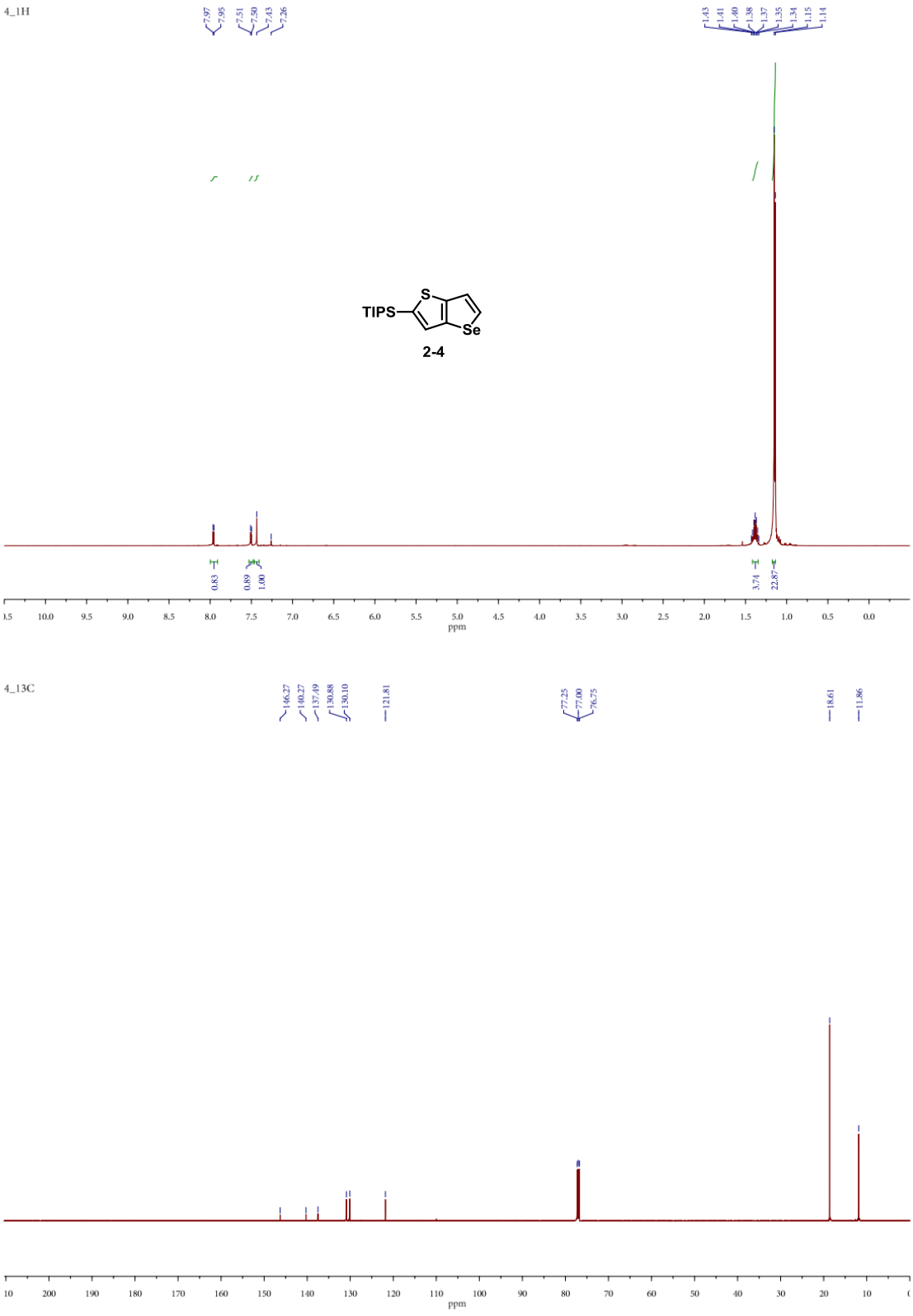

Figure A-3. ^{1}H and ^{13}C NMR spectra of compound **2-4**.

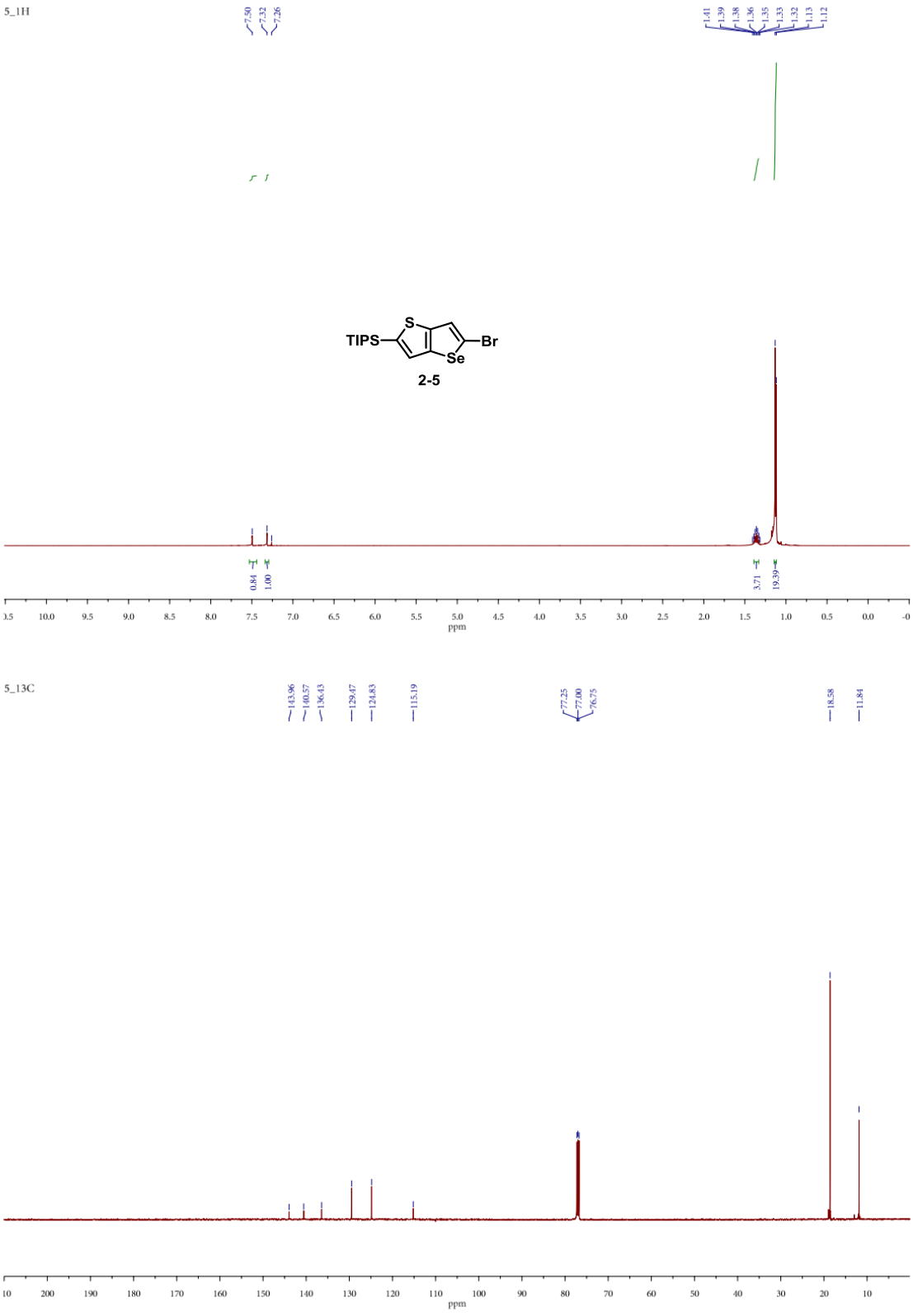

Figure A-4. ^{1}H and ^{13}C NMR spectra of compound **2-5**.

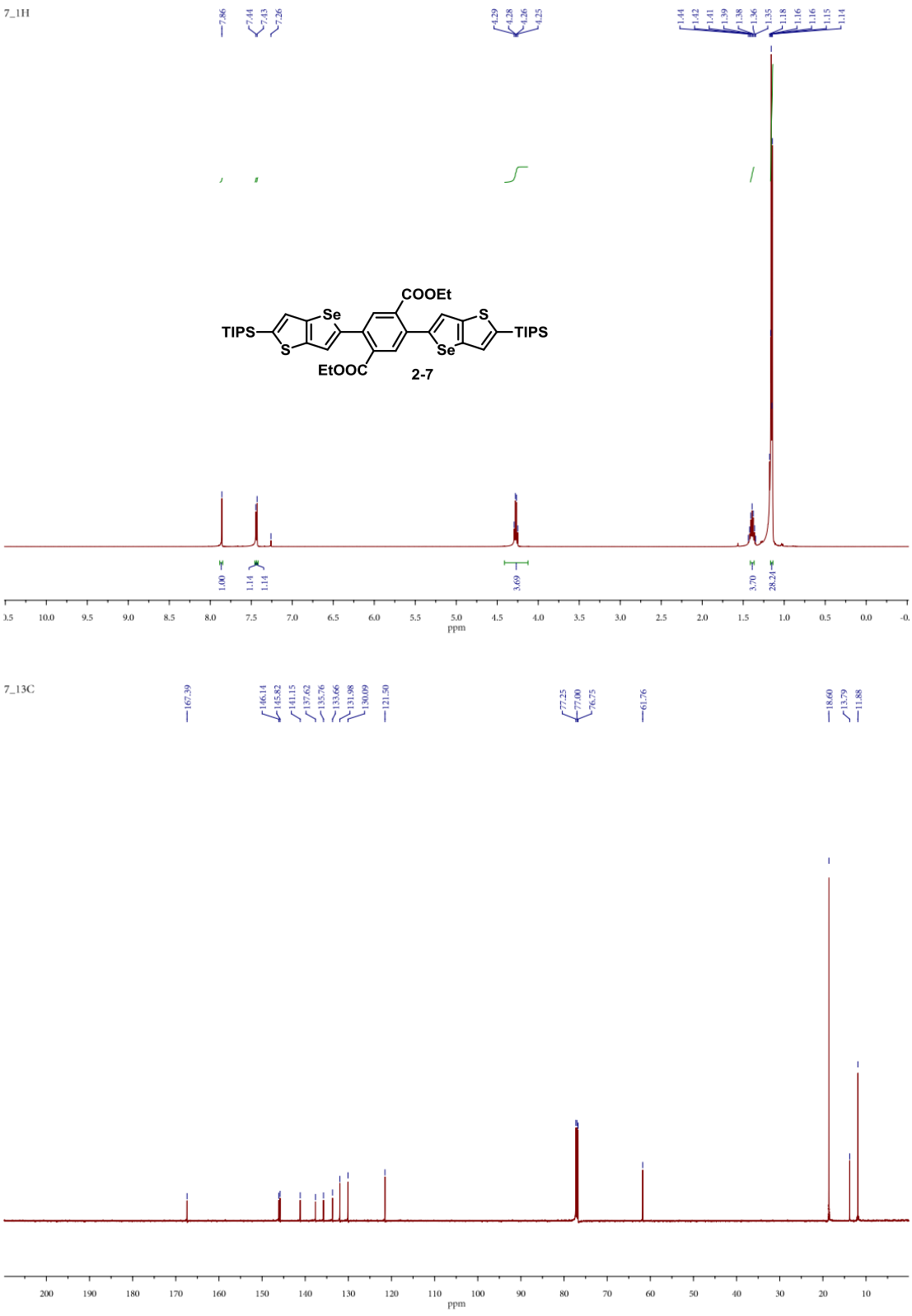

Figure A-5. ^{1}H and ^{13}C NMR spectra of compound **2-7**.

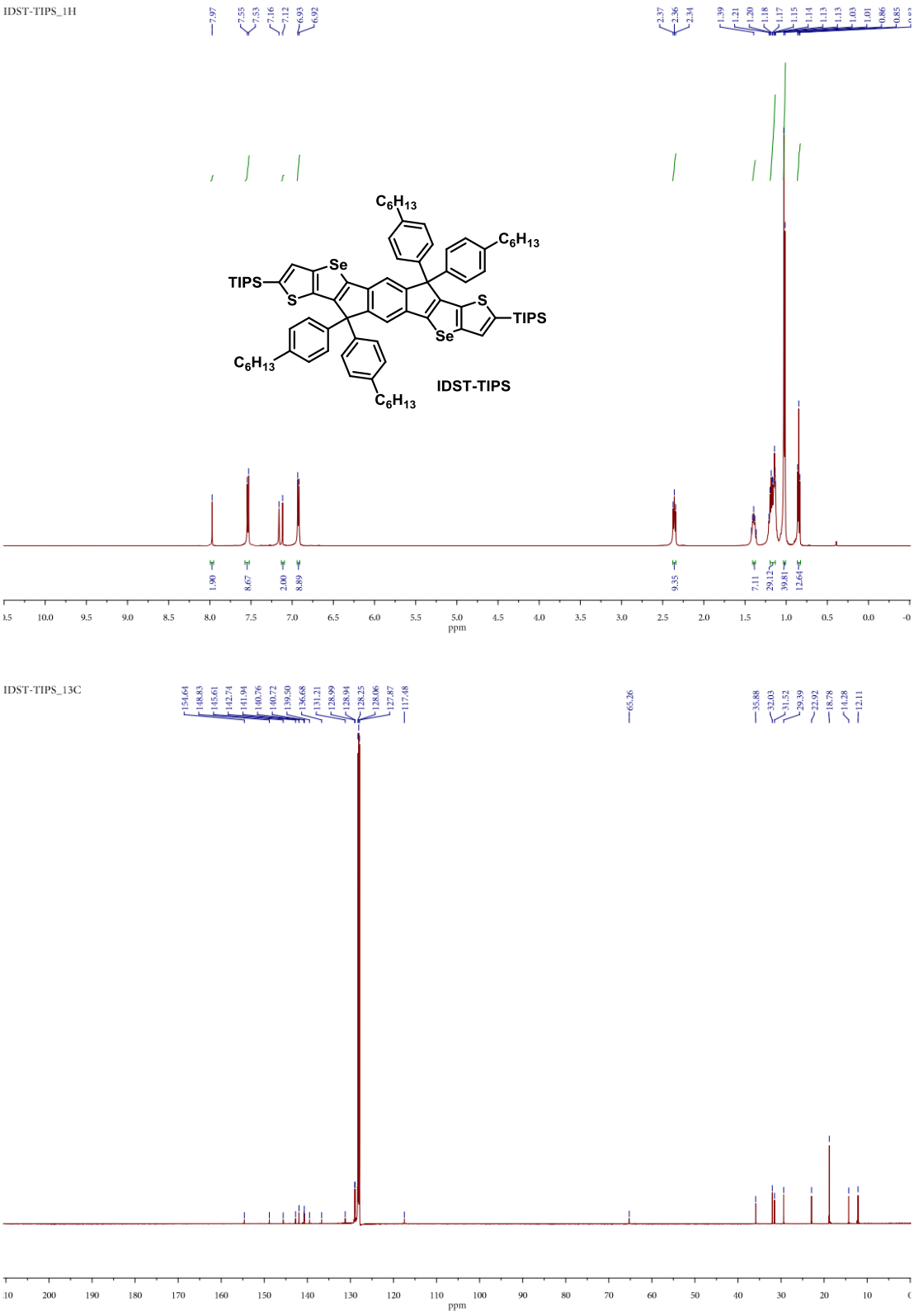

Figure A-6. ^{1}H and ^{13}C NMR spectra of **IDST-TIPS**.

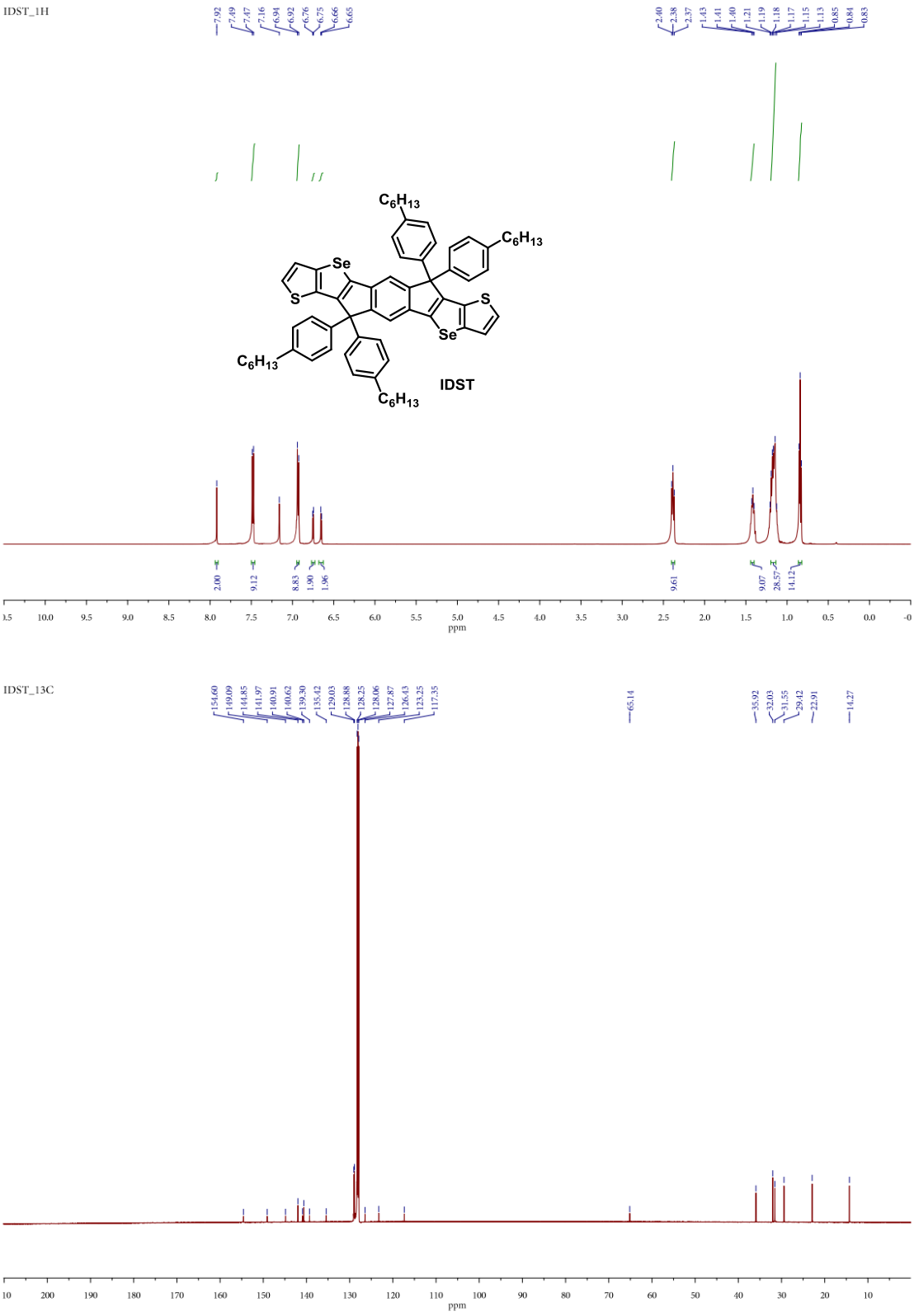

Figure A-7. ^{1}H and ^{13}C NMR spectra of **IDST**.

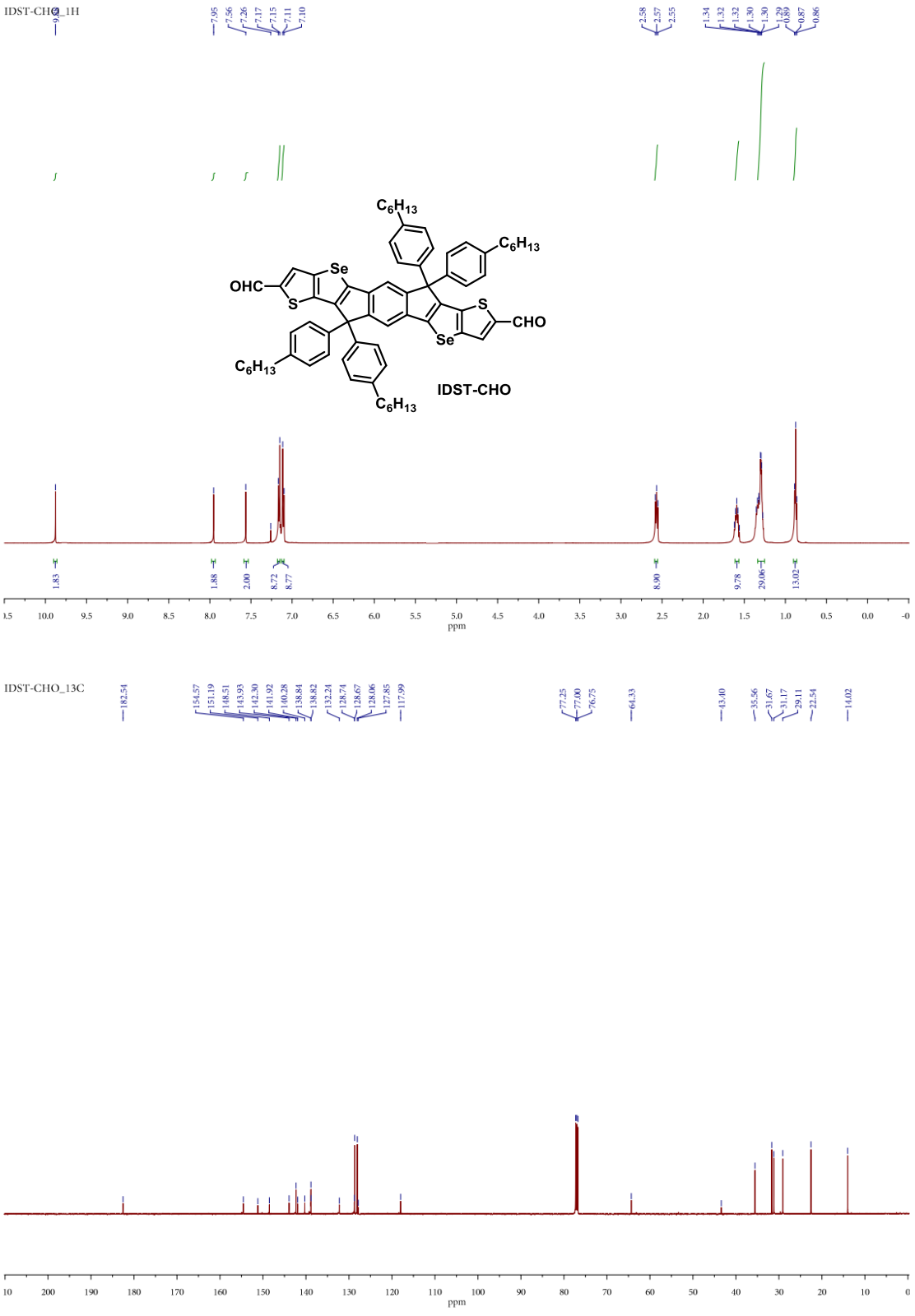

Figure A-8. ^{1}H and ^{13}C NMR spectra of **IDST-CHO**.

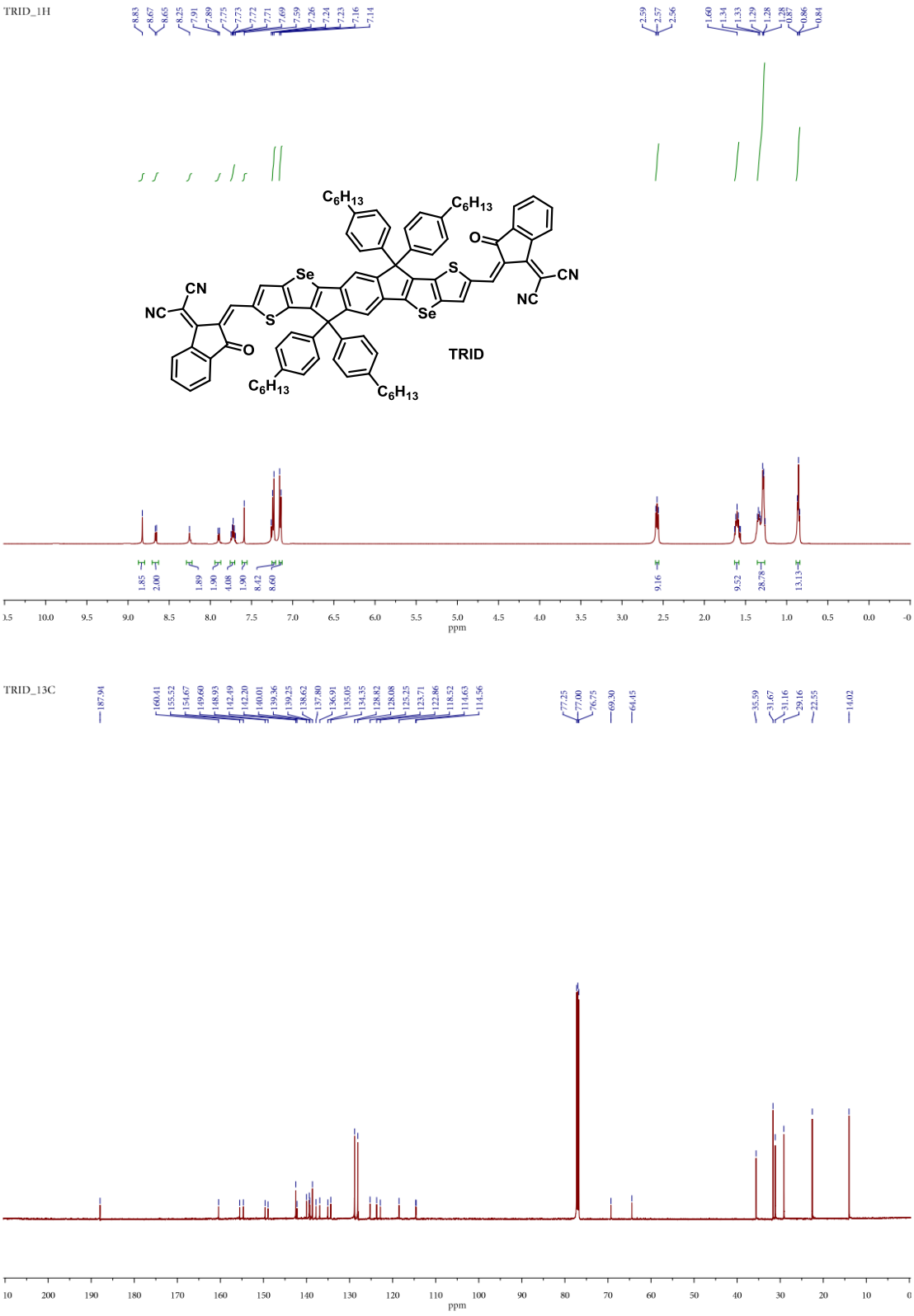

Figure A-9. ^{1}H and ^{13}C NMR spectra of **TRID**.

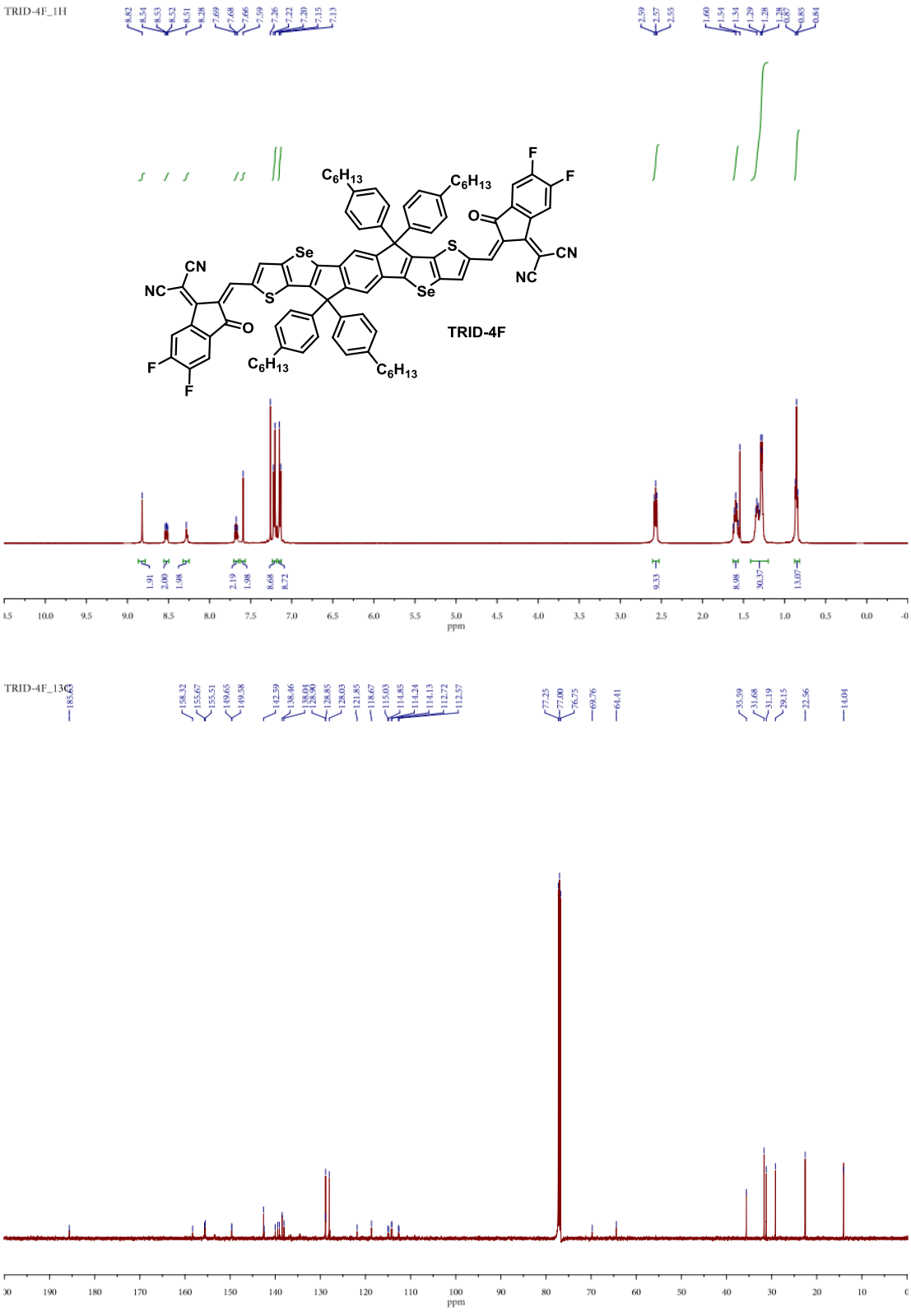

Figure A-10. ^{1}H and ^{13}C NMR spectra of **TRID-4F**.

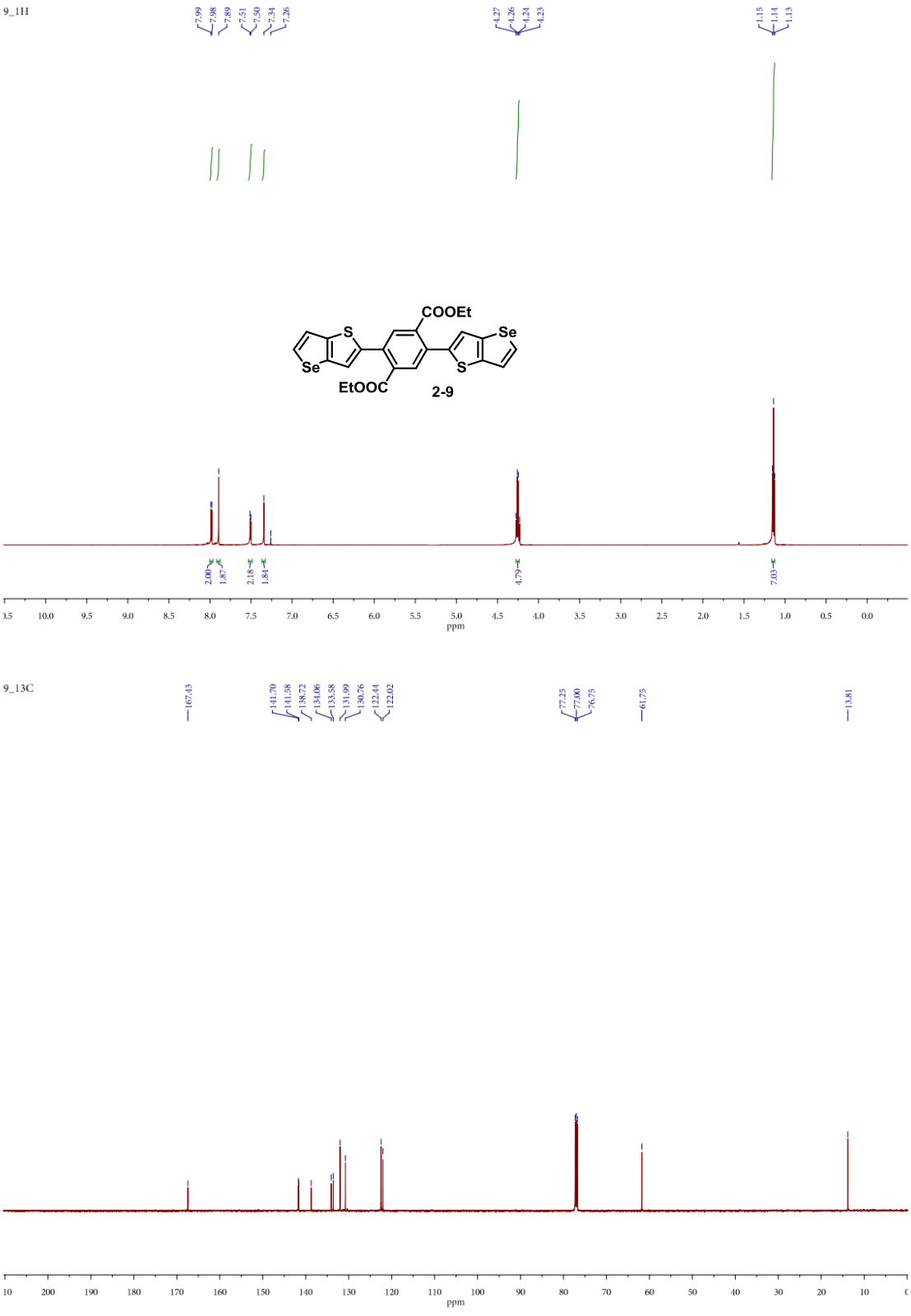

Figure A-11. ^{1}H and ^{13}C NMR spectra of compound **2-9**.

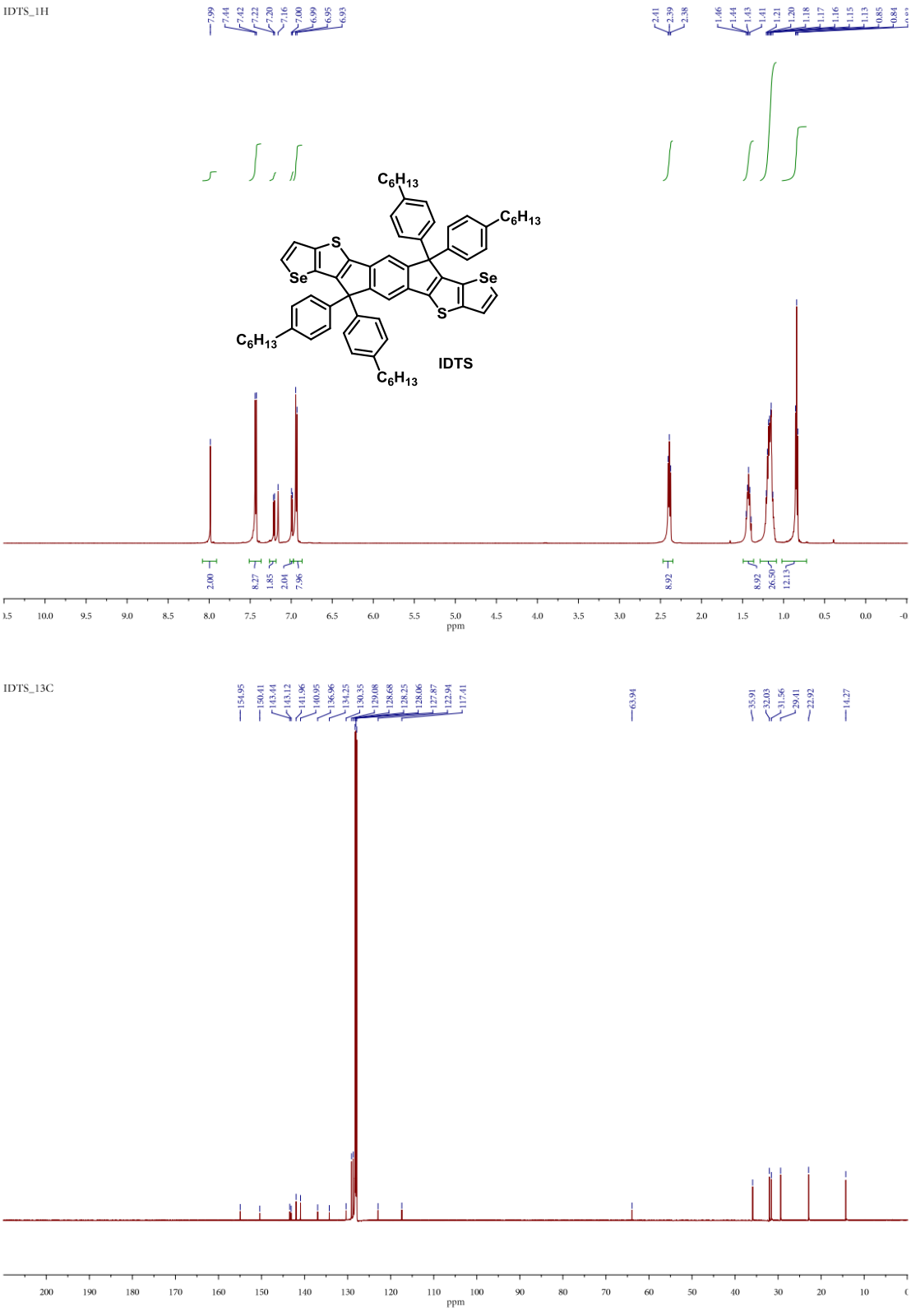

Figure A-12. ^{1}H and ^{13}C NMR spectra of **IDTS**.

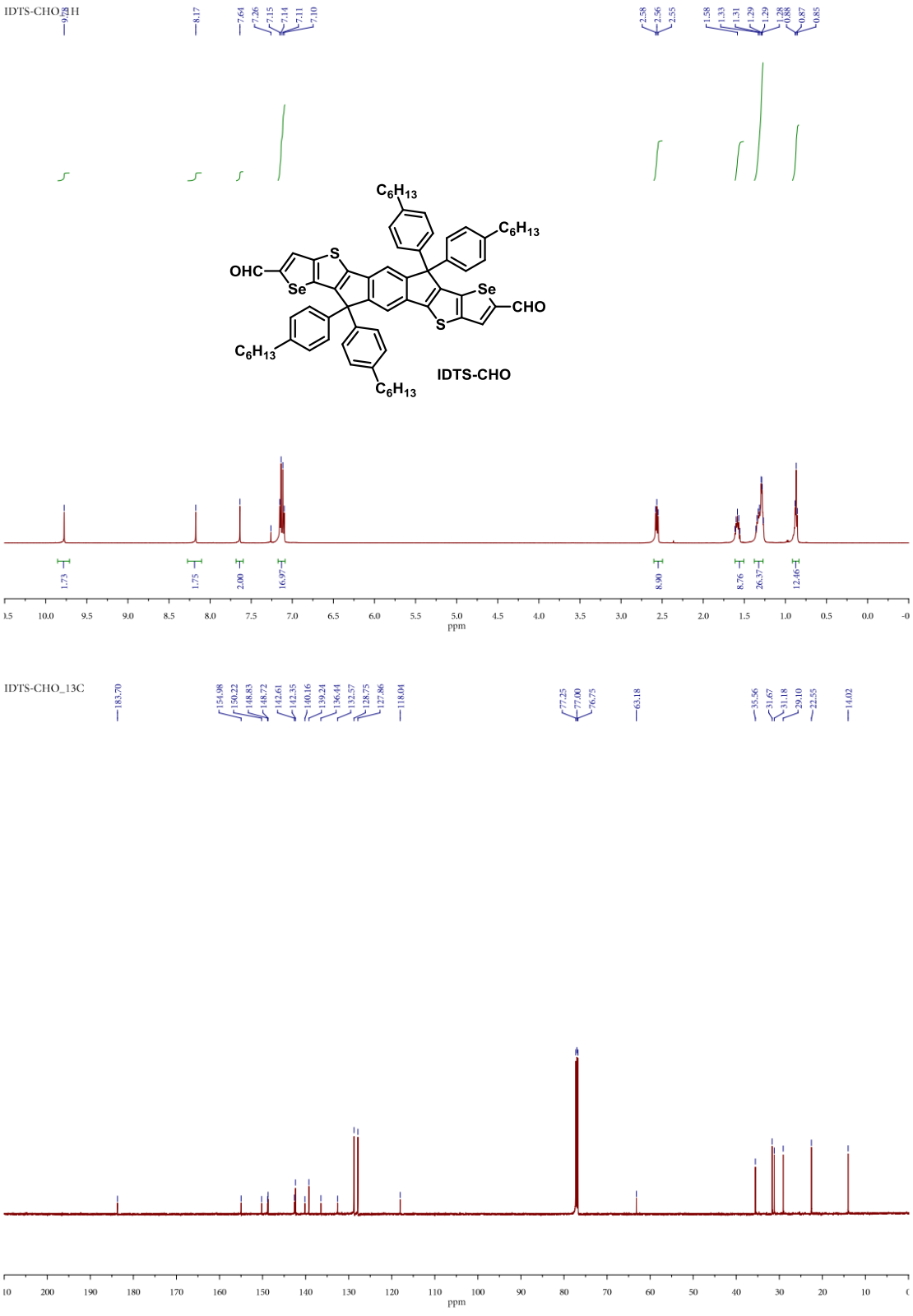

Figure A-13. ^{1}H and ^{13}C NMR spectra of **IDTS-CHO**.

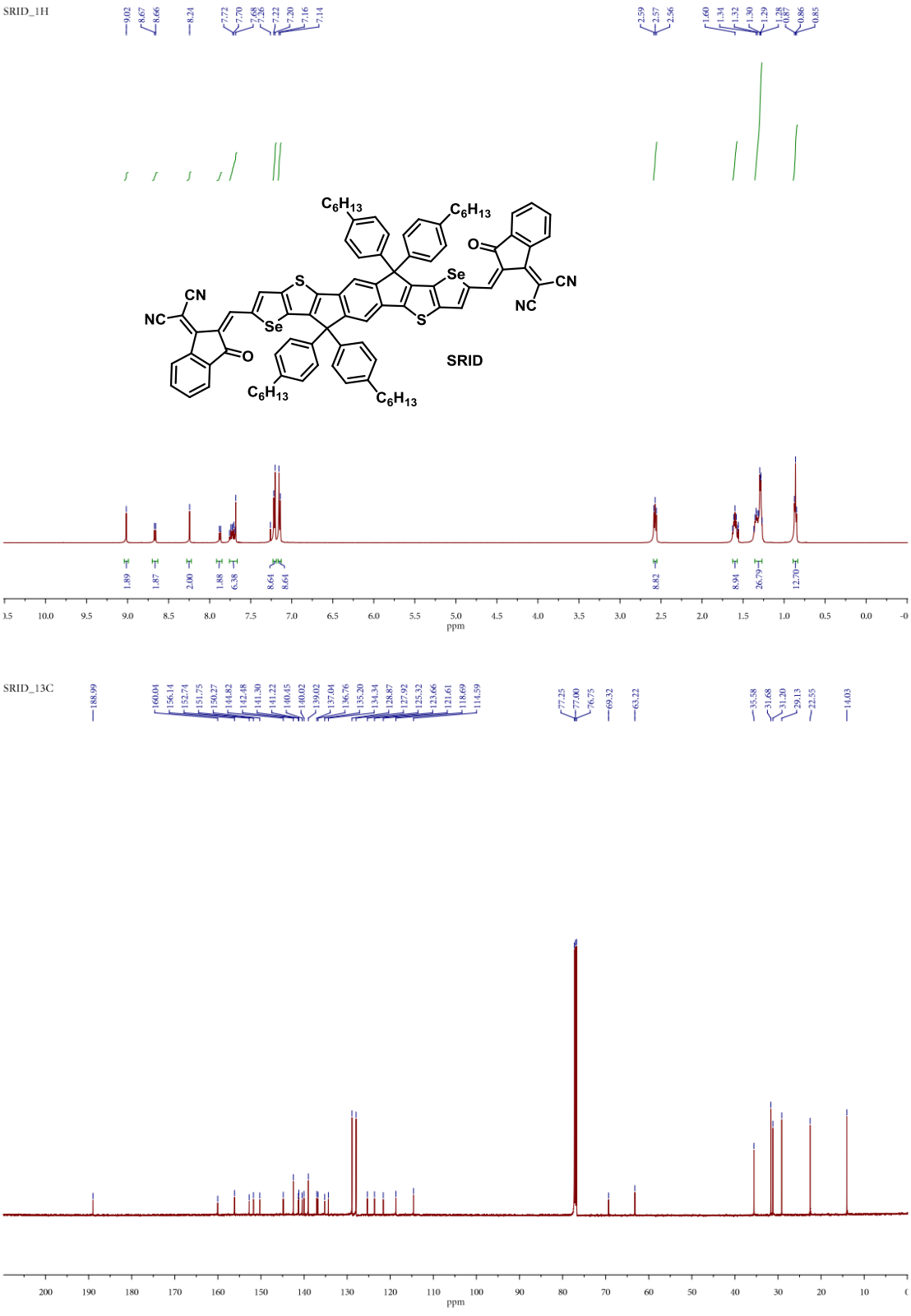

Figure A-14. ^{1}H and ^{13}C NMR spectra of **SRID**.

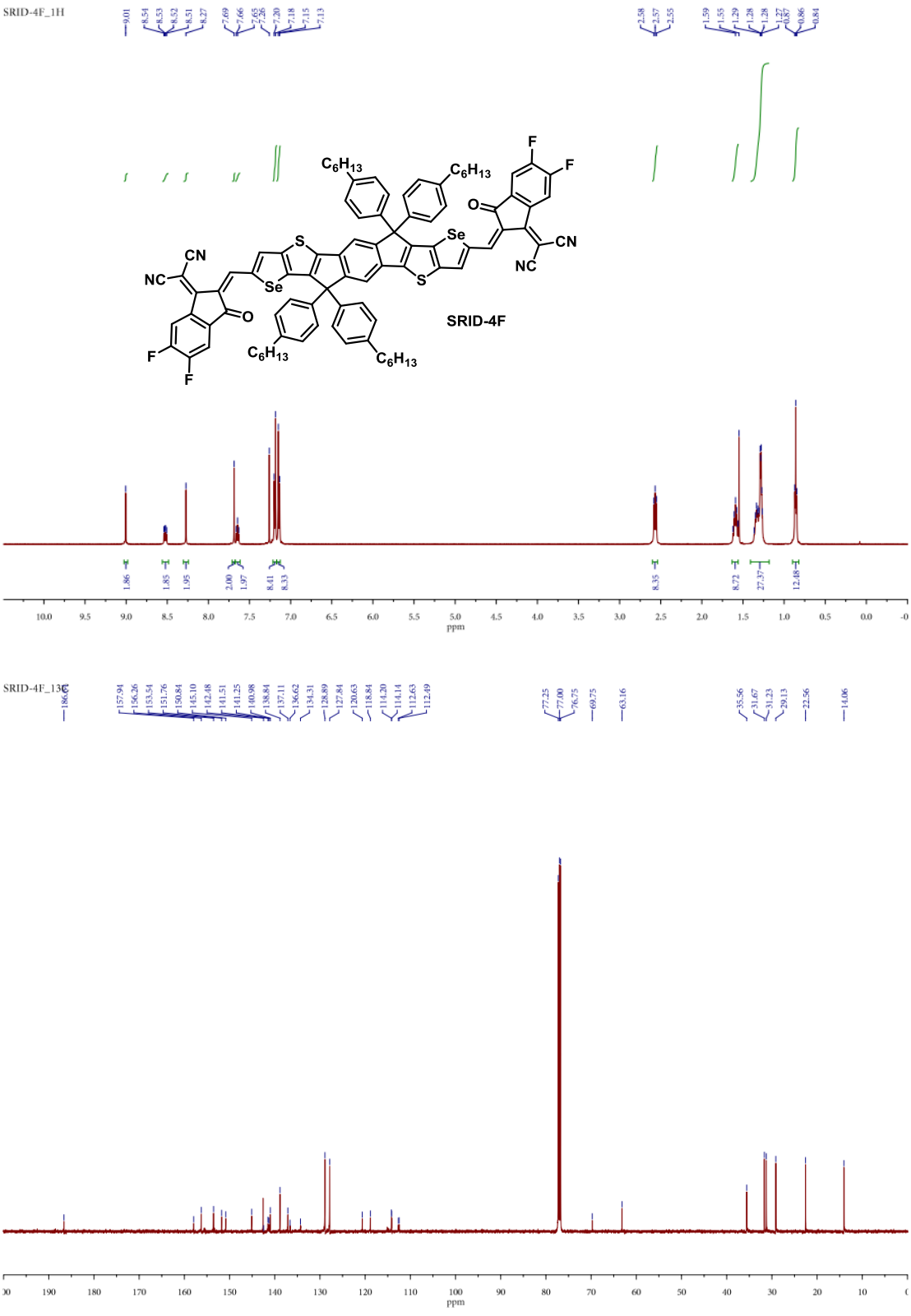

Figure A-15. ^{1}H and ^{13}C NMR spectra of **SRID-4F**.

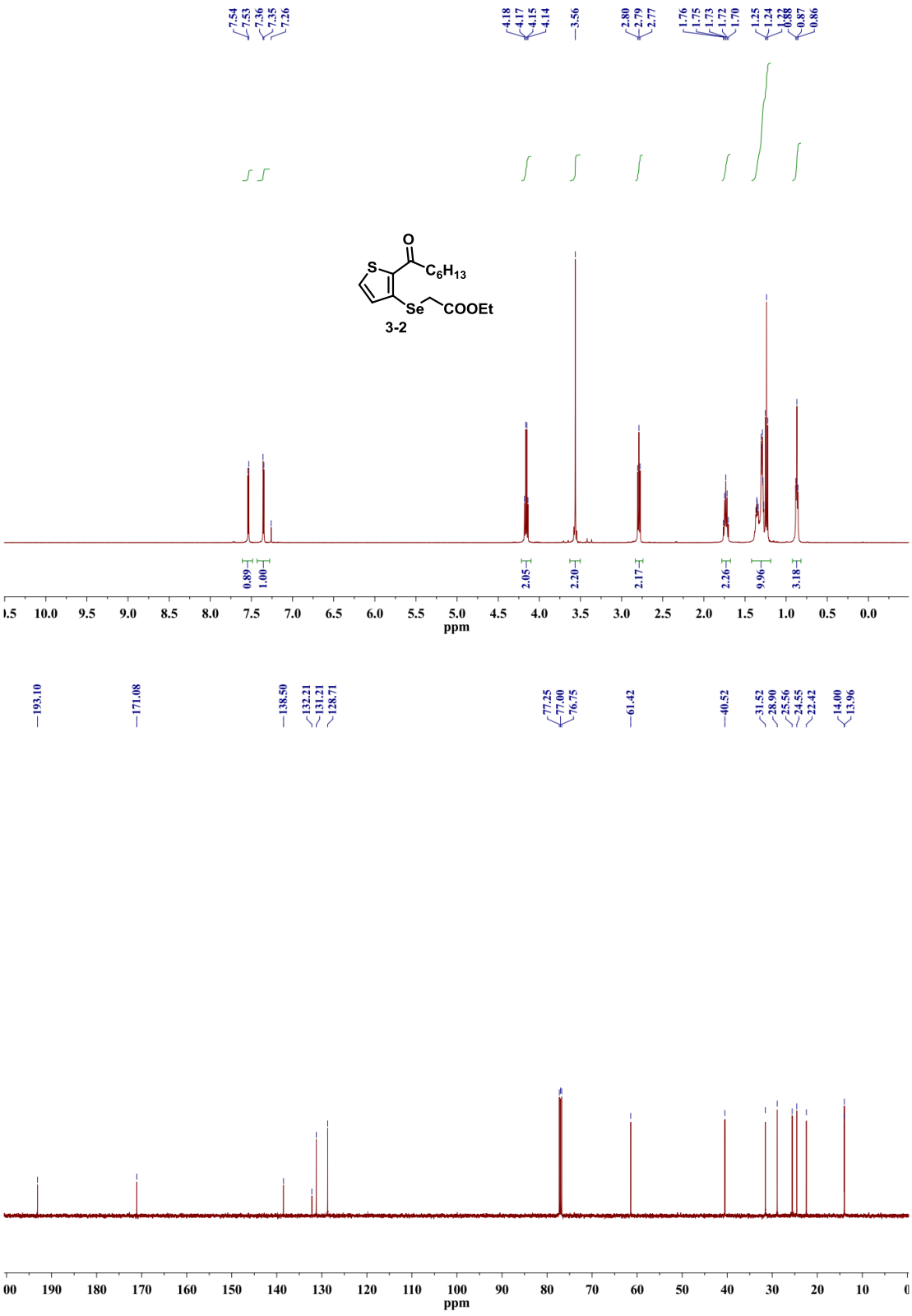

Figure A-16. ^{1}H and ^{13}C NMR spectra of compound **3-2**.

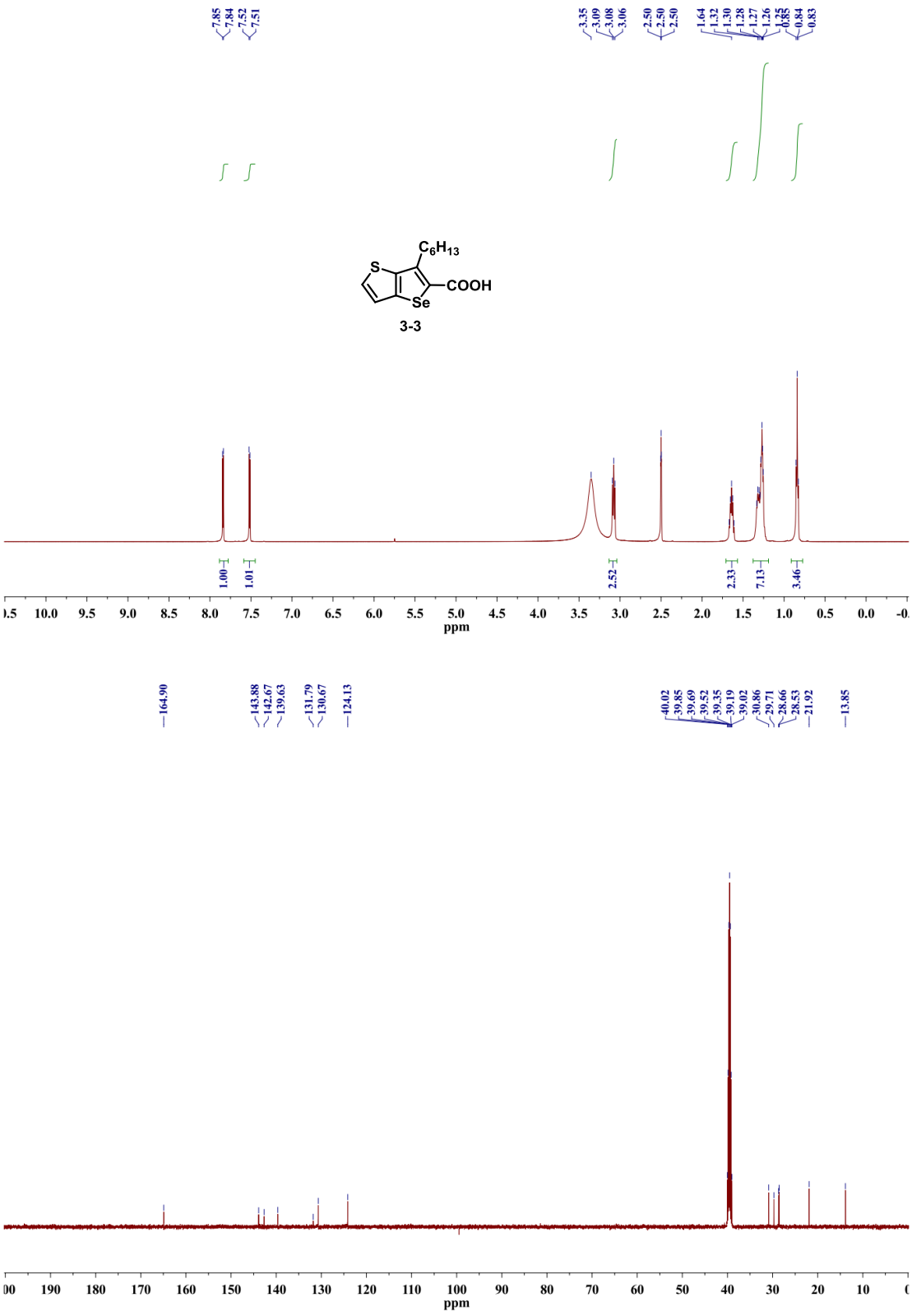

Figure A-17. ^{1}H and ^{13}C NMR spectra of compound **3-3**.

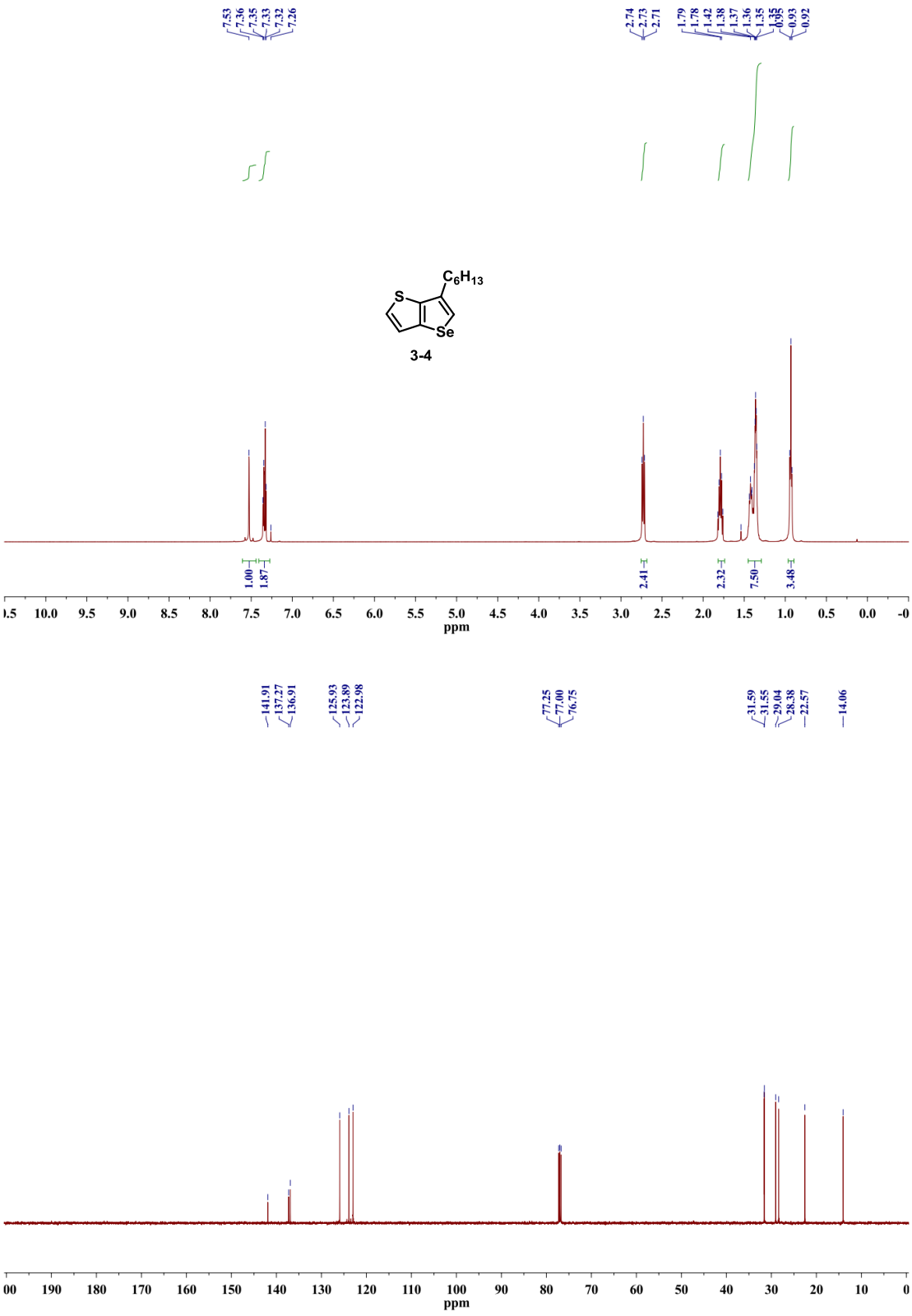

Figure A-18. ^{1}H and ^{13}C NMR spectra of compound **3-4**.

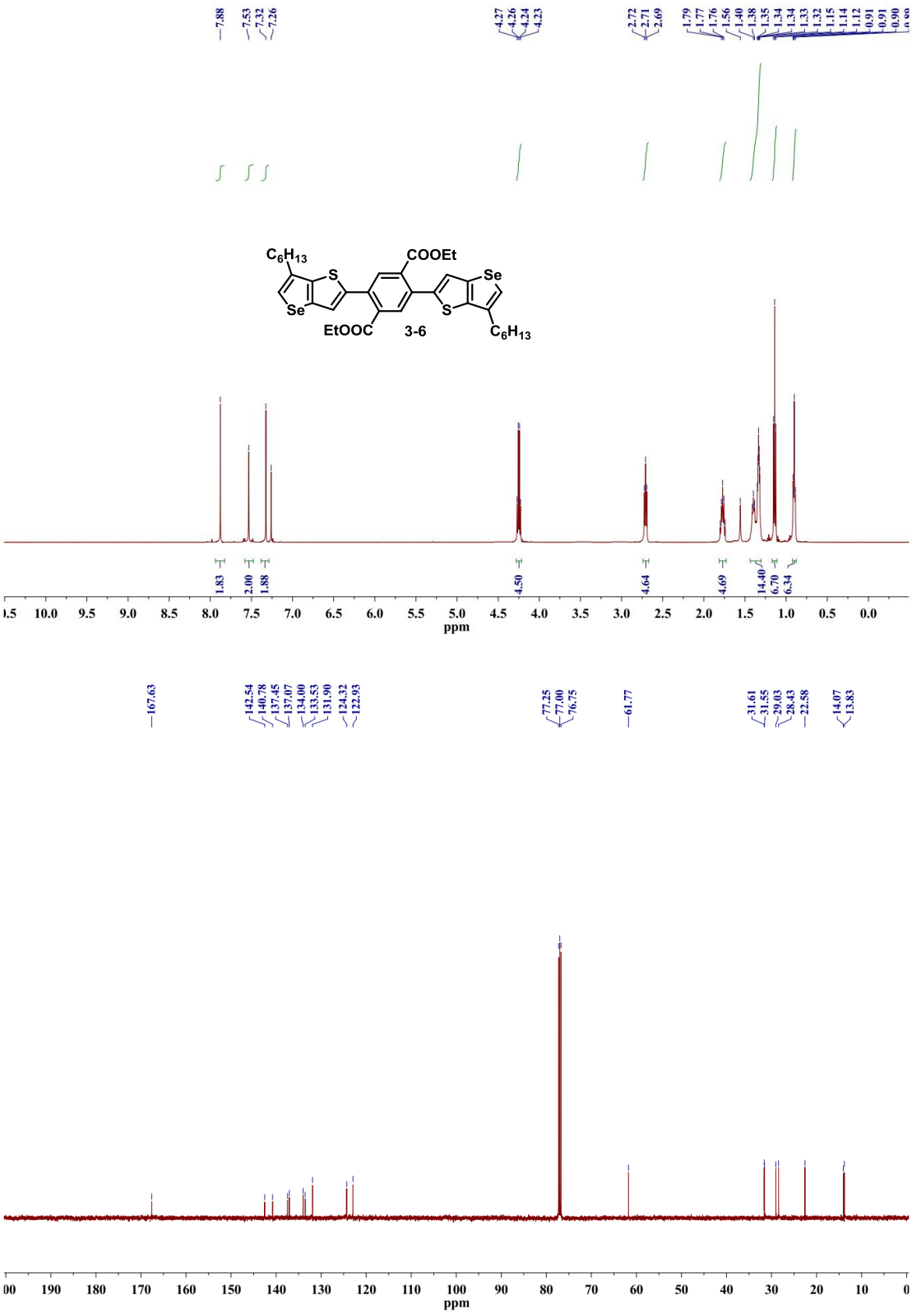

Figure A-19. ^{1}H and ^{13}C NMR spectra of compound **3-6**.

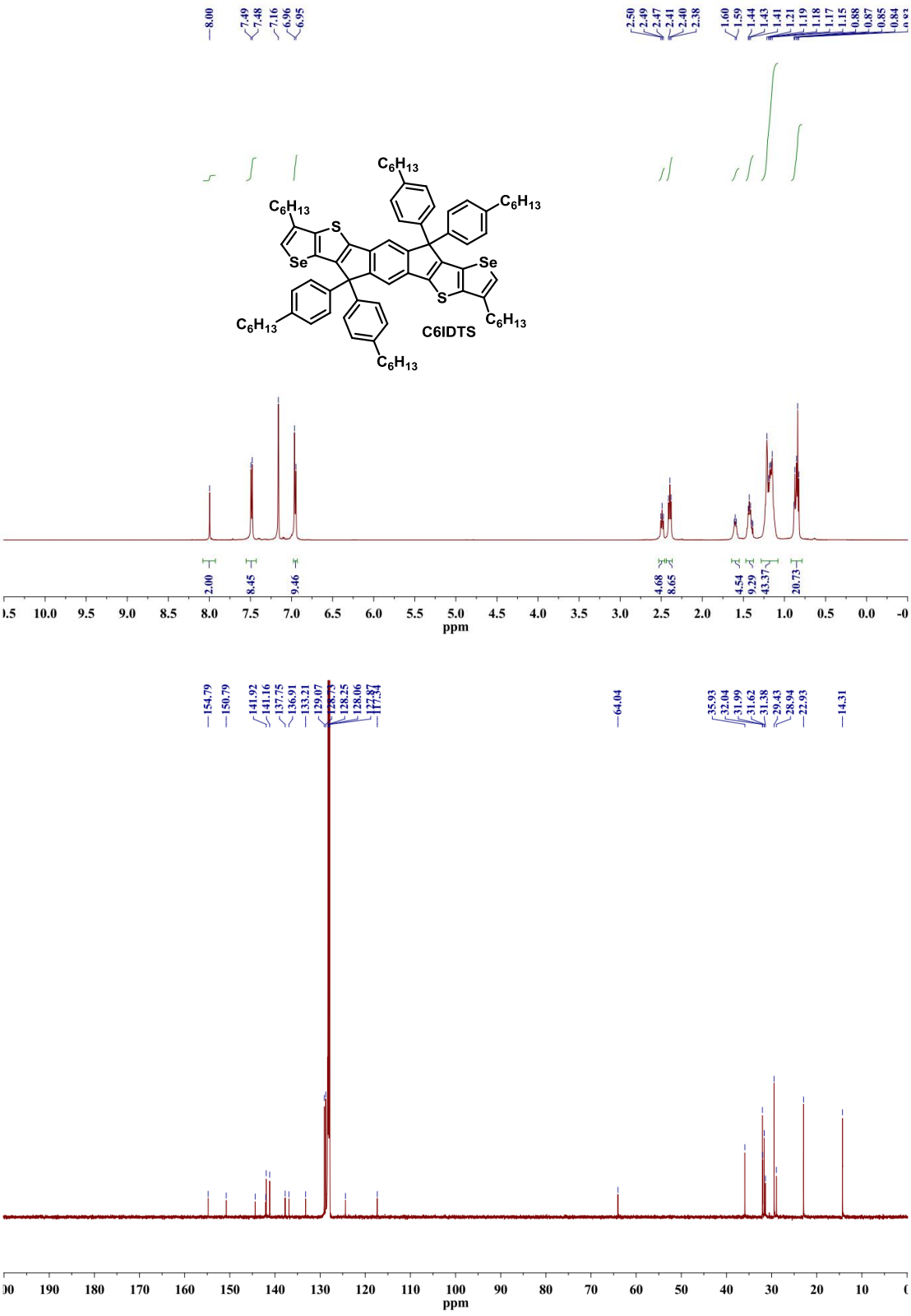

Figure A-20. ^{1}H and ^{13}C NMR spectra of **C6IDTS**.

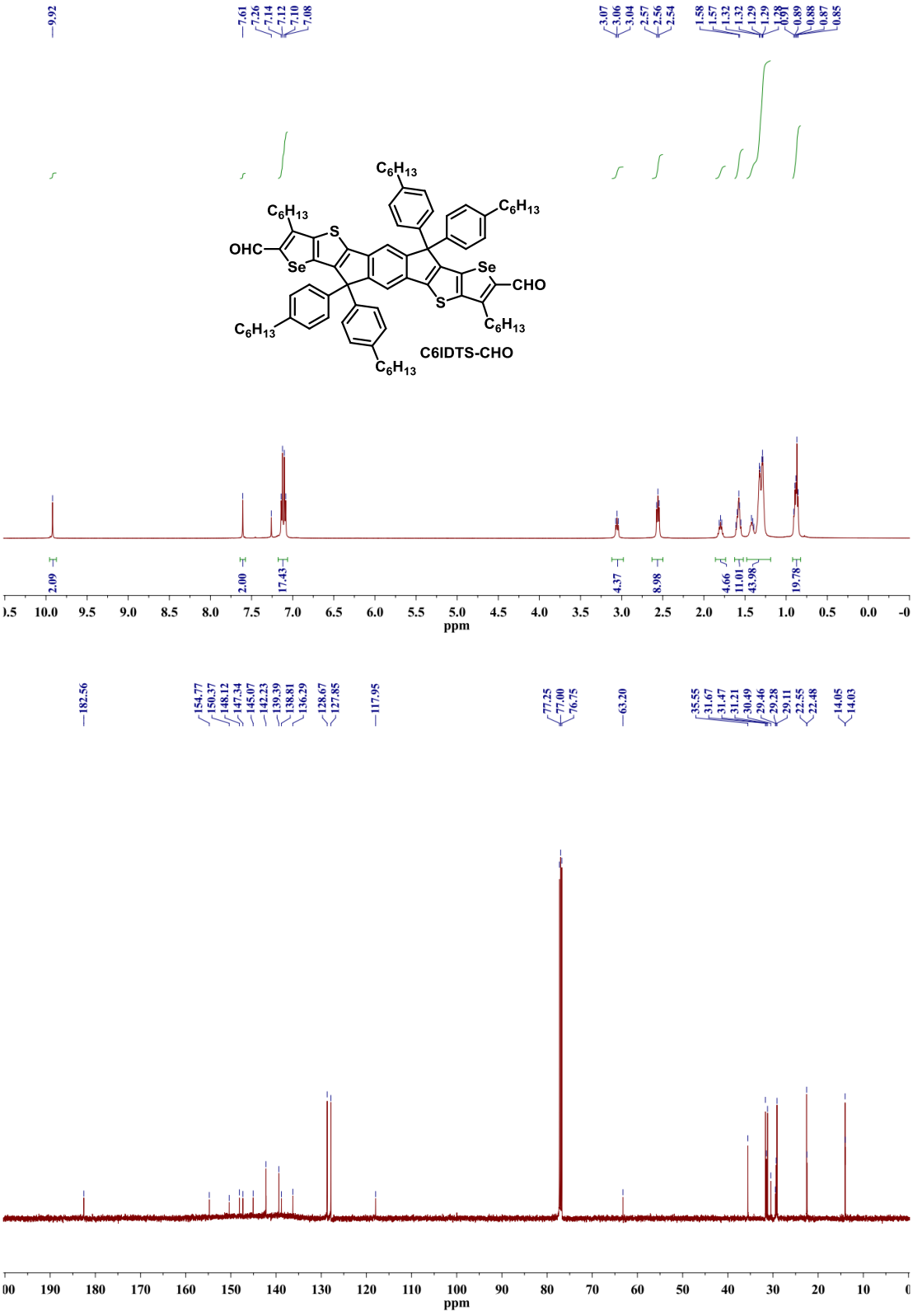

Figure A-21. ^{1}H and ^{13}C NMR spectra of **C6IDTS-CHO**.

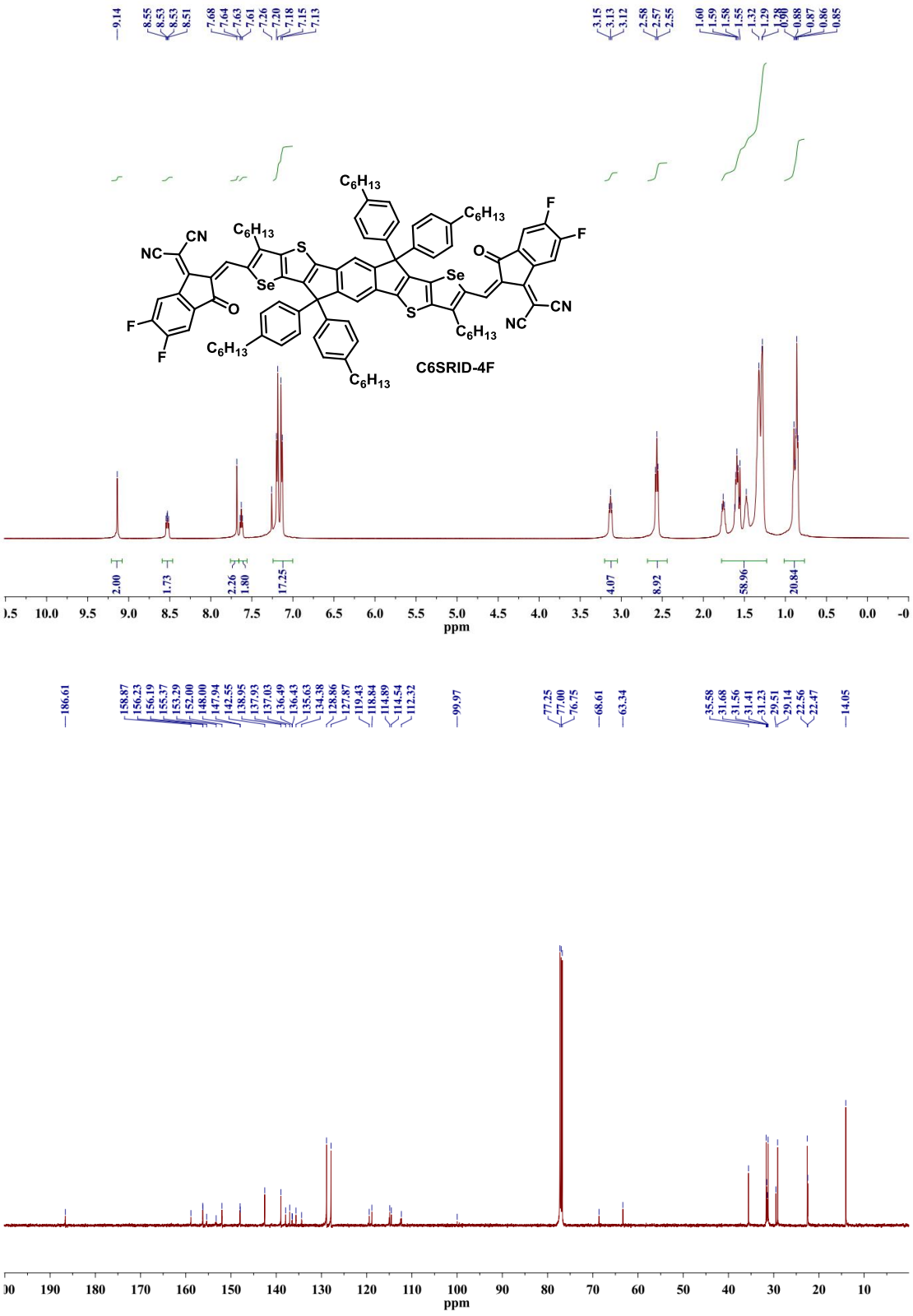

Figure A-22. ^{1}H and ^{13}C NMR spectra of **C6SRID-4F**.

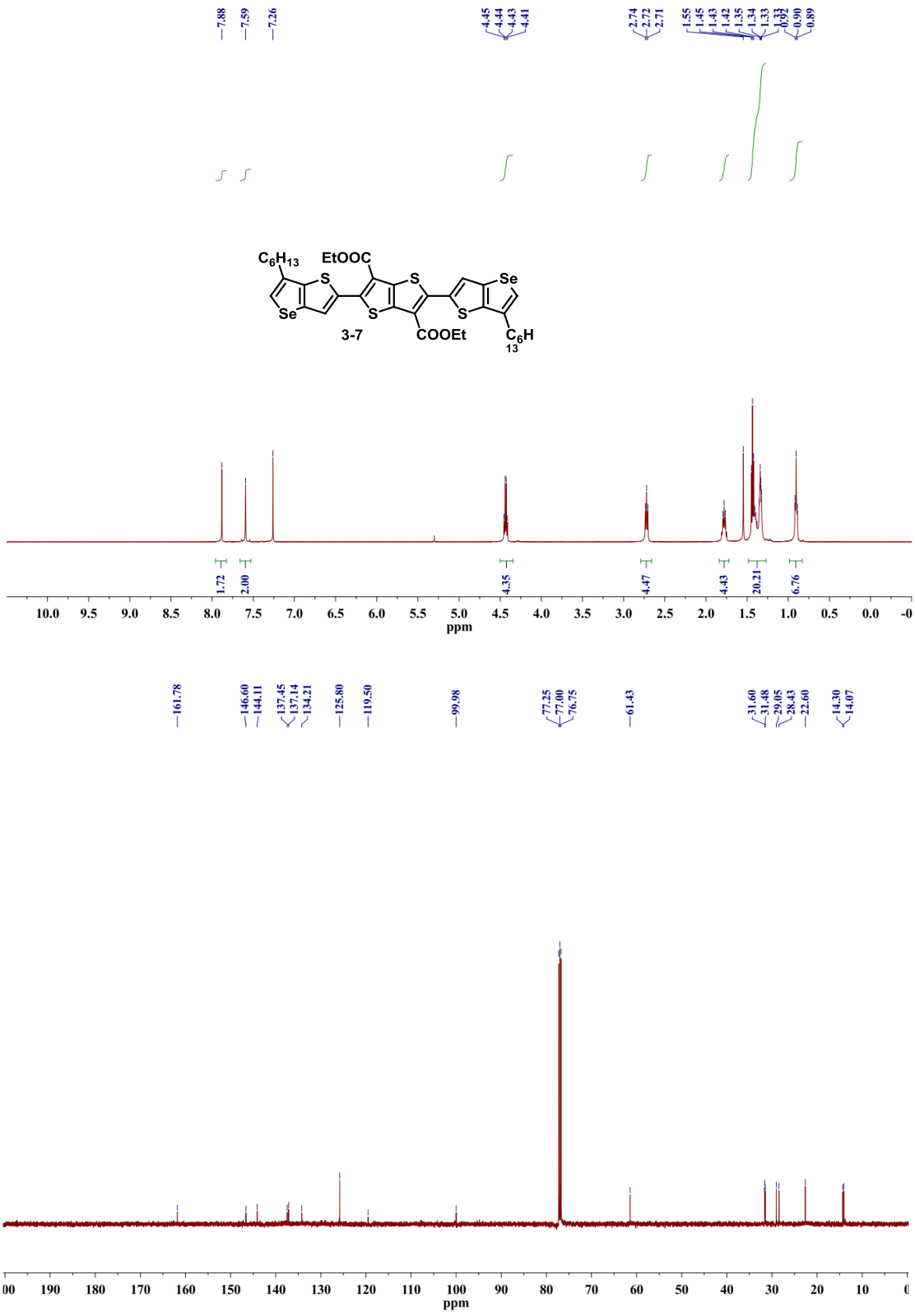

Figure A-23. ^{1}H and ^{13}C NMR spectra of compound **3-7**.

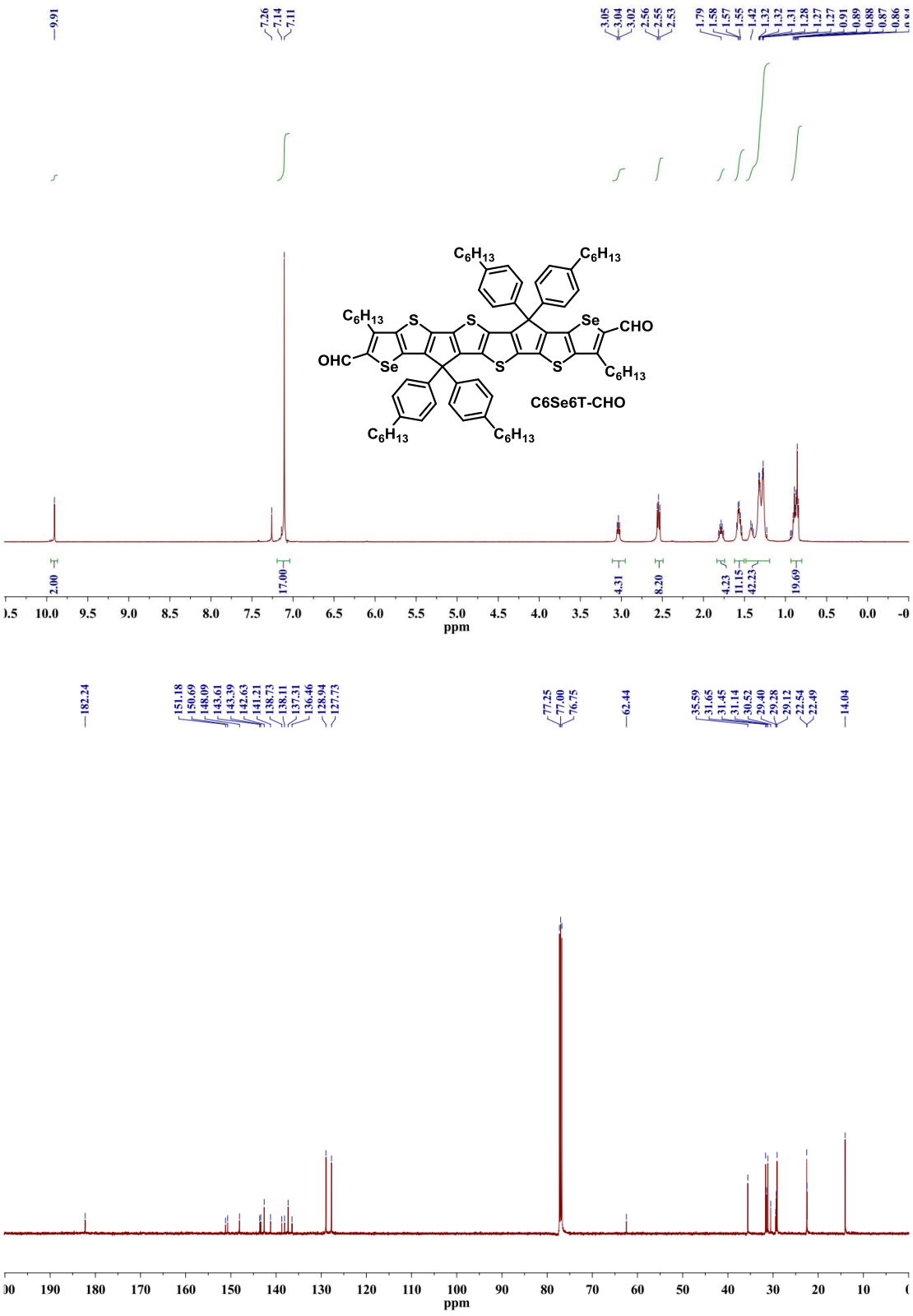

Figure A-24. ^{1}H and ^{13}C NMR spectra of **C6Se6T-CHO**.

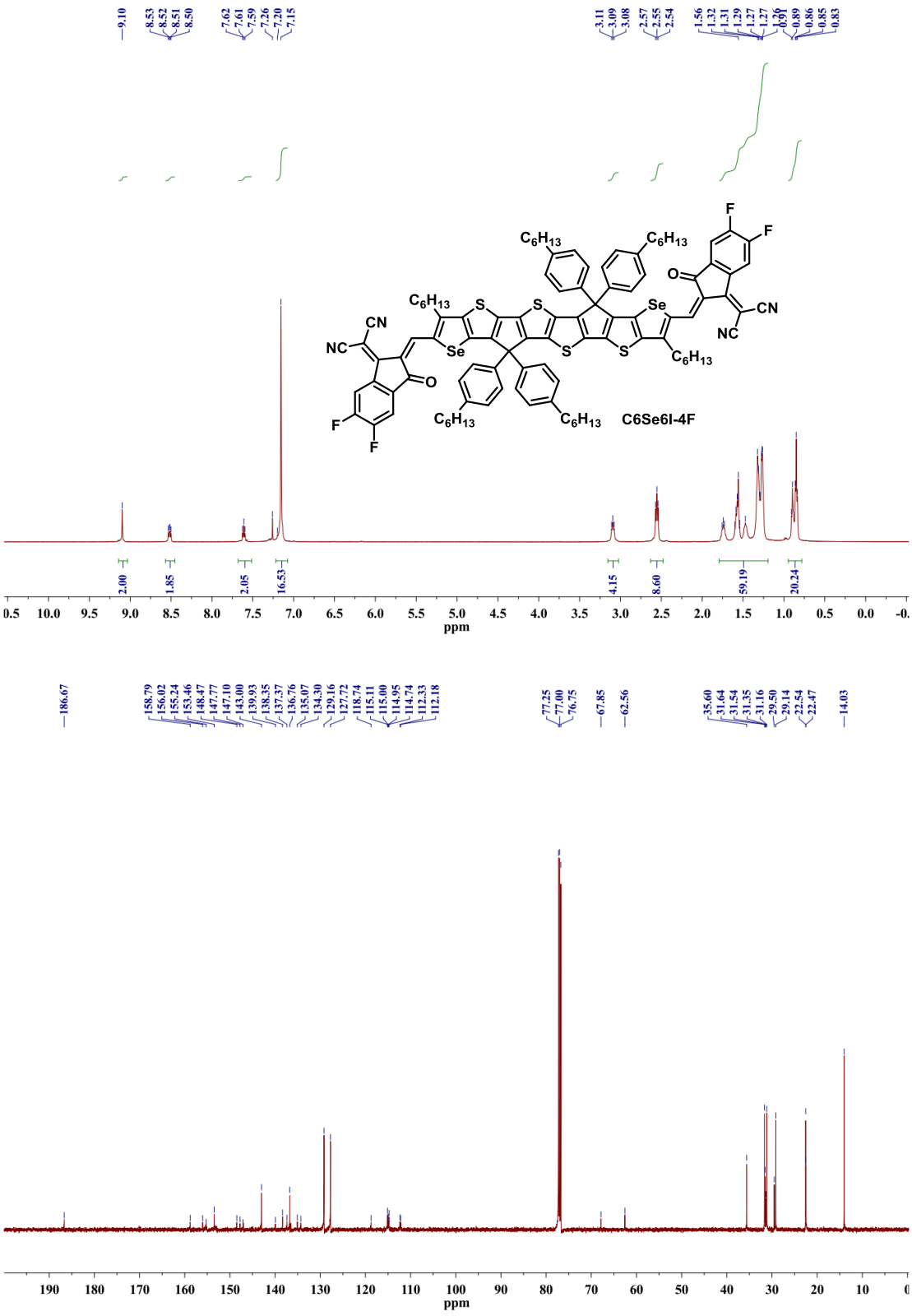

Figure A-25. ^{1}H and ^{13}C NMR spectra of **C6Se6I-4F**.

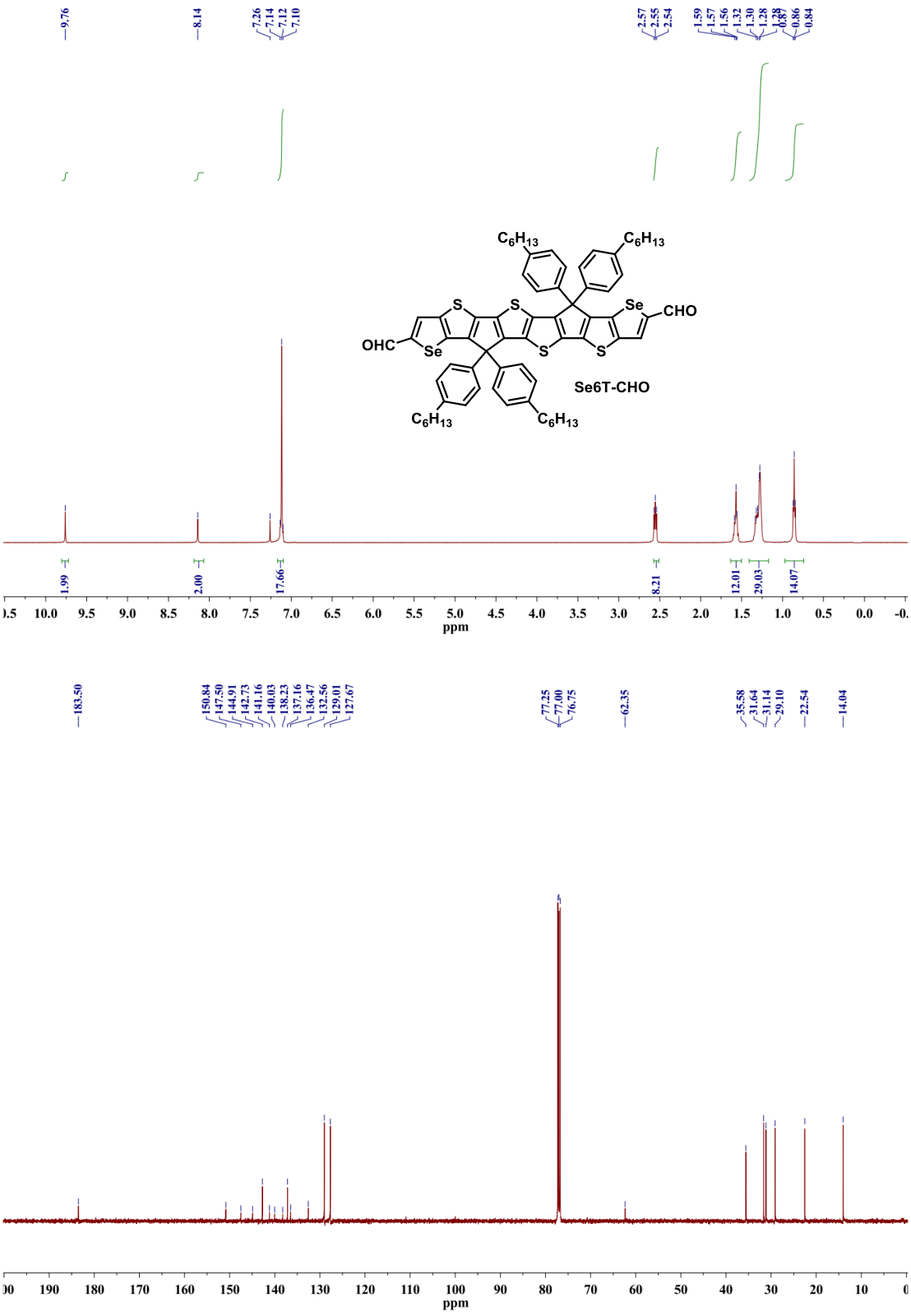

Figure A-26. ^{1}H and ^{13}C NMR spectra of **Se6T-CHO**.

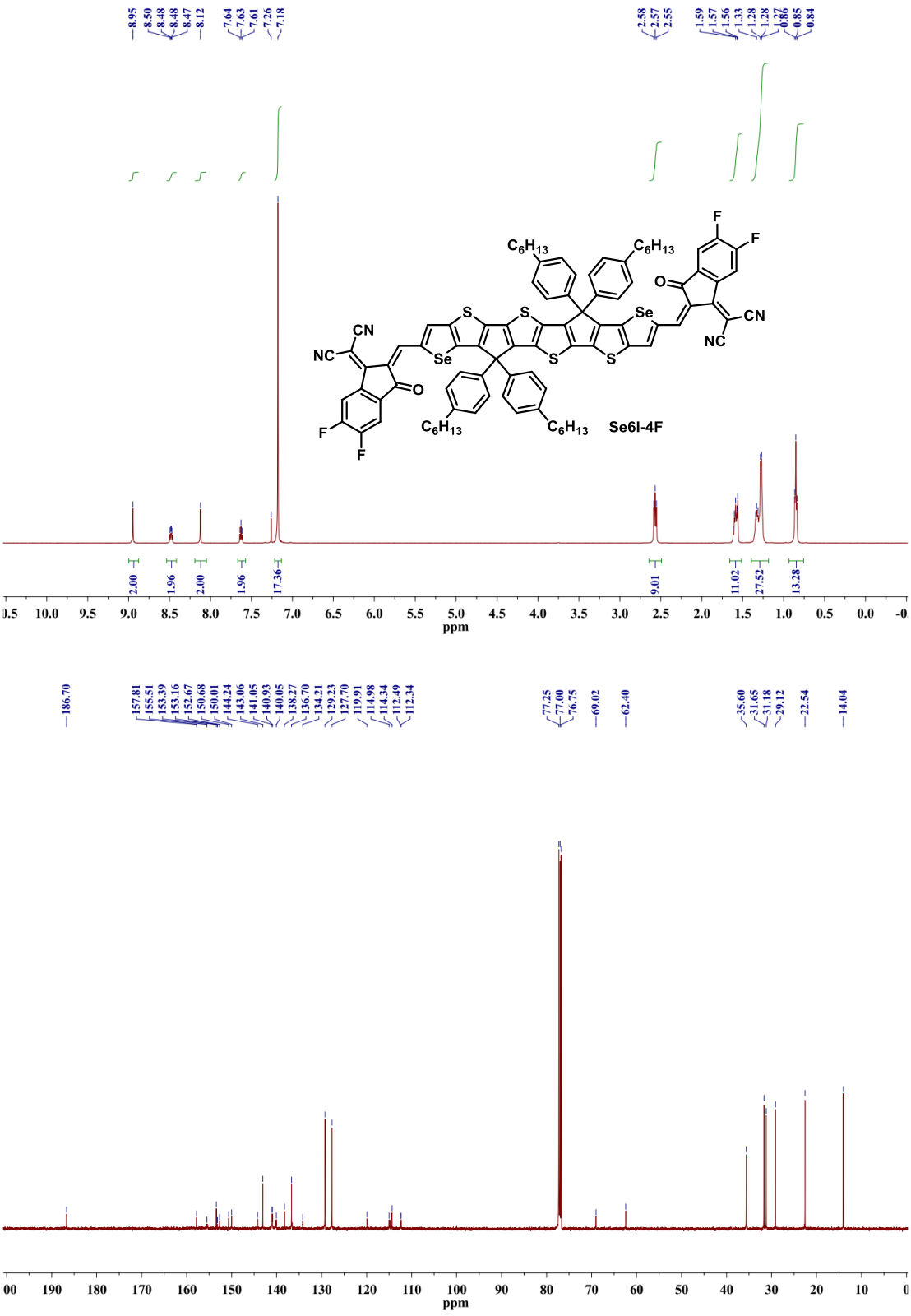

Figure A-27. ^{1}H and ^{13}C NMR spectra of **Se6I-4F**.

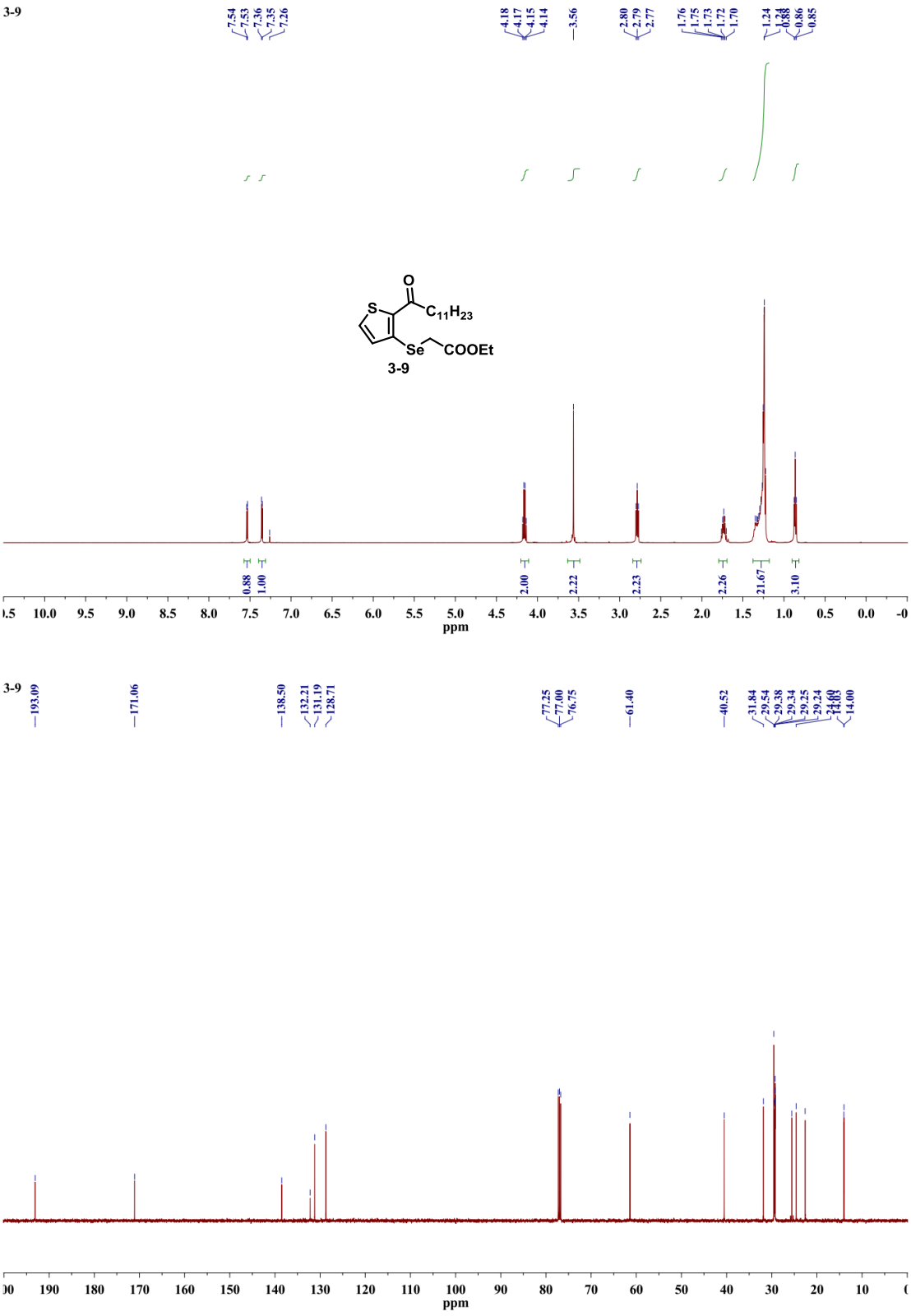

Figure A-28. ^{1}H and ^{13}C NMR spectra of compound **3-9**.

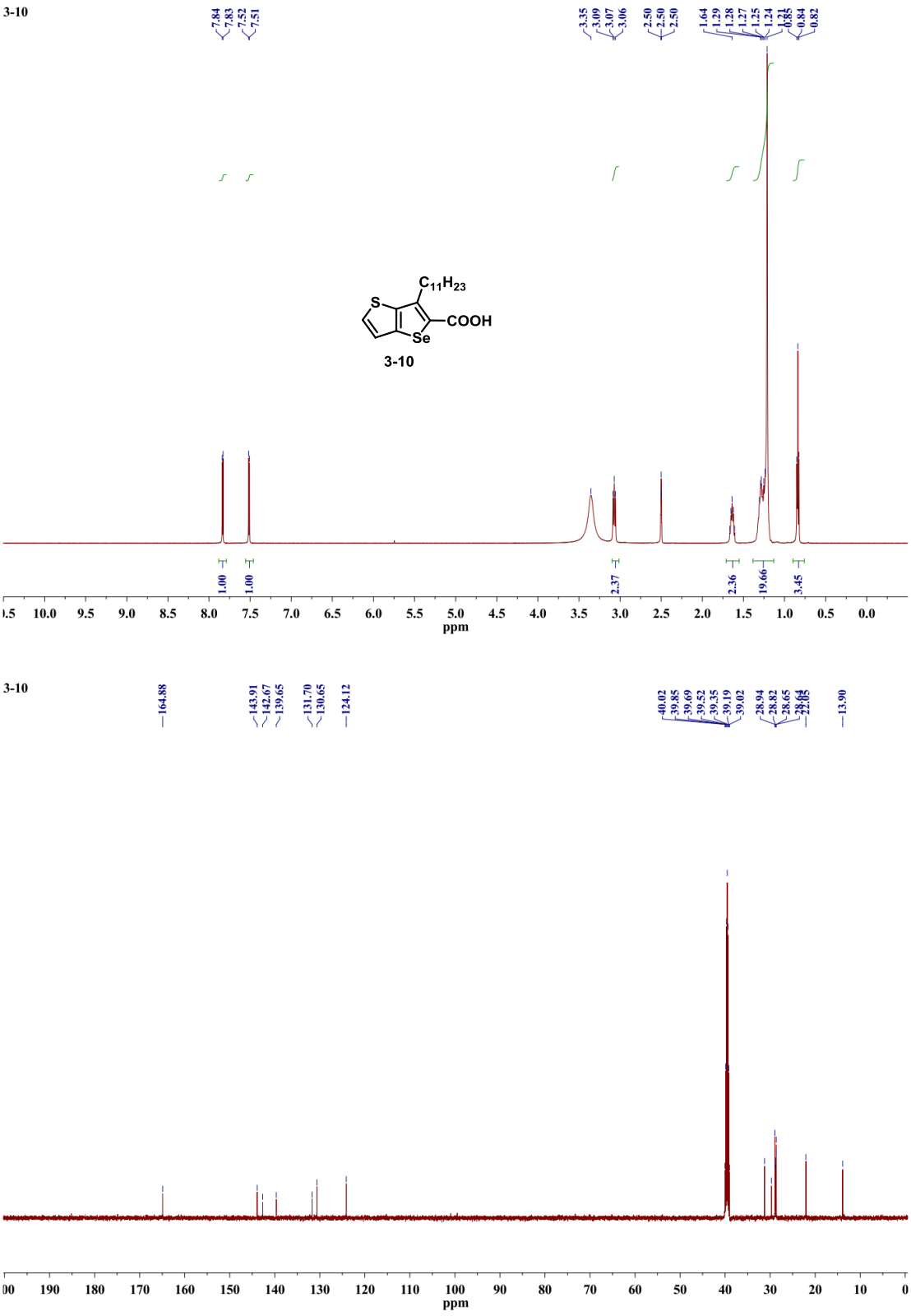

Figure A-29. ^{1}H and ^{13}C NMR spectra of compound **3-10**.

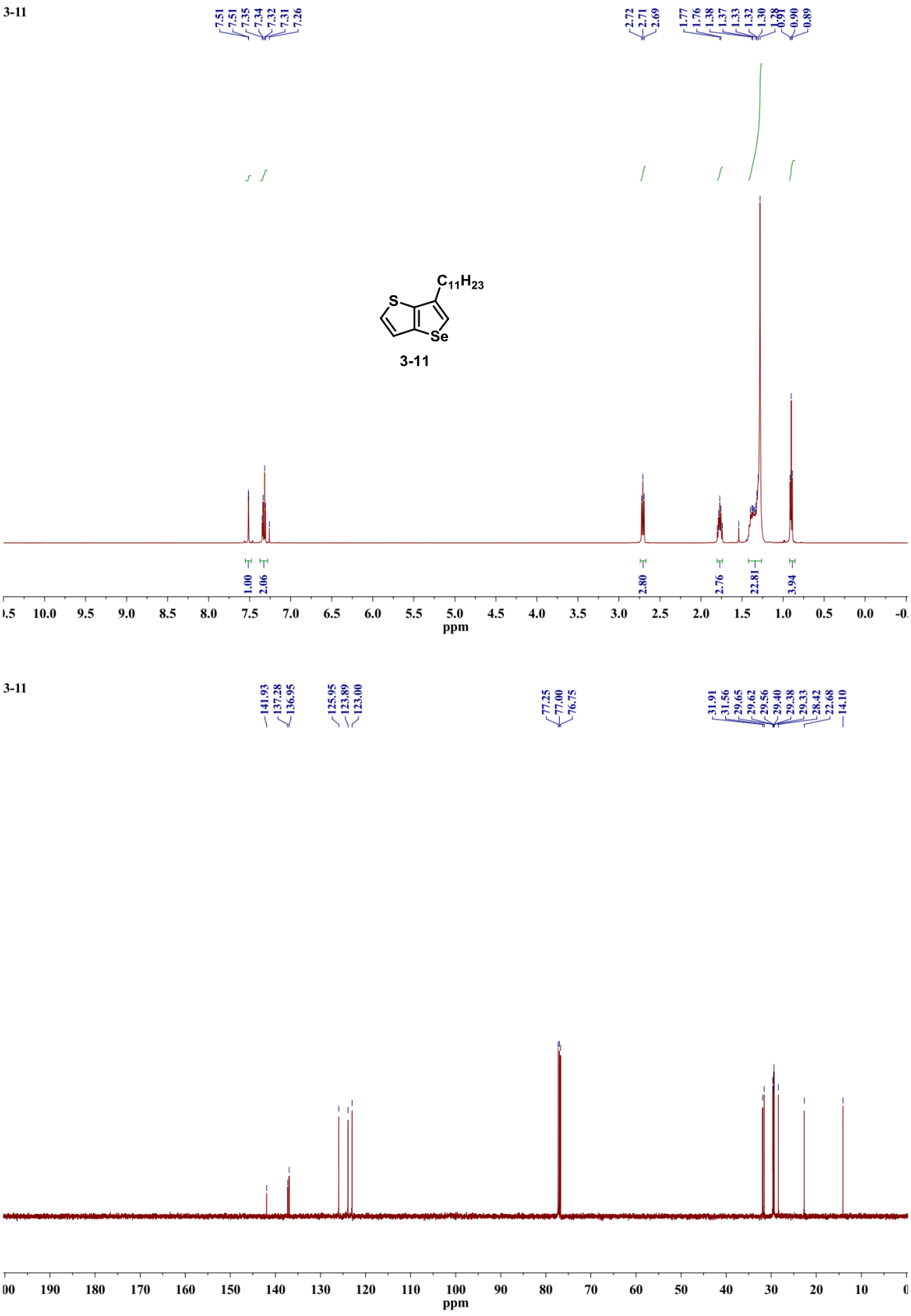

Figure A-30. ^{1}H and ^{13}C NMR spectra of compound **3-11**.

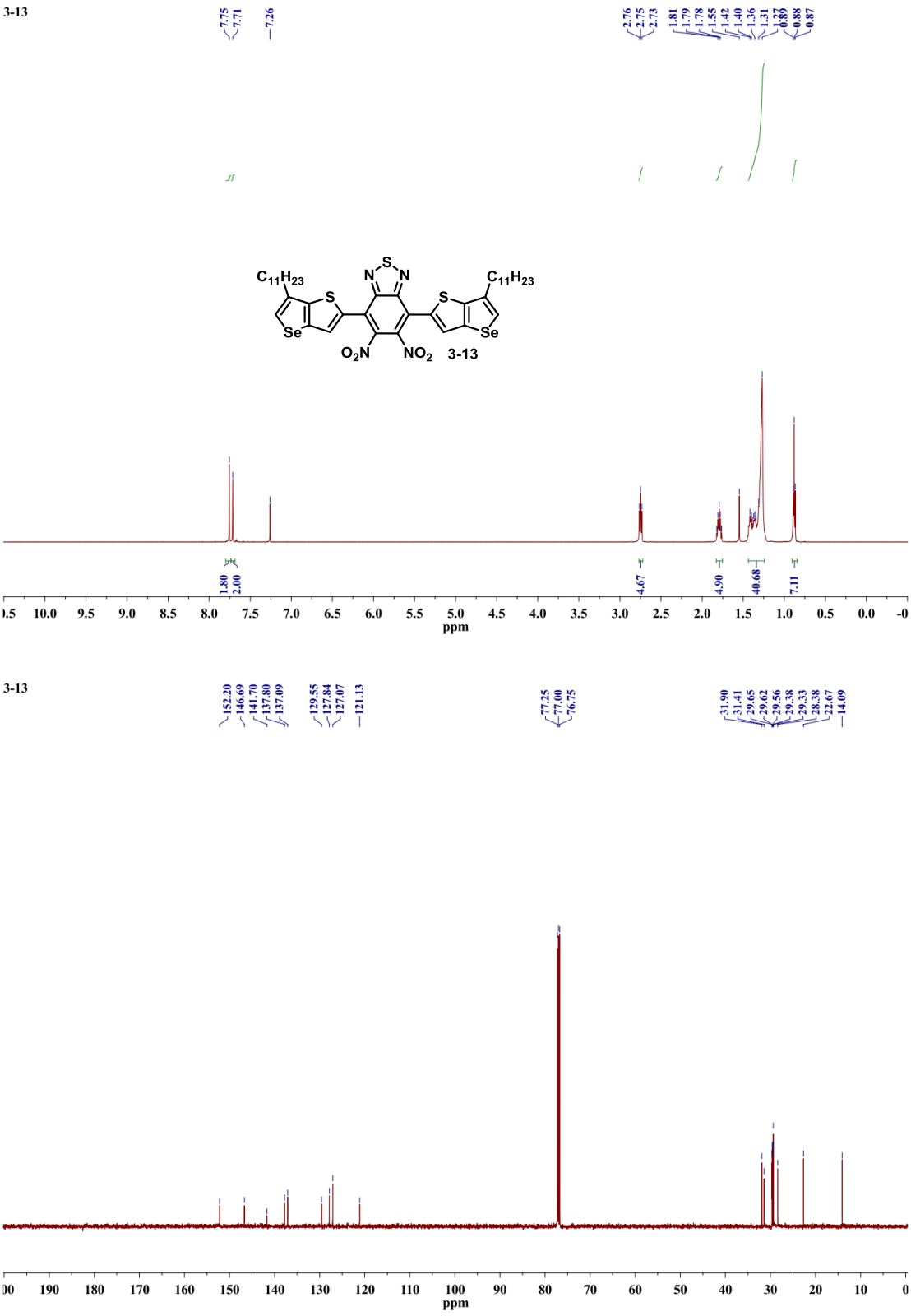

Figure A-31. ^{1}H and ^{13}C NMR spectra of compound **3-13**.

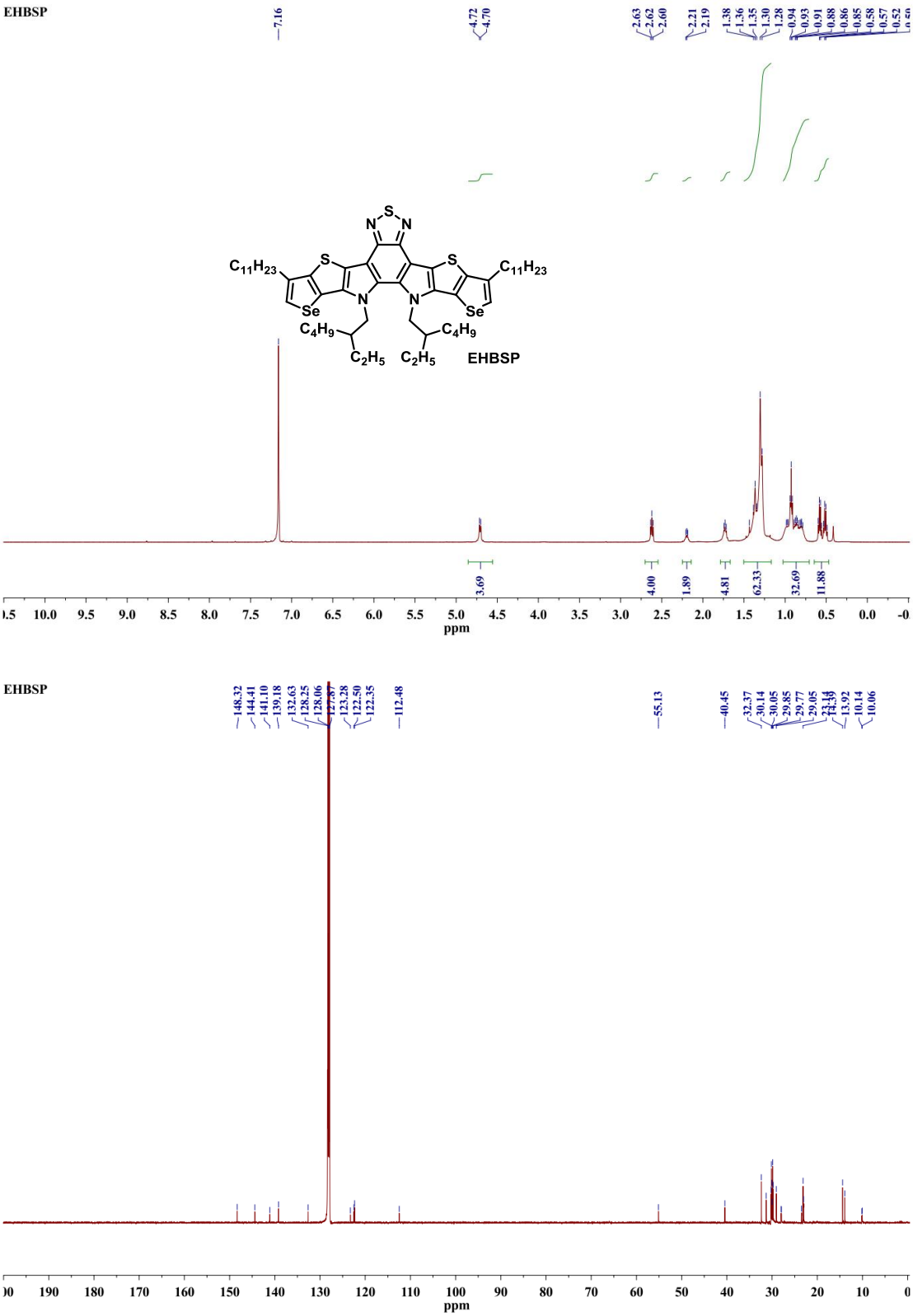

Figure A-32. ^{1}H and ^{13}C NMR spectra of **EHBSP**.

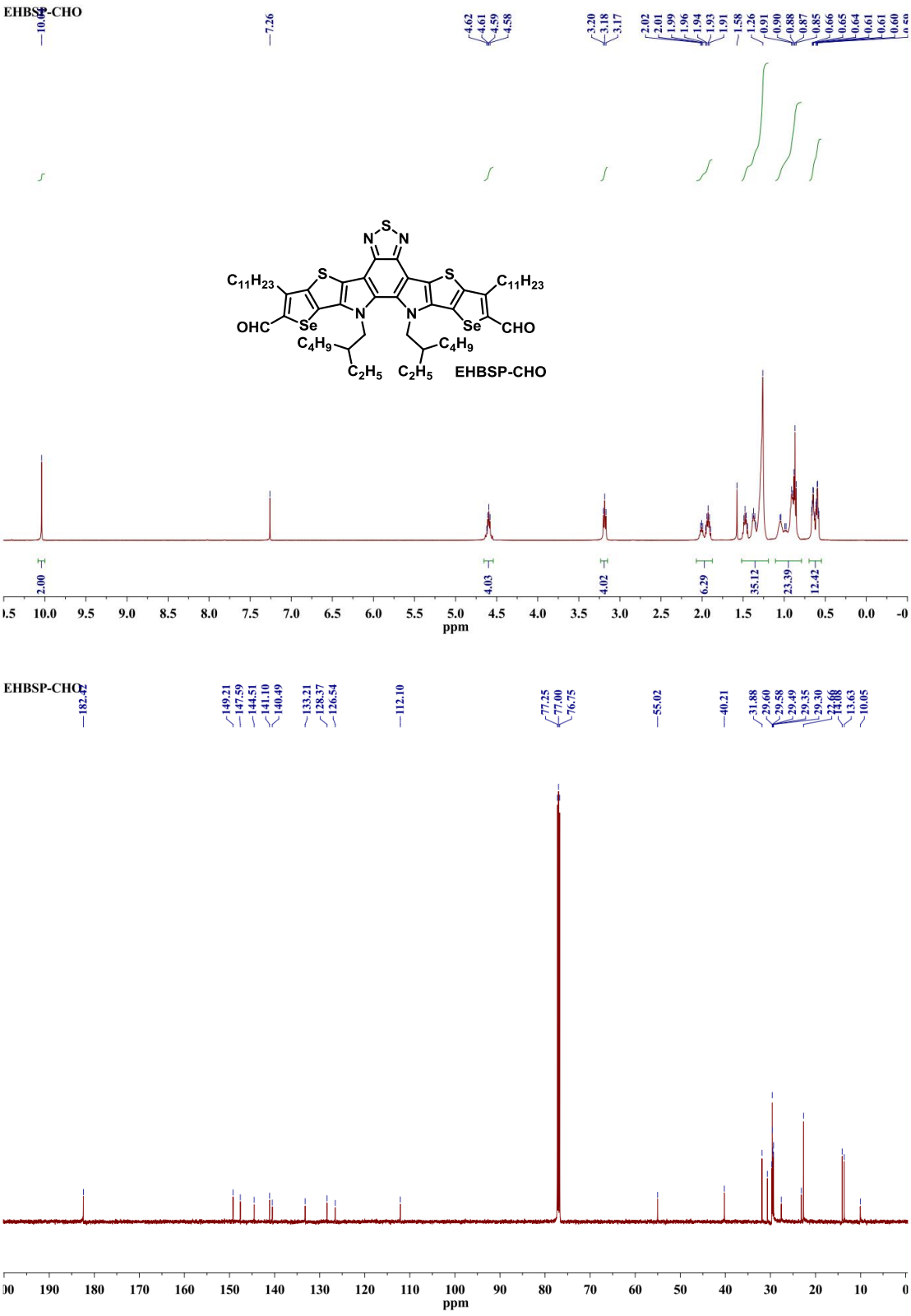

Figure A-33. ^{1}H and ^{13}C NMR spectra of **EHBSP-CHO**.

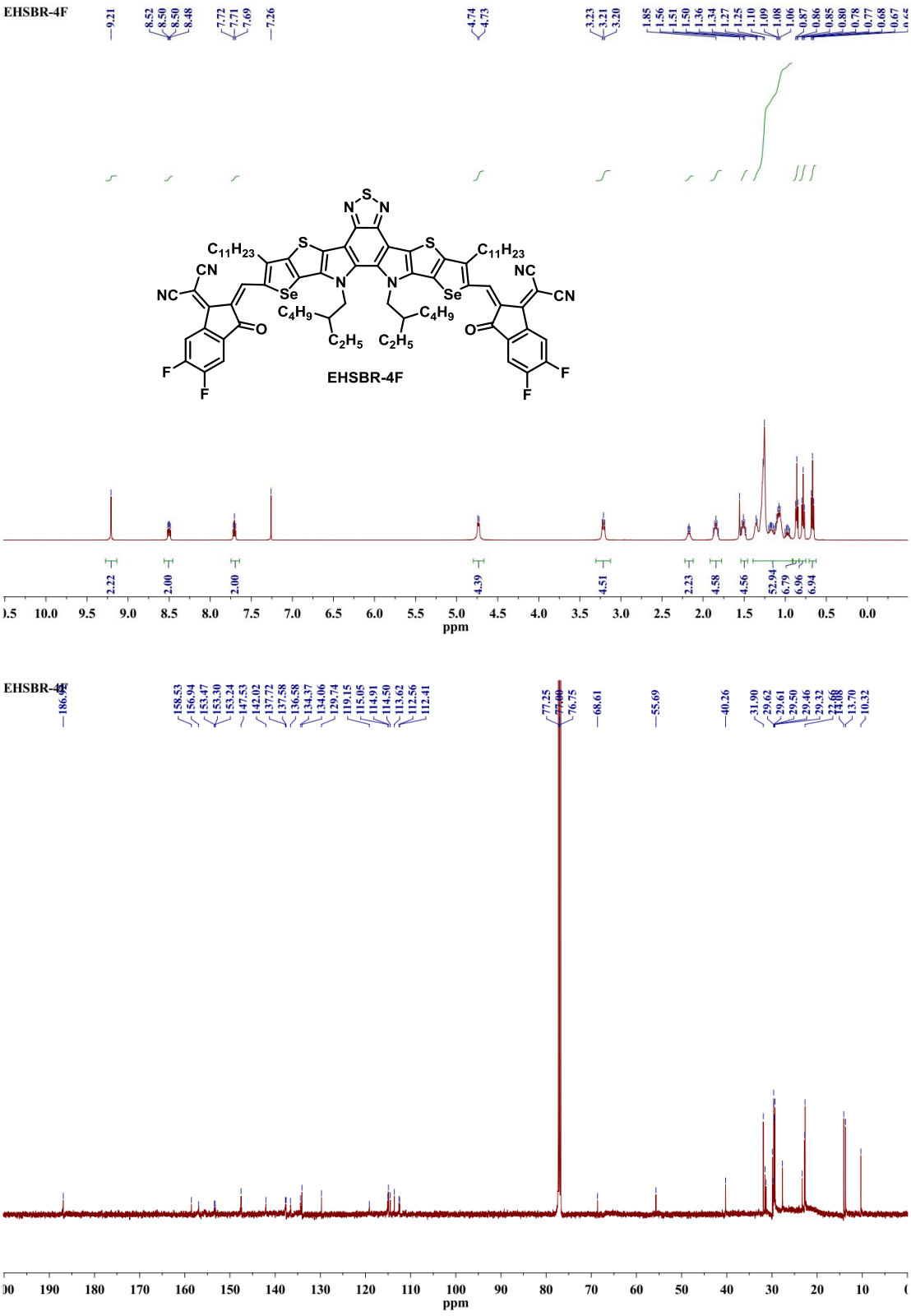

Figure A-34. ^{1}H and ^{13}C NMR spectra of **EHSBR-4F**.

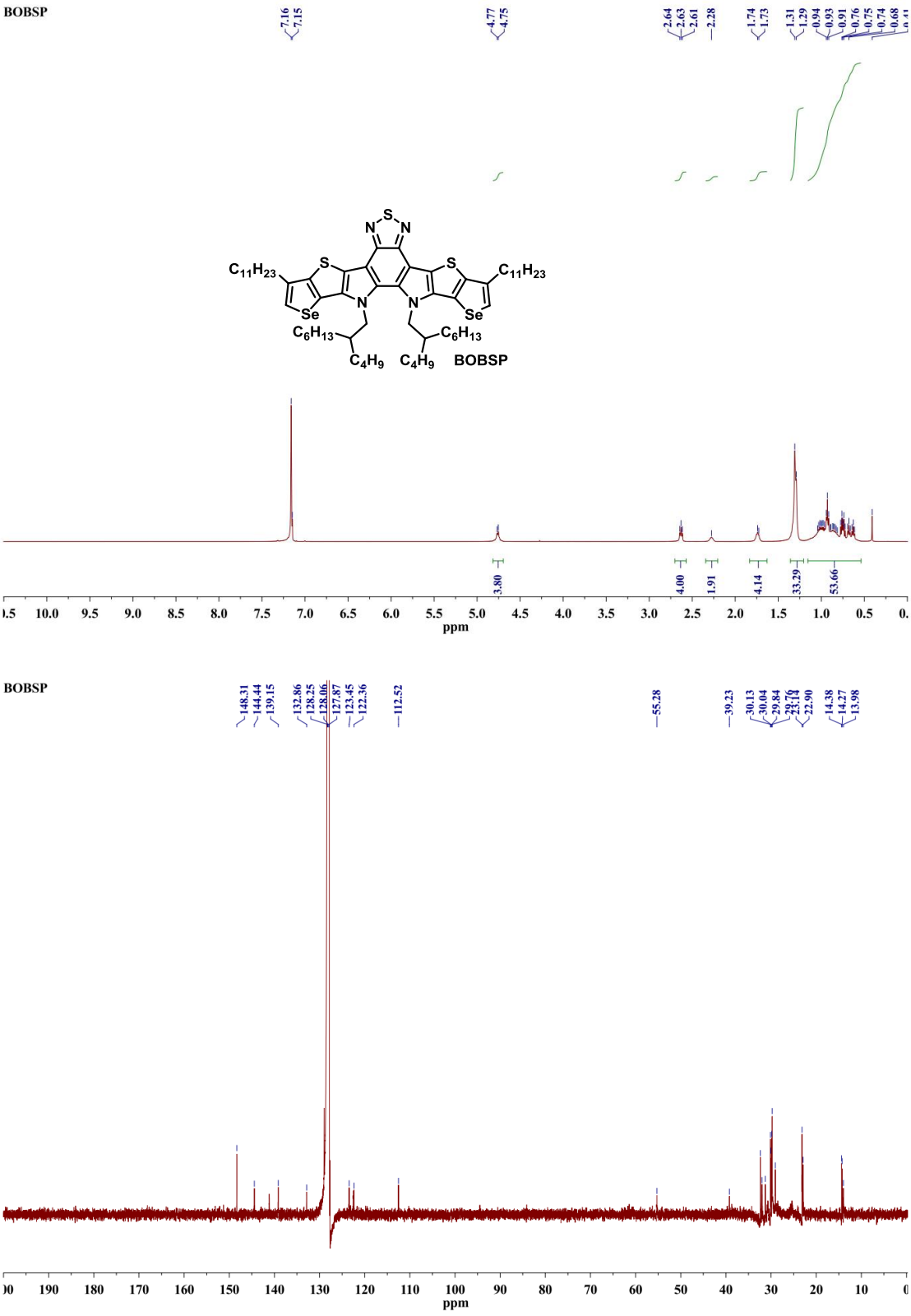

Figure A-35. ^{1}H and ^{13}C NMR spectra of **BOBSP**.

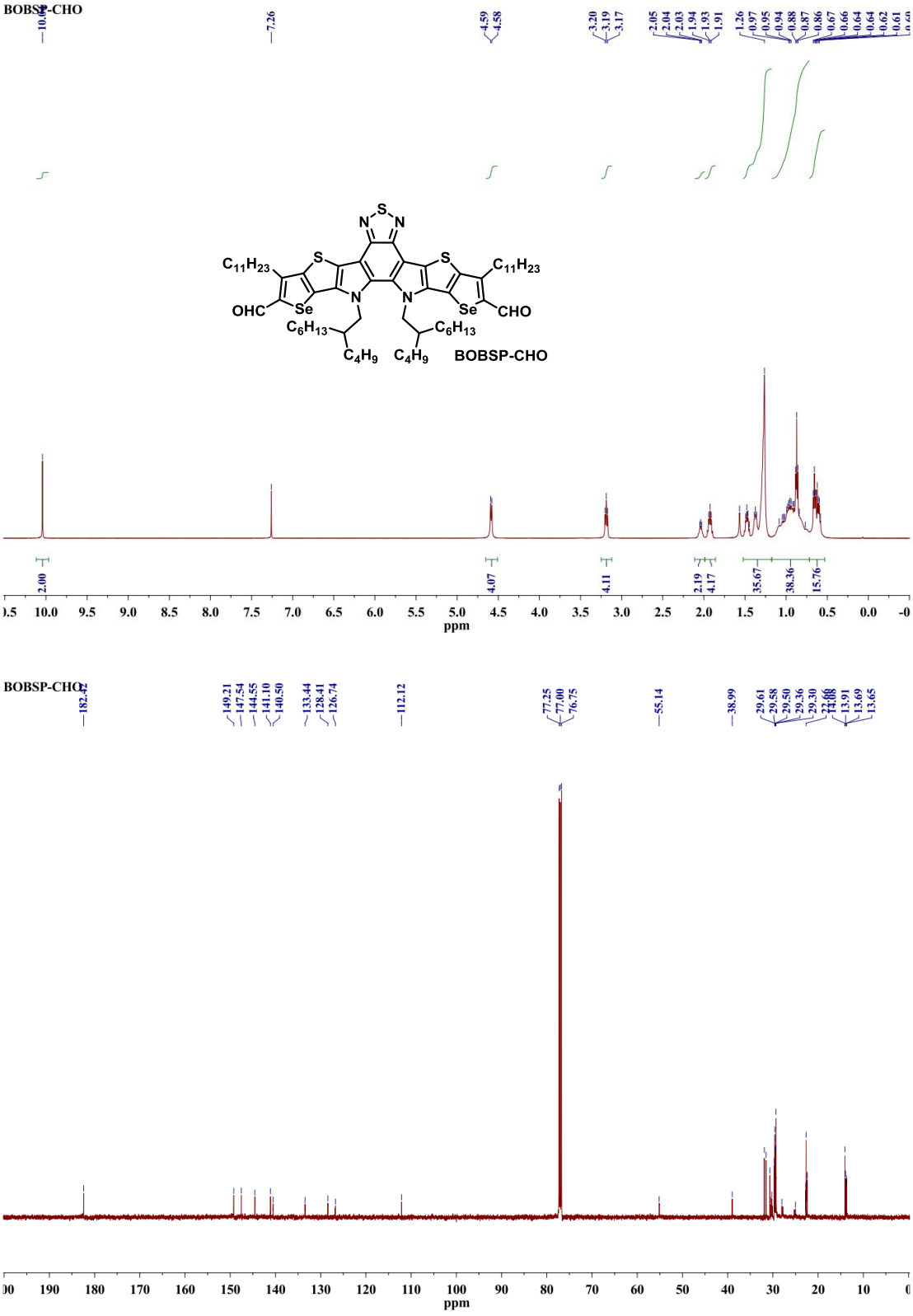

Figure A-36. ^{1}H and ^{13}C NMR spectra of **BOBSP-CHO**.

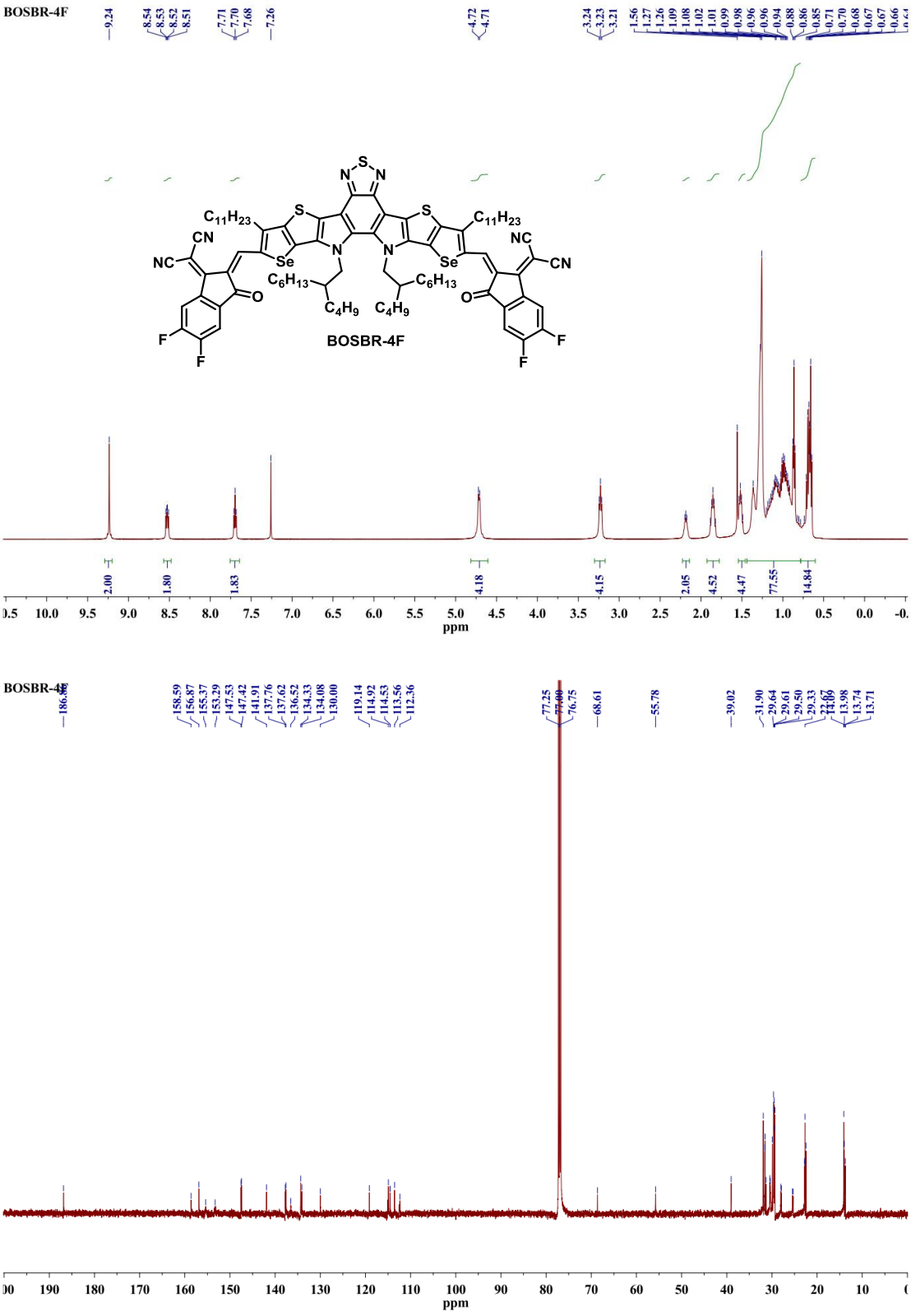

Figure A-37. ^{1}H and ^{13}C NMR spectra of **BOSBR-4F**.

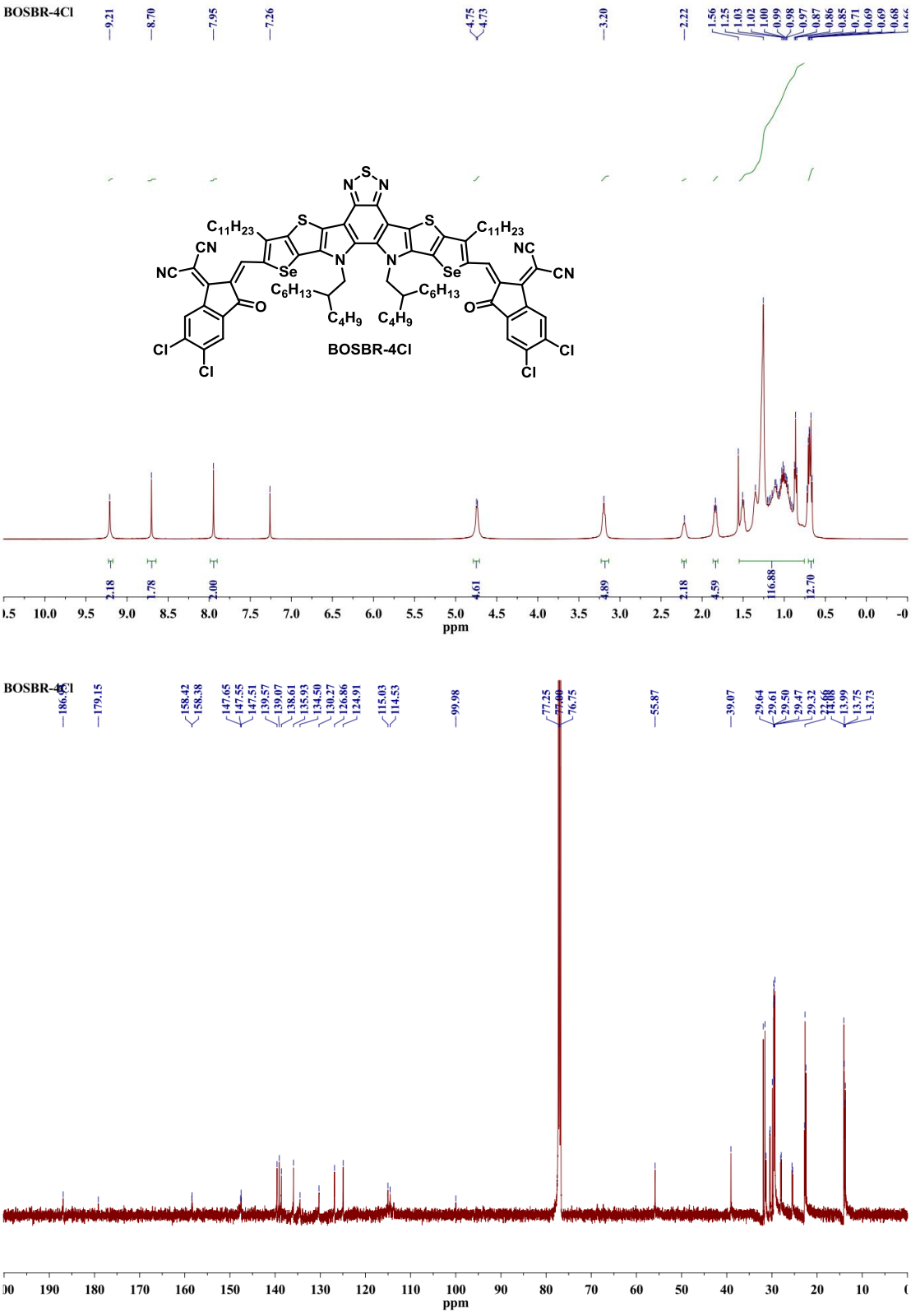

Figure A-38. ^{1}H and ^{13}C NMR spectra of **BOSBR-4Cl**.

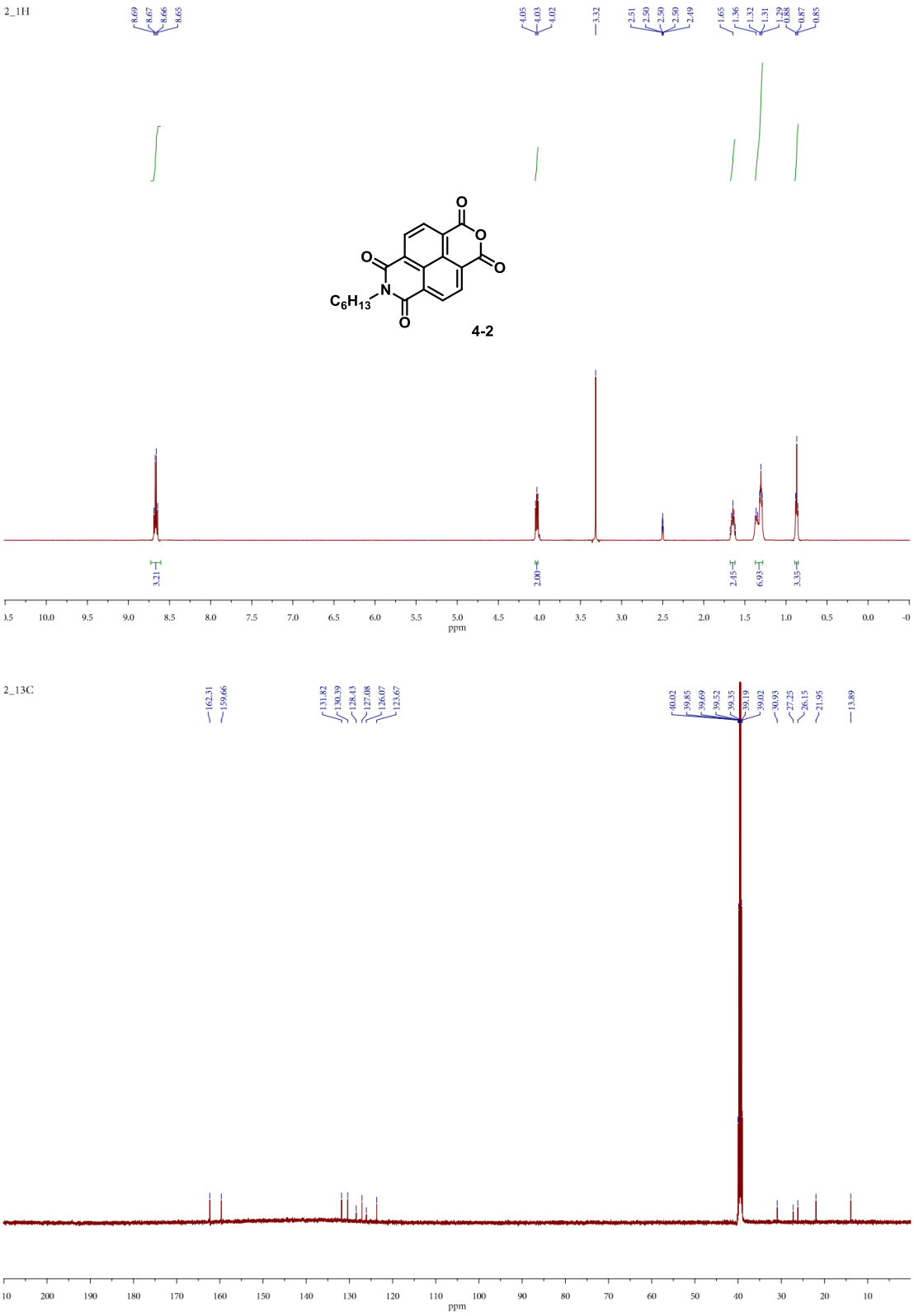

Figure A-39. ^{1}H and ^{13}C NMR spectra of compound **4-2**.

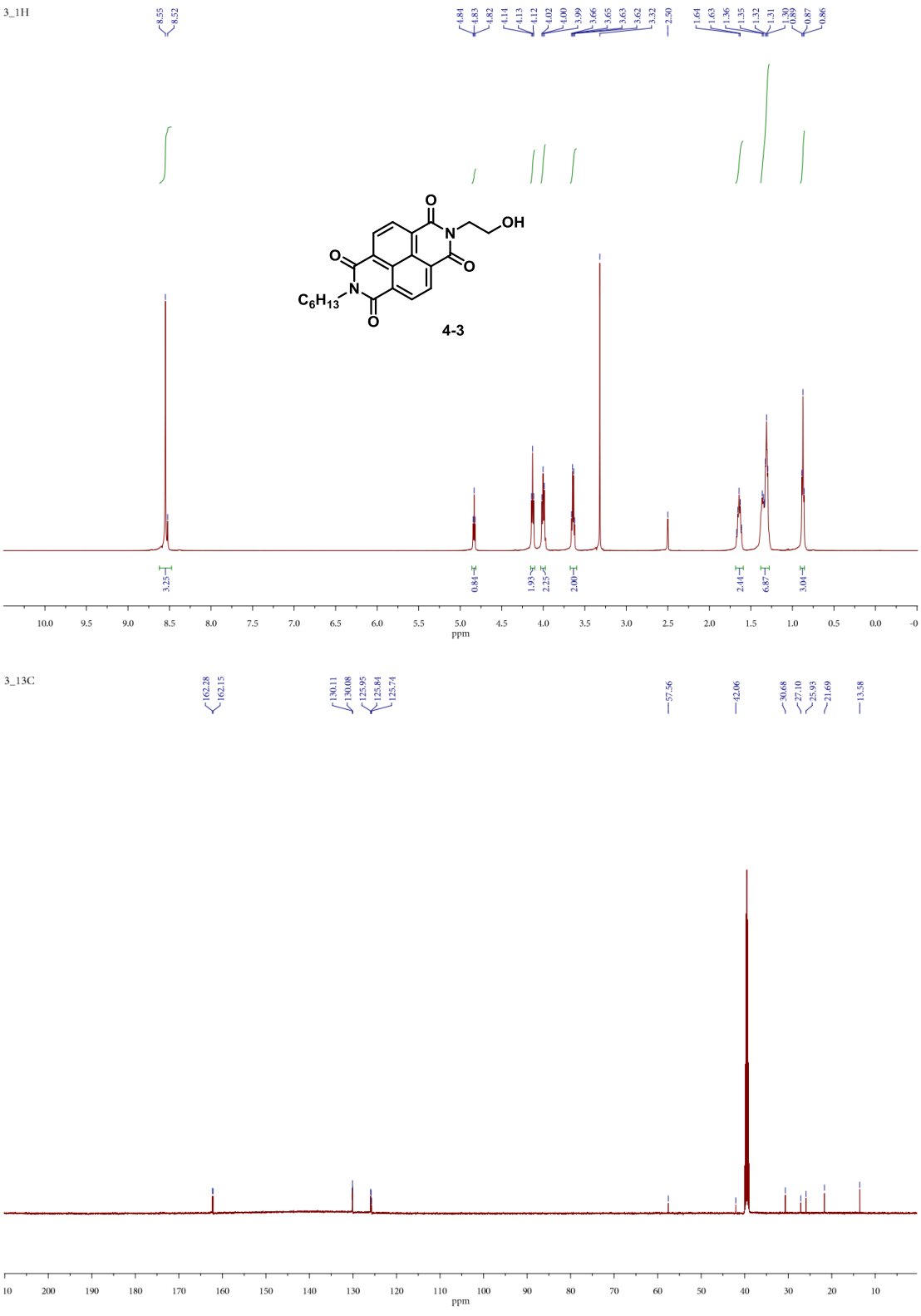

Figure A-40. ^{1}H and ^{13}C NMR spectra of compound **4-3**.

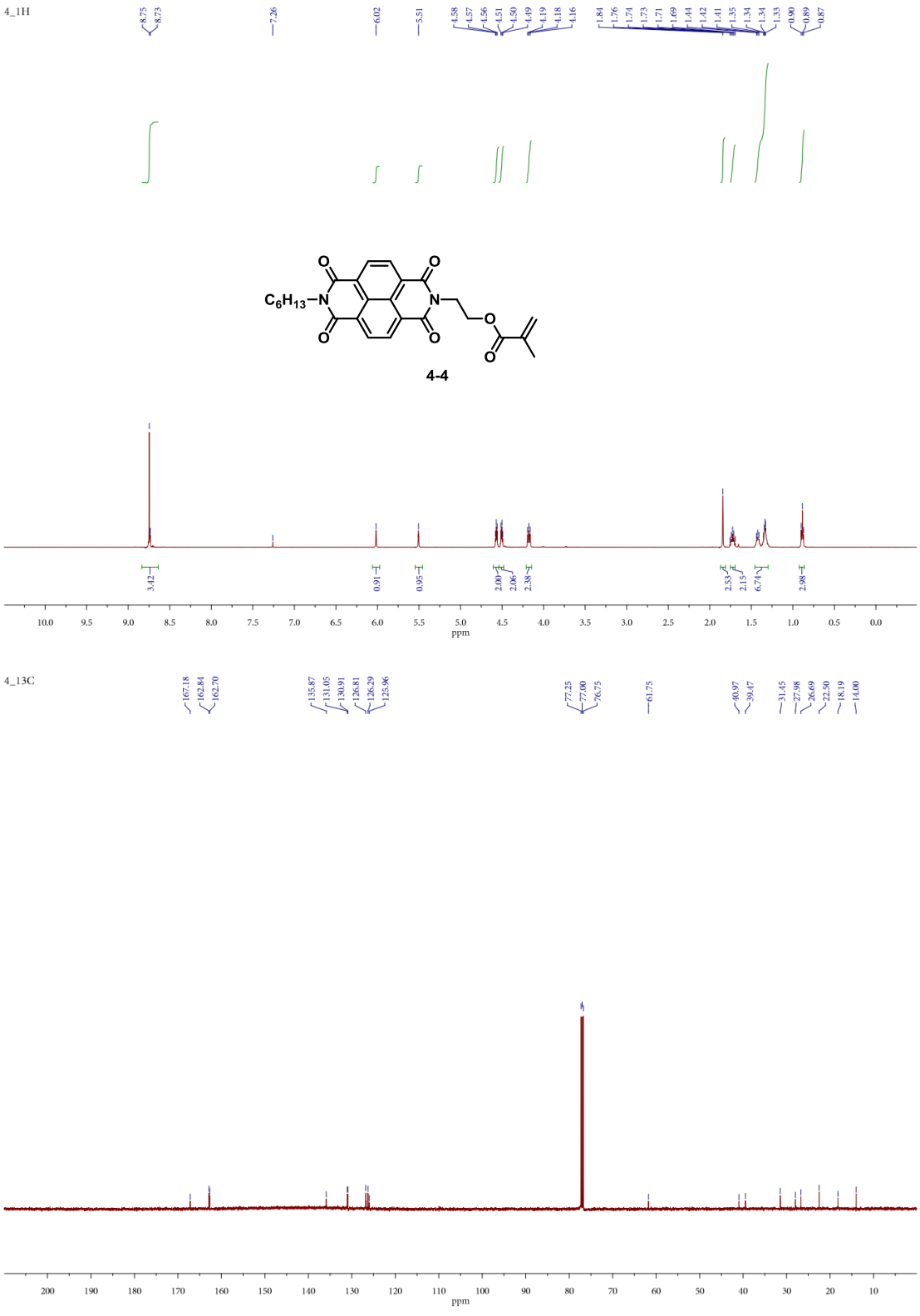

Figure A-41. ^{1}H and ^{13}C NMR spectra of compound **4-4**.

VITA

Francis Lin, AKA Ray or DDR, was born in California and grew up in Taiwan. He has been working in the field of organic functional materials for renewable energy applications since 2010 at National Taiwan University under the supervision of Prof. Ken-Tsung Wong. After he got a B.S. degree in Chemistry, he went to University of Washington where he joined the research group of Prof. Alex Jen in the year of 2014 to pursue a Ph.D. degree. He has a solid background on design and synthesis of organic functional materials, and has authored or co-authored over 40 publications (h-index = 23) in the field of organic photovoltaics, Perovskite solar cells and lithium ion batteries.

Besides doing research, he is a good cook in the kitchen, an adventurous backpacker in the mountains, and a sharp shooter who focuses on his targets.